DESIGN OF INHERENTLY SAFER COMPLEX REACTIVE PROCESSES: APPLICATION ON THE *N*-OXIDATION OF ALKYLPYRIDINES

A Dissertation

by

ALBA LUCIA PINEDA SOLANO

Submitted to the Office of Graduate and Professional Studies of
Texas A&M University
in partial fulfillment of the requirements for the degree of

DOCTOR OF PHILOSOPHY

Chair of Committee,	M. Sam Mannan
Committee Members,	Mahmoud El-Halwagi
	Charles Glover
	Debjyoti Banerjee
Head of Department,	M. Nazmul Karim

May 2014

Major Subject: Chemical Engineering

ABSTRACT

Alkylpyridine *N*-oxides are important intermediates in the pharmaceutical industry. The *N*-oxides are produced via the homogeneously catalyzed *N*-oxidation of the respective alkylpyridines using hydrogen peroxide as the oxidizing agent and phosphotungstic acid as the catalyst. The *N*-oxidation is accompanied by the undesired, condition-dependent decomposition of hydrogen peroxide. A runaway of this reaction may result in a rapid generation of oxygen and temperature rise in the alkylpyridine flammable environment, with the additional potential to overpressurize the reaction vessel and/or trigger secondary decompositions of the product. The decomposition of hydrogen peroxide is exacerbated during the *N*-oxidation of higher order alkylpyridines due to the mass transfer resistance caused by the formation of an organic phase and an aqueous phase. The water-soluble catalyst promotes severe decomposition of hydrogen peroxide, jeopardizing the safety of the process, and reducing its efficiency.

This research focused on the development of a more efficient and inherently safer process for the *N*-oxidation of alkylpyridines. Isothermal calorimetry, incorporating a factorial design of experiments (DOE), was used to study operating conditions that minimize the decomposition of hydrogen peroxide. Adiabatic calorimetry was used to study the thermal stability of alkylpyridines and their *N*-oxides. The compounds studied in this work included 3-picoline, 3,5-lutidine, 2,6-lutidine and 2,4,6-collidine, and their corresponding *N*-oxides. In addition, this research evaluated the use of *in-situ* FTIR spectroscopy to monitor this reaction system.

Thermal stability analyses showed that the alkylpyridines studied are stable up to 400 °C, while the corresponding *N*-oxides decompose significantly above 230 °C. The factorial DOE revealed that the conversion of 3-picoline is most influenced by the interaction between the factors catalyst mass and dosing rate. Conversions of 3-picoline

and 3,5-lutidine obtained were as high as 98% and 95%, respectively, using only a stoichiometric amount of hydrogen peroxide. Significant decomposition was observed during the *N*-oxidation of 2,6-lutidine and 2,4,6-collidine. Knowledge acquired on the *N*-oxidation of alkylpyridines indicates that reaction efficiency, selectivity and safety can be greatly improved a) by increasing the operating temperature and using a system working under pressure, and b) in the case of the higher order alkylpyridines, by avoiding operating conditions where a heterogeneous mixture is formed.

This work demonstrates the complexity and the multiple studies required for the design of inherently safer reactive processes and it can serve as a model for similar studies on different complex reactions and in the development of inherently safer reactor design.

DEDICATION

To my parents Martha Lucia Solano and Julio Roberto Pineda, for always giving me their love and unconditional support, and for being the main motivation to move forward and become a better person every day.

A mis padres Martha Lucía Solano y Julio Roberto Pineda, porque siempre me han brindado su amor y apoyo incondicional y han sido mi mayor motivación para seguir adelante y convertirme en una mejor persona cada día.

ACKNOWLEDGEMENTS

Many people have been part of my journey through Texas A&M University who have helped me overcome challenges, accomplish my goals, supported me in difficult moments, or simply made graduate school happier and memorable, and for that I am very thankful to each one of them.

I would like to offer my special thanks to my advisor, Dr. M. Sam Mannan for his mentoring, which has gone beyond the academic level, and for his kindness and understanding during difficult times. I also thank him for giving me multiple opportunities to learn about real world problems, contribute with solutions and gain valuable experience to develop myself personally and professionally. I admire Dr. Mannan as a researcher, a leader and a person. He is a visionary and an inspiration for students to make a contribution in the process safety field.

I am deeply grateful to Dr. Maria Papadaki from the University of Patras, Greece whose advice and expertise allowed me to complete my research project successfully. I am also thankful to Dr. Papadaki for her continuous encouragement and support, and for making me realize the value of good and bad results, as there is always something to learn from them in the research process. Thank you for helping me see things in perspective, even life; your advice has made me a better researcher and a stronger person.

I would like to thank Dr. Mahmoud El-Halwagi, Dr. Charles Glover and Dr. Debjyoti Banerjee for serving as my committee members and for their assistance during the doctoral program.

I would like to thank the Chemical Engineering Program at Texas A&M University at Qatar for allowing me to perform some of my experiments at the process safety

laboratory. I would also like to thank Dr. Simon Waldram for his technical advice during and after my stay in Qatar. Thanks also to Dr. Subramanya Nayak for his help and support in the laboratory, and thanks to all of those who made my stay in Qatar a memorable and fruitful experience.

I would like to express my deep gratitude to Dr. Victor Carreto and Dr. Lina Saenz for their constant and unconditional support, encouragement and friendship throughout my graduate studies. I am also grateful for their technical advice and insightful discussions about my research. I am particularly thankful to Dr. Carreto for his help and teachings in the laboratory.

I also want to express my thanks to Randy Marek for his help with the maintenance, repair and troubleshooting of laboratory equipment, and to Olga Reyes and Akshay Jain for their assistance with some experimental work.

I would also like to extend my thanks to the staff and members of the Mary Kay O'Connor Process Safety Center. Special thanks to Dr. Mentzer for helping keep my writing progress on schedule and for his advice during the last stages of my PhD. Thanks to Valerie Green for her care and encouragement and to Tricia Hasan for her assistance in the review of several manuscripts, including this dissertation.

There are not enough words to thank my parents, Martha and Julio, for their unconditional love, understanding and support during every step towards reaching my goals. I am deeply thankful to them for instilling in me the importance of education and perseverance, and for their contribution towards shaping the person I am today. I thank them for being my motivation and pillar of strength. Thanks also to my sister, and to my extended family for their support and for making the most out of the few moments spent together during my graduate studies.

I would like to express my very great appreciation to Devin for his love and support and for helping me keep in mind the big picture and focus on my studies. I also thank his family for their care and generosity, and for accepting me as one of their own.

Thanks also go to my friends and colleagues, and to the department faculty and staff for making my time at Texas A&M University a wonderful experience. Special appreciation goes to Bibian and Diego for their long-standing friendship, encouragement and wholehearted support, for helping me overcome setbacks, and for the old and new memories. Special thanks also to Camilo for his understanding and for adding fun and laughter to a serious environment.

Finally, I thank God for giving the strength and clarity needed to complete my studies, for the happy and difficult moments lived, and for making my experience at Texas A&M one I will cherish forever.

TABLE OF CONTENTS

Page

LIST OF FIGURES

Page

LIST OF TABLES

Page

1. INTRODUCTION[*]

Many processes in the pharmaceutical, fine chemicals, and agrochemical industries involve hazardous chemicals for which the knowledge of their chemistry, thermochemistry, and thermodynamic properties is very limited. In addition, due to the wide variety of chemicals and reactions employed, as well as time and economic constraints, the reaction kinetics are usually not determined. Therefore, this type of application relies on empirically designed multipurpose batch and semi-batch reactors, in which a runaway scenario is more likely to occur.[1, 2] This is because not only are the systems of reactions usually complex and have strong non-linear dynamics, but these types of reactors (*i.e.*, batch and semi-batch) also have more human intervention, and thus are more prone to human error.[2] There are many situations that can upset the process and cause a rapid increase in temperature, leading to a runaway reaction, including poor temperature control, presence of impurities, stirring or cooling failure, incorrect or wrong order of recipes, and inadequate operational procedures.[3, 4] Moreover, the negative environmental impact of these empirically designed batch-reactor processes is very high since the ratio of byproducts to desired product is very high.[5]

In 1989, Barton and Nolan[6] published a study on incidents occurred in batch reactors. The study revealed a "lack of understanding of the process carried out" as one of the main causes of incidents. The U.S. Chemical Safety and Hazard Investigation Board (CSB) also conducted a study on incidents involving uncontrolled chemical reactivity in the United States.[7] The CSB study showed that inadequate knowledge of the systems and inadequate hazard identification are still among the main causes of incidents involving reactive chemicals.

---

[*] Part of this section is reprinted with permission from "Toward an inherently safer design and operation of batch and semi-batch processes: The *N*-oxidation of alkylpyridines" by A. Pineda-Solano, L.R. Saenz, V. Carreto, M. Papadaki and M. S. Mannan, 2012. *Journal of Loss Prevention in the Process Industries*, 25, 797-802, Copyright [2012] by Elsevier.

After the CSB study, many other accidents related to chemical reactivity have occurred.[8-13] Therefore, it is essential to investigate carefully and understand the hazards related to chemical processes in order to prevent process safety incidents, which can severely impact people, the environment, and the company. The best way to prevent incidents is through the implementation of alternatives that eliminate or reduce the hazards in the process rather than control them; these are called inherently safer alternatives. By applying inherently safer alternatives, safe conditions can be maintained in the process, even if an abnormality occurs. Incidents that have had a worldwide impact, such as the Bhopal incident in 1984,[14] highlight the importance of these alternatives and the potential catastrophic consequences that can result when their application is not seriously considered.

In order to apply inherent safety concepts in the reactive chemicals field, it is important to understand the hazards associated with a particular material or process.[15-18] There are multiple screening techniques and empirical methods to evaluate chemical reactivity hazards.[19-21] For simple processes, these methods offer a rapid alternative to identify process hazards. However, complex reaction systems require a more thorough understanding of the process under different conditions. To provide an example of complex reaction systems in semi-batch processes, the *N*-oxidation of alkylpyridine is used as the subject of this study.

The *N*-oxidation of alkylpyridines is a homogeneously catalyzed reaction, where an aqueous solution of hydrogen peroxide in excess is used as the oxidizing agent and phosphotungstic acid acts as the catalyst. The *N*-oxidation is accompanied by the undesired, condition-dependent decomposition of hydrogen peroxide. A runaway of this reaction may result in a rapid generation of oxygen and temperature rise in the alkylpyridine flammable environment with the additional potential to overpressurize the reaction vessel and/or trigger secondary decompositions of the product. The decomposition of hydrogen peroxide is exacerbated during the *N*-oxidation of higher

order alkylpyridines due to the mass transfer resistance caused by the formation of an organic phase and an aqueous phase. The water-soluble catalyst promotes the severe decomposition of hydrogen peroxide, jeopardizing the safety of the process, and reducing its efficiency.

The *N*-oxide production is based on a good study of the underlying chemistry in a chemist's laboratory. However, this is not sufficient for the industrial process, as efficiency, safety, and environmental issues, which are very important for the chemical engineer, also need to be considered.[22] The *N*-oxidation of alkylpyridines will be used as a case study to illustrate how an adequate process design can integrate high efficiency, low environmental impact, and inherent safety principles during the development of new process technologies. This reaction itself is of great interest for the pharmaceutical industry and it employs hydrogen peroxide, which is a widely spread industrial oxidizer. Thus, many of the hazards related to this reaction system are typical of other batch processes, so the approach used in this study can be incorporated in the design of other systems involving batch reactions.

1.1 Dissertation Outline

The remaining of Section 1 describes the main properties and uses of the reactants and products in the *N*-oxidation of alkylpyridines. It also provides an overview of the typical industrial process and outlines the hazards associated with it. A summary of previous works on the *N*-oxidation of alkylpyridines is also included in Section 1. Finally, the strategies to achieve an inherently safer design are described, and the importance of reaction calorimetry as a tool for process design is discussed.

Section 2 defines the research problem and describes the objectives of this work. Section 3 explains the methodology, equipment and procedures used to fulfill the objectives.

Sections 4 to 7 are dedicated to the discussion of results obtained from experiments performed and summarize the knowledge acquired through this research. Section 4 presents the results from the thermal stability study of several alkylpyridines and their *N*-oxides. Section 5 is dedicated to the *N*-oxidation of 3-picoline; this section discusses the results from the factorial design of experiments (DOE) and summarizes the reaction parameters obtained such as heat of reaction and power output. Section 6 discusses the results from calorimetric experiments with higher order alkylpyridines (3,5-lutidine, 2,6-lutidine and 2,4,6-collidine). Section 7 evaluates the use of *in-situ* Fourier Transform Infrared (FTIR) spectroscopy to monitor the *N*-oxidation of alkylpyridines and describes the advantages and disadvantages of this technique.

Section 8 proposes alternatives to achieve an inherently safer process for the *N*-oxidation of alkylpyridines based on the results obtained in this and previous works. Finally, Section 9 summarizes the main findings of the work presented in this dissertation and outlines the opportunities to continue this research.

1.2 Alkylpyridines and Their *N*-oxides – Properties and Uses

Alkylpyridines are considered specialty chemicals, mostly used as chemical intermediates in the manufacture of final consumer products.[23] These compounds can be readily found in nature as constituents of alkaloids, vitamins, and coenzymes.[24] Due to their bioactivity, some of the major applications of alkypyridines are in the pharmaceutical industry for the fabrication of medical drugs and feed supplements, and in the agricultural industry for the fabrication of herbicides, fungicides, pesticides, and plant growth regulators.[23, 24] Other uses include solvents and reagents, chemicals for polymers, and within the textile industries.[24]

The alkylpyridines are heterocyclic, aromatic compounds similar in structure to benzene but with a ring-carbon substituted with a nitrogen atom and one or more alkyl

substituents.[24, 25] Methylpyridines are commonly called picolines, dimethylpyridines are called lutidines, and trimethylpyridines are called collidines. Figure 1 shows examples of commercially important alkylpyridines;[23] alkylpyridines (b) through (e) have been studied in this work.

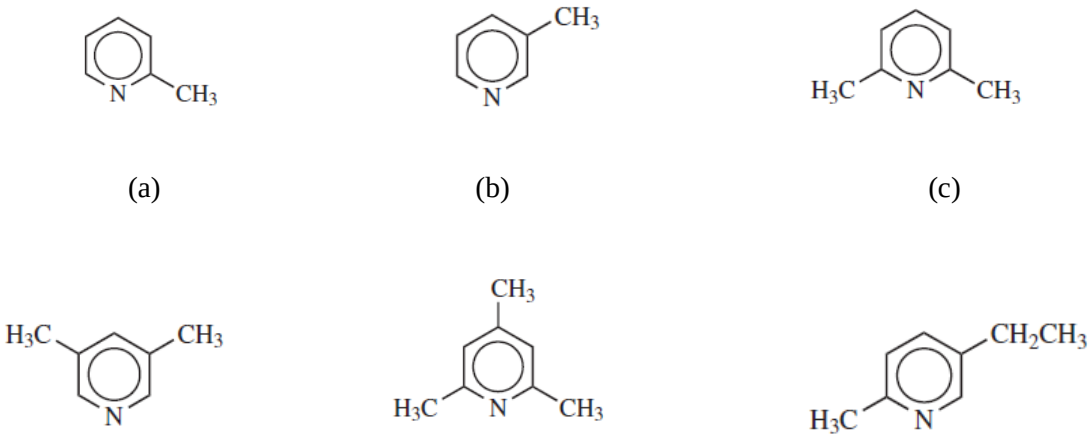

Figure 1. Commercially important alkylpyridines. (a) 2-picoline, (b) 3-picoline, (c) 2,6-lutidine, (d) 3,5-lutidine, (e) 2,4,6-collidine, and (f) 5-ethyl-2-methylpyridine.

Table 1. Physical properties of some commercially important alkylpyridines[23, 25]

Substance	Molecular weight (g/mole)	d_4^{20} (g/ml)	Normal boiling point (°C)	Flash point (°C)
2-picoline	93.1	0.945	129.4	27
3-picoline	93.1	0.956	144.1	38
2,6-lutidine	107.2	0.924	144.5	37
3,5-lutidine	107.2	0.944	171.9	53
2,4,6-collidine	121.2	0.913	170.4	58

Alkylpyridines are stable compounds, slightly alkaline,[24] and have relatively low reactivity.[26] Lower order alkylpyridines (picolines) are miscible with water, while mixtures of higher order alkylpyridines and water present two phases under certain conditions. Table 1 shows some of the physical properties of the alkylpyridines mentioned above. As seen in Table 1, alkylpyridines have low flash points, for which they are considered flammable compounds under the Globally Harmonized System (GHS). In addition, these compounds are toxic in contact with skin, harmful if swallowed or inhaled and cause skin and eye irritation.[27-30]

Alkylpyridines *N*-oxides are particularly useful due to their rich chemistry. Owing to the increased and versatile reactivity provided by the *N*-oxide function,[25] alkylpyridine *N*-oxides facilitate the synthesis of some compounds which are more difficult to obtain directly from alkylpyridines.[24] Similarly to the alkylpyridines, the *N*-oxides are also widely used in the pharmaceutical industry.

1.3 Hydrogen Peroxide – Properties and Uses

Hydrogen peroxide is a clear, colorless liquid with a sharp odor; its chemical formula is H_2O_2, and its molecular weight is 34.02 g/mol. Table 2 shows some physico-chemical properties of hydrogen peroxide at different concentrations. Hydrogen peroxide is miscible in water in all proportions. It is typically used in aqueous solutions of concentrations no higher than 70 wt. %. Pure hydrogen peroxide (100 wt. %) is not produced at industrial scale and it is usually of interest for academic purposes only.[31]

Hydrogen peroxide is a strong oxidizer and can react with a variety of organic and inorganic compounds. However, it can also act as a reducing agent for strong oxidizers. Because of its dual properties as an oxidizing and reducing agent, hydrogen peroxide is used in a wide range of applications.[32] In addition, as the only liquid by-product from its

use is water, hydrogen peroxide is considered a clean oxidizer, and it is ideal for chemical synthesis where by-products are undesired.

Table 2. Physico-chemical properties of aqueous solutions of hydrogen peroxide at different concentrations

Property	**70%**	**60%**	**50%**	**35%**	**30%**
Density* (g/ml)	1.290	1.242	1.197	1.132	1.112
Liters of O_2 at 0 °C/760 mmHg released by liter of H_2O_2 at 20 °C‡	298	246	197	130	110
Active O_2 content‡, %	32.8	28.2	23.5	16.4	14.1
Boiling point at 1 atm‡, °C	125	119	114	108	106

*Source:[33]
‡ Source:[34]

The most common application of hydrogen peroxide is in pulp and paper bleaching, where its use has grown mostly due to stricter environmental legislation. Other uses include chemical purification and hydrometallurgy and metal finishing, in which hydrogen peroxide has also had increased used due to interests in environmental issues.[31, 32, 35]

Due to the weakness of the peroxide bond (–O–O–), hydrogen peroxide decomposes easily. The decomposition reaction is exothermic and occurs according to the following chemical equation:

$$H_2O_2 \rightarrow \frac{1}{2}O_2 + H_2O \qquad \Delta H_{rxn} = -98.3\ \text{kJ/mole}$$

The decomposition of hydrogen peroxide is condition dependent and at standard conditions it releases approximately 100 kJ per mole of hydrogen peroxide reacted.[31, 32]

The reaction is highly sensitive to pH, temperature, and impurities, in particular to metals such as iron, chromium, manganese, nickel and zinc.[32]

Due to its instability, commercial solutions of hydrogen peroxide contain stabilizers, which maintain the rate of decomposition well below 1% a year. However, a large amount of hydrogen peroxide can evolve an amount of oxygen that is sufficient to pressurize sealed equipment or create an oxygen-rich atmosphere in the vapor space of the container vessel.[36]

Multiple accidents involving hydrogen peroxide have occurred.[37-41] The typical causes of incidents are associated with the exothermic, gas-generating decomposition of hydrogen peroxide and with its instability, as it reacts violently with organic compounds under certain conditions.[31, 38] Moreover, the oxygen generated during the decomposition can form a hazardous environment, particularly, in the presence of flammable compounds.

Due to the high reactivity of hydrogen peroxide, and its condition dependent decomposition, it is necessary to study the decomposition simultaneously with the synthesis reaction in order to have an adequate evaluation of the hazards involved in the process.

1.4 Phosphotungstic Acid – Properties and Uses

Phosphotungstic acid, also called tungstophosphoric acid hydrate, is a heteropolyacid (HPA) with chemical formula $[H_3PW_{12}O_{40}]\cdot nH_2O$.[42] It has a Keggin-type structure, which means that it is constituted by heteropolyanions of formula $[XM_{12}O_{40}]^n$, where M, the polytatoms, are tungsten (W), and X, the central atom or heteroatom, is phosphorus (P).[43, 44] The structure of phosphotungstic acid consists of a central tetrahedral PO_4, surrounded by 12 octahedral WO_6, as shown in Figure 2.[42-44] This Keggin-type of heteropolyacid is widely used due to their commercial availability and thermal stability;

phosphotungstic acid is thermally stable up to 465 °C, temperature at which it loses all acidic protons.[43]

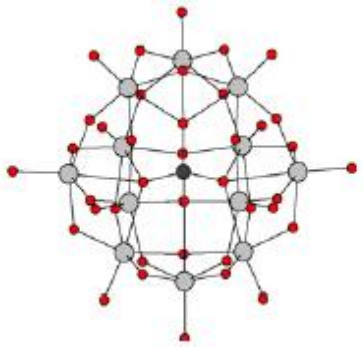

Figure 2. Structure of Keggin heteropolyanion $[XM_{12}O_{40}]_n$. For phosphotungstic acid, the central atom is phosphorus (black ball) and the polyatoms are tungsten (grey balls); oxygen atoms are represented by red balls. Source: [43]

Phosphotungstic acid is a highly selective and environmentally friendly complex metal compound, which has increasingly found industrial applications due to its unique physicochemical properties and environmentally friendly, or green, benefits.[44-48] Because of its strong Brønsted acidity, the catalytic activity of phosphotungstic acid is higher than that of conventional solid catalysts, which allows it to operate more efficiently.[46] Its green benefits are associated with its high selectivity and efficiency, which reduces the amount of waste generated.[45]

Phosphotungstic acid can be used as homogeneous or heterogeneous catalyst in different reactions, including dehydration, cyclization, esterification, amine oxidation, and olefin epoxidation, which are reactions typically employed in the production of fine chemicals, pharmaceuticals, and fragrances.[44]

In the *N*-oxidation of alkylpyridines, phosphotungstic acid, hereafter referred as the catalyst, has shown to be highly selective, with alkylpyridine *N*-oxides being the only

product of the reaction.[49] Furthermore, previous studies have suggested that phosphotungstic acid used in the *N*-oxidation of alkylpyridines can potentially be recovered and reused without decreasing its catalytic activity.[50]

1.5 Typical Production of Alkylpyridine *N*-oxides

Alkylpyridines *N*-oxides are obtained by oxidizing the nitrogen atom in the pyridine ring. The *N*-oxidation is a homogeneously catalyzed reaction, where an aqueous solution of hydrogen peroxide is used as the oxidizing agent and phosphotungstic acid as the catalyst.

The industrial *N*-oxidation of alkylpyridines is usually carried out isothermally, in a semi-batch mode at temperatures close to 100°C, which is the boiling point of the mixture.[49, 51] First, the alkylpyridine and the catalyst are loaded into the reactor and heated up to the reaction temperature. Then, a 30 to 50% excess of an aqueous solution of hydrogen peroxide is gradually dosed to the reactor in order to control the heat generated. At the end of the reaction, the residual hydrogen peroxide is neutralized by adding the appropriate chemicals.[49] The reaction is performed in a reactor vented to the atmosphere to allow the escape of oxygen produced during the reaction. An overhead condenser is used to condensate any escaping vapors.

The *N*-oxidation reaction (i) occurs simultaneously with the undesired and exothermic decomposition of hydrogen peroxide (ii), which generates oxygen. The macroscopically observed reactions are the following:

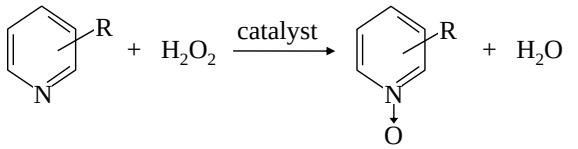

(i)

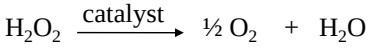

(ii)

1.6 Hazards Associated to the *N*-oxidation of Alkypyridines

The decomposition of hydrogen peroxide (ii), represents one of the major hazards of the *N*-oxidation of alkylpyridines. Should a runaway reaction occur due to an abnormality in the process (*e.g.*, due to lack of cooling/stirring), the system behaves adiabatically and the temperature of the reaction mass increases up to the boiling point of the mixture, which is approximately 100 °C. The heat released by the reaction is then removed by evaporation; the temperature remains constant until all the reactants are consumed or the mixture has completely evaporated. However, if the disturbance occurs by the end of the dosing period when there is a high accumulation of hydrogen peroxide, an inadequately vented reactor might be at risk of overpressurization due to the rapid generation of vapors and oxygen gas.

Furthermore, due to the flammable properties of the alkylpyridines and the oxygen-rich atmosphere caused by the hydrogen peroxide decomposition, there is a significant hazard of fire and explosion associated with this process. The temperature rise during a runaway reaction may also trigger the decomposition of the products, further increasing the temperature and pressure due to the generation of non-condensable gases. In the case of the *N*-oxidation of 2-picoline for example, the decomposition of hydrogen peroxide can trigger the decomposition of the product (2-picoline-*N*-oxide) if the temperature reaches 200 °C.[52] Moreover, it has been shown that the decomposition of 2-picoline-*N*-oxide generates non-condensable gases, posing a hazard of overpressurization in the reactor.[52, 53]

The potential for such a runaway scenario has been demonstrated in a previous study by Papadaki *et al.*[54] In this study, different runaway scenarios of the excess of hydrogen peroxide used in the *N*-oxidation of alkylpyridines were simulated. The study showed that the maximum temperature attained in all the scenarios was higher than the temperature at which the *N*-oxide decomposes. This finding emphasizes the need to

minimize the decomposition of hydrogen peroxide in order to prevent a runaway reaction during the *N*-oxidation of alkylpyridines.

The decomposition of hydrogen peroxide becomes more pronounced during the *N*-oxidation of higher order alkylpyridines *i.e.*, lutidines and collidines, due to the formation of two liquid phases in the reaction mixture: an organic phase and an aqueous phase. Because of the poor solubility of phosphotungstic acid in organic compounds,[42, 46] most of the catalyst remains in the aqueous phase, promoting the decomposition of hydrogen peroxide. Thus, the phase separation not only affects the safety of the process but also the selectivity. In turn, efficiency is also affected due to the mass transfer resistance. As a result, very little of the hydrogen peroxide supplied to the system is effectively consumed in the *N*-oxidation.

The hazardous situations mentioned above are typical in batch processes and clearly demonstrate the need for a more efficient and inherently safer process, in particular for the *N*-oxidation of alkylpyridines. The hydrogen peroxide decomposition not only jeopardizes the safety of the process, but being used in a 50% excess also renders the process inefficient.[55]

1.7 Previous Research on the *N*-oxidation of Alkylpyridines

Previous research on the *N*-oxidation of alkylpyridines, using phosphotungstic acid as the catalyst and hydrogen peroxide as the oxidizing agent, has focused on the development of a kinetic model that can represent the *N*-oxidation of different members in the alkylpyridines family, using isothermal calorimetry and an open system working at atmospheric pressure.[50, 51, 54, 56-59] The main findings of these studies are summarized in the following paragraphs.

Sempere *et al.*[51] developed an empirical kinetic model for the *N*-oxidation of 2-picoline from experiments performed at temperatures between 85 and 100 °C. Due to the particular reaction profiles obtained, the kinetic model developed was based on the Langmuir-Hinshelwood mechanism for heterogeneous catalysis, which involves fast equilibrium reactions between catalyst sites and reactants to form intermediates that react to form the final products. The kinetic model by Sempere *et al.* was later modified and completed by Papadaki and Gao,[57] after proving some of the initial assumptions of Sempere *et al.* were incorrect. The refined model showed good agreement for the *N*-oxidation of picolines; however, the agreement for the *N*-oxidation of higher order alkylpyridines, *i.e.*, 3,5-lutidine, 2,6-lutidine and 2,4,6-collidine, was only partial due to the existence of more than one phase in the mixture. Unfortunately, the seven rate and equilibrium constants for the model were not made available, as their reliable estimation was difficult due to the complexity of the study.

The study of the kinetics of the *N*-oxidation of alkylpyridines is inherently complex due to several reasons. At temperatures below 85 °C the decomposition of hydrogen peroxide prevails, leaving little oxidant for the *N*-oxidation. The upper limit of the temperature range for the study in an open, atmospheric system is set by the thermodynamics of the system, as the maximum temperature at which the *N*-oxidation can be performed is at the boiling point of the mixture, *i.e.*, around 100 °C. With regard to the catalyst, at high concentrations the *N*-oxidation occurs very fast, such that the data collected for kinetic analyses is not sufficient; while at low concentrations of catalyst, the decomposition is favored and therefore, the rate of the *N*-oxidation is controlled by the availability of hydrogen peroxide. Furthermore, the decomposition of hydrogen peroxide must not be studied in isolation, as the reaction is condition dependent.[60, 61] Papadaki *et al.*[59] have previously shown that the decomposition reaction occurs slower in the presence of alkylpyridines, as compared to the decomposition of hydrogen peroxide in isolation; consequently, it is necessary to study the decomposition reaction simultaneously with the *N*-oxidation reaction.

Despite the challenging study of the *N*-oxidation of alkylpyridines, previous studies have made a significant contribution to the knowledge and understanding of this system of reactions and have opened the door for the improvement of the safety and efficiency of the process. Apart from the kinetic model developed,[51] previous works have indicated that the selectivity of the *N*-oxidation is improved with increased temperature and catalyst concentration.[50, 57, 59] Therefore, the use of higher temperatures (>100 °C) and pressures to reduce and potentially eliminate the decomposition of hydrogen peroxide has been suggested. In addition, it has also been argued that by operating the process at higher temperatures and pressures, a homogeneous mixture may be achieved, which would dramatically favor the *N*-oxidation of higher order alkylpyridines such as lutidines and collidines; however, it must be pointed out that the findings of these studies were based on experiments performed in a narrow range of temperature (85-100 °C) and their arguments require experimental validation in a wider range of temperature.

More recently, Saenz-Noval[62] studied the *N*-oxidation of alkylpyridines based on the abovementioned findings, and addressed three major issues: the evaluation of the *N*-oxidation of alkylpyridines in a system operating at higher temperatures and pressures; the decomposition of the product (alkylpyridine-*N*-oxide), and the runaway behavior of hydrogen peroxide in isolation and mixed with alkylpyridine-*N*-oxide; and the prediction of phase diagrams for higher order alkylpyridines.

Saenz-Noval[62] studied the *N*-oxidation of 2-picoline and 2,6-lutidine at temperatures between 110 and 125 °C using a reaction calorimeter working under pressure, which allowed the operation at temperatures above the boiling point of the mixtures. This work demonstrated that for the *N*-oxidation of 2-picoline, it is possible to reduce dramatically the decomposition of hydrogen peroxide by increasing the temperature of the reaction. However, the role of the catalyst was unclear, as experiments performed using different amounts of catalyst led to similar conversions of 2-picoline. Saenz-Noval's experiments with 2,6-lutidine showed that even with an increase in temperature and catalyst

concentration, the decomposition of hydrogen peroxide is significant due to the phase separation; these results emphasize the need for identifying conditions at which it becomes possible to achieve a homogeneous mixture during the *N*-oxidation of higher order alkylpyridines. In addition, it is necessary to test other higher order alkylpyridines, *e.g.*, 3,5-lutidine and 2,4,6-collidine, to determine their behavior during the *N*-oxidation at higher temperatures.

Saenz-Noval[52, 53] also conducted calorimetric studies to determine the effect of catalyst and hydrogen peroxide on the rate of the decomposition of 2-picoline-*N*-oxide.[52, 53, 62] From these studies, it was concluded that both temperature and catalyst accelerate the decomposition of 2-picoline-*N*-oxide. The studies on the decomposition of 2-picoline-*N*-oxide also revealed the generation of non-condensable gases. This finding represents an additional serious hazard in the *N*-oxidation of alkylpyridines, as the decomposition of the product may worsen the consequences of a runaway reaction.

Saenz-Noval[62] also studied the runaway behavior of hydrogen peroxide with and without catalyst and developed a kinetic model that represents the catalytic decomposition of hydrogen peroxide. It was concluded that the presence of catalyst accelerates significantly the "onset" of the decomposition of hydrogen peroxide.

Regarding phase-equilibrium studies, Saenz-Noval[62] used the Gibbs minimization method to predict the phase diagrams of binary and tertiary systems involving 2,6-lutidine. The use of a third component in the mixture was considered as a potential alternative to reduce the phase separation. The study showed that by adding acetic acid to a 2,6-lutidine/water system, the region where two phases are present is significantly reduced. However, the issues associated with the addition of a third component, including formation of by-products, effect on the runaway behavior of the mixture, and cost of separation from the desired product must be assessed before this alternative can be implemented.

1.8 Inherently Safer Design

Inherently safer processes are those which accomplish a hazard elimination or reduction by means that are permanent and inseparable parts of the process;[63] that is, the process is safer because of its own nature and not because of added on features (*e.g.*, alarms, safety interlocks).[22]

There are four major strategies for the design of inherently safer processes:[63]

Minimization or intensification: Although there are several types of minimization strategies, this basically consists of reducing the inventory of hazardous materials. "Process intensification" is a term generally used to describe operation and design strategies that reduce the size of the equipment needed. In order to achieve an intensified process, it is necessary to completely understand the reaction system (*e.g.*, reaction mechanism, kinetics, mass transfer). This allows the design of reactor configurations that maximize selectivity and yield and minimize the size of the equipment, which in turn results in more efficient and economical processes. Additionally, the environmental impact associated to these processes is usually lower due to the lower generation of waste and by-products.[15]

Substitution: This entails changing a hazardous material, *e.g.*, toxic or flammable, or synthesis route with a less hazardous one. An inherently safer synthesis route would be one that avoids the formation of unstable intermediates, strongly exothermic reactions, and highly hazardous materials. The selection of a solvent is also an important aspect for the safety of a chemical process; highly toxic or flammable solvents, as well as solvents hazardous for the environment should be avoided.[64]

Moderation or attenuation: This consists of using operating conditions that reduce or eliminate the hazards, or less hazardous forms of materials, in order to reduce the

consequences of a release of a hazardous material or energy.[65] In the case of chemical reactions, the goal is to reduce the potential for a runaway reaction.

Simplification: This consists of eliminating complexities in the system in order to make it less apt to human errors.

More details on the implementation and examples of the aforementioned strategies are given elsewhere.[15, 65-67]

The design of inherently safer chemical processes requires as a first step, the identification and understanding of chemical reaction hazards. Chemical reaction hazards are not only related to the intrinsic properties of a substance itself or the chemistry used, but also to process specific conditions.[15] Therefore, in order to design a reliable, robust, and inherently safer process, consideration should be given to all the different sources of chemical process hazards.

In the *N*-oxidation of alkylpyridines, the semi-batch process is an example of an inherently safer alternative to a batch process because it prevents the accumulation of hydrogen peroxide in the reactor.[20] However, a sufficiently harmful amount of hydrogen peroxide can accumulate at the end of the dosing period if an excess amount is used. Therefore, the possibility of a runaway reaction is still possible.

1.9 Calorimetry as a Tool for the Evaluation of Thermal Risk of Chemical Processes

The identification of reactive hazards and assessment of thermal risk of a chemical reaction are crucial for the safe design and operation of a chemical process. A thorough understanding of the chemistry of desired and undesired process reactions is necessary in order to prevent reactive incidents.[68]

The identification of reactive hazards can be a complex task as it may involve external process conditions. Any event that can lead to a large temperature or pressure increase, or release of hazardous materials or energy should be considered.[68] Some information on reactivity hazards may be available in the literature. However, it is often necessary to obtain reactivity data experimentally.

Reactive hazards are typically identified by using calorimetric techniques.[20, 69] Calorimetry is the science dedicated to the measurement and quantification of heat during a chemical reactions or physical transformation. Several calorimetric techniques and equipment are available depending on the objective of the application. In general, there are four techniques commonly used for the evaluation of chemical reactivity: temperature-programmed, isoperibolic, isothermal, and adiabatic.[70] Aldeeb *et al.*,[70] divide these four techniques into screening (temperature-programmed and isoperibolic) and advanced techniques (isothermal and adiabatic). In this work only the advanced analyses techniques were used.

Screening techniques are used to determine whether a reactive hazard exists in a quick manner and using few resources, and define a temperature range to perform further analyses. Screening tests can be performed in a Differential Scanning Calorimeter (DSC) or in a Reactive Screening System Tool (RSST). For a detailed assessment, more sophisticated equipment, such as the Vent Sizing Package (VSP) or the Adiabatic Pressure Tracking Adiabatic Calorimeter can be used.[69]

Isothermal and adiabatic calorimetry are advanced techniques that can provide more accurate data. Isothermal reaction calorimetry is typically used to study the desired reaction, while adiabatic calorimetry is used for the study of undesired and runaway reactions.

Isothermal reaction calorimetry is a powerful tool in the design and scale-up of processes[71]. It allows the study of the process in conditions similar to plant scale in order to develop an understanding of the heat effects and cooling requirements of the system. Reaction calorimetry studies can also reveal process flaws and ways to improve the safety, efficiency, and environmental impact of a process.[72] This technique offers multiple advantages to process safety and process development.[73] Some of the data that can be obtained from a reaction calorimeter include reaction kinetics and related data (*e.g.*, heat release rate, accumulation of reactants), heat transfer and thermal data (*e.g.*, enthalpy of reaction, heat transfer coefficient, heat capacity), and mass transfer data, which are essential for the safe design of a process and for risk assessment.[71]

Adiabatic calorimetry is a useful technique to assess the consequences of a runaway reaction and the thermal stability of a reaction mixture; they are also useful for relief vent-sizing.[74] This is important not only for risk assessment, and to ensure adequate safety measures for the process, but also for the quality of the product. Typical data obtained from adiabatic tests include: adiabatic temperature rise ($\triangle T_{ad}$), self-heating rate (dT/dt) and maximum self-heating rate $(dT/dt)_{max}$, pressure increase (P), and maximum pressure rate $(dP/dt)_{max}$. Kinetic data can also be obtained for simple reactions. For more complex systems of reactions the analysis of adiabatic data can be challenging.[75, 76]

1.9.1 Thermal risk assessment

The thermal risk associated to a chemical reaction is the risk to have a runaway reaction, and the resulting consequences. In order to assess the thermal risk, a scenario must be identified. The worst case scenario for a batch or semi-batch reactor would be the exposure to an event or process deviation that causes the reactor to continue operation under adiabatic conditions, *e.g.*, a cooling or stirring failure.[77]

The cooling failure scenario developed by Gygax[76] can be used to explain the parameters necessary to calculate the thermal risk associated to a chemical reaction. However, similar scenarios can result from other process upsets, *e.g.*, stirring failure. The cooling failure scenario depicts the temperature course after a cooling failure and is visually represented in Figure 3. In the normal process, the reactants are loaded to the reactor and heated to the reaction temperature, $T_{process}$, where they are maintained until the reaction is completed. After completion of the reaction, the final product mixture is cooled down. The scenario assumes that a cooling failure occurs at some point during the reaction, while the contents of the reactor are at $T_{process.}$ Depending on the accumulation of reactants at the time of the cooling failure, which in turn depends on the process conditions, the reaction will continue until all unconverted materials are finished. Consequently, the temperature of the rector increases and reaches a temperature value known as the Maximum Temperature of the Synthesis Reaction (MTSR). This increase in temperature can trigger secondary reactions, which may increase the temperature further to T_{end}. Secondary reactions are typically accompanied by the evolution of vapors and/or gases, which increase the hazards of the process due to the potential overpressurization of the reactor.

In order to assess the risk of a runaway scenario, it is necessary to have adequate knowledge on the chemical reaction during normal and abnormal conditions. First of all, it is necessary to determine the heat release rate ($\dot{Q}_{rxn}$) and the cooling capacity of the reactor in order to ensure that the cooling system can remove the heat generated by the reaction. These quantities are typically obtained using reaction calorimetry.

It is also important to determine the maximum temperature reached by the reaction mixture during a runaway of the desired reaction, the MTSR. The MTSR will determine the potential to trigger a secondary reaction, which is typically a decomposition reaction. The MTSR can be calculated as follows:[76, 77]

$$MTSR = T_{process} + X_{ac}\Delta T_{ad1} \quad \text{(Eq. 1)}$$

where

$T_{process}$ is the desired reaction temperature;

X_{ac} is the thermal accumulation at the time of the cooling failure; and

ΔT_{ad1} is the adiabatic temperature rise

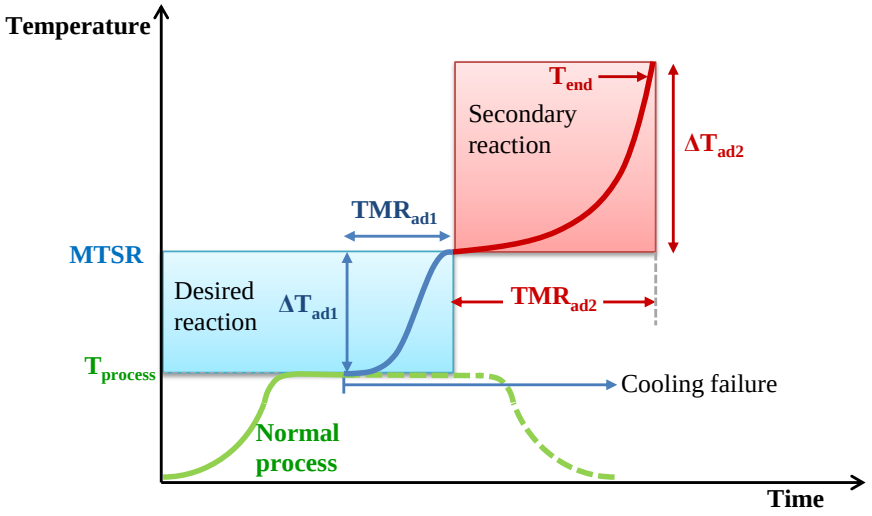

Figure 3. Cooling failure scenario. Adapted from[64, 76]

Since the cooling failure can occur at any point in time during the reaction, MTSR is a function of time. The worst case scenario, for which MTSR(t) is maximum, is characterized by a maximum accumulation of reactants and minimum stability of the reaction mixture, taking into consideration any available safety measures.[77] The accumulation of reactants and MTSR can also be determined using reaction calorimetry, while the thermal stability of the mixture is evaluated using Differential Scanning Calorimetry (DSC) or adiabatic calorimetry.

The final temperature, T_{end}, is determined by the adiabatic temperature rise during the secondary reactions or decompositions triggered by the initial runaway reaction:

$$T_{end} = MTSR + \Delta T_{ad2} \quad \text{(Eq. 2)}$$

The final temperature provides an estimation of the severity of the potential consequences of a runaway reaction. Therefore, it is critical to collect thermal data not only on the desired reaction but also on the potential secondary reactions or decompositions in order to have an accurate evaluation of the potential consequences. Adiabatic calorimetry, DSC or Calvet calorimetry are generally used to obtain the required data for this evaluation.

It is also important to determine the time that will take to reach MTSR and T_{end} under adiabatic conditions. This is called the Time to Maximum Rate (TMR_{ad}) and it is a function of the reaction kinetics.[76-78]

Risk is the combination of probability and consequence. For the estimation of the thermal risk, the consequences are determined by the temperature and pressure that could be achieved if the reactor is under adiabatic or nearly-adiabatic conditions. The probability of a runaway scenario is evaluated based on the time available to respond. If the time available to take corrective measures is very short (*i.e.*, minutes), a runaway reaction is likely to occur. Conversely, if the time available is long (*i.e.*, several hours or days), corrective actions can be taken before the runaway fully develops.[72, 76, 77]

2. PROBLEM STATEMENT

From a safety point of view, there are several key safety issues to consider in the *N*-oxidation of alkylpyridines, either as isolated factors or as factors in synergy, such as: the flammability of alkylpyridines, the oxygen generation by the undesired hydrogen peroxide decomposition during the reaction, the potential accidental decomposition of stored hydrogen peroxide, the potential accidental release of hydrogen peroxide during transport, the high amount of heat generated by both, the *N*-oxidation and decomposition reactions, and the thermal decomposition of the formed *N*-oxide in case of a runaway.

An inherently safer process for the *N*-oxidation of alkylpyridines would be one where the undesired hydrogen peroxide decomposition can be eliminated (or reduced), and in the case of higher order alkylpyridines, one where a homogenous mixture can be achieved. As mentioned in Section 1.7, previous studies suggest that the operation at higher temperatures, which imposes the need of operation under pressure to prevent boiling of the reaction mixture, can have an important positive impact on the process safety and efficiency.[57, 62] As these suggestions are partially based on the predictions of a complex kinetic model, and the extrapolation of findings at lower temperatures, the current work focuses on their experimental investigation and validation.

In addition, this dissertation presents a methodology based on the combination of *in-situ* Fourier Transform Infrared (FTIR) spectroscopy and reaction calorimetry to obtain further understating of the reaction kinetics and reaction pathways involved in the *N*-oxidation of alkylpyridines, via the measurement of concentrations of reactants products and intermediates. Since reaction calorimetry is a sensitive technique to small disturbances, such as sampling, *in-situ* FTIR offers an alternative as a non-intrusive technique for the monitoring and analysis of complex reaction systems. However, it is

necessary to evaluate its performance and determine its adequacy as an analytical tool for the study of the *N*-oxidation of alkylpyridines.

2.1 Objectives

The ultimate goal of this study is to design a much more efficient and inherently safer process for the *N*-oxidation of alkylpyridines. In order to achieve this goal, it is necessary to collect the data that will provide more understanding of the reaction and will serve as the foundation for such inherently safer process. The specific objectives of this work are:

- To evaluate the thermal stability of the alkylpyridines: 3-picoline; 3,5-lutidine; 2,6-lutidine; and 2,4,6-collidine; and of their corresponding alkylpyridine *N*-oxides: 3-picoline-*N*-oxide; 3,5-lutidine-*N*-oxide; 2,6-lutidine-*N*-oxide; and 2,4,6-collidine-*N*-oxide using adiabatic calorimetry, to determine their runaway behavior and ensure that new process conditions will not compromise the safety of the process or affect the quality of reactants or products. In addition, the effect of the accumulation of hydrogen peroxide at different catalyst concentrations on the decomposition of 3-picoline-*N*-oxide is also evaluated using adiabatic calorimetry to determine synergistic effects among all three compounds. This objective also includes the analysis of 3-picoline-*N*-oxide decomposition products to determine the major components and potential paths of the decomposition reaction.

- To study the *N*-oxidation of 3-picoline in a semi-closed reactor working under pressure using isothermal calorimetry and a factorial design of experiments. This objective is twofold: a) to validate and complement previous studies arguing that an increase in catalyst and temperature can potentially eliminate the decomposition of hydrogen peroxide, thus favoring the selectivity toward the *N*-oxidation; and b) to assess the effect of additional factors, such as dosing and stirring rate, and

determine the most dominant factors on the *N*-oxidation of 3-picoline by using a two-level full factorial design of experiments. In addition, this objective includes the calculation of heat of reaction of the *N*-oxidation of alkylpyridines and the power output, as these are important parameters for the design of a reactor.

- To study the *N*-oxidation of 3,5-lutidine, using isothermal calorimetry, to determine the effect of temperature, catalyst concentration, dosing rate, and phase separation on the overall safety and efficiency of the process.

- To study the *N*-oxidation of 2,6-lutidine and 2,4,6-collidine to observe the effect of the phase separation on the safety and efficiency of the process and compare their reactive behavior to that of other alkylpyridines studied in this work.

- To propose improvements to the process for the *N*-oxidation of alkylpyridines, incorporating the findings of this and previous works.

- To evaluate the use of *in-situ* Fourier Transform Infrared (FTIR) spectroscopy in combination with reaction calorimetry to obtain further understating of the *N*-oxidation of alkylpyridines. This objective includes: a) obtaining reliable concentration data to compare with concentrations obtained from calorimetric data; b) estimating the end point of the *N*-oxidation reaction; and c) determining the advantages and disadvantages of *in-situ* FTIR as an analytical tool for the study of complex reactions, such as the *N*-oxidation of alkylpyridines

3. METHODOLOGY[*]

As mentioned earlier in Subsection 1.8, the development of an inherently safer process requires a deep understanding of the chemical reaction and its hazards. This section explains the steps followed to further the understanding on the *N*-oxidation of alkylpyridines, and also provides details on the experimental techniques, equipment, methods, and procedures used to collect the data necessary to address efficiency and inherent safety issues associated with this complex reaction system.

3.1 Research Methodology

A schematic of the research methodology is depicted in Figure 4. The methodology can be divided into three main parts: the evaluation of thermal stability and runaway behavior of reactants and products in the *N*-oxidation of alkylpyridines, the evaluation of operating conditions to minimize the decomposition of hydrogen peroxide during the *N*-oxidation reaction, and the evaluation of the *N*-oxidation using *in-situ* FTIR. As can be seen in Figure 4, the research methodology was mostly based on the use of isothermal and adiabatic calorimetry to characterize the reaction system and improve the safety and efficiency of the process. Overall, the methodology aims to the application of the "moderation" strategy to achieve an inherently safer process (See Subsection 1.8). However, as will be explained later in Section 8, the operation of the process at temperatures higher than 100 °C also results on "process intensification", which is another strategy for inherently safer design.

[*] Part of this section is reprinted with permission from "Inherently safer reactors: Improved efficiency of 3-picoline *N*-oxidation in the temperature range 110–125 °C" by A. Pineda-Solano, L. Saenz-Noval, S. Nayak, S. Waldram, M. Papadaki and M. S. Mannan, **2012**. *Process Safety and Environmental Protection*, 90, 5, 404-410, Copyright [2012] by Elsevier.

3-picoline and 3,5-lutidine were selected to evaluate the *N*-oxidation reaction at different operating conditions. These two members of the alkylpyridine family were selected for this study due to the unavailability of data on their *N*-oxidation at temperatures higher than 100 °C, and because they represent two different cases of the *N*-oxidation of alkylpyridines. 3-picoline is miscible with water; therefore, it represents the case in which the *N*-oxidation occurs in a homogeneous mixture. In contrast, 3,5-lutidine is not soluble in water in a wide range of conditions; thus, it represents the case in which (at least) two phases form during the *N*-oxidation, and the difficulties associated with the limited solubility of higher order alkylpyridines in water. The *N*-oxidation of 2,6-lutidine and 2,4,6-collidine, in which the formation of two phases also occurs, was briefly studied as well, mostly for comparison purposes. A list of the chemicals studied in this work is shown in Table 3.

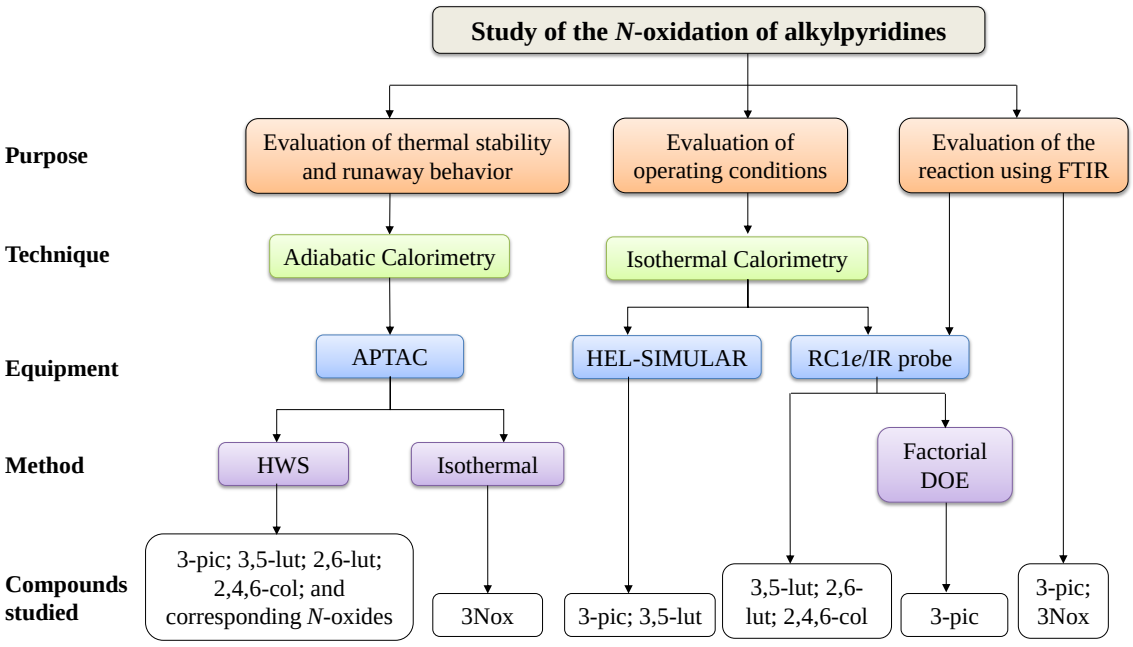

Figure 4. Research methodology for the current study

The thermal stability of all the alkylpyridines included in this study, along with their corresponding *N*-oxides, was evaluated using the HWS mode of the Automatic Pressure Tracking Adiabatic Calorimeter (APTAC). The APTAC and its different modes of operation are described in Subsection 3.2.1. A more in depth study was performed on the decomposition of 3Nox, using the isothermal mode of the APTAC, to determine the effect of temperature and catalyst concentration on its decomposition. In addition, the effect of hydrogen peroxide accumulation in the reactor on the severity of the potential consequences of a runaway reaction was evaluated by performing experiments with 3Nox mixed with a quantity of hydrogen peroxide and different amounts of catalyst, using the HWS mode of the APTAC. The results of all experiments conducted in the APTAC are discussed in Section 4.

Table 3. List of chemicals used in this study

Material	CAS number	Product number
3-picoline 99%	108-99-6	P42053 Aldrich
3,5-lutidine ≥98%	591-22-0	L4206 Aldrich
2,6-lutidine 98%	108-48-5	31531 Alfa Aesar
2,4,6-collidine 99%	108-75-8	A11058 Alfa Aesar
3-picoline-*N*-oxide 98%	1003-73-2	P42401 Aldrich
3,5-lutidine-*N*-oxide	3718-65-8	**
2,6-lutidine-*N*-oxide	1073-22-0	**
2,4,6-lutidine-*N*-oxide	3376-50-9	**
Phosphotungstic acid hydrate	12501-23-4	P4006 Sigma-Aldrich
Hydrogen peroxide 35 wt. % in water	7722-84-1	349887 Sigma-Aldrich

**Note: These chemicals were prepared in the laboratory

For the evaluation of operating conditions to minimize the decomposition of hydrogen peroxide, preliminary experiments with 3-picoline and 3,5-lutidine were conducted using

an HEL-SIMULAR isothermal calorimeter (see Subsection 3.2.1), at Texas A&M University at Qatar. A more extensive study was then conducted on both compounds using a Mettler-Toledo RC1*e* isothermal calorimeter at Texas A&M University at College Station. A factorial design of experiments was used for the study of 3-picoline in order to determine the most dominant parameters on the *N*-oxidation of alkylpyridines, along with other important parameters for the design of a reactor, such as heat of reaction and heat transfer coefficients. The *N*-oxidation of 2,6-lutidine and 2,4,6-collidine was also studied using the Mettler-Toledo RC1*e* isothermal calorimeter. The results of experiments performed with 3-picoline using isothermal calorimetry are shown in Section 5, while the study of higher order alkylpyridines is shown in Section 6.

During isothermal measurements in the RC1*e* calorimeter, an FTIR probe was used to obtain quantitative concentration data from infrared peak profiles and to identify any potential intermediates. This information could be used to obtain a better understanding of the chemical reaction. In order to illustrate this technique, an analysis was performed on infrared data from the *N*-oxidation of 3-picoline. The results from the IR analysis are presented in Section 7.

3.2 Equipment, Methods and Procedures

As mentioned earlier in this section, the data collected in this work was acquired mostly by using isothermal and adiabatic calorimetry. Two different isothermal calorimeters, the HEL-SIMULAR and the RC1*e* from Mettler-Toledo, and one adiabatic calorimeter, the Automatic Pressure Tracking Adiabatic Calorimeter (APTAC), were used in this work. This subsection describes the calorimeters used and experimental procedures followed. The infrared probe used for the evaluation of the reaction using *in-situ* FTIR is incorporated in the RC1*e* calorimeter and will also be described in this subsection.

3.2.1 Isothermal calorimeters

Overall, the two calorimeters are very similar in their hardware configuration and operation. Both calorimeters were operated in heat flow mode, meaning that the temperature of the oil jacket is constantly adjusted in order to maintain isothermal conditions inside the reactor. A general schematic that represents both calorimeters is shown in

Figure **5**. A detailed description of each calorimeter is given in the following paragraphs.

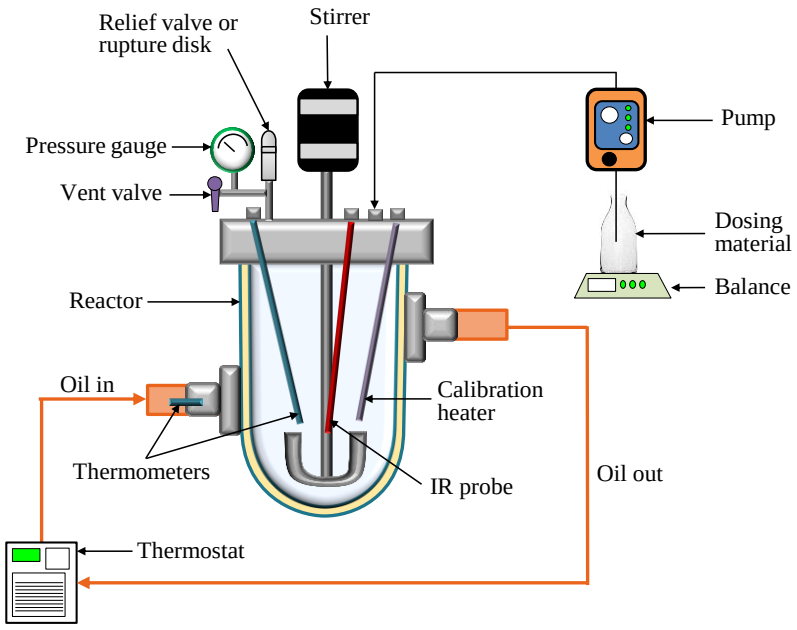

Figure 5. Schematic representation of the isothermal calorimeters used in this work. The IR probe was only available in the RC1*e*

HEL-SIMULAR isothermal calorimeter

The HEL-SIMULAR isothermal calorimeter consists of a stirred high pressure reactor vessel, which has a maximum operating pressure of 6 bar absolute and a maximum

temperature of 200 °C. The reactor vessel is equipped with a platinum resistance thermometer, a stirrer, a pressure transducer and a relief valve, which is set at 5 bar to ensure that the pressure inside the reactor does not exceed the maximum operating pressure. The temperature of the reactor is controlled by a cooling/heating Julabo bath which operates between −50 °C and 200 °C. The oil is circulating in the jacket at high speed so that its temperature while in the jacket does not practically change. The temperatures of the oil at the inlet of the jacket and inside the reactor are measured with platinum resistance thermometers. The reactor vessel is also equipped with an electrical heater which is used for calibration purposes. The dosing of materials to the reactor vessel in the semi-batch mode is done by means of a Prominent® solenoid metering pump and an Oxford scale. All temperatures, scales indication, heater power, current and voltage, reactor pressure and a number of other quantities are recorded every 20 s.

During preliminary experiments performed in the HEL-SIMULAR calorimeter, it was observed that even small quantities of oxygen produced during the decomposition of hydrogen peroxide can rapidly increase the pressure inside the reactor and make it reach the maximum operating pressure. For this reason, in some measurements, it was necessary to cool down the reactor, and vent to let the non-condensable gases escape in order to continue the experiment. However, in the worst cases, the experiment had to be terminated before the desired measurement was completed.

In order to solve this problem, it was necessary to increase the head space of the reactor. A stainless steel vessel with a volume of approximately 1 L was connected to the reactor. The vessel and connections were maintained at the desired temperature by means of a heating tape connected to a Variac, *i.e.,* the temperature was controlled by varying the voltage provided to the heating tape. The temperature inside the vessel was measured with a J-type thermocouple and regulated by an OMEGA CN7800 controller. The stainless steel vessel was also equipped with a relief valve set at 4 bar.

The volume of the system was measured with two different methods (a) by inserting a known quantity of air at isothermal conditions and recording the difference in pressure and (b) by introducing a known volume of water and recording the pressure change. The pressure change was then used to evaluate the volume of the reactor, assuming ideal gas. In both cases the volume of the empty system was calculated as 2.1 L

Mettler-Toledo RC1e isothermal calorimeter

The Mettler-Toledo RC1*e* MP10 calorimeter consists of a 1.2 L glass reactor with a maximum operating pressure of 10 barg and a maximum operating temperature of 162 °C. The reactor vessel is equipped with a thermometer, an anchor stirrer, a calibration heater, and a rupture disc set at 12 barg. All inserts in the reactor are made of Hastelloy. Pressure is measured through a pressure transmitter, which is incorporated into a pressure controller that maintains the desired pressure within the reactor. During the experiments performed in the RC1*e*, no pressure control was utilized; the pressure was continuously changing throughout the experiment due to changes in the vapor pressure of the mixture, compression of the gas volume and generation of oxygen through the decomposition of hydrogen peroxide. The addition of materials to the reactor can be done either manually or by using a ProMinent® solenoid metering pump.

The RC1*e* is comprised of 3 modules assembled in a single unit: an electronic control and monitoring system, a thermostat and pump for the circulating oil, and a measuring system. The equipment is fully automated and connected to a personal computer (PC) through a Universal Control Box (UCB).[79]

To acquire data, set safety limits, and calibrate sensors, the calorimeter incorporates the *iControl* software. A microprocessor receives parameters and set values from the PC, acquires measured values, and controls the temperature and stirrer speed in the reactor. The microprocessor also monitors the safe operation of the RC1*e*. In case unsafe

conditions are detected or the connection to the PC is interrupted, the microprocessor sets the reactor temperature to a predetermined value. The temperature of the reactor contents, the circulating oil, the coolant, stirrer speed, pressure, and other quantities are recorded every 2 seconds. These values are used to control the RC1*e* and also to trigger warnings or activate the emergency programs.[79]

The temperature of the reactor is controlled by a high performance thermostat, which uses silicone oil as the heat transfer fluid. The oil circulates around the jacket at high speed so that its temperature while in the jacket is practically constant. The oil circulation system consists of a hot oil reservoir and a cold oil reservoir. The hot oil reservoir is heated by an electrical heater and the cold oil reservoir is cooled by a cooling coil connected to a chiller unit. A control valve regulates the amount of cold oil to be mixed with hot oil in order to achieve the required jacket temperature.[79] In order to minimize heat losses, the lid of the reactor can be heated at the desired temperature by circulating oil through it at a high speed.

The RC1*e* also includes the RTCal option. It consists of two metal bands (heat flux sensors), one horizontal and one vertical, attached to the outer wall of the reaction vessel. The sensors measure the heat flow through the horizontal sensor band, and the vertical band determines the fill level. The RTCal option allows the heat flow to be determined in real time for the calculation of thermal data, constants, and further evaluation of data.[79]

ReactIR 15™

The RC1*e* incorporates the ReactIR 15™, an automated *in-situ* spectrometer that uses Fourier Transform Infrared technology (FTIR) to monitor changes of chemical species throughout the course of the reaction. The ReactIR 15™ uses a DS FiberConduit probe as the sampling technology. The FiberCounduit consists of silver halide fibers that

transfer the infrared (IR) source light from the ReactIR 15^{TM} to the probe in contact with the reactor contents and then back to the detector. A Mercury Cadmium Telluride detector collects infrared absorbance of the different components of the reaction mixture. This detector must be kept cool with liquid nitrogen in order to be functional. The ReactIR 15^{TM} is connected to a PC through a USB cable. The PC incorporates the iC IR 4.2 Mettler Toledo software to collect, visualize, and analyze real time infrared data.[80]

Experimental procedure

The procedure to perform experiments in both isothermal calorimeters was similar, and it is outlined below (see Figure 6):

First, the alkylpyridine and a certain amount of phosphotungstic acid, dissolved in 15-20 g of water, are loaded into the reactor and heated up to the desired temperature, followed by a stabilization period (1). Then, a calibration is performed (2) by means of the electrical heater to determine the heat transfer coefficient (UA) and baseline at the initial conditions. After this, the system is allowed to stabilize once again (3). An equimolar amount (with alkylpyridine) of hydrogen peroxide 35 wt. % in water is then added (4) to the reactor at the desired rate. Once the dosing step is finished, the reaction mixture is left to stabilize for a period of 30-60 min (5). After this, a second calibration step is performed (6) followed by stabilization (7) to determine the heat transfer coefficient (UA) and baseline at the end of the reaction. The reaction mixture is then cooled down (8) to ambient temperature. Figure 6 shows typical temperature and pressure profiles obtained during the calorimetric measurements.

The power of the reaction, $\dot{Q}_{rxn}$, is calculated via an energy balance over the reactor:

$$\dot{Q}_{rxn} = \dot{Q}_{flow} - \dot{Q}_{heater} + \dot{Q}_{dosing} + \dot{Q}_{accum} + baseline \qquad \text{(Eq. 3)}$$

Where

$\dot{Q}_{flow}$ is the power exchanged with the cooling medium, in W;

$\dot{Q}_{heater}$ is the power from the electrical heater, which is measured directly, in W;

$\dot{Q}_{dosing}$ is the power loss to bring the dosed material to the temperature of the reaction mixture, in W; and

$\dot{Q}_{accum}$ is the accumulated heat, in W. During isothermal operation this term is zero.

The term *baseline* includes the power due to stirring and the power losses. The total heat generated by the reaction can be calculated as the integral of $\dot{Q}_{rxn}$ over the total time of the reaction. More details on the calculations of power and heat of reaction are given in Section 6 and 7 along with the results from isothermal measurements.

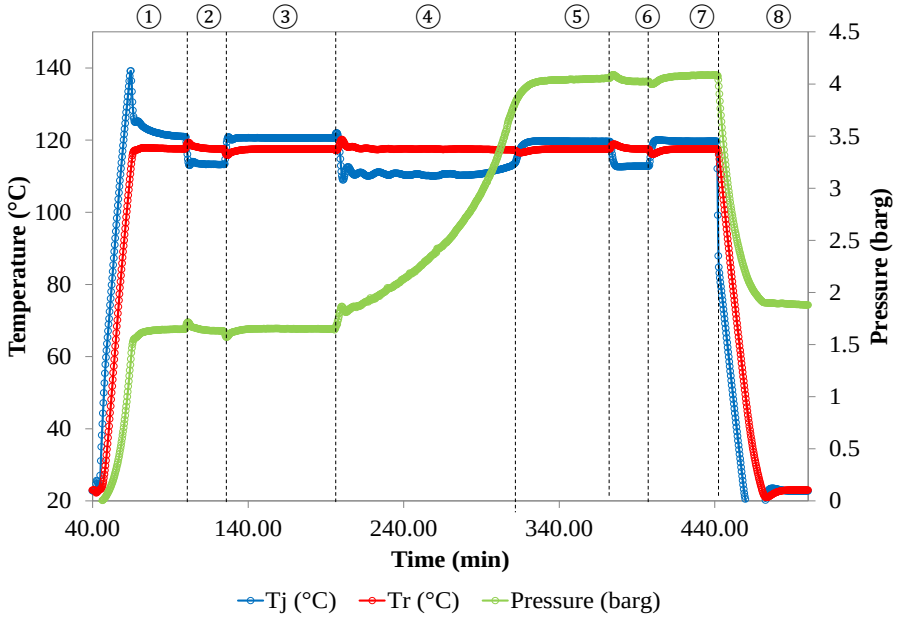

Figure 6. Typical temperature and pressure profiles obtained during experiments in the HEL-SIMULAR and RC1e isothermal calorimeters

3.2.2 Adiabatic calorimeter

Automatic pressure tracking adiabatic calorimeter (APTAC)

The APTAC is a fully automated adiabatic calorimeter, which can operate at temperatures between ambient temperature and 500 °C, and pressures from vacuum to 138 bar (2000 psi). Heat losses are minimized by keeping the temperature of the surroundings as close as possible to the temperature of the sample. The equipment consists of three well-insulated main heaters located in a pressure containment vessel, which maintain the reaction cell under adiabatic conditions (see Figure 7). Two of the heaters are placed on the sides of the containment vessel and one at the bottom. An additional heater is located at the top head of the containment vessel which regulates the temperature of a fitting where injection tubing and probes pass through.

The reaction cell is attached to the top heater and placed inside a containment vessel. The temperature of the sample is measured with a type N thermocouple. The cell is prevented from bursting due to pressure build up during a reaction by injecting nitrogen in the containment vessel at a fast rate, such that the pressure differential across the cell wall is kept at a minimum throughout the experiment (typically 0.3 bar).

The APTAC is able to track pressures up to 1380 bar/min (20000 psi/min), depending on the material of the reaction cell. For glass cells, this number is reduced by approximately an order of magnitude.[75] Reaction cells are available in different materials, including glass, titanium, stainless steel, and tantalum. In this work, only glass cells were used.

A MagnaDrive stirrer is placed at the bottom of the containment vessel, below the heated space, and a magnet is attached to the shaft, such that it is sufficiently close to the bottom of the reaction cell to provide good stirring,[75] as shown in Figure 7. The heaters, nitrogen flow, stirring rate, and data acquisition system are controlled by a PC.

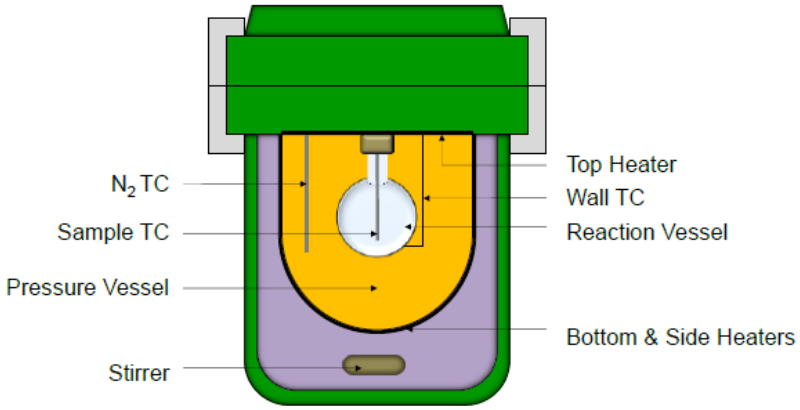

Figure 7. Simplified diagram of the APTAC.[62]

The APTAC can operate in several different modes, including Heat-Wait-Search (HWS), Heat-Soak-Search (HSS), temperature ramp and isothermal mode. In this work, only the HWS and isothermal modes were used. The HWS mode consists on heating up the sample at a rate predefined by the operator to the starting temperature. From this temperature, the equipment increases the temperature in steps, searching for an exotherm. At each step, the sample is allowed to stabilize (wait period) for a few minutes and then the equipment searches for an exotherm. An exotherm is identified when the self-heat rate of the sample is greater than the predetermined threshold (0.04 °C/min). Once an exotherm is identified, the APTAC switches over to adiabatic mode in order to track the exotherm. During this period the surroundings of the sample are kept at approximately the same temperature as the sample to avoid heat losses.[75] The minimum temperature at which the exotherm is identified is known as the "onset temperature" of the reaction,[81] and it depends strongly on the sensitivity of the equipment. Figure 8a shows a typical temperature-time curve obtained during an experiment using the HWS mode.

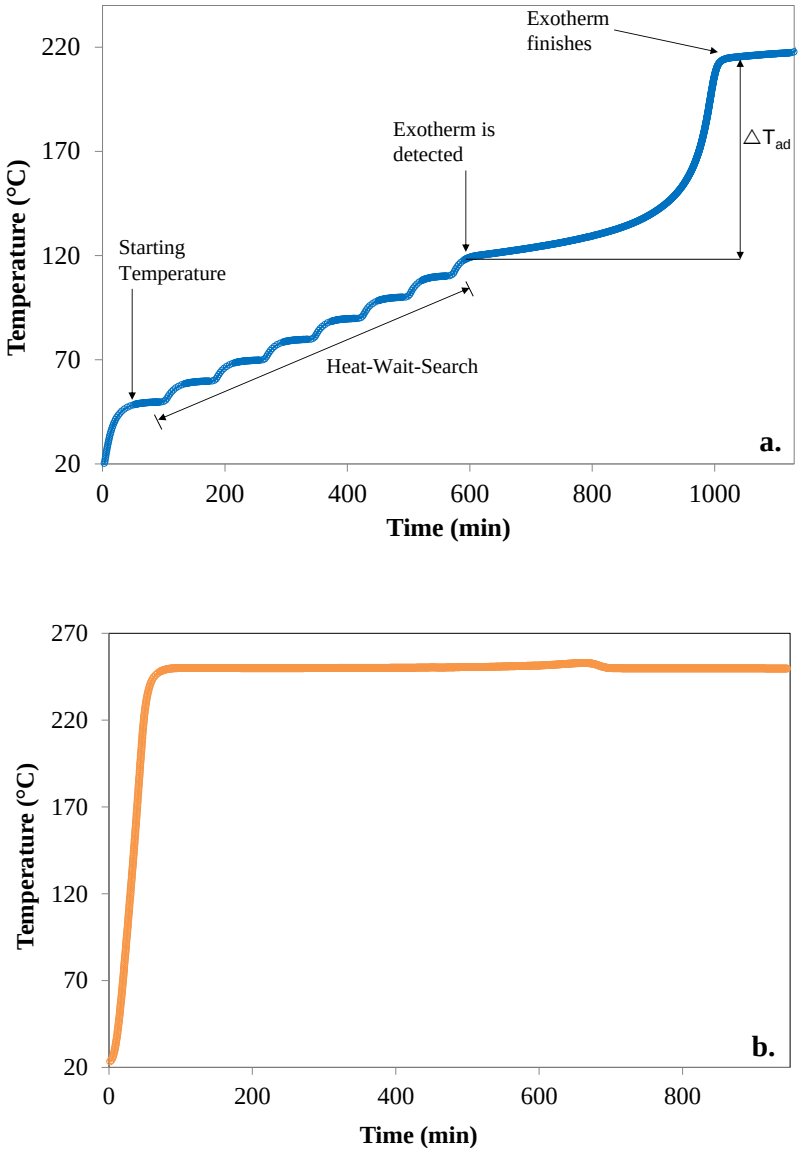

Figure 8. Typical temperature profiles obtained from experiments in the APTAC using a) HWS mode; and b) isothermal mode

In the isothermal mode, the sample is heated up at a specified heating rate to the desired experiment temperature. Then, the sample is maintained at isothermal conditions for a predetermined period of time. If the equipment detects an exotherm, it switches over to adiabatic conditions. Two criteria must be met for the equipment to switch over to

adiabatic mode to track an exotherm: the self-heating rate must be greater than 0.02 °C/min and the sample temperature must be at least 1 °C higher than the soak temperature. Once the time limit is exceeded, the sample is cooled down. Figure 8b shows a typical curve obtained during an isothermal measurement.

Reactions are performed in a small spherical cell of about 100 ml. Samples of 15-30 g are needed for each run. Once the sample is placed in the cell, the cell is attached to the top heater. The equipment is closed and two safety clamps are put in place to seal the equipment. Then the desired operating mode and experiment parameters are set using the software. During the experiment, several variables are recorded by the software, including the temperatures of the sample, the nitrogen in the containment vessel, the cell wall, and the pressure of the sample. At the end of the experiment, the cell is weighted to determine whether any mass was lost during the experiment. Samples collected at the end of the experiments were analyzed using Gas Chromatography/Mass Spectrometry (GC/MS) and Liquid Chromatography/Mass Spectrometry (LC/MS).

In a perfectly adiabatic system, all the heat generated by the sample would be absorbed by the sample, increasing its temperature. However, in the APTAC, part of the heat generated is absorbed by the sample cell. The full adiabatic temperature rise and maximum reaction rate are therefore lowered. The heat balance can be written as:[78]

$$M\bar{C}_v\Delta T_{ad} = \left(M\bar{C}_v + M_c\bar{C}_{v_c}\right)\Delta T_{ad,s} \qquad \text{(Eq. 4)}$$

where

$\Delta T_{ad,exp}$ is the adiabatic temperature rise for the system consisting of the sample and the cell, which is measured experimentally;

M is the mass of the sample;

M_c is the mass of the cell;

$\bar{C}_v$ is the average heat capacity of the sample; and

$\bar{C}_{vc}$ is the average heat capacity of the cell.

The adiabatic temperature rise of the sample, ΔT_{ad}, can then be written as:[78]

$$\Delta T_{ad} = \frac{\left(M\bar{C}_v + M_c\bar{C}_{v_c}\right)}{M\bar{C}_v}\Delta T_{ad,exp} = \left(1 + \frac{M_c\bar{C}_{v_c}}{M\bar{C}_v}\right)\Delta T_{ad,exp} \quad \text{(Eq. 5)}$$

$$\Delta T_{ad} = \varphi\Delta T_{ad,exp} \quad \text{(Eq. 6)}$$

$$\varphi = 1 + \frac{M_c\bar{C}_{v_c}}{M\bar{C}_v} \quad \text{(Eq. 7)}$$

The heat of reaction can be calculated as:

$$\Delta H_r = \frac{M\bar{C}_v\Delta T_{ad}}{N_{rxn}} \quad \text{(Eq. 8)}$$

where

N_{rxn} are the moles reacted during the experiment; and

φ is the thermal inertia factor

The φ factor is used as a measure of the adiabaticity of the reactants.[75] The closer the φ factor is to one, the more adiabatic the system is. It must be emphasized that Equation 12 is only valid if there is no change in the reaction mechanism over the temperature range studied.

3.2.3 Factorial design of experiments

The study of the *N*-oxidation of 3-picoline was conducted following a two-level factorial design of experiments (DOE), in order to determine the statistical significance of each factor on the conversion of 3-picoline into its *N*-oxide.

A factorial design of experiments is a tool used to determine cause and effect relationships between the process variables, called factors, and one or more response variables.[82, 83] The effect of a factor is defined as "the change in response produced by a change in the level of the factor".[84] When the effect of a factor on the response depends on the level of another factor, it is said that there is an interaction between the factors.

The most widely used experimental design is the two-level factorial, in which each factor is set at a high level and a low level. A full factorial design of experiments consists of all combinations of high/low levels for all factors.[82, 85] Thus, a two-level factorial design with k factors requires 2^k observations. Because each factor is studied only at two levels, it is assumed that the response is approximately linear over the range of conditions chosen for each factor.[84] Therefore, the response variable can be described by a linear model. The significance of each main and interaction effects are determined through statistical analysis.

The procedure to analyze a 2^k design of experiments has been outlined by Montgomery.[84] The first step in the statistical analysis is to determine the signs and magnitudes of factor effects. In order to determine the effect of a factor, the contrast associated with that effect must be calculated. The contrast is defined by NIST/SEMATECH[85] as "a linear combination of two or more factor level means with coefficients that sum to zero". The contrast for a factor or interaction effect is calculated as

$$Contrast_{AB\ldots K} = (a \pm 1)(b \pm 1)\cdots(k \pm 1) \quad \text{(Eq. 9)}$$

where the factors are represented by the capital letters A, B,…K, and the lowercase letters represent the high level of the corresponding factor in the treatment combination. The absence of a lowercase letter represents the low level of the corresponding factor in the treatment combination, *e.g.*, the letter a, by itself, represents a treatment combination where factor A is at the high level and other factors are at the low level, while the combination ab represents a treatment combination where both factors, A and B, are at the high level. When all the factors are at the low level the treatment combination is denoted by (1). The signs in the parentheses in Equation 4 are defined by the presence or absence of a factor in the effect, *i.e.*, the sign is negative if the factor is included and positive if it is not.[84]

Once the contrasts for each effect and interaction are calculated, the effect and the sum of squares are calculated using Equation 5 and 6, respectively:[84]

$$AB\cdots K = \frac{2}{n2^k}(Contrast_{AB\cdots K}) \quad \text{(Eq. 10)}$$

$$SS_{AB\cdots K} = \frac{2}{n2^k}(Contrast_{AB\cdots K})^2 \quad \text{(Eq. 11)}$$

where n is the number of replicates.

After all effects are calculated, the initial linear model for the experiment is formed. If at least one run in the DOE has been replicated, the initial model includes all factor and interaction effects. For an unreplicated DOE, it is typically assumed that higher order interactions are negligible, as it is not possible to estimate all parameters for the full model with a single replica factorial. The assumption is based on the "sparsity of effects principle", which says that most systems are dominated by some of the main factors and

low order, typically two-order, interactions. Instead, the mean squares of higher order interactions are combined to estimate the error. The regression model is[84, 85]

$$y = \beta_0 + \beta_1 x_1 + \beta_2 x_2 + \cdots + \beta_k x_k \qquad \text{(Eq. 12)}$$

where x_k is a coded variable (+1 or -1), β_k are the model parameters and y is the response variable.

The statistical significance of all factor and interaction effects is tested by using Analysis of Variables (ANOVA). P-values can be used as criteria to determine the significance of an effect. Once the statistical analysis has revealed the most significant effects, the model is refined by eliminating non-significant terms from the full model.

Finally, an analysis of the residuals is performed to check the assumptions (*e.g.*, linearity) and adequacy of the model. The residuals are the differences between the experimentally observed response values and the response values predicted by the model. The adequacy of a model is verified if a straight line is obtained in the normal probability plot of the residuals.[84, 85]

Due to the high number of terms that may result during the analysis of DOE, the calculations are typically done using statistical packages. In this work, the analysis of the full factorial design was performed using the statistical package Minitab 16. This software provided an estimation of the main and interaction effects, statistical parameters, and plots typically used in the analysis of statistical design of experiments. The DOE used for the study of the *N*-oxidation of 3-picoline was a 2^4 factorial design for four independent variables: temperature, mass of catalyst, dosing rate, and stirring rate, where the response variable was the conversion of 3-picoline.

4. THERMAL STABILITY STUDY OF ALKYLPYRIDINES AND THEIR *N*-OXIDES

This section presents the results of experiments conducted using the Automatic Pressure Tracking Adiabatic Calorimeter (APTAC) described in Section 3.2.2, to study the thermal stability of the alkylpyridines: 3-picoline; 3,5-lutidine; 2,6-lutidine; and 2,4,6-collidine; and of their corresponding alkylpyridine *N*-oxides: 3-picoline-*N*-oxide; 3,5-lutidine-*N*-oxide; 2,6-lutidine-*N*-oxide and 2,4,6-collidine-*N*-oxide. In addition, the effect of the accumulation of hydrogen peroxide at different catalyst concentrations on the decomposition of 3-picoline-*N*-oxide is also evaluated to determine synergistic effects among all three compounds. The analysis of 3-picoline-*N*-oxide decomposition products to determine the major components and potential paths of the decomposition reaction is also shown.

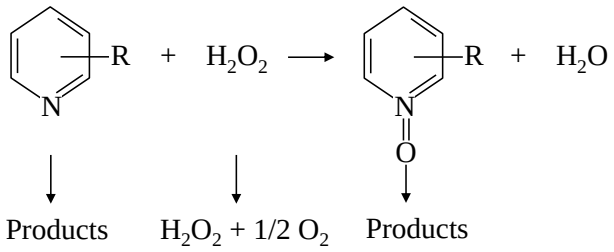

Figure 9. Schematic representation of the *N*-oxidation of alkylpyridines and potential decomposition reactions

The *N*-oxidation of alkylpyridines can be represented by the schematic shown in Figure 9. As discussed earlier, the synthesis reaction is accompanied by the undesired, gas-generating decomposition of hydrogen peroxide. In addition to the hydrogen peroxide decomposition, Figure 9 shows the potential decomposition that alkylpyridines and their corresponding *N*-oxides may undergo under certain conditions. During the *N*-oxidation

of alkylpyridines, hazardous scenarios could arise if the reaction gets out of control, *i.e.*, if there is a runaway reaction. A runaway during the *N*-oxidation of alkylpyridines could increase the temperature to a value above which the product – alkylpyridine *N*-oxide – starts decomposing. However, the conditions under which such decomposition may occur are unknown.

The decomposition of hydrogen peroxide catalyzed by phosphotungstic acid under different conditions has been previously studied by Saenz-Noval.[62] This work is concerned with the thermal stability of alkylpyridines and their *N*-oxides. The main purpose of this study is to ensure that the operating conditions used do not compromise the safety of the process while the process efficiency is maximized and the product quality guaranteed.

The results of the thermal stability study on the abovementioned alkylpyridines is shown in Subsection 4.1, while the results for alkylpyridine *N*-oxides are shown in Subsection 4.2.

4.1 Thermal Stability of Alkylpyridines

The thermal stability of 3-picoline; 3,5-lutidine; 2,6-lutidine; and 2,4,6-collidine was studied using a glass cell and the HWS mode of the APTAC between 150 °C and 400 °C, with heating steps of 10 °C. For each experiment, the glass cell was loaded with approximately 15.5 g of alkylpyridine; then, the cell was placed in the containment vessel and the containment was sealed. A pressure of 1.7 bar (25 psi) of nitrogen was then applied to the cell in order to avoid rapid vaporization of the alkylpyridine. After that, the sample was heated to the starting temperature (150 °C), where the HWS process started. In order to confirm the data obtained in the APTAC, the experimental vapor pressure was compared to the vapor pressures found in the literature for each alkylpyridine. The experimental vapor pressure was obtained from APTAC data by

subtracting from each data point the initial nitrogen pressure, appropriately modified using the ideal gas law.

Figure 10 shows the temperature and pressure profiles obtained from the experiment with 3-picoline. As shown in Figure 10, no exotherm was observed. Figure 11 shows a comparison of the vapor pressures obtained from the APTAC and the values from literature for 3-picoline. The literature values of vapor pressure were obtained from the following equation taken from DIPPR Project 801:[86]

$$P = exp\left[93.075 - \frac{8172.2}{T} - 10.444 * \ln(T) + 0.0000060393 * T^2\right] \qquad \text{(Eq. 13)}$$

Equation 13 is valid in the temperature range 255.0 to 645.0 K (-18 to 372 °C).

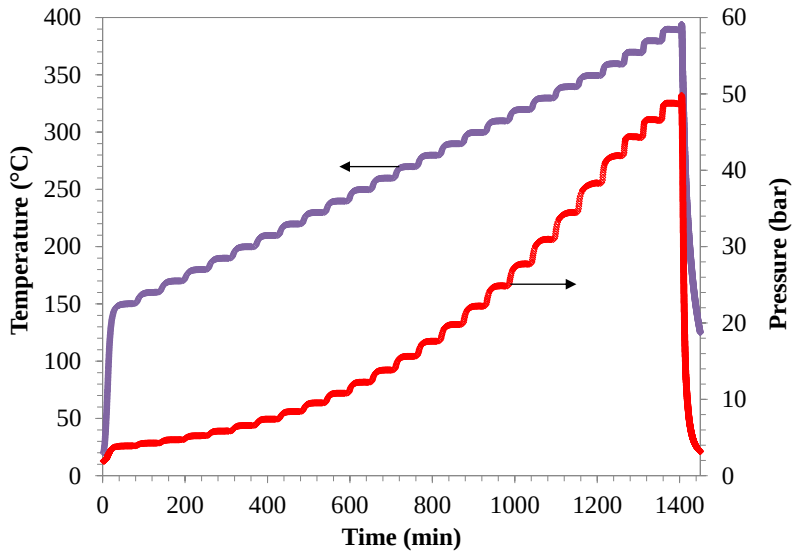

Figure 10. Temperature (purple) and pressure (red) profiles for a HWS experiment with 15.14 g of 3-picoline

It can be seen in Figure 11 that the vapor pressures generated from APTAC data match literature data very well up to a temperature of 350 °C. After this point, there is some disagreement between the data. The disagreement is likely because Equation 13 is valid only up to 372°C. Therefore, some disagreement is expected at higher temperatures. The fact that the measured vapor pressure remains smaller than the calculated one, verifies further that no decomposition gases have been produced. At the end of the experiment the sample cell was removed from the containment vessel. It was observed that the final sample appeared darker (coffee-colored) than the original clear yellow.

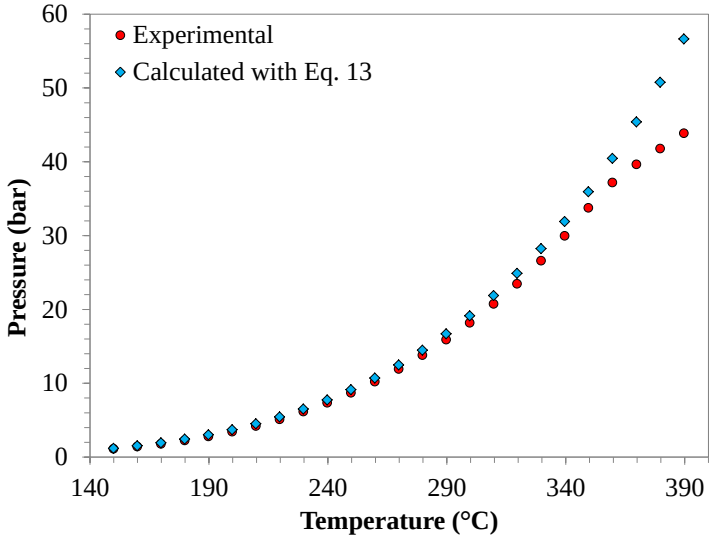

Figure 11. Comparison of vapor pressure of 3-picoline calculated using data generated by the APTAC and using the vapor pressure correlation from DIPPR Project 801[86]

From the comparison, it can be seen that it is unlikely that 3-picoline decomposed at temperatures below 350 °C, and if it did, it was at a non-detectable rate.

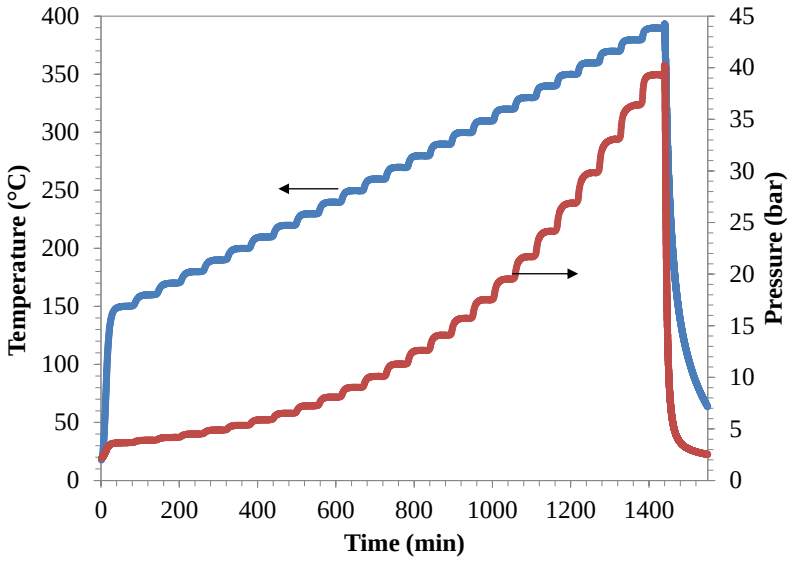

Figure 12. Temperature (blue) and pressure (red) profiles for a HWS experiment with 15.52 g of 3,5-lutidine

Figure 12 shows the temperature and pressure profiles generated during the experiment performed with 3,5-lutidine and Figure 13 shows the comparison of experimental and literature vapor pressure values. The literature values, in mmHg, were obtained from the following equation and converted to bar:[33]

$$P = 10^{\left[A - \frac{B}{T+C}\right]} \qquad \text{(Eq. 14)}$$

where

A = 7.314893;

B = 1765.913; and

C = 226.3593

Equation 14 is valid in the temperature range 11 to 412.9 °C.

It can be seen in Figure 12 that no exotherm was observed during the experiment. Also, in Figure 13, it can be seen that there is very good agreement between experimental and theoretical data up to 350 °C. After this temperature, there is some disagreement between the data; however, the error is lower than 10%. In the temperature range where there is disagreement, the experimental values are always lower than literature values, indicating that non-condensable gases were not generated, *i.e.*, no decomposition occurred. The final sample collected was also darker than the original color (yellow).

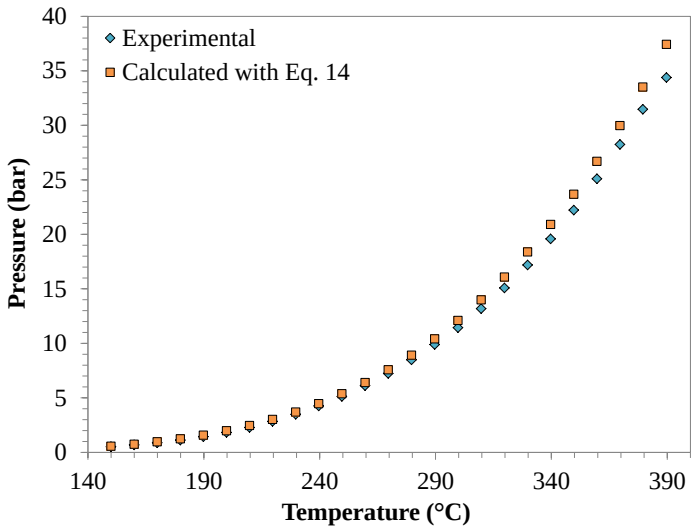

Figure 13. Comparison of the vapor pressure of 3,5-lutidine calculated using experimental data from the APTAC and using the vapor pressure correlation from Yaws' Critical Property Data for Chemical Engineers and Chemists.[33]

Figure 14 shows the temperature and pressure profiles obtained during an experiment with 2,6-lutidine. Figure 15 shows the comparison of experimental and literature vapor pressure values for the same compound. The literature vapor pressure values were obtained, in Pa, from the following equation and converted to bar:[86]

$$P = exp\left(78.801 - \frac{7637.8}{T} - 8.2293 * ln(T) + 0.0000039754 * T^2\right) \qquad \text{(Eq. 15)}$$

Equation 15 is valid in the temperature range -6 to 350 °C.

It can be seen in Figure 15 that the experimental and literature vapor pressure values agree very well up to 340 °C, which is close to the upper limit of the valid range of Equation 15. Similarly to previous analyses, this confirms that no gases were generated throughout the experiment up to this temperature. The color of the final sample was tea-like, which is darker than the original yellow color.

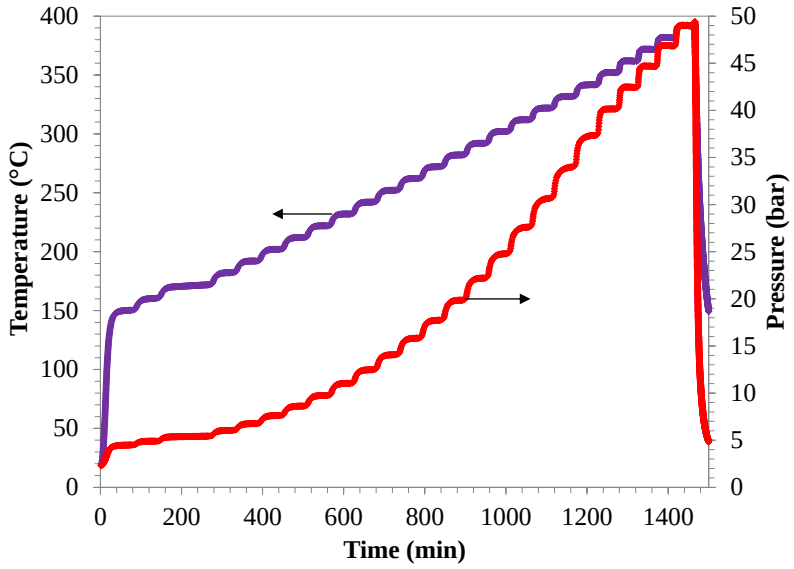

Figure 14. Temperature (blue) and pressure (red) profiles for a HWS experiment with 15.51 g of 2,6-lutidine

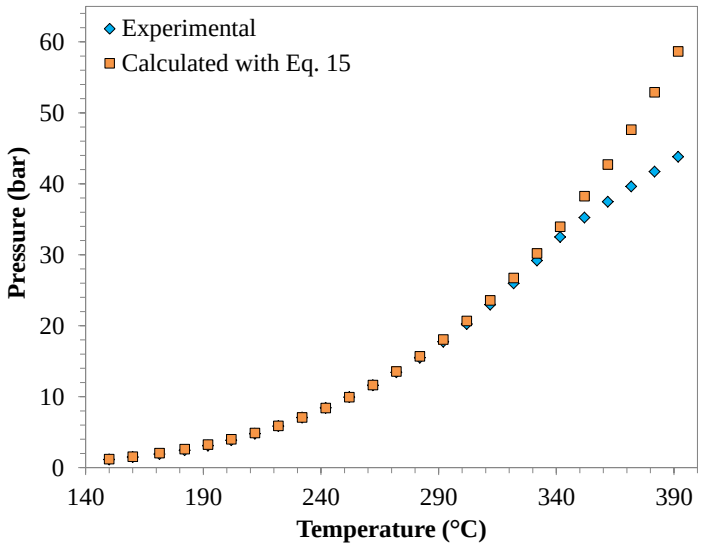

Figure 15. Comparison of the vapor pressure of 2,6-lutidine calculated using experimental data from the APTAC and using the vapor pressure correlation from DIPPR Project 801[86]

Figure 16 shows the temperature and pressure profiles obtained during an experiment with 2,4,6-collidine. Figure 17 shows the comparison of experimental and literature vapor pressure values for 2,4,6-collidine. The literature values were obtained, in Pa, using the following equation and then converted to bar:[86]

$$P = exp\left[54.46 - \frac{7031.1}{T} - 4.4481 * ln(T) + 2.0586E - 18 * T^6\right] \qquad \text{(Eq. 16)}$$

Equation 16 is valid in the temperature range -45 to 380 °C.

Similar to the other alkylpyridines studied, no exotherm was observed and the experimental and literature values of vapor pressure were in agreement up to the upper temperature limit of validity of the vapor pressure equation (380 °C). The color of the final sample was reddish-brown, which is also darker than the original dark yellow color. In summary, all the alkylpyridines included in this study were found to be stable up to the tested temperature of 400 °C. Vapor pressure values obtained from experimental data

were found to be in good agreement with those from literature, which confirmed that no gases were produced during the experiments.

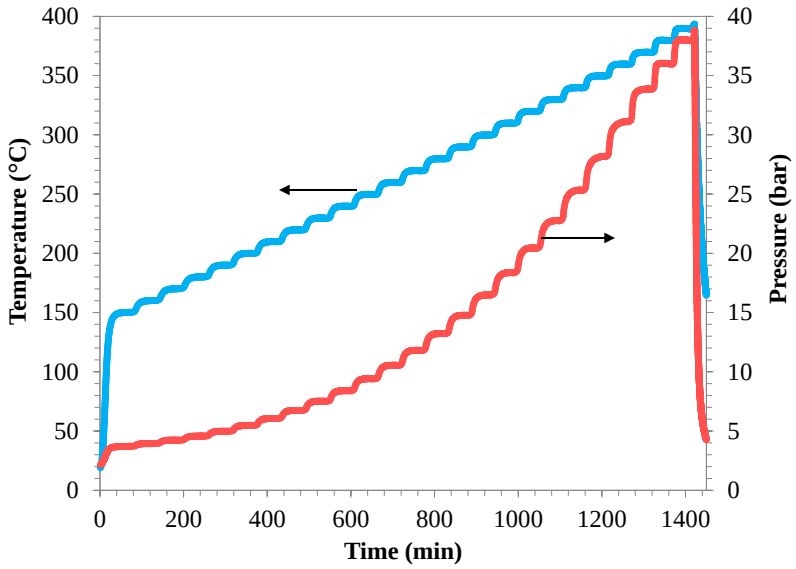

Figure 16. Temperature (blue) and pressure (red) profiles for a HWS experiment with 15.53 g of 2,4,6-collidine

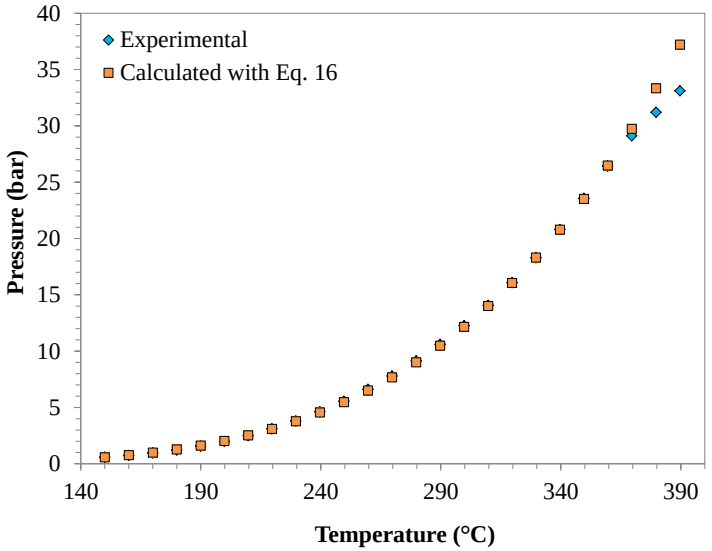

Figure 17. Comparison of the vapor pressure of 2,4,6-collidine calculated using experimental data from the APTAC and using the vapor pressure correlation from DIPPR Project 801[86]

4.2 Thermal Stability of Alkylpyridine *N*-oxides

4.2.1 3-picoline-N-oxide

3-picoline-*N*-oxide (3Nox) was first studied in HWS mode between 200 and 280 °C with heating steps of 5 °C to determine the "onset" temperature of decomposition. The experimental procedure was similar to the procedure described earlier for the thermal stability study of alkylpyridines. An aqueous solution of 3Nox was loaded to the cell and placed in the containment vessel, which was subsequently sealed. A pressure of 1.4 bar (20 psi) of nitrogen was applied to the cell to prevent rapid vaporization of the sample. At the end of the experiment, the sample was weighted to determine the mass converted to non-condensable gases. Table 4 shows the details of the HWS experiments performed with 3Nox.

Table 4. Quantities used for HWS experiments with 3Nox. The HWS was performed between 200 and 280 °C with heating steps of 5 °C

Experiment	3Nox solution 43.7 wt. %	Water (g)	Catalyst (g)
1	15.09	0.00	0.10
2	15.08	0.00	0.30
3	7.54	7.53	0.10

3Nox is a very hygroscopic solid, which makes it difficult to handle in the laboratory. It absorbs moisture from the environment and becomes a liquid rapidly. Therefore, it is difficult to obtain an accurate measure of the mass of *N*-oxide in each experiment. For this reason, a series of measurements were performed using an aqueous solution of 3Nox 43.7 wt. % so as to have a minimal unaccounted for quantity of water in the sample and also to standardize the mass of 3Nox used in those experiments. The concentration of the aqueous solution used was similar to the concentration of a mixture at the end of an *N*-

oxidation reaction. The same solution was used for all experiments performed with 3Nox.

Figure 18 shows the temperature and pressure profiles obtained during experiments 1 and 2 from Table 4. An exotherm was detected at around 250 °C in experiment 1 and around 255 °C in experiment 2. The difference in the detected "onset" temperature is expected, since the error associated with HWS experiment is as large as the heating step, 5 °C. In both experiments, the shutdown parameters set were reached and the experiments were finished before the decomposition reaction reached completion.

Experiment 3 was performed with a lower amount of 3Nox solution so the decomposition could finish before the shutdown parameters were reached, thus, allowing the calculation of the heat of reaction. Figure 19 shows the temperature and pressure profiles obtained from experiment 3. It can be seen that the exotherm was detected around 255 °C and finished at 279 °C ($\Delta T_{ad,exp}$ = 24 °C). The heat of the decomposition of 3Nox was calculated using Equations 10-12. The thermal inertia factor, φ, was 1.66 and the estimated heat of decomposition was 102 kJ/mole. It is expected that the heat of reaction has a large error associated to it given that the extent of decomposition of 3Nox is unknown. As discussed later in this subsection, 3Nox was found in final samples collected, which indicates that not all the 3Nox initially loaded decomposed during the experiments.

Once the temperature range of decomposition was identified, experiments using the isothermal mode of the APTAC were conducted to determine the influence of the catalyst and temperature on the decomposition reaction. In a typical experiment, the initial mixture contained approximately 6.5 g of 3Nox, 8.4 g of water, and a mass of catalyst that varied between 0 and 2 g.

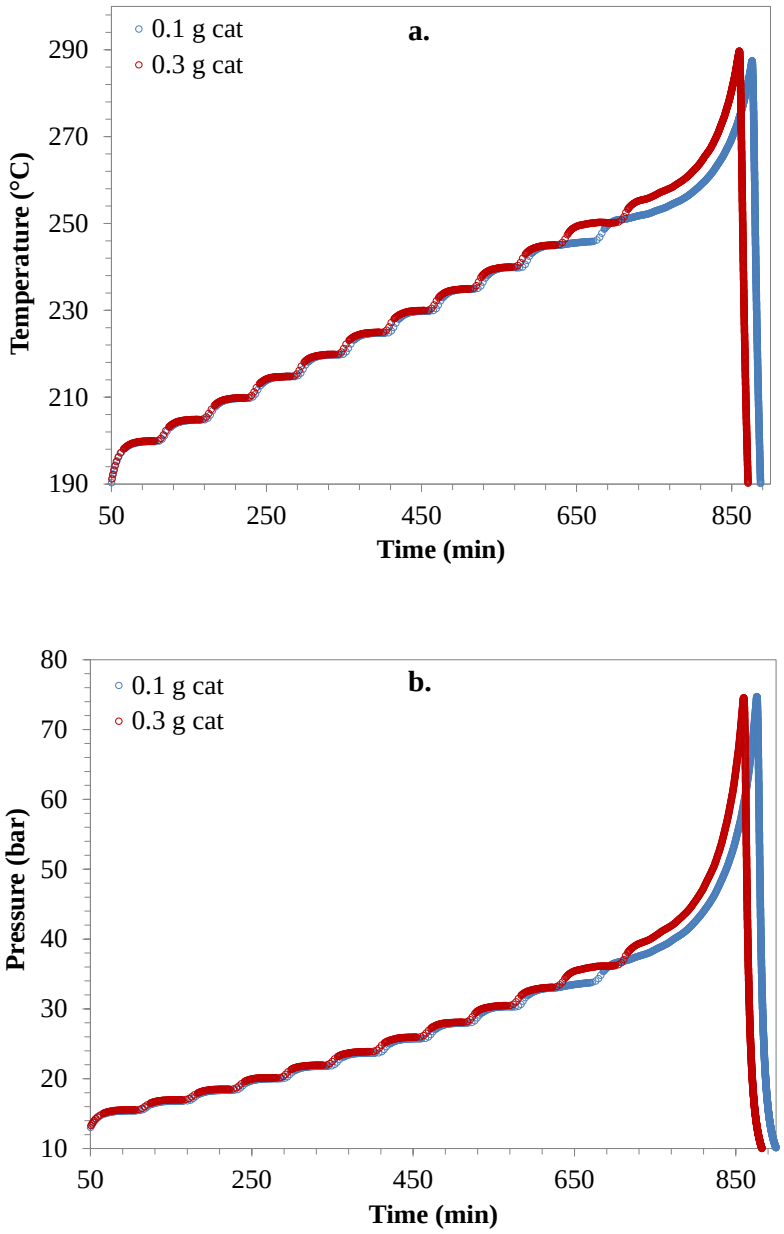

Figure 18. a) temperature and b) pressure profiles obtained during HWS experiments with 3Nox and catalyst at two different concentrations (Experiments 1 and 2)

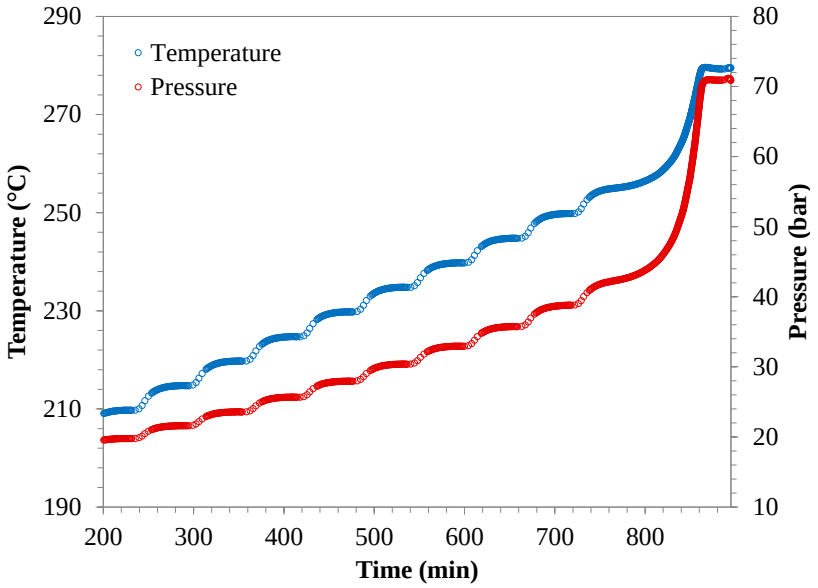

Figure 19. Temperature and pressure profiles obtained during a HWS experiment with 3Nox and 0.1 g of catalyst (Experiment 3)

Table 5. Details of experiments for the study of the decomposition of 3Nox using the isothermal mode of the APTAC

Temperature (°C)	3Nox (g)	Water (g)	Catalyst (g)	Mass Lost (g)	O_2 moles calculated
250	6.56	8.45	0.0	0.24	0.008
250	6.56	8.46	0.1	0.70	0.022
250	6.56	8.45	0.3	0.79	0.025
250	6.56	8.46	1.0	0.73	0.023
250	6.64	8.56	2.0	0.71	0.022
240	6.53	8.42	0.1	0.73	0.023
240	6.57	8.47	0.3	0.87	0.027
230	6.53	8.42	0.1	0.78	0.024
230	6.53	8.22	0.3	0.67	0.021

The temperatures selected for the study were based on the results obtained from the HWS experiments. Table 5 shows the details of the experiments performed in isothermal mode with 3Nox. Scanning experiments at 210 °C with different amounts of catalyst (0.1

and 0.3 g) were also performed but they are not included in Table 5 because no exotherm was detected for the 1000 min duration of those measurements.

The decomposition of 3Nox was very slow during experiments performed at 230 °C and 240 °C, even when 0.3 g of catalyst was used. For this reason, the rest of the experiments were conducted at 250 °C. Figure 20 shows the temperature and pressure profiles generated during the experiments listed in Table 5.

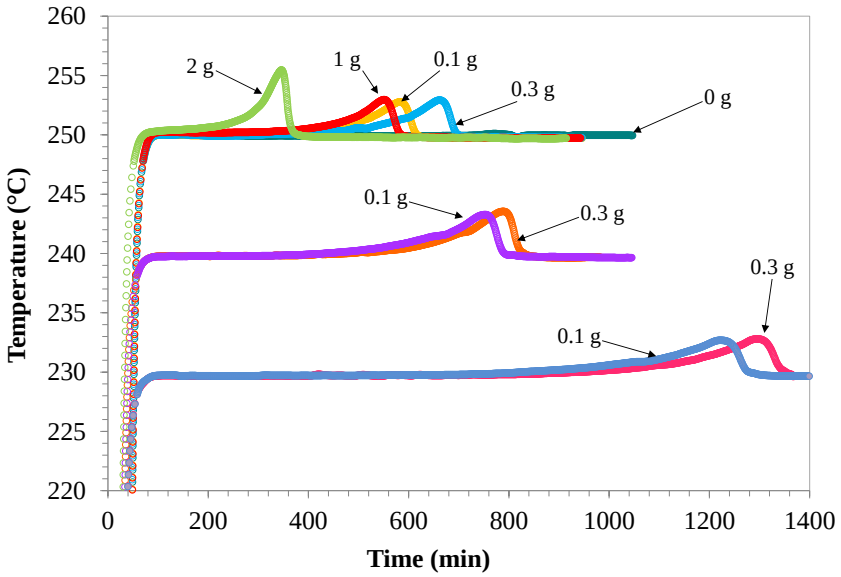

Figure 20. Temperature profiles from isothermal experiments with 3Nox in the APTAC at different temperatures and catalyst amounts

During isothermal experiments, the APTAC controls the power supplied to the heaters so the cell is maintained at a constant temperature. Because of the unavailability of cooling in the APTAC, there is a small increase in the sample temperature during the reaction. The power supplied to the heaters is then reduced so that heat losses allow the sample to return to the measurement set-temperature. Once an exotherm is identified, the

APTAC switches over to adiabatic mode if the two criteria described in Subsection 3.2.2 are met.

During the isothermal experiments shown in Figure 20 it can be seen that the decomposition reaction caused a temperature increase of 3 °C. However, this increase was not fast enough to make the APTAC switch over to adiabatic mode. Instead, the power supplied to the heaters was decreased to maintain isothermal conditions, so the experiment was not adiabatic during this time and the real temperature rise cannot be observed. However, these measurements were useful to observe the effect of temperature on the decomposition of 3Nox. As shown in Figure 20, the decomposition reaction occurs earlier at higher temperatures. At 230 °C, the reaction is detected after 800 min, while at 240 °C it can be detected after approximately 450 min. That is, increasing the temperature by 10 °C reduced the detection time by almost half. At 250 °C, the decomposition starts 120 min after the set temperature is reached, at around 200 min.

With regards to the effect of the catalyst on the decomposition of 3Nox, it can be seen in Figure 20 that there are mixed results. During the experiment at 250 °C and 0 g of catalyst, no temperature increase was observed throughout the experiment. However, the pressure profile revealed that the decomposition was occurring slowly (See Figure 21a).

Experiments at 230, 240, and 250 °C were initially performed with 0.1 g and 0.3 g of catalyst to compare its effect at different temperatures. In all experiments performed, the "onset" of the decomposition of 3Nox occurred later when 0.3 g of catalyst were used, as compared to 0.1 g. However, the difference in detection of the onset was small compared to the duration of the test; the difference between the times at which the maximum temperature was recorded was only 80 minutes for the experiments at 250 °C, 35 minutes for the experiments at 240 °C, and 75 minutes for the experiments at 250 °C. The same effect was also identified during the HWS experiments conducted as seen in

Figure 18, *i.e.*, the experiment performed with 0.3 g of catalyst showed a later onset of decomposition compared to the experiment performed with 0.1 g of catalyst.

At first sight, it appeared that a higher amount of catalyst delayed the decomposition reaction. In order to confirm this trend, experiments with a higher mass of catalyst (1 and 2 g) were conducted at 250 °C. However, it can be seen in Figure 20 that increasing the mass of catalyst showed the opposite trend, *i.e.*, a larger mass of catalyst accelerated the decomposition reaction. Nevertheless, a tenfold increase in the amount of catalyst (from 0.1 g to 1 g) only decreased the time at which the maximum temperature was recorded by 32 minutes. A stronger effect was observed in the experiment with 2 g of catalyst, in which the decomposition started approximately 120 min after the set temperature was reached. Additionally, a temperature increase of 5 °C was observed with a faster decomposition rate than the rest of the experiments. However, it must be pointed out that a catalyst mass of 1 or 2 g is too large to be used in an *N*-oxidation reaction for the production of the employed amount of 3Nox. In reality, a much smaller quantity would be used. The large amounts of catalyst used in this study aimed at magnifying the effect of the catalyst on the *N*-oxide decomposition and to determine whether there was a correlation between the catalyst concentration and the decomposition rate.

According to the results obtained, it is difficult to draw a straightforward conclusion regarding the effect of the catalyst on the decomposition of 3Nox. It is likely that different decomposition mechanisms occur depending on the concentration of catalyst in the mixture.

Figure 21a and Figure 21b show the pressure and pressure rate profiles, respectively, during the isothermal decomposition of 3Nox at 250 °C, employing different amounts of catalyst. From Figure 21a it can be seen that the decomposition of 3Nox without catalyst was slowly occurring at 250 °C, although no temperature increase can be observed in Figure 20. Additionally, Figure 21a shows that the pressure increase in all the

experiments performed with 0.1 g or more of catalyst reached approximately the same maximum pressure of 52 bar at 250 °C, meaning that nearly the same amount of gases was produced.

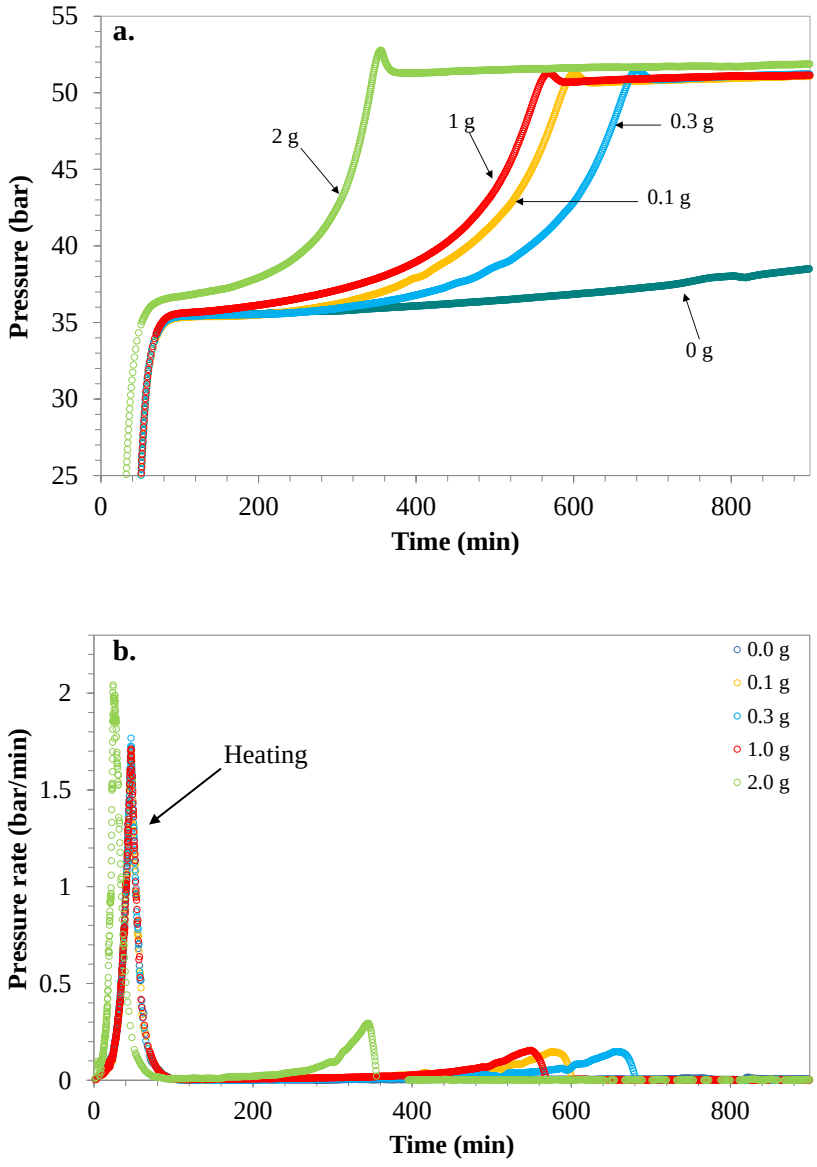

Figure 21. a) Pressure profiles and b) pressure rate profiles generated during the isothermal decomposition of 3Nox in the APTAC at 250 °C and different amounts of catalyst

It is observed in Figure 21a that after the exotherm finished, the pressure continues increasing at a much slower rate, which indicates a change in the mechanism of decomposition of 3Nox. In Figure 21b, the first peak observed corresponds to the heating step of the experiment, when the reaction mixture is brought from ambient temperature to the isothermal test temperature. During the heating step, the padding gas pressure increases, along with the vapor pressure of the mixture. The second peak observed in the profiles shown in Figure 21b corresponds to the decomposition of 3Nox. During the decomposition reaction, the pressure increases due to the temperature increase and the generation of non-condensable gases.

In the case of the experiments performed with 0.1 g, 0.3 g, and 1.0 g of catalyst, it can be seen in Figure 21a-b that although the decomposition reaction is detected at different times, the reaction occurs at approximately the same rate in all three cases (see Table 6), indicating the lack of sensitivity of 3Nox to the amount of catalyst. It can be seen that the decomposition of 3Nox is accelerated only when a large mass of catalyst are used. As shown in Figure 21a, the decomposition of 3Nox using 2 g of catalyst is not only detected much earlier, but it also occurs at a faster rate. From Figure 21b and Table 6, it can be seen that the pressure rate of the experiment performed with 2 g of catalyst nearly doubles the pressure rate of the other experiments conducted at 250 °C.

Table 6. Maximum pressure rate for experiments shown in Figure 21 and Figure 22

Temperature (°C)	**Catalyst (g)**	**Max. pressure rate (bar/min)**
250	0.10	0.147
250	0.30	0.148
250	1.00	0.154
250	2.00	0.294
240	0.10	0.125
230	0.1	0.070

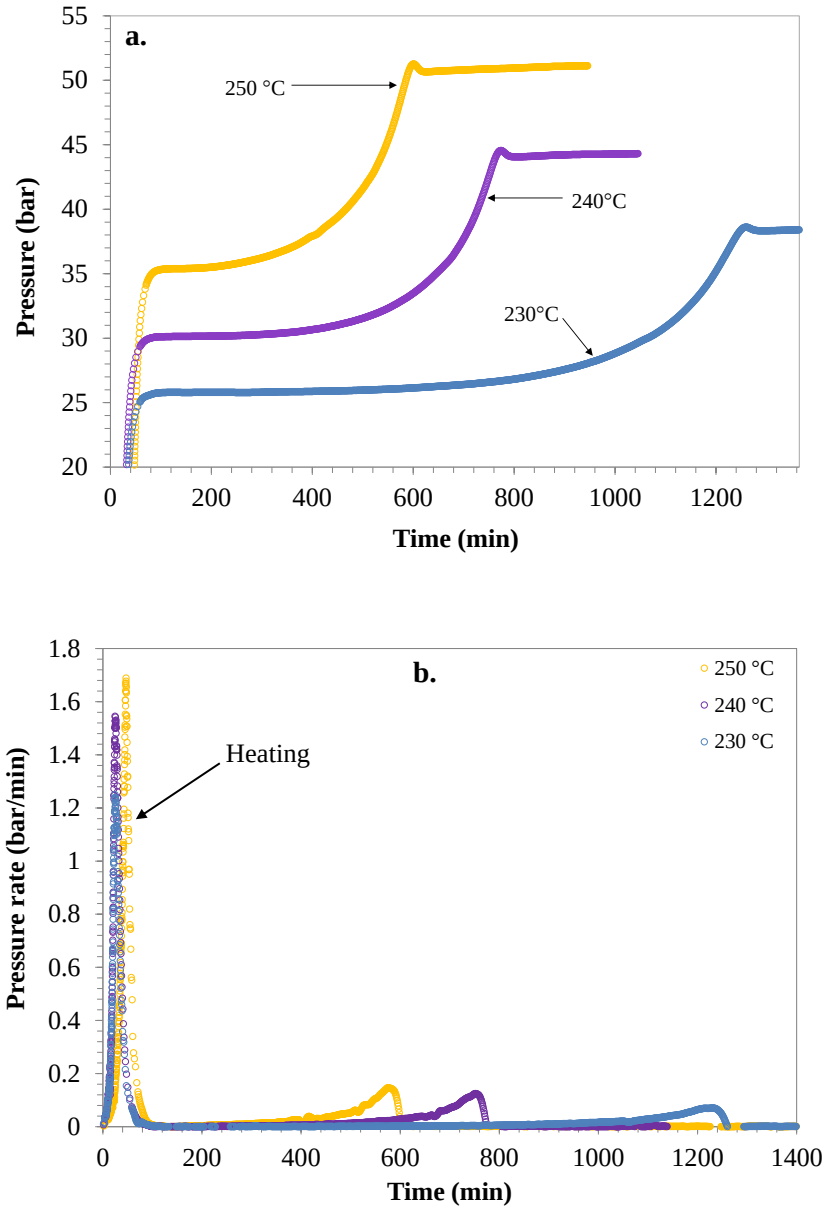

Figure 22. a) Pressure profiles and b) pressure rate profiles generated during the isothermal decomposition of 3Nox in the APTAC at different temperatures, employing 0.1 g of catalyst

Figure 22a and Figure 22b show the pressure and pressure rate profiles, respectively, during the isothermal decomposition of 3Nox at different temperatures, employing 0.1 g of catalyst. It is clear from these figures that temperature accelerates the decomposition

of 3Nox, as expected. The slope of the pressure rise (Figure 22a) indicates the rate of the reaction.

The behavior of 3Nox proved to be different from that of 2-picoline-*N*-oxide (2Nox), which decomposition was studied by Saenz *et al*.[52] The results published by Saenz *et al.* indicate that the decomposition of 2Nox is accelerated by both temperature and catalyst mass. In addition, 2Nox is more sensitive to the mass of catalyst; an increase of 0.1 g in the catalyst mass had a stronger effect in the decomposition of 2-picoline-*N*-oxide (2Nox) than in the decomposition of 3Nox. Additionally, 3Nox was found to be more stable than 2Nox at higher temperatures. According to Saenz, the decomposition of 2Nox is detectable at temperatures as low as 192 °C, using 0.3 and 0.5 g, within 1000 minutes. Instead, the decomposition of 3Nox was not detected at 210 °C within the same time, 1000 min, when using 0.1 and 0.3 g of catalyst. Also, while the decomposition of 2Nox at 250 °C using 0 g of catalyst started as soon as the set temperature was reached, the decomposition of 3Nox at the same conditions occurred slowly (Figure 21a) and when using 2 g of catalyst, at the same temperature of 250 °C, it was detected after 200 min, which as mentioned earlier, is a large mass of catalyst.

The mass lost during the experiments provided a rough estimation of the amount and type of non-condensable gases generated during the decomposition reaction. It was assumed that the main pathway in the decomposition of 3Nox is the detachment of the oxygen atom from the 3Nox molecule to form oxygen gas (O_2), as proposed by Saenz-Noval.[62] In order to verify this assumption, the mass lost, *i.e.*, the difference between the initial and final sample weights, was used to calculate the number of O_2 moles produced during the decomposition, and these values were compared to the oxygen moles contained in the initial 3Nox sample. Table 5 contains the number of O_2 moles calculated for each experiment and Figure 23 shows a visual comparison of the O_2 moles calculated and the moles contained in the 3Nox sample.

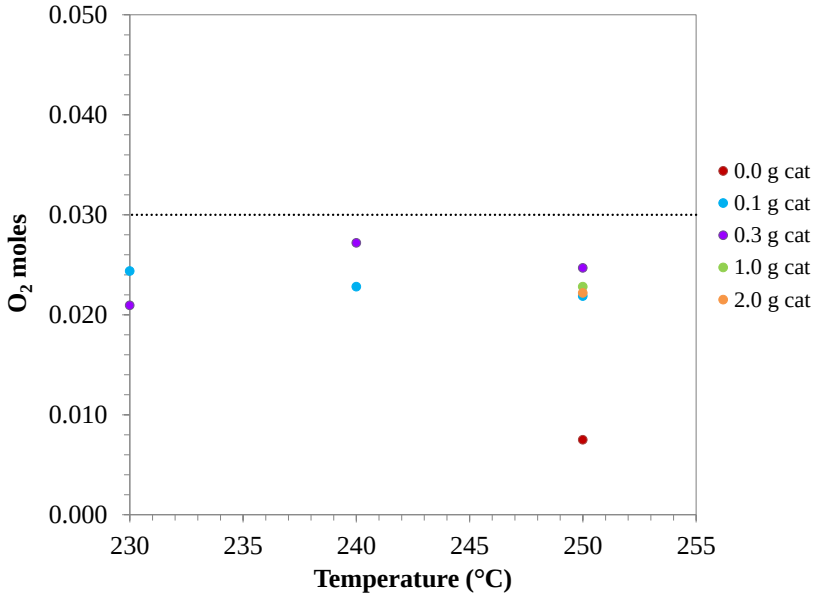

Figure 23. Comparison of O_2 moles calculated from mass lost during the decomposition of 3Nox at different temperatures and catalyst amounts. The dotted line indicates the O_2 moles contained in the initial 3Nox mass

It can be seen in Figure 23 that in all cases, the number of O_2 moles calculated from the mass lost during isothermal experiments were lower than the number of moles contained in the initial mass of 3Nox (0.03 moles). This indicates that not all the 3Nox was consumed in the decomposition. However, it is possible that not all the 3Nox reacted to form oxygen gas, but also other compounds. The red dot in Figure 23 represents the experiment conducted at 250 °C with 0.0 g of catalyst, in which the decomposition was very slow. Therefore, the mass lost was considerably lower for this experiment.

The samples collected at the end of the experiments were analyzed using Gas-Chromatography/Mass spectrometry (GC/MS). However, because only volatile components can be detected using GC/MS, the samples were also analyzed using Liquid-Chromatography/Mass Spectrometry (LC/MS). All samples were analyzed at the Laboratory for Biological Mass Spectrometry in the Chemistry Department at Texas A&M University.

GC/MS was performed on Ultra GC/DSQ (ThermoElectron, Waltham, MA). The chromatographic column used was a Rxi-5ms with dimensions of 60 m x 0.25 mm x 0.25 μm (Restek; Bellefonte, PA). Helium was used as a carrier gas at a constant flow of 1.5 ml/min. Split (1:50) injection was used. The column temperature was maintained at 50°C for 5 min, then raised to 320°C at 20°C/min. The transfer line and ion source were held at 250°C. The mass spectra were acquired in full scan mode in the range of 30-500 m/z.

The LC/MS analysis was performed on a LCQ-DECA, ThermoFinnigan with Surveyor HPLC system (ThermoFinnigan, San Jose, CA), using a Betasil C18 column (Thermo Hypersil-Keyston, Bellefonte, PA) of 2.1 x 150 mm x 3 μm. The mobile phase was solvent A (10 mM Ammonium acetate, pH 5.8) and B (acetonitrile), with a flow rate of 300 μL/min. Table 7 shows the solvent gradient used throughout the LC/MS analysis. For the MS, Electrospray Ionization (ESI) in positive mode was used for ionization.

Table 7. Solvent gradient used during LC/MS analyses

Time (min)	**Solvent A (%)**	**Solvent B (%)**
0	100	0
3	100	0
20	0	100
24	0	100
25	100	0
30	100	0

In all the samples collected, the mixture contained a solid black residue, the mass of which was larger than the mass of catalyst added initially. This means that the solid residue was constituted not only by the catalyst, but also by other products formed during the decomposition of 3Nox. For the GC/MS and LC/MS analyses, the sample was

dissolved in different solvents and centrifuged. However, the black solid precipitated in all cases and for this reason only the liquid residue was analyzed.

Figure 24a and 24b show typical chromatograms obtained during the GC/MS analyses. It can be seen in Figure 24a that the main decomposition product found was 3-picoline. Many other compounds were detected, which produced small peaks in the chromatogram, as seen in Figure 24b. However, due to the complex nature of the mixture, it is not possible to identify with certainty the components detected in the GC/MS.

Figure 25 shows a typical chromatogram obtained during the LC/MS analyses. Same as the GC/MS analyses, 3-picoline was identified as the main component of the decomposed mixture. Both the GC/MS and LC/MS analyses confirm the assumption that the main mechanism of decomposition of 3Nox involves the detachment of oxygen from the 3Nox molecule to form 3-picoline.

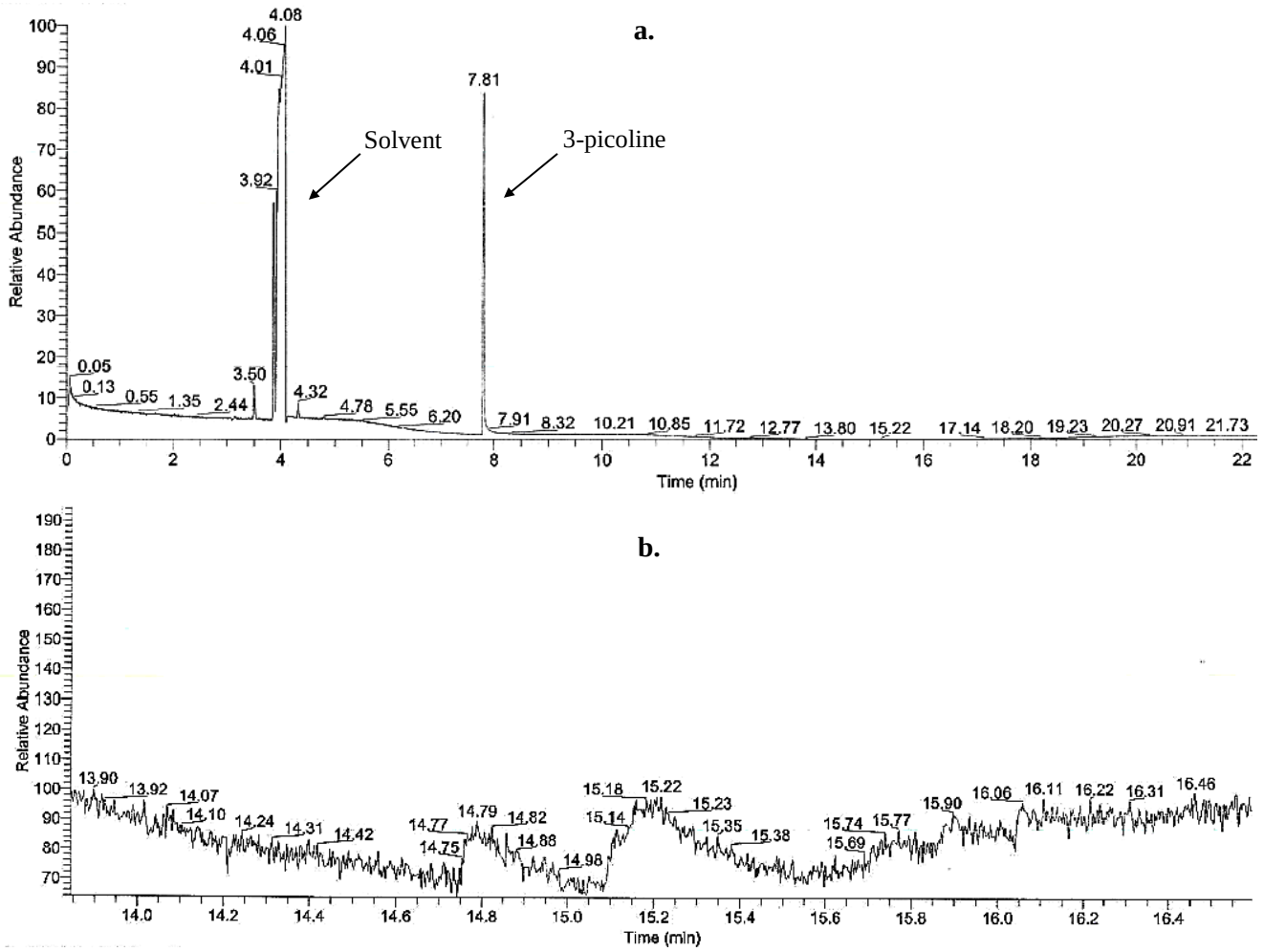

Figure 24. Typical chromatogram obtained from GC/MS analyses of samples from the decomposition of 3Nox. a) entire time of analysis (0 – 22 min); b) retention time: 13.84 – 16.59 min

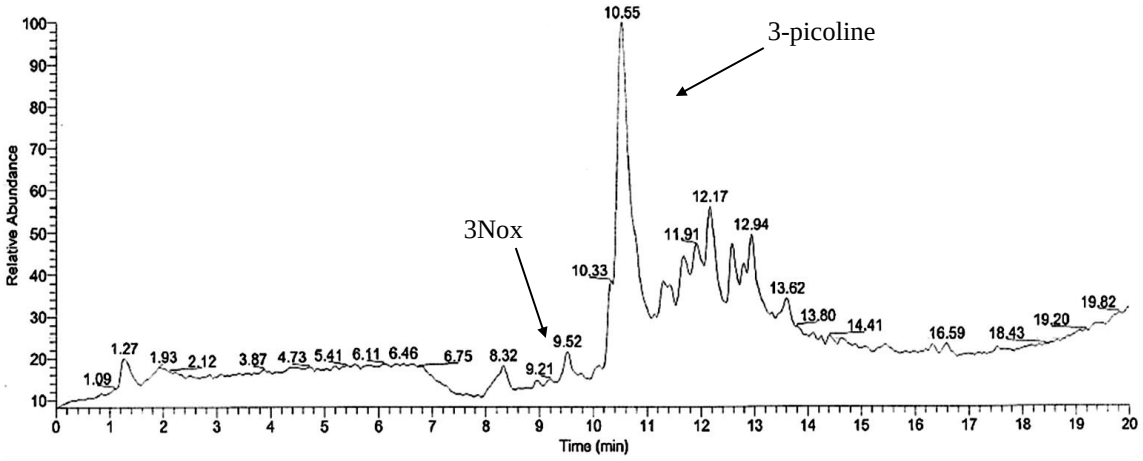

Figure 25. Typical chromatogram obtained from LC/MS analyses of samples from the decomposition of 3Nox

The LC/MS analyses also showed residues from 3Nox, which confirmed that not all 3Nox was converted to 3-picoline during decomposition. This could have happened because of catalyst poisoning, because an equilibrium was reached, or perhaps there is a concentration of 3Nox beyond which the mechanism changes and the rate of reaction is so slow that thermal effects are no longer measurable. Residues from pyridine (m/z = 80) were also present in the final mixture. It is important to point out, however, that 3-picoline was not found to decompose up to the tested temperature of 400 °C (see Subsection 4.1). Therefore, the origin of the small amounts of pyridine found in the sample is not known with certainty, as it may have resulted from potential decomposition reactions or it could also be present as an impurity in the initial mixture.

Many other compounds of different mass-to-charge ratio (m/z) were detected in the LC/MS analyses; most m/z are listed in Table 8. The m/z ratios with higher intensity in the mass spectra are highlighted in red in Table 8; m/z ratios higher than 300 were very weak in the mass spectra and in the chromatogram, indicating that those compounds were present only in low concentrations or traces. The high m/z ratios obtained in the LC/MS analyses indicate that polymerization reactions likely occurred during the

decomposition of 3Nox. However, the mechanism and pathways involved in the decomposition of 3Nox were beyond the scope of this study.

Table 8. Molecular weight of base molecules and corresponding molecular weight if two or more base molecules are combined. Mass to charge ratios (m/z) obtained in LC/MS analyses of samples from 3Nox decomposition

	Molecular weight[§] (g/mole)	**x 2**	**x 3**	**x 4**	**x 5**
Pyridine	80	160	240	320	400
3-picoline	93	186	279	372	465
3Nox	109	218	327	436	545
Combination of base molecules*				**Molecular weight[§] (g/mole)**	
(1) pyridine + (1) 3-picoline				173	
(1) pyridine + (1) 3Nox				189	
(1) 3-picoline + (1) 3Nox				202	
(1) pyridine + (1) 3-picoline + (1) 3Nox				282	
(1) pyridine + (2) 3-picoline				266	
(1) pyridine + (2) 3-picoline + (1) 3Nox				375	
m/z detected in LC/MS[ǂ]					
80.07	180.85	239.5	340.96	399.12	
92.06	185.35	276.23	341.37	428.62	
94.13	187.25	278.30	355.12	443.12	
110.11	189.63	282.99	356.25	468.88	
140.98	199.31	289.75	364.45	476.34	
150.66	201.28	292.26	383.18	481.26	
166.18	215.25	304.25	385.59	484.84	
171.38	225.60	325.08	396.52		

Notes:
* the numbers in parenthesis indicate the number of molecules
§ numbers highlighted in blue indicate molecular weights that approximately match m/z ratios detected in the LC/MS
ǂ numbers highlighted in red indicate m/z ratios with higher intensity in the mass spectra

Unfortunately, the LC/MS equipment only provides the m/z ratios of compounds detected, but it does not identify the compounds by name. However, if pyridine, 3-picoline, and 3Nox are assumed to be the base molecules for the formation of other substances during the decomposition of 3Nox, the combination of these base molecules gives molecular weights that match some of the m/z ratios obtained in the LC/MS analyses. Table 8 shows the molecular weight of the assumed base molecules and the molecular weights that would be obtained when two or more base molecules are combined with the same or different type base molecules. However, the numbers shown in Table 8 do not account for any atoms lost when molecules bond. The molecular weights that match m/z ratios detected in the LC/MS are highlighted in blue in Table 8. Potential structures of some of the compounds formed are shown in Figure 26.

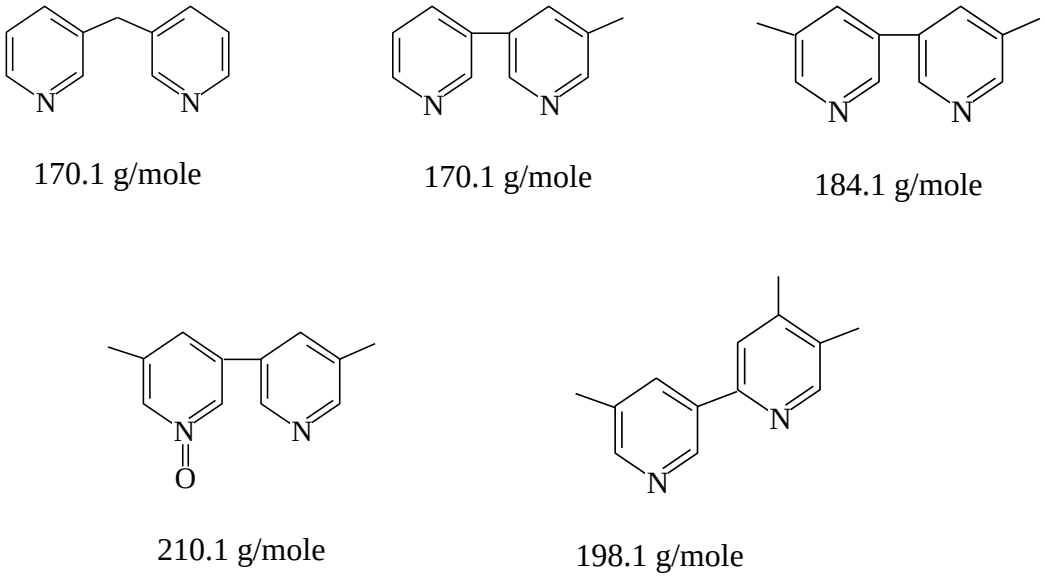

Figure 26. Potential structures formed during the decomposition of 3Nox

4.2.2 Decomposition of 3Nox in presence of hydrogen peroxide with and without catalyst

This study represents the case in which a runaway reaction can trigger the decomposition of the product, if the temperatures reached are sufficiently high. In the *N*-oxidation of alkylpyridines, hydrogen peroxide accumulates in the reaction mixture towards the end of the dosing period, when the concentration of alkylpyridine has dropped to a value such that the rate of the *N*-oxidation is no longer competitive. A cooling failure or similar upset can lead to a runaway decomposition of hydrogen peroxide, particularly when an excess of this reactant is used. The consequences of the runaway will depend on the amount of hydrogen peroxide accumulated in the reactor and the reaction conditions. The decomposition of 3Nox in the presence of hydrogen peroxide, with and without catalyst, was studied to assess the potential consequences if a runaway reaction occurs towards the end of the dosing period, when a significant amount of hydrogen peroxide has been accumulated.

The methodology followed to perform the experiments is identical with the one described in previous sections, but the HWS was conducted between 50 and 270 °C, using heating steps of 10 °C. The amounts of 3Nox, water, and hydrogen peroxide were the same in all experiments, except for one (experiment 2) where only half of the amount of hydrogen peroxide was used to determine the effect of accumulation on the decomposition of 3Nox. The amount of water in experiment 2 was increased to maintain the same sample mass for all experiments. The amount of catalyst varied between 0.0 g and 0.2. Table 9 summarizes the details of the measurements presented in this subsection.

Table 9. Details of the experiments with 3Nox, hydrogen peroxide and catalyst

Exp.	3Nox (g)	H_2O_2 wt. 35 % (g)	Water (g)	Catalyst (g)
1	1.53	7.00	7.00	0.00
2	1.53	3.50	10.50	0.00
3	1.53	7.00	7.00	0.10
4	1.53	7.00	7.00	0.20

Figure 27a-b show the temperature and pressure profiles generated during the experiments listed in Table 9. Three different thermal behaviors can be observed from Figure 27a-b. The first case is represented by experiment 1 (orange markers), where no catalyst was used and the concentration of hydrogen peroxide in the mixture was high. In this case, the "onset" temperature for the decomposition of hydrogen peroxide occurred around 100 °C. The reaction quickly accelerated, reaching a temperature higher than the "onset" temperature of decomposition of 3Nox. In the temperature profile, it can be seen that a change in the rate of the reaction occurs in the last few minutes of the experiment. The change in the rate occurs when the decomposition of hydrogen peroxide has finished and only 3Nox continues to decompose. However, the pressure generated during the decomposition of hydrogen peroxide (Figure 27b) reached a value close to the shutdown criteria of the equipment, and therefore, the experiment finished shortly after the decomposition of 3Nox had started. This experiment, which had the highest temperatures and pressure rates generated, represents the worst case scenario.

In the second case (experiment 2 – purple markers), where no catalyst and a lower concentration of hydrogen peroxide were used, only the decomposition of hydrogen peroxide was detected. The "onset" temperature of decomposition was around 120 °C, and due to the low concentration of hydrogen peroxide in the mixture and the absence of catalyst, the reaction occurred slowly with an adiabatic temperature rise ($\triangle T_{ad}$) of 95 °C. Once the decomposition of hydrogen peroxide finished, the HWS continued until the end of the experiment without detecting another exotherm.

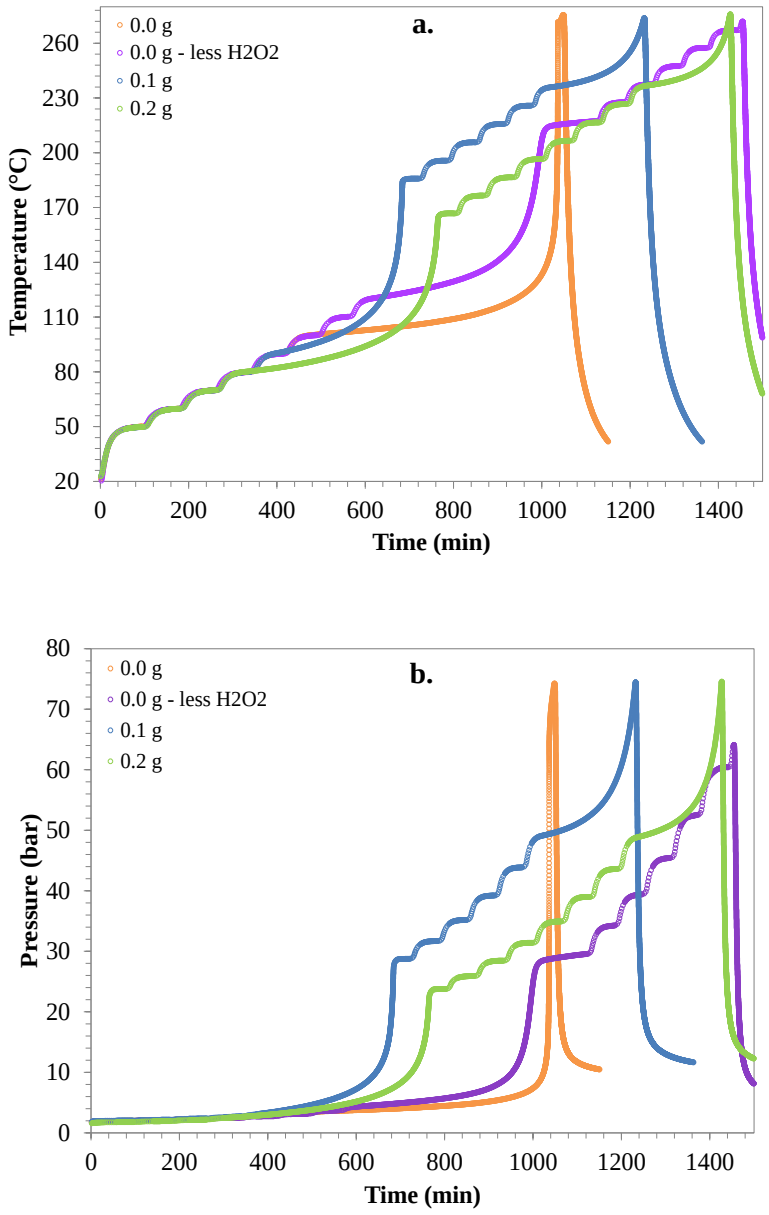

Figure 27. a) Temperature, and b) Pressure profiles during the decomposition of 3Nox and hydrogen peroxide 35 wt. %, employing different amounts of catalyst

From previous results obtained for the decomposition of 3Nox, it is known that in the absence of catalyst, the decomposition occurs very slowly at 250 °C. Therefore, most likely some decomposition of 3Nox occurred during experiment 2, but the self-heat rate

did not exceed the detection threshold of the APTAC. This experiment demonstrates the importance of limiting the accumulation of hydrogen peroxide in the reactor, as it has a dramatic effect on the severity of the consequences.

In the third case (experiments 3 and 4 – blue and green lines, respectively), both decomposition reactions were detected. The presence of the catalyst decreased the "onset" temperature of decomposition of hydrogen peroxide, but the maximum temperatures reached were far below the temperature of decomposition of 3Nox. The "onset" temperatures for the decomposition of hydrogen peroxide were decreased to 90 °C for experiment 3 (0.1 g of catalyst) and to 80°C for experiment 4 (0.2 g of catalyst), with adiabatic temperature rises of 95°C and 87°C, respectively. After the decomposition of hydrogen peroxide finished, the HWS continued until it detected the decomposition of 3Nox at a temperature of 236 °C in both experiments, once again showing the lack of sensitivity of 3Nox to the amount of catalyst.

The decrease in the "onset" of the decomposition of hydrogen peroxide decreases the severity of the consequences of a runaway reaction, if hydrogen peroxide is not accumulated in large amounts. The reason for this is that at lower temperatures, the decomposition of hydrogen peroxide would occur at a slower rate, and the maximum temperature reached would be far below that of the decomposition of 3Nox. This is only if the accumulation of hydrogen peroxide is low. Otherwise, the temperature rise can be sufficiently high to trigger the decomposition of the 3Nox, potentially leading to catastrophic consequences. It can be seen in Figure 27b that experiments 1, 3, and 4 reached the set pressure criteria for the shutdown of the equipment, while experiment 2 was allowed to continue through the end of the experiment.

Figure 28 shows the self-heat rate as a function of temperature during the decomposition of hydrogen peroxide for the experiments included in this subsection. It can be seen in Figure 28 that although the increase in the mass of catalyst from 0.1 to 0.2 g decreased

the “onset” temperature of decomposition of hydrogen peroxide, the maximum self-heat rate was lower in the experiment with 0.2 g of catalyst (experiment 4). This is because the rate of reaction increases with temperature and concentration. In experiment 4, the “onset” occurs at a lower temperature, thus the rate of reaction is lower. The reaction increases the temperature of the mixture, but at the same time, the concentration of hydrogen peroxide decreases until it has decomposed fully, producing no more heat. Also seen in Figure 28 is the dramatic difference between the two experiments performed with 0.0 g of catalyst. The self-heat rate of the experiment with more hydrogen peroxide was two orders of magnitude higher than the experiment performed with less hydrogen peroxide. This is also due to the dependency of the reaction rate on temperature and concentration.

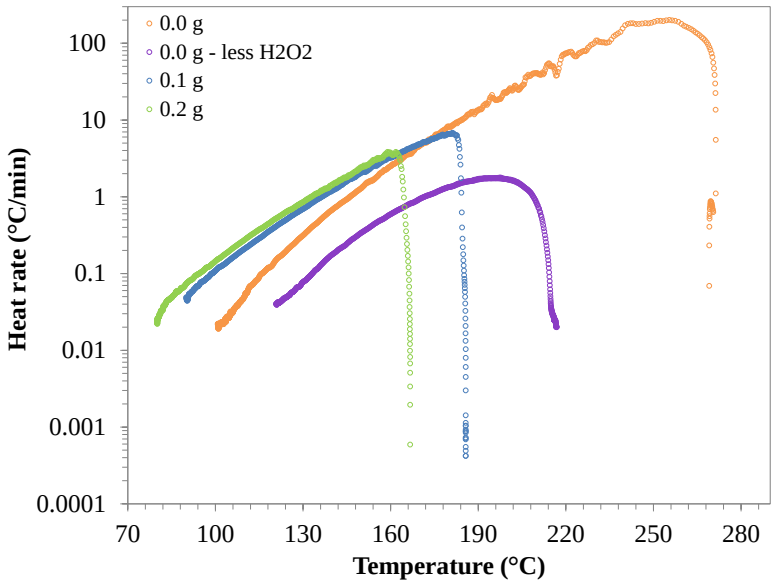

Figure 28. Heat rate profiles during the decomposition of hydrogen peroxide 35 wt. %, in the presence of 3Nox, employing different amounts of catalyst

4.2.3 Decomposition of higher order alkylpyridine N-oxides

The decomposition of 3,5-lutidine-*N*-oxide (35Nox); 2,6-lutidine-*N*-oxide (26Nox); and 2,4,6-collidine-*N*-oxide (246Nox) was briefly studied in order to identify the onset temperature of decomposition. The samples used for this study were prepared in our laboratory. They were taken from the final mixture of the *N*-oxidation of the corresponding parent alkylpyridine.

The *N*-oxidation of 3,5-lutidine was performed using 1 g of catalyst, which was fully dissolved in the product mixture obtained (see subsection 6.2). The *N*-oxidation of the remaining two alkylpyridines was performed using 10 g of catalyst, which were also fully dissolved in the final product mixtures. The composition of those mixtures is reported in Section 6.2 and 6.3. No additional catalyst was added to the samples used for experiments in the APTAC.

All experiments were conducted in HWS mode, and a pressure of approximately 1.7 bar (25 psi) of nitrogen was initially applied to the reaction cell to avoid rapid vaporization of the sample. The sample mass in all experiments was 15 g, although the proportion of alkylpyridine *N*-oxide solution to water was changed in the experiments with 26Nox to observe the effect of the concentration of 26Nox on the decomposition reaction. Table 10 shows the details of the experiments conducted.

Figure 29 shows the temperature and pressure profiles obtained during the decomposition of 35Nox. The “onset” of the decomposition reaction was detected around 250 °C. The pressure generated during the experiment reached the shutdown criteria of the equipment, and therefore, the experiment finished before the reaction reached completion.

Table 10. Details of experiments conducted with higher order alkylpyridine *N*-oxides

Compound	HWS range	Heating step (°C)	Solution* (g)	Water (g)
3,5-lutidine-*N*-oxide	120-280 °C	5	15.00	0.00
2,6-lutidine-*N*-oxide	150-280 °C	10	7.54	7.50
2,6-lutidine-*N*-oxide	50-280 °C	10	11.25	3.75
2,4,6-collidine-*N*-oxide	150-280 °C	10	15.03	0.00

*Note: The term "solution" refers to the final mixture obtained from the *N*-oxidation of the corresponding alkylpyridine in the RC1*e*

Before the experiment finished, the temperature rise due to the decomposition was 50 °C. Similar to the decomposition of 3Nox, the decomposition of 35Nox produced non-condensable gases, and a black solid and liquid residue was observed in the final mixture.

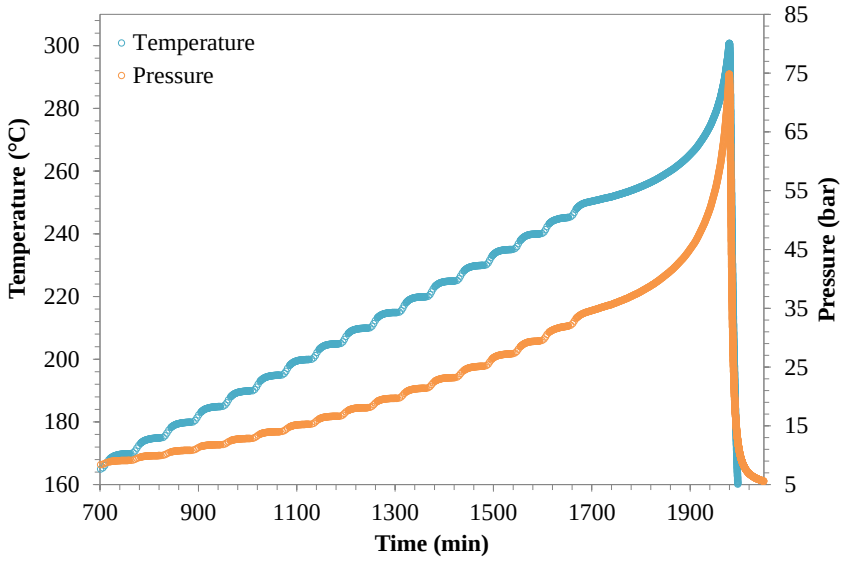

Figure 29. Temperature and pressure profiles obtained during the decomposition of 35Nox

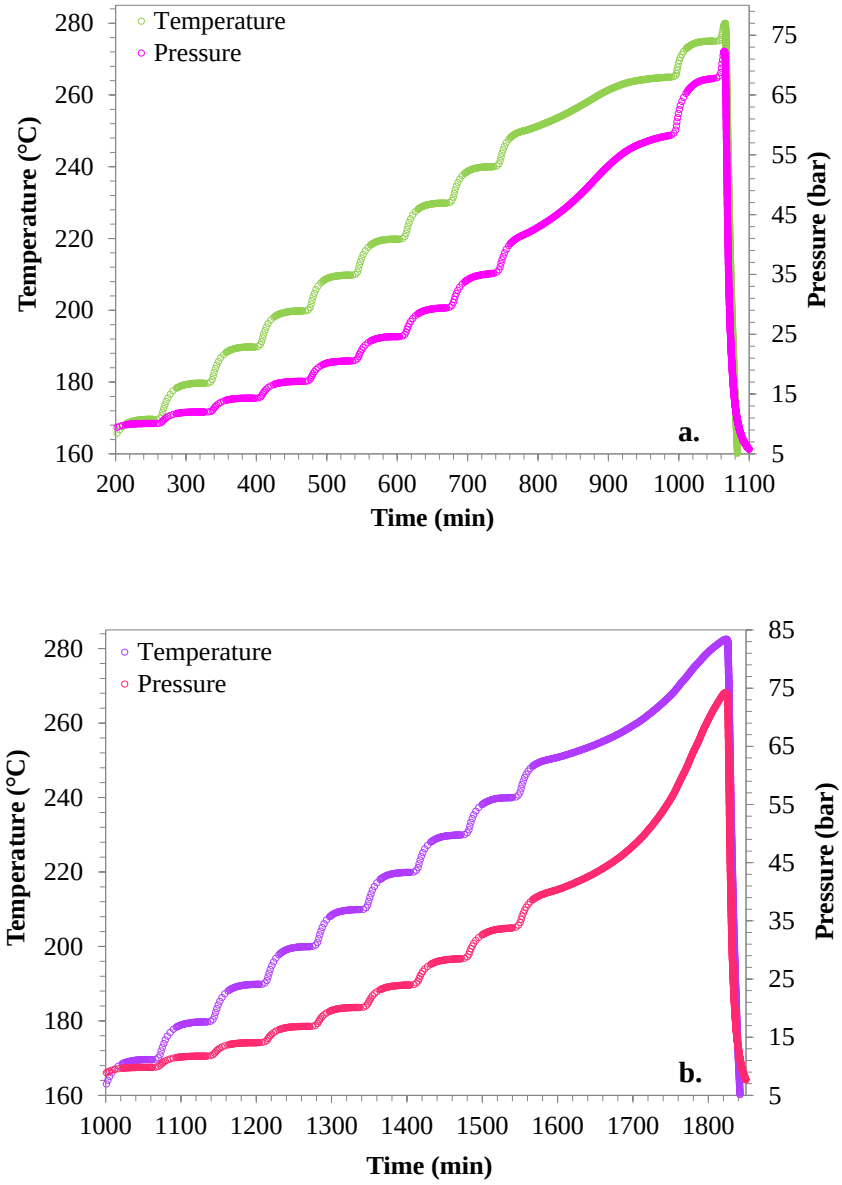

Figure 30. Temperature and pressure profiles obtained during the decomposition of 26Nox; a) using 7.54 g of 26Nox solution; b) using 11.25 g of 26Nox solution

Figure 30a-b show the temperature and pressure profiles obtained during the decomposition of 26Nox, using different initial quantities of 26Nox. In both experiments, the "onset" of the decomposition was detected around 250 °C; however, due to the difference in concentration of 26Nox in the samples, the temperature and

pressure profiles of the two experiments are different. From Figure 30a, it can be seen that the exotherm occurs very slowly and finishes within 200 min, with an adiabatic temperature rise of 15 °C. At the same time, there is a pressure increase of 18.6 bar. Once the exotherm finished, the HWS continued until the upper temperature limit set was reached.

For the experiment with a higher amount of 26Nox (Figure 30b), the decomposition occurs at a faster rate. However, the pressure generated by the non-condensable gases produced in the reaction reached the shutdown criteria of the equipment and the reaction did not reach completion. The adiabatic temperature had risen by 32 °C when the equipment shut down and the pressure had increased by 35.5 bar, though these values would have been higher if the equipment had not shutdown. The final sample collected was constituted by a black liquid and solid residue.

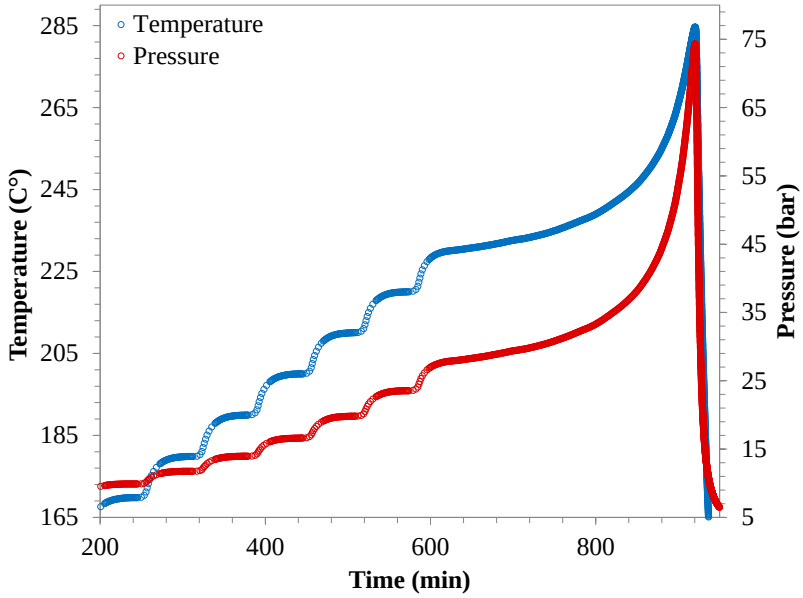

Figure 31. Temperature and pressure profiles obtained during the decomposition of 246Nox

Figure 31 shows the temperature and pressure profiles obtained during the decomposition of 246Nox. The "onset" temperature of decomposition of this compound, 230 °C, was lower than that of the other *N*-oxides included in this study. The pressure generated during the experiment reached the shutdown criteria of the equipment, and therefore, the experiment finished before the reaction reached completion. The adiabatic temperature had risen by 54 °C when the equipment shut down and the pressure had increased by 46.7 bar, though these values would have been higher if the equipment had not shut down. The final sample collected was mostly composed of a black tar with thicker consistency than the residues obtained from the decomposition of other *N*-oxides.

4.3 Conclusions

This section was concerned with the study of the thermal stability of alkylpyridines and their *N*-oxides under different conditions. The main purpose of this study was to ensure that operating conditions used do not compromise the safety of the process nor the quality of the materials involved in the reaction. The main findings presented in this section are summarized below:

The thermal stability study of 3-picoline; 3,5-lutidine; 2,6-lutidine; and 2,4,6-collidine did not reveal any exothermic behavior. Therefore, these compounds are considered thermally stable up to the tested temperature of 400 °C. On the contrary, all corresponding alkylpyridine *N*-oxides decompose at temperatures above 230 °C. Non-condensable gases were generated during the decomposition of all *N*-oxides included in this study. All final samples from the decomposition of *N*-oxides contained a black liquid and a solid residue, the mass of which was higher than the initial mass of catalyst in the sample. This means that the solid residue was constituted not only by the catalyst, but also by other products formed during the decomposition.

The effect of temperature and catalyst concentration on the decomposition of 3Nox was studied using isothermal tests in the APTAC. These tests indicated that 3Nox decomposes significantly at temperatures above 230 °C, and that an increase in temperature accelerates the rate of the decomposition. Conversely, 3Nox appears to have low sensitivity to small changes in the catalyst concentration. The rate of the decomposition reaction using 0.1 g of catalyst was slightly faster than when using 0.3 g of catalyst at all temperatures tested. Only when excessive amounts of catalyst were used was the decomposition of 3Nox accelerated. This behavior may suggest that different decomposition mechanisms occur depending on the concentration of catalyst in the mixture.

Samples collected at the end of experiments with 3Nox were analyzed by GC/MS and LC/MS. The analyses revealed that the main product of the decomposition of 3Nox is 3-picoline, which confirms that one of the main pathways of the decomposition involves the detachment of oxygen from the 3Nox molecule; the analyses also showed that not all 3Nox was consumed in the decomposition reaction. In addition, multiple compounds of a wide range of m/z ratios were detected in LC/MS analyses. This indicates that the decomposition of 3Nox occurs through a complex mechanism in which some polymerization likely occurs, accompanied by the generation of non-condensable gases.

Experiments involving 3Nox, hydrogen peroxide and catalyst demonstrated the dramatic effect of the accumulation of hydrogen peroxide in the reaction mixture. A runaway decomposition of hydrogen peroxide may increase the temperature of the mixture sufficiently to trigger the decomposition of the *N*-oxide, leading to severe consequences. This finding emphasizes the importance of maintaining a low accumulation of hydrogen peroxide throughout the process.

5. STUDY OF THE *N*-OXIDATION OF 3-PICOLINE USING ISOTHERMAL CALORIMETRY[*]

This section presents the results of measurements performed in two isothermal calorimeters, the HEL-SIMULAR and the RC1*e*, which have been previously described in Subsection 3.2.1. Preliminary experiments with 3-picoline were conducted in the HEL-SIMULAR isothermal calorimeter to study the effect of an increase of temperature and catalyst mass on the *N*-oxidation reaction. The results of preliminary experiments are shown in Subsection 5.1. A full 2^4 factorial design of experiments was used in order to complement preliminary studies and to determine the factors that have the strongest effect on the conversion of 3-picoline; these experiments were performed in the RC1*e* and the results are shown in Subsection 5.2. Calculations of the power output and enthalpy of the *N*-oxidation of 3-picoline are also included in this section.

5.1 Study of the *N*-oxidation of 3-picoline in the HEL-SIMULAR Isothermal Calorimeter

Presently, the industrial *N*-oxidation of alkylpyridines is carried out in an open semi-batch reactor to allow for the generated oxygen to escape. Hydrogen peroxide in approximately 50% excess is added gradually to the reactor so as to control the heat generated and the accumulation of hydrogen peroxide in the reactor.

Previous works on the *N*-oxidation of alkylpyridines have proposed a kinetic model for the *N*-oxidation of alkylpyridines based on a Langmuir-Hinshelwood type of kinetics.[51, 57] This type of kinetics involves fast equilibrium reactions to form intermediates that

[*] Part of this section is reprinted with permission from "Inherently safer reactors: Improved efficiency of 3-picoline *N*-oxidation in the temperature range 110–125 °C" by A. Pineda-Solano, L. Saenz-Noval, S. Nayak, S. Waldram, M. Papadaki and M. S. Mannan, **2012**. *Process Safety and Environmental Protection*, 90, 5, 404-410, Copyright [2012] by Institution of Chemical Engineers.

then react to form the final products. The kinetic model developed shows that the *N*-oxidation reaction is proportional to the concentration of both alkylpyridine and hydrogen peroxide, while the hydrogen peroxide decomposition rate is proportional to the square of hydrogen peroxide concentration. Therefore, the selectivity towards the *N*-oxidation is favored by low concentrations of hydrogen peroxide and by maintaining a low accumulation of this reactant. Also, previous studies have suggested that the selectivity of the synthesis reaction can be improved if more favorable operating conditions (higher temperatures) for the *N*-oxidation are used.

The primary objectives of this study were to investigate whether a reasonable process temperature and catalyst concentration exist at which the *N*-oxidation is so fast that practically no hydrogen peroxide decomposes, and to identify the maximum conversion of 3-picoline that can be achieved before hydrogen peroxide decomposition becomes competitive.

Table 11. Details of measurements presented in Section 6.1. In all measurements 1.933 mole of 3-picoline was added in the reactor with the catalyst dissolved in 15 g of water before mixed with the picoline. In all cases 188 g of H_2O_2, 35 wt. % aqueous solution (1.933 mole of H_2O_2) were dosed at the same constant rate of 0.25 g/min. P_o (pressure at T_o) = 0.99 bar. T_f indicates final temperature after cooling and before venting.

Exp.	Temp. (^{o}C)	Catalyst (g)	T_o (°C)	T_f (°C)	Pressure at T_f (bar)	moles of H_2O_2 decomposed
A	125	6	21.6	22.6	1.1	-
B	125	2	25.6	22.5	1.7	0.12
C	125	4.2	22.1	21.3	2.4	0.20
D	125	4.2	24.8	21.2	1.8	0.12
E	125	3	25.3	22.1	1.7	0.11
F	120	6	25.4	21.2	1.7	0.10
G	110	4.2	24.3	20.7	1.6	0.10

Isothermal calorimetric measurements were conducted in the HEL-SIMULAR isothermal calorimeter at 110 °C, 120 °C, and 125 °C using 2, 3, 4.2, or 6 g of catalyst and approximately 2 mole of alkylpyridine per batch. For the purpose of this study, unlike the industrial process, only stoichiometric quantities of reactants were used. The dosing of material was done at the slowest possible rate in order to ensure practically zero accumulation of hydrogen peroxide at all times. The details of each measurement are shown in Table 11. Unless otherwise reported, the experimental procedure followed during the calorimetric measurements discussed in this section was as explained in Subsection 3.2.1. One of the measurements performed at 125 °C was identical to the ones performed for the 3-picoline *N*-oxidation, however, instead of hydrogen peroxide, it employed an equal amount of pure water dosed over the 3-picoline-catalyst mixture.

The final conversion of 3-picoline was estimated from the difference between the initial and final pressures. The initial pressure, P_1, is the pressure measured once the reactor is closed and before it begins to heat up; it is equal to the pressure of the air plus the vapor pressure of the mixture at ambient temperature. Likewise, the final pressure, P_2, is measured at the end of the experiment, once the reactor has been completely cooled down to ambient temperature (~23 °C). The final pressure accounts for the air pressure, the vapor pressure of the mixture, and the oxygen generated throughout the course of the reaction.

Due to lack of information in the literature, it was assumed that the vapor pressures of the initial and final mixtures are equal to the vapor pressure of water. Since the initial and final pressures are both measured at ambient temperature, the change in the vapor pressure of the mixture would be equal to zero. The error introduced by this assumption is insignificant given that both 3-picoline and its *N*-oxide are by far less volatile than water. The pressure of the non-condensable gases is also affected by the headspace volume contraction owing to the addition of hydrogen peroxide. Thus, the partial pressure of the oxygen generated can be calculated as follows:

$$\Delta P_{O_2} = P_2 - P_1 \cdot \frac{V_1}{V_2} \quad \text{(Eq. 17)}$$

where V_1 and V_2 are the volume of the vessel headspace before and after dosing, respectively. The oxygen moles generated during the reaction are calculated with the ideal gas law. At the conditions of the reaction, the accumulation of hydrogen peroxide in the reactor at the end of dosing is zero. Thus, the hydrogen peroxide that has been added into the reactor has either decomposed or reacted with 3-picoline.

From the stoichiometry of the hydrogen peroxide decomposition reaction, the moles of hydrogen peroxide that decomposed are equal to the oxygen moles multiplied by two. Similarly, from the stoichiometry of the *N*-oxidation reaction, the number of moles of hydrogen peroxide that participated in the *N*-oxidation is equal to the number of moles of 3-picoline that reacted to form 3-picoline-*N*-oxide. Therefore, the final conversion of 3-picoline can be calculated, as shown below:

$$n_{H_2O_2\ dec} = 2 \cdot n_{O_2} \quad \text{(Eq. 18)}$$

$$n_{H_2O_2\ reacted} = n_{H_2O_2\ added} - n_{H_2O_2\ dec} \quad \text{(Eq. 19)}$$

$$n_{H_2O_2\ reacted} = n_{3-pic\ reacted} \quad \text{(Eq. 20)}$$

$$X_{3-pic} = \frac{n_{3-pic\ reacted}}{n_{3-pic\ loaded}} \quad \text{(Eq. 21)}$$

where n_{O_2} , $n_{H_2O_2}$, and n_{3-pic} are the moles of oxygen, hydrogen peroxide, and 3-picoline, respectively, and $X_{3\text{-pic}}$ is the final conversion of 3-picoline.

The increase of pressure during the course of the reaction was used to assess the extent of the decomposition. For this purpose, it was necessary to determine the contribution of

the vapor pressure of the mixture to the overall pressure increase. The pressure of the vapors of the initial mixture, which is 70 mole % 3-picoline, is much lower than that of water. Water is added into the system as part of the aqueous hydrogen peroxide solution and it is also produced via the reactions. Consequently, its molar concentration in the mixture rapidly increases, inevitably provoking a respective increase in the reactor pressure. In order to assess the influence of water concentration on the experiments, experiment A, shown in Table 11, where pure water was added over 3-picoline, was performed.

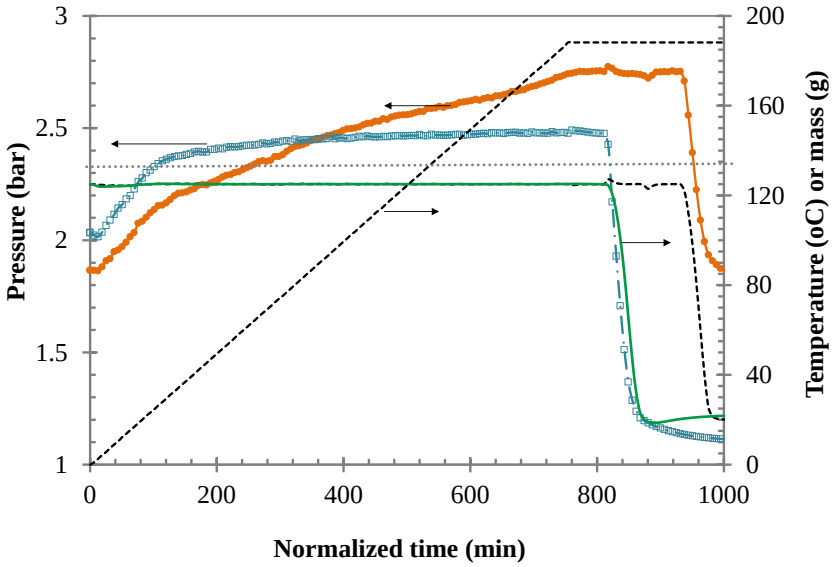

Figure 32. Comparison of the pressure profiles of measurement A (blue) and B (orange). On the right hand axis are shown the cumulative addition (--) and temperature (---), which is identical for both measurements A and B. The dotted horizontal line indicates the vapor pressure of water at 125 ^{o}C

Figure 32 shows a typical profile of the reactor temperature and pressure profiles during measurement B of Table 11, performed at 125 °C, and the respective measurement A performed under identical conditions but employing water instead of hydrogen peroxide.

As can be seen in Figure 32, the pressure profile of the measurement A with water shows a steep pressure rise during the first 80 min, during which 20–30 g of water has been added, followed by a smoother pressure rise until approximately 400 min, when practically half of the amount of water has been added. The first steep rise is most likely owed to water (or mixture) rapid evaporation, so that the mixture reaches its equilibrium pressure which is higher than the existing one. The speed of pressure rise is most likely controlled by the heat transferred to the reactor by the jacket, which has to provide the energy for heating of water to the reactor temperature and the latent heat for the evaporation.

The reactor pressure at the time dosing started was approximately 2 bar-a, and the reactor contained 1.933 mole of alkylpyridine and 0.83 mole of water. Because of its low molar mass compared to that of 3-picoline, water mole fraction in the mixture rapidly increases, affecting significantly the overhead equilibrium pressure. When 20 g of water had been added in the reactor, water mole fraction in the mixture was over 0.5, after the addition of 40 g of water in total, its mole fraction rose to over 0.6; when half of the water had been added it was 0.7, and its mole fraction when all water had been added was 0.85.

Water vapor pressure at 125 °C is 2.32 bar-a, shown with a gray dotted line in Figure 32, as opposed to approximately 0.65 bar-a vapor pressure of 3-picoline. As the molar composition of the mixture changes, water vapors are rapidly formed. The pressure rise of measurement B, shown here in orange dots, does involve a steep pressure rise in the beginning, but with a smaller slope than the one involving pure water. This pressure rise is slower, because water is not added directly, but formed through a reaction, and also due to the formation of *N*-oxide, which has a lower vapor pressure than 3-picoline, which it replaces in equimolar quantities.

As can be seen in Figure 32 and Table 11, the overall pressure increase in measurement B with reaction was 0.7 bar, while in the measurement with water the pressure increase was practically only half of that. So, the change of pressure due to the increased vapor pressure of the mixture is significant and cannot be neglected or grossly approximated.

Water and 3-picoline form homogeneous mixtures at any composition in the temperature range examined, with a significant enthalpy of mixing.[87] Therefore, the mixture is not expected to be ideal and Raoult's law is not expected to apply. The vapor pressure of the initial mixture was calculated as explained later and the vapor pressure of an ideal solution was compared with the measured vapor pressure of the system to have an idea of the degree of non-ideality of the mixture.

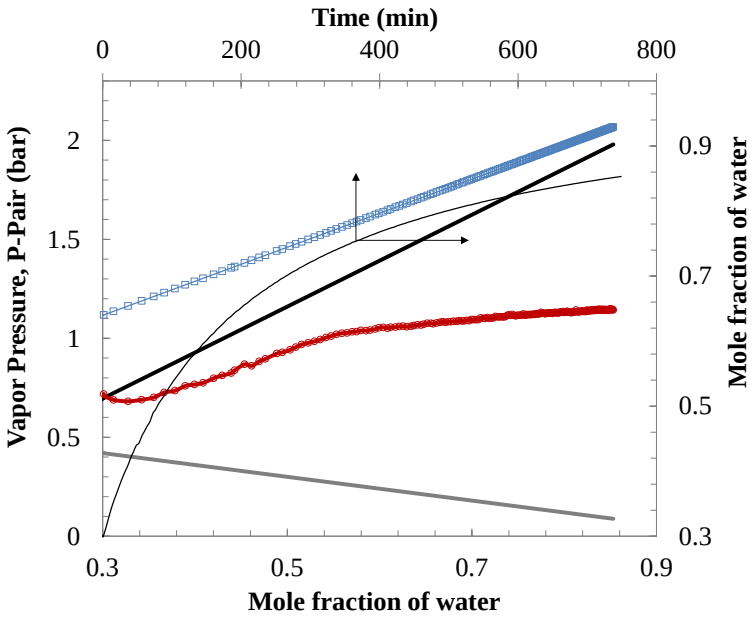

Figure 33. Pressure of vapors as measured (red) and as calculated (blue) at 125 °C, assuming Raoult's law. The thick, solid black line shows the water vapor pressure, and the thick, gray line shows the vapor pressure of 3-picoline. The thin, black line shows the change of water mole fraction, and it is read on the secondary axes of the figure

Figure 33 shows the vapor pressure of measurement A, employing water, and the total pressure that the mixture should have, if it behaved as an ideal solution, as a function of the mole fraction of water. The values of the vapor pressure of the mixture were calculated from the measured pressure after subtraction of the pressure of the air contained in the system. The latter was calculated as pressure increase of the gas initially contained in the headspace of the reactor, according to the ideal gas law.

As can be seen in Figure 33, the system of 3-picoline and water displays negative deviations from Raoult's law. However, the pressure of the system during the first 100 min of dosing could well be controlled by the rate of heat supply in the reactor, so the accuracy of those values has to be tested in a different calorimeter. Consequently, the evaluation of the contribution of vapors in the overall changes of the system pressure is not an easy task.

Table 12. Vapor pressure of solutions of 2 mole of 3-picoline with 15 g of water and a few grams of phosphotungstic acid. The numbers in bold are the arithmetic average of the vapor pressure values at the respective temperature shown in column 2

Temperature (°C)	Vapor Pressure (bar)	Average vapor pressure	From DIPPR Project 801[86]
125	0.553 0.540 0.470 0.524 0.627 0.705 0.703	**0.589**	0.585
120	0.379 0.354 0.454	**0.395**	0.502
110	0.247 0.221	**0.234**	0.364

The measured for 1 h equilibrium pressure values of the alkylpyridine was averaged for each measurement performed at 110, 120 and 125 °C, and the average of all measurements at a specific temperature was fitted to an Antoine type equation for 3-picoline vapor pressure. The values of vapor pressures obtained from ten different measurements are shown in Table 12. In the same table the values of DIPPR project 801[86] properties are also shown. As can be seen in Table 12, there is a good agreement in the value of the vapor pressure at 125 °C between the values obtained experimentally in this work and DIPPR project 801.[86]

Experimental vapor pressure values together with the normal boiling point of 144.1 °C[25] were fitted to an Antoine equation (Equation 22). Figure 34 shows the experimental points employed with open circles and the Equation 22 calculations with closed squares.

$$Log\ [P^o\ (bar)] = 0.82 - \frac{63.31}{T\ (°C) - 66.69} \qquad \text{(Eq. 22)}$$

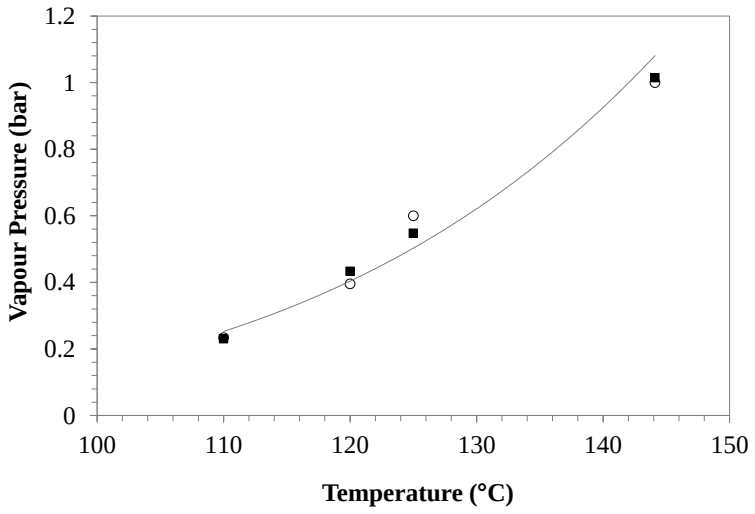

Figure 34. Vapor pressure of the initial reaction mixture: 180 g of 3-picoline and 15 g of water. Experimental values are shown in open circles and calculated values via Equation 22 are shown in closed squares

As mentioned earlier, the addition of hydrogen peroxide was chosen to be very slow. In order to prevent back pressure, the end of the addition tube was positioned above the liquid level so that hydrogen peroxide was dripping in the liquid content of the reactor. However, the high temperatures of the measurements resulted in a substantial decomposition of hydrogen peroxide in the air, before it reached the alkylpyridine solution. The metal dosing tube was therefore extended so that its tip was submerged into the liquid. This resulted in a substantial reduction of gas generation. However, the gas generation was still significant because the metal tube was catalyzing hydrogen peroxide decomposition. As the dosing tube could not be replaced, a nylon tube was inserted inside most of the length of the metal tube. This resulted in a significant reduction of hydrogen peroxide decomposition.

The residual pressure after the reactor was cooled and HPLC measurements performed on the liquid showed that less than 5% of hydrogen peroxide had decomposed and the conversion of 3-picoline was over 95%.

Figure 35 shows two measurements (C and D in Table 11) performed using the metal dosing tube submerged in the liquid (measurement C) and the dosing tube with the inserted nylon tube (measurement D). Both measurements were performed otherwise under identical conditions. The cumulative dosed mass is shown on the right-hand ordinate as a function of time. On the left-hand ordinate, the measured pressure for each measurement is shown. Also, shown on the left hand ordinate are the normalized pressures of the two measurements.

The normalization of pressure was performed by subtracting the pressure of measurement A, using water, from the respective measured pressures of experiments C and D. As can be seen from the comparison of the latter two, in the measurement where hydrogen peroxide was in direct contact with the metal tube, the pressure rise due to the production of oxygen (1.2 bar) was twice the value of the pressure generated in the one

with the nylon tube (0.6 bar). The conversion of 3-picoline in the latter was over 95%. It is worth mentioning here that the nylon tube did not eliminate contact of hydrogen peroxide with the metal; it merely reduced the area of contact. It is thus expected that even in the measurements where the nylon tube was used, some hydrogen peroxide actually decomposed before reaching the alkylpyridine. In other words, it is believed that carefully selected inert materials for the transport of hydrogen peroxide may further enhance the efficiency of the *N*-oxidation.

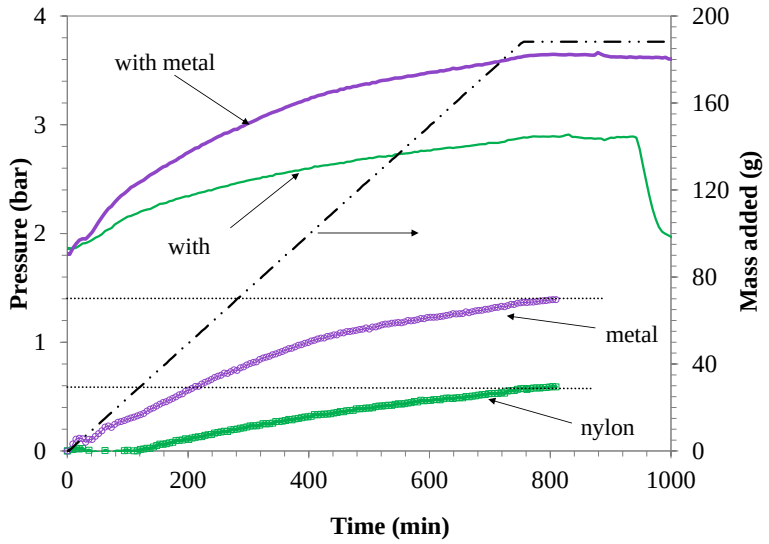

Figure 35. Total and normalized pressure history of measurements C (purple) and D (green). Measurement C was performed with a metal dosing tube, while in measurement D, a nylon tube was inserted inside the metal tube. On the right-hand axis the dosed mass is read, which is identical for both measurements

Figure 36 shows the pressure rise during dosing in three measurements performed at 125 °C, employing different masses of catalyst. The inset figure shows the normalized pressure for the three measurements; the normalization was conducted in a similar manner as discussed earlier.

As can be seen in Figure 36, the catalyst does not seem to have any positive effect in the range of catalysts used. Similar results were obtained for the measurements performed at 110 and 120 °C. The differences shown are well within the experimental error, although there is an indication that at the higher temperature (125 °C) there is an optimum quantity of catalyst beyond which, catalyst has a detrimental effect on the *N*-oxidation, probably by enhancing hydrogen peroxide decomposition. This has been further investigated using the RC1*e* calorimeter and the results which confirm this indication are reported in Subsection 5.2.1. In addition, adiabatic tests conducted by Saenz-Noval[62] using the APTAC also indicate that phosphotungstic acid accelerates the decomposition of hydrogen peroxide.

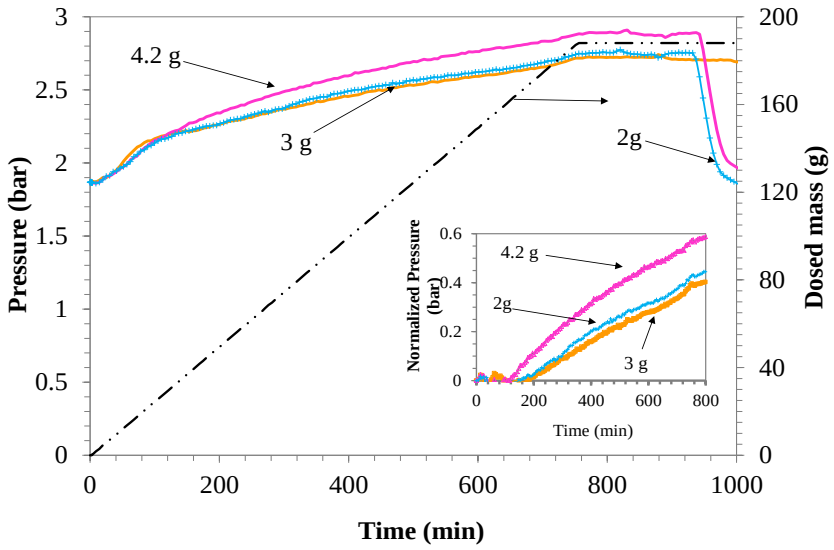

Figure 36. Pressure history of three *N*-oxidations at 125 °C (measurements B, D, and E) employing different masses of catalyst. Inset figure: normalized pressure of measurements shown in the main figure. The mass dosed, which is identical for all three measurements, is read on the right-hand axis

Figure 37 shows the effect of temperature for three measurements performed at different temperatures (measurements D, F, and G in Table 11). In one of them (measurement F), a

higher amount of catalyst was employed. In Figure 37a, the measured pressure for each experiment is shown. However, the comparison is not straightforward since the pressure of vapors is different in each of them. The normalized pressure values are shown in Figure 37b. This time normalization was performed by subtraction of the equilibrium pressure value before dosing from all subsequent pressure values of the respective measurement. The effect of the reactor headspace volume reduction due to mass addition was ignored. It must be pointed out however, that this approach is approximate. Thus, the conclusions cannot be accurate.

As can be seen in Figure 37b, the pressure stabilizes in all three cases as soon as dosing is stopped. This clearly indicates, that at the end of dosing, when the rate of the *N*-oxidation is the slowest in this process, there is no significant accumulation of hydrogen peroxide in the reactor, hence no hazard of its runaway exists. Consequently, at those higher temperatures tested in this study (compared to lower temperatures used in previous studies), high conversions can be achieved without the need to increase much the temperature or the catalyst concentration.

In Figure 37b, the normalized pressure rise during the course of the reaction appears to increase faster at higher temperature, indicating more decomposition of hydrogen peroxide. However, all three measurements display practically the same pressure profiles, and in all three of them 0.1 mole of hydrogen peroxide was found to have decomposed. Thus, the increased pressure rise at higher temperatures can be merely due to the error associated to the normalization of the pressure. Alternatively, this may indicate that hydrogen peroxide decomposition may have happened before it came in contact with the liquid solution and not in the course of the reaction. It is worth mentioning here that the measurements at 120 °C and 110 °C were performed with the bare metal dosing tube. Thus, it appears that the catalytic decomposition of hydrogen peroxide because of the contact with the metal is significant at higher temperatures. However, additional studies are needed to investigate this possibility.

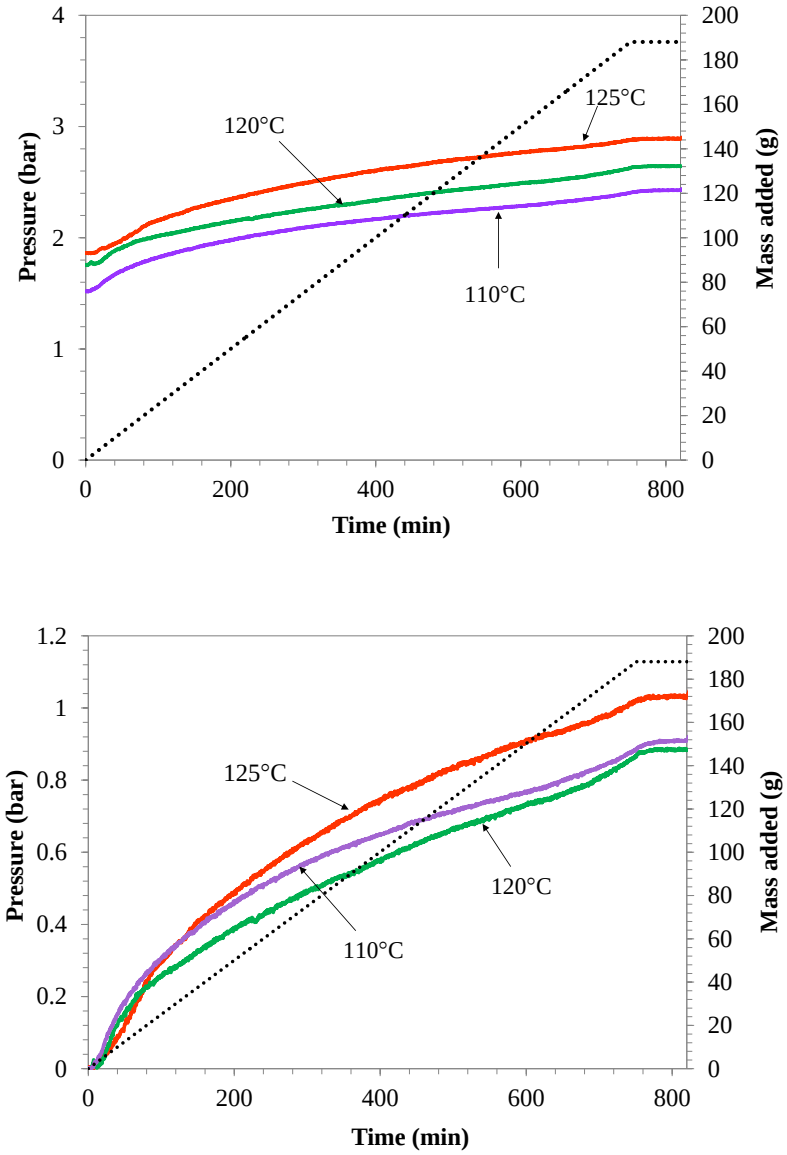

Figure 37. a) Total pressure, and b) Normalized pressure profiles as a function of time for three *N*-oxidations of 3-picoline at different temperatures (measurements D, F and G)

5.2 Study of the *N*-oxidation of 3-picoline Using a Factorial Design of Experiments

The experiments with 3-picoline *N*-oxidation discussed in the previous section and the work of Saenz-Noval[62] performed with 2-picoline *N*-oxidation led to the same

conclusion that the temperature appears to play an important role, but the role of the catalyst is unclear. The effect of the catalyst was possibly masked by the temperature effect, or because the quantities of catalyst used were in excess of the kinetically required amount, or because other parameters were left constant. During the experiments conducted by Saenz-Noval[62] and the experiments discussed in Subsection 5.1, the stirring rate, as well as the dosing rate, were kept constant in all experiments. However, it is scientifically necessary to determine the role of as many parameters as possible that can affect the reaction.

The main objective of this study is to obtain a clear understanding of the effect of each parameter of interest for the *N*-oxidation of alkylpyridines and determine which ones are the most significant. For this work, the *N*-oxidation of 3-picoline was used as a case study. The information obtained from this study is key for the design of inherently safer and more efficient *N*-oxidation of alkylpyridines, and the results from this study can be extended to other members in the alkylpyridine family.

A two-level full factorial design of experiments (DOE) was used in order to determine the variables – or factors – that have the strongest effect on the conversion of 3-picoline, the response variable. The design chosen for the current work was a 2^4 factorial design for four independent variables: temperature (A), catalyst mass (B), dosing rate (C) and stirring rate (D). The factor levels were selected based on preliminary experiments, safety of the operation, and operability at the conditions selected. All experiments for the factorial DOE were performed in the RC1*e* isothermal calorimeter.

Preliminary experiments discussed in Section 5.1 showed that it is not necessary to use temperatures higher than 125 °C to obtain a high conversion of 3-picoline. Therefore, a temperature of 125 °C was set as the high level for the factorial design. The typical amount of catalyst used for the *N*-oxidation of alkylpyridines is 7 g of catalyst / 300 g of alkylpyridine. For the experiments performed in the RC1*e* calorimeter, 240 g of 3-

picoline were used, so the normal amount of catalyst would be 5.6 g. It was decided to set the catalyst levels as 1 and 10 g, respectively.

All preliminary experiments discussed in the previous section were performed at the same dosing rate of 0.25 g/min. The use of this dosing rate would prevent the accumulation of hydrogen peroxide in the reactor, thus limiting the decomposition. However, using this dosing rate in the experiments discussed in this section would lead to a dosing time of 16.7 h. This dosing would be extremely slow and not viable in an industrial process. Therefore, it was decided to start with a dosing rate of 0.5 g/min which would still be sufficiently slow to prevent accumulation, but at the same time it would reduce the dosing time by half. The high level of dosing rate was set based on preliminary experiments not reported here. It was determined that a dosing rate higher than 4 g/min would lead to a high heat generation and temperature increase, which would be difficult to control by the calorimeter. Additionally, the pressure generation could be very fast, depending on the other operating conditions, which could endanger the operator and the equipment.

For the stirring rate, the low level was set at the normal 250 rpm (revolutions per minute). The high level of the stirring rate was selected based on the operability of the equipment. Stirring rates greater than 400 rpm cause the liquid to go over the allowed level in the RC1*e*. Therefore, the high level of stirring rate was set at 400 rpm.

Table 13 contains the 16 required runs for the 2^4 full factorial design. The upper part of the table displays the factors coded as (-1) for the low level and (1) for the high level of each factor. In addition, two center points were added to the design, coded as (0). The last column of the upper section of the table contains the values obtained for the response variable, *i.e.*, degree of conversion of 3-picoline. The lower part of the table shows the actual values of the factor levels.

Table 13. Experimental matrix for the full 2^4 factorial design with center points

Run	Temperature	Catalyst	Dosing rate	Stirring rate	$X_{3\text{-pic}}$
1	-1	-1	-1	-1	0.97
2	1	-1	-1	-1	0.95
3	-1	1	-1	-1	0.98
4	1	1	-1	-1	0.97
5	-1	-1	1	-1	0.63
6	1	-1	1	-1	0.81
7	-1	1	1	-1	0.98
8	1	1	1	-1	0.97
9	-1	-1	-1	1	0.94
10	1	-1	-1	1	0.96
11	-1	1	-1	1	0.97
12	1	1	-1	1	0.95
13	-1	-1	1	1	0.74
14	1	-1	1	1	0.83
15	-1	1	1	1	0.96
16	1	1	1	1	0.97
17	0	0	0	0	0.97
18	0	0	0	0	0.96

Factors	Levels		
	-1	0	1
Temperature (°C)	110	117.5	125
Catalyst (g)	1	5.5	10
Dosing rate (g/min)	0.5	2.25	4
Stirring rate (rpm)	250	325	400

The experiments were conducted randomly to avoid systematic errors. However, Table 13 shows the runs in the standard order of a factorial design of experiments.

Table 14 shows the uncoded factors and quantities necessary to calculate the conversion of 3-picoline.

Table 14. Details of factorial design runs. Initial mixture composition: 240.1 g (2.578 moles) of 3-picoline, and catalyst dissolved in 20 g of water. P_i (pressure at T_i) = 0 barg. T_f indicates final temperature after cooling and before venting. $V_1 = 271$ ml, and $V_2 = 52$ ml. All experiments were performed in the RC1*e* isothermal calorimeter.

Run	Temp. (°C)	Catalyst (g)	Dosing rate (g/min)	Stirring rate (rpm)	Mass dosed (g)	T_i (°C)	T_f (°C)	$\triangle PO_2$ (bar)	nO_2	H_2O_2 moles decomp.	3-picoline moles reacted	3-picoline conv.
1	110	1	0.5	250	250.45	22.77	22.98	1.635	0.045	0.090	2.488	0.97
2	125	1	0.5	250	250.45	22.96	25.68	2.247	0.061	0.123	2.455	0.95
3	110	10	0.5	250	250.45	23.02	23.01	0.933	0.026	0.051	2.527	0.98
4	125	10	0.5	250	250.45	22.90	22.99	1.604	0.044	0.088	2.490	0.97
5	110	1	4	250	93.70	21.94	23.30	5.831	0.198	0.396	0.569	0.22
					95.45	24.66	23.60	6.164	0.185	0.370	0.613	0.46
					61.30	24.29	20.64	3.454	0.096	0.192	0.439	0.63
6	125	1	4	250	125.18	23.01	23.23	2.749	0.090	0.179	1.109	0.43
					125.27	24.07	22.99	5.410	0.149	0.298	0.991	0.81
7	110	10	4	250	250.45	22.85	22.99	1.069	0.029	0.059	2.519	0.98
8	125	10	4	250	250.45	22.88	22.86	1.258	0.035	0.069	2.509	0.97
9	110	1	0.5	400	250.45	22.34	22.99	2.872	0.079	0.158	2.420	0.94
10	125	1	0.5	400	250.45	22.97	22.99	1.757	0.048	0.097	2.481	0.96
11	125	10	4	400	250.45	23.22	23.00	1.570	0.043	0.087	2.492	0.97
12	110	10	0.5	400	250.45	23.61	22.99	1.316	0.036	0.073	2.506	0.97
13	110	1	4	400	141.20	23.21	22.98	6.531	0.209	0.418	1.035	0.40
					109.25	22.94	23.00	4.432	0.122	0.244	0.880	0.74
14	125	1	4	400	160.45	23.07	22.96	4.365	0.136	0.273	1.379	0.53
					90.00	22.89	22.96	2.872	0.079	0.158	0.768	0.83
15	110	10	4	400	252.45	22.97	22.98	1.711	0.047	0.094	2.484	0.96
16	125	10	0.5	400	251.45	23.52	22.99	2.297	0.063	0.127	2.451	0.95
17	117.5	5.5	2.25	325	250.45	22.70	22.99	1.505	0.042	0.083	2.495	0.97
18	117.5	5.5	2.25	325	250.45	23.54	22.96	1.678	0.046	0.093	2.486	0.96

Note: Highlighted rows indicate experiments with more than one dosing step. For these experiments, the cumulative conversion was calculated for each step.

It can be seen in Table 13 and Table 14 that in most runs, the conversion of 3-picoline obtained was between 0.94 and 0.98; four of the runs fell below this range, and they are highlighted in Table 13 and Table 14. All runs that resulted in conversions lower than 0.9 were performed at the low level of catalyst (-1) and high level of dosing rate (1).

Table 15 shows the results of the statistical analysis performed in the software Minitab 16. For the statistical analysis, it was assumed that three and higher order interactions are negligible for the model and were instead used to estimate the standard error (see subsection 3.2.3).[84, 88] Main and interaction effects were estimated, along with the coefficients of the linear model and the standard error of the coefficients. The test of statistical significance shows that the only significant effects at the 5% probability level ($P<0.05$) are the catalyst amount, dosing rate, and the interaction between these two factors. All effects with a P value lower than 0.05 were significant. The fit model presented a square correlation coefficient (R^2) of 95.66%, fitting well the statistical model. The conversion of 3-picoline can then be expressed via the following equation:

$$X_{3-pic} = 0.912 + 0.057B - 0.049C + 0.051BC \quad \text{(Eq. 23)}$$

where B represents the catalyst level and C represents the dosing rate level. Equation 23 has the values of the factors coded and its levels are valid only to the levels described in Table 13.

It can be seen in Table 15 that the effect of the catalyst mass is positive, meaning that an increase of catalyst produces an increase in the conversion of 3-picoline, the response variable. On the other hand, the effect of the dosing rate is negative, which means that an increase in dosing rate from the low level to the high level leads to a decrease in the conversion of 3-picoline. However, the interaction effect between the mass of catalyst and dosing rate is positive, meaning that an increase in the dosing rate associated with an increase in the catalyst mass leads to an increase in the conversion of 3-picoline.

Table 15. Estimated effects and statistical significance of the full 2^4 factorial design for the *N*-oxidation of 3-picoline using Minitab 16

Term	Effect*	Coef*.	SE Coef.	P-value
Constant		0.912	0.009	0.000
Temperature	0.0313	0.016	0.009	0.119
Catalyst	0.114	0.057	0.009	0.001
Dosing	-0.098	-0.049	0.009	0.001
Stirring	0.009	0.004	0.009	0.617
Temperature*Catalyst	-0.040	-0.020	0.009	0.057
Temperature*Dosing	0.037	0.019	0.009	0.073
Temperature*Stirring	-0.007	-0.004	0.009	0.682
Catalyst*Dosing	0.101	0.051	0.009	0.001
Catalyst*Stirring	-0.020	-0.010	0.009	0.291
Dosing*Stirring	0.019	0.009	0.009	0.313
Center Point		0.054	0.026	0.080
Standard error	0.034			
Square correlation factor (R^2)	95.66%			

*Note: The effects and coefficients for the linear model are given in coded units. Coef: Coefficient, SE Coef: Standard error of the coefficient, Ct Pt: central point

Figure 38 shows the 2-factor interaction plots. These plots show the change of a factor depending on the levels of another factor. The green lines represent the high level and the black lines represent the low level of the corresponding factors. The red dot represents the center point. The numbers at the top horizontal axis represent the coded levels high (1), low (-1) and center point (0). The vertical axis on the right represents the response variable, in this case, the conversion of 3-picoline, for which the range is 0-1 (or 0-100%). Parallel lines in an interaction plot mean that there is no interaction between the factors. An interaction is present when the lines cross each other.

It can be seen from Figure 38 that that the catalyst-dosing rate is the strongest interaction. When the catalyst mass is at the low level and the dosing rate is at the high

level there is not enough catalyst for the *N*-oxidation and because of the high dosing rate, hydrogen peroxide is accumulated. Higher accumulation of hydrogen peroxide leads to more decomposition because the rate of the decomposition reaction is proportional to the square of the concentration of hydrogen peroxide. In contrast, when both the catalyst amount and dosing rate are at the low level, there is no accumulation of hydrogen peroxide and therefore, the *N*-oxidation reaction becomes more competitive.

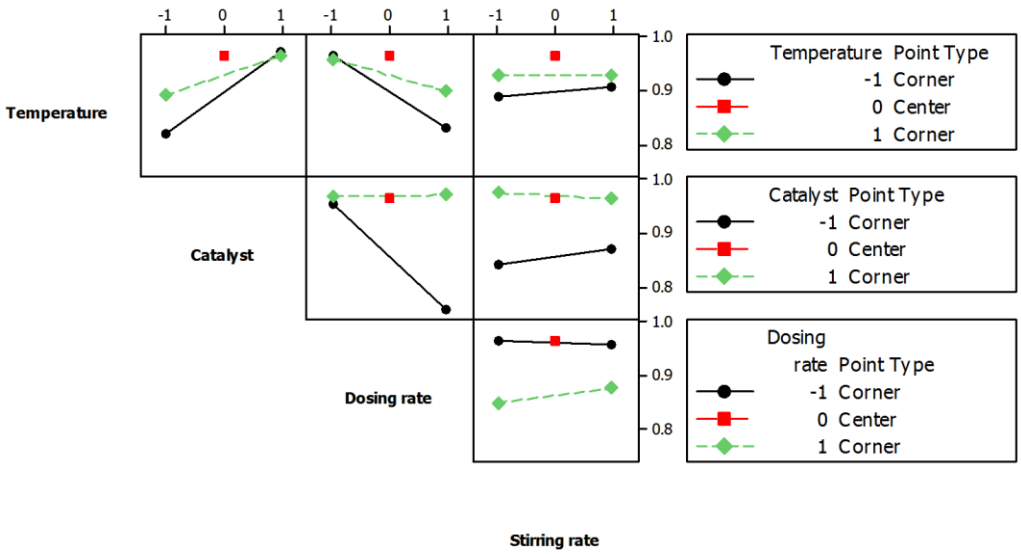

Figure 38. Interaction plots for conversion of 3-picoline obtained from Minitab 16

Other important interactions are those of temperature-catalyst, and temperature-dosing rate. All the interactions with stirring rate seem to be weak. This means that for the arrangement and levels used for this study, the stirring rate did not have a strong effect on the conversion of 3-picoline. However, it must be taken into account that as the volume of the reactor increases, mixing effects are more prominent, thus, the effect of the stirring rate would likely be more significant.

Figure 39 shows a Pareto chart of the absolute value standardized effects at the 5% significance level. For this type of applications, a Pareto chart is a tool that displays the relative importance of factors in a format that is easy to interpret. This plot visually represents the absolute values of the effects of the main factors and the effects of their interaction. The significance of the effects is represented by the length of its corresponding bar.[89] Factors and interactions with an absolute standardized value of the effect higher than 2.447 were significant at the 5% significance level. The absolute standardized value of the effect of each factor and interaction appear at the right of each bar.

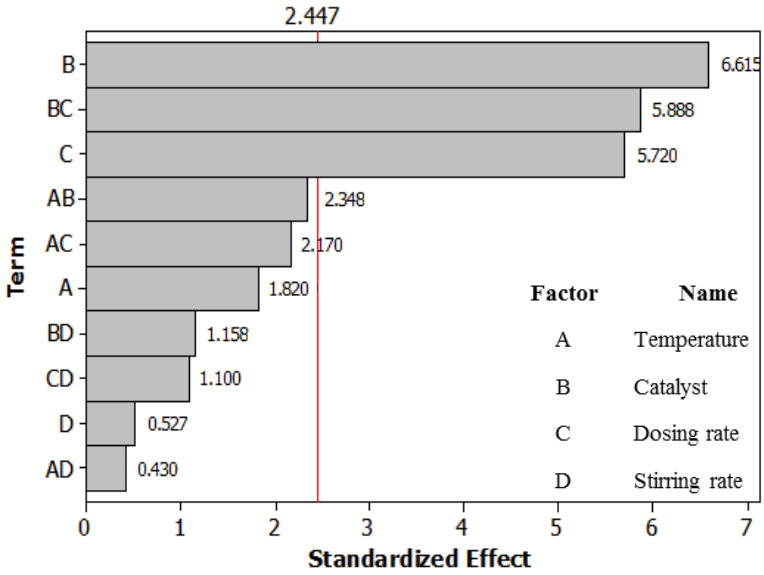

Figure 39. Pareto chart of standardized effects obtained from Minitab 16. The response variable is conversion of 3-picoline; alpha=0.05

The largest effects, as shown by the statistical significant test, were the catalyst mass, dosing rate, and the interaction between those two factors, with the catalyst mass being the factor with the largest effect. Although the dosing rate is important, the interaction

with the catalyst mass is slightly more significant than the main factor (dosing) alone. This information would not be acquired using an univariate procedure for the study of the *N*-oxidation of alkylpyridines, where the factors are varied one at a time while maintaining the other factors fixed.

The center points were used to obtain the standard error of the coefficients, determine curvature in the model and to test the reproducibility of the experiments. It can be seen in the interaction plots (Figure 38) that there is a slight curvature when the levels are changed from the lower to the higher level going through the central point. However, according to the P value, the center point was not significant in the chosen model (P=0.08) at the 5% significance level.

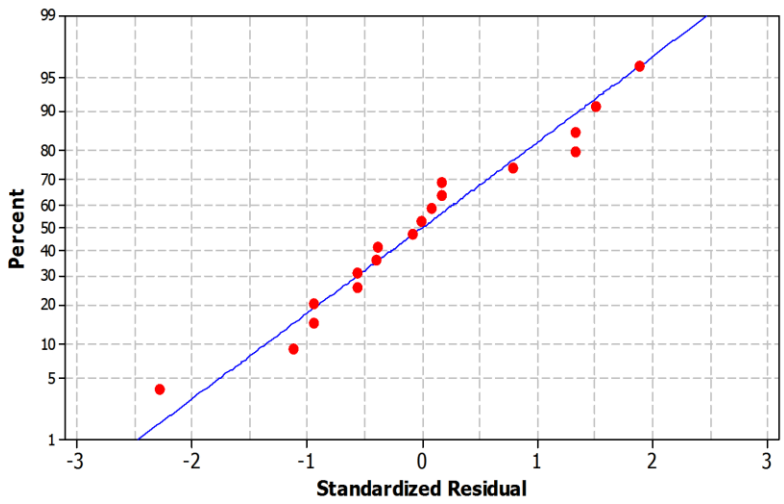

Figure 40. Normal probability plot of standardized residuals

A normal probability plot of the data in terms of standardized residuals was also generated in Minitab 16 in order to confirm the normality of the data. The residual plot was used to evaluate the goodness of fit in the regression analysis and ANOVA (analysis of variance). The normal probability plot of residuals is generally used to verify the

assumptions of the ordinary least squares are adequate to produce unbiased coefficient estimates with minimum variance.[89] As shown in Figure 40, all of the points in the normal probability plot of the standardized residuals are fairly close to the straight line, which indicates that the data satisfy a normally distributed population.

5.2.1 Analysis of pressures

Figure 41 shows the pressure increase during the experiments conducted at the center point. It can be seen that there is a slight difference between the curves, even though they were performed at identical conditions. The estimated conversions for the center point differ in 1%. Thus, this is the error associated with all measurements. However, it was observed that higher stirring rates caused more noise in pressure and power measurements.

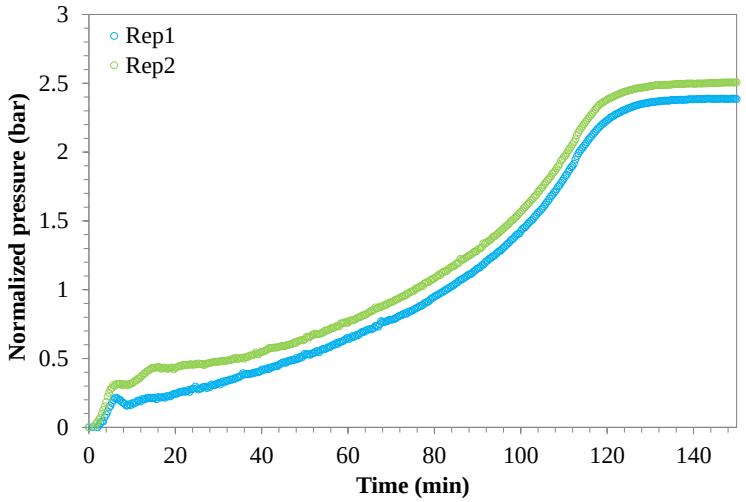

Figure 41. Pressure increase during two replica experiments conducted at the center point. Conditions: 117.5°C, 5.5 g of catalyst, dosing rate of 2.25 g/min and stirring rate of 325 rpm (runs 17 and 18 in Table 14)

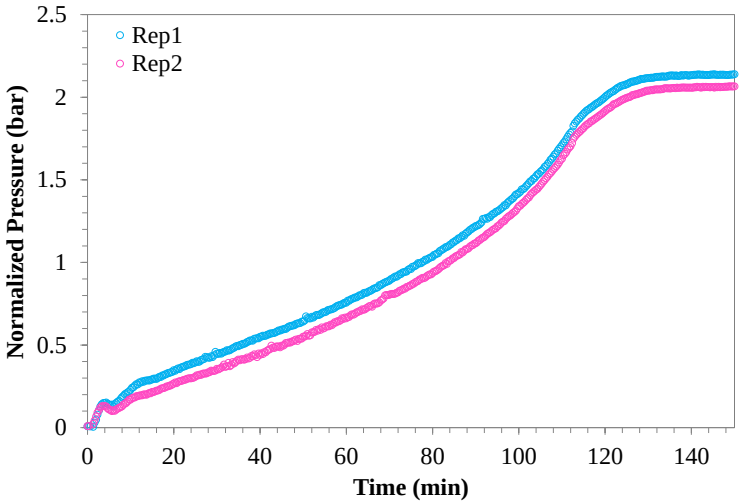

Figure 42. Pressure increase during two replica experiments conducted at 117.5°C, 5.5 g of catalyst, dosing rate of 2.25 g/min and stirring rate of 250 rpm.

Experiments conducted at the same temperature, catalyst mass and dosing rate as the center point, but using a stirring rate of 250 rpm were almost identical, and the conversions obtained differed only by 0.02%. However, these measurements are not part of the factorial DOE (See Figure 42).

Figure 43 shows the normalized pressure of measurements at the high and low levels of temperature (110 °C and 125 °C) and catalyst mass (1 and 10 g) and high level of dosing rate (400 rpm). The normalization was performed by subtraction of the equilibrium pressure value before dosing from all subsequent pressure values of the respective measurement. The effect of the reactor headspace volume reduction due to mass addition was ignored. As mentioned earlier in Subsection 5.1, this approach is approximate, thus the conclusions are not accurate. However, this analysis provides a good estimation and understanding of the behavior of the *N*-oxidation at different conditions.

As can be seen in Figure 43 the measurements performed at 110 ^{o}C and 125 ^{o}C, both at high level of catalyst mass (10 g), are very similar, with the measurement performed at 125 ^{o}C having a slightly larger pressure increase. Adiabatic tests have shown that self-

decomposition of hydrogen peroxide becomes very vigorous at temperatures higher than 120°C.[62] In addition, it has also been shown in previous studies that the catalyst accelerates the decomposition of hydrogen peroxide.[62] The 10 g of catalyst used in the measurement at 125 °C (run 8 in Table 14) was likely a much larger mass of catalyst than the kinetically required mass at that temperature. Consequently, the combination of high temperature and high catalyst mass in run 8 likely increased the decomposition of hydrogen peroxide. A lower mass of catalyst combined with a high temperature may be appropriate to reduce the decomposition. However, the catalyst mass cannot be too low such that it is not sufficient to make the *N*-oxidation competitive. Further studies are needed to determine the optimum mass of catalyst to use at a given temperature.

In the case of the experiments performed with low catalyst mass (see Figure 43), the decomposition of hydrogen peroxide was so vigorous that the pressure generated reached the maximum operating pressure of the reactor; consequently, dosing of hydrogen peroxide had to be stopped and the reactor was then cooled down and vented. For the measurement at 110 °C and 1 g of catalyst (run 5 in Table 14), dosing had to be interrupted twice, while in the measurement performed at 125 °C and 1 g of catalyst (run 6 in Table 14), dosing was interrupted once. Typically, as a precautionary measure, dosing of hydrogen peroxide to the reactor was interrupted before the pressure reached the maximum operating pressure. Due to the high dosing rate, it was known that the large accumulation of hydrogen peroxide would cause the pressure to continue increasing, even after dosing was interrupted.

Figure 43 shows only the first dosing step of each of the two measurements conducted at the low level of catalyst mass. It can be seen in Figure 43 that the pressure generated in the first dosing step of the experiment at 110 °C and 1 g of catalyst was more than 4 times the pressure increase of the entire experiment performed at the high catalyst level (10 g). In the case of the measurement at 125 °C and 1 g (run 6 in Table 14), the pressure increase for the first dosing step was about twice the pressure increase for the entire

experiment performed at high catalyst mass. With regards to the pressure rates, it can be seen that the pressure rate increases much faster during the measurement at 110 °C.

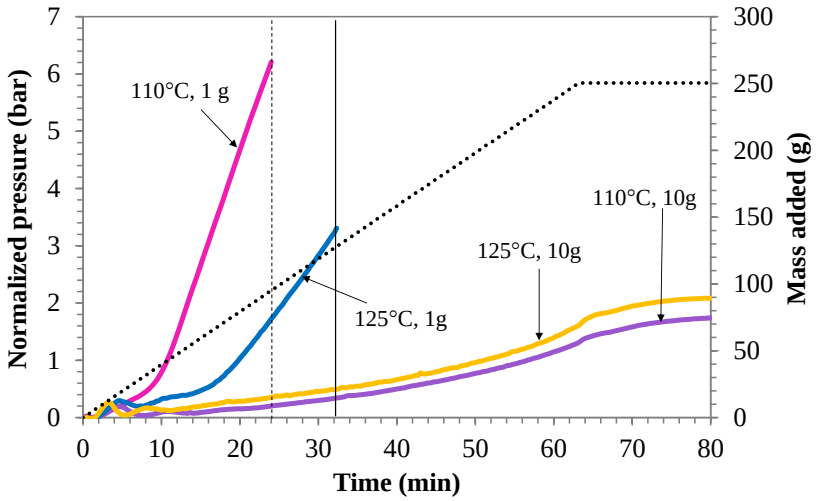

Figure 43. Normalized pressure increase of runs at different temperatures and mass of catalyst. All runs shown in this figure were performed at 250 rpm and 4 g/min (Runs 5 to 8 from Table 14)

The vertical dashed line in Figure 43 indicates the point where dosing was interrupted for the first time in the experiment at 110 °C and 1 g of catalyst, which was after adding 93.75 g of hydrogen peroxide solution. The vertical solid line represents the point at which dosing was interrupted in the measurement at 125 °C and 1 g of catalyst, which was after adding 125.18 g of hydrogen peroxide solution. Figure 44a-b show the complete measurement data for the experiments conducted at 110 °C and 125 °C at the low level of catalyst amount.

For the measurement at 110 °C and 1g shown in Figure 43, the pressure continued to increase about 1.3 bar after interrupting dosing (refer to Figure 44a), which indicates there was an accumulation of hydrogen peroxide in the reactor. In contrast, for the measurement at 125 °C and 1g, even though a larger amount had been dosed before

dosing was interrupted, the pressure increased by only 0.57 bar (refer to Figure 44b). This is due to the faster rate of the *N*-oxidation at 125 °C, which limits the accumulation of hydrogen peroxide.

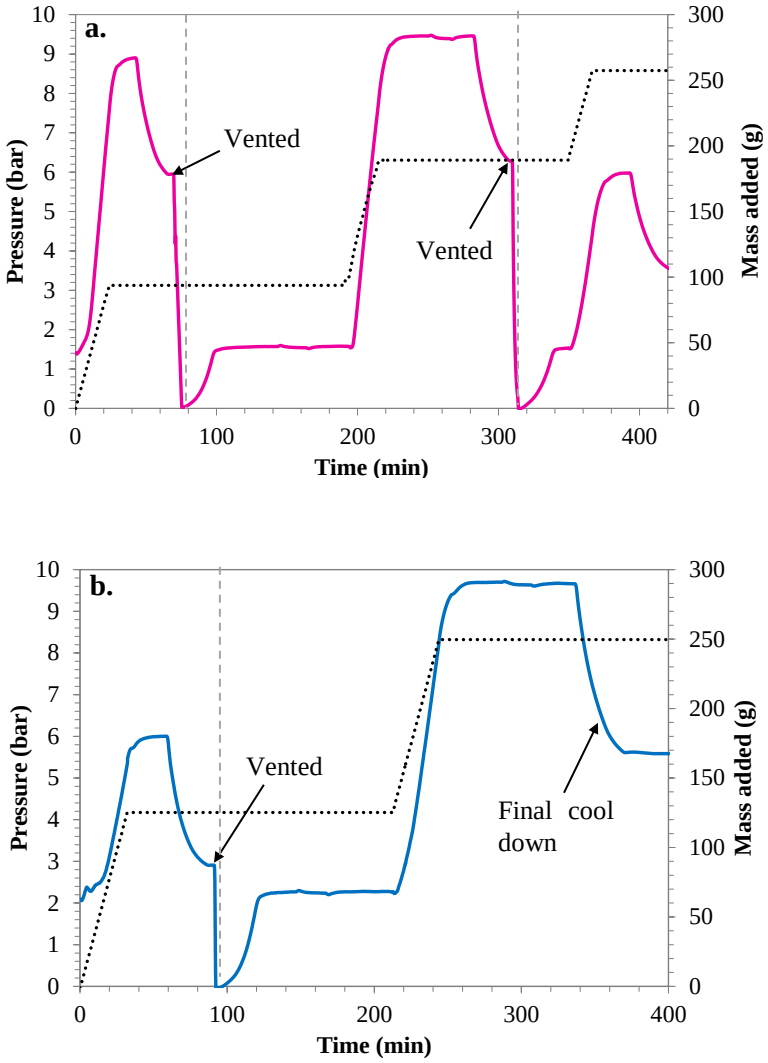

Figure 44. Pressure history of the *N*-oxidation of 3-picoline at two different temperatures using 1 g of catalyst. (a) 110 °C (run 5 from Table 14); (b) 125 °C (run 6 from Table 14). A dosing rate of 4 g/min and a stirring rate of 250 rpm were used in both experiments shown. Pressure is read in the left-hand ordinate and the mass added is read in the right-hand ordinate.

The conversion of 3-picoline obtained in the experiment at 125 °C (run 6 in Table 14) was 81%, while the conversion in the experiment at 110 °C (run 5 in Table 14) was only 63%. Despite the fact that the catalyst mass/temperature interaction was not found statistically significant, it can be seen from Figure 43 and Figure 44 that there is a quite noticeable interaction, which can make the difference in the efficiency of the process. The catalyst mass/temperature interaction shows that the effect of the catalyst at the low level changes with the different levels of the temperature. In other words, this interaction shows that a low mass of catalyst may be inadequate when operating at 110 °C, but it is much less adequate when operating at 125 °C. Although severe decomposition accompanied of pressure generation occurred in both experiments, there was much less decomposition in the experiment at 125 °C.

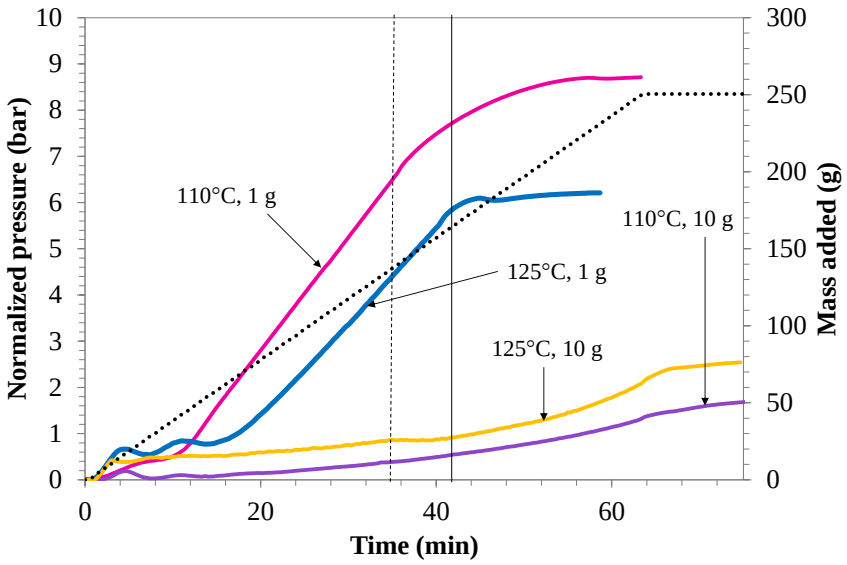

Figure 45. Normalized pressure increase during the *N*-oxidation of 3-picoline at different temperatures and mass of catalyst. All runs shown in this figure were performed at 400 rpm and 4 g/min (runs 13 to 16 in Table 14)

Similar conclusions can be drawn from measurements conducted at the high level of stirring rate (Figure 45). Although in this case, the measurement performed at 110 °C

and 1 g of catalyst (run 13 in Table 14) was benefited by the higher stirring, which contributed to a better distribution of hydrogen peroxide. In this measurement, more hydrogen peroxide was added before dosing had to be interrupted. However, because of the larger amount added, there was also more hydrogen peroxide accumulation. As a result, after dosing was stopped, the pressure was increased further by 1.84 bar.

From Figure 43 and Figure 45, it can be seen the benefit of the catalyst at the high dosing rate, at both high and low levels of temperature. It is also observed that when the catalyst mass is high, an increase in temperature provides no benefit, at least in the range of temperatures selected. This is consistent with the interaction plots shown in Figure 38. However, this finding disagrees with previous studies that indicate a positive effect of the temperature on the selectivity towards the *N*-oxidation reaction.[50, 51, 57] Overall, it can be concluded that the temperature can have a positive effect on the *N*-oxidation of alkylpyridines up to a certain level, where its effect becomes detrimental by promoting the thermal decomposition of hydrogen peroxide, particularly when combined with a large mass of catalyst.

Figure 46 shows runs 1-4 (see Table 14), which were performed at 250 rpm and 0.5 g/min. All runs performed were finished without interrupting dosing. From Figure 46, it can be seen that the experiment with the lowest pressure increase, and consequently the higher conversion of 3-picoline, was the experiment conducted at 110 °C and 10 g of catalyst. In contrast, the experiment with the highest pressure increase was the one performed at 125 °C and 1 g of catalyst.

The measurement at 110 °C and 1 g of catalyst in Figure 46 is of particular interest. It can be seen that the pressure increase is linear for most of the measurement up to the point where about 222 g of the hydrogen peroxide solution have been added. After this point, the slope of the pressure increase curve becomes much steeper. The linear increase of the pressure indicates that the reaction is limited by dosing and that the pressure

increase is the result of the reduction of the headspace (gas volume). As this indicates that the decomposition of hydrogen peroxide is insignificant up to this point, the conversion of 3-picoline can therefore be estimated at approximately 88%. Due to the sharp increase at the end of the experiment, the run at 110 °C and 1 g of catalyst, which seemed to be going smoothly and without significant decomposition, ended up having about the same increase as the measurement at 125°C and 10 g of catalyst.

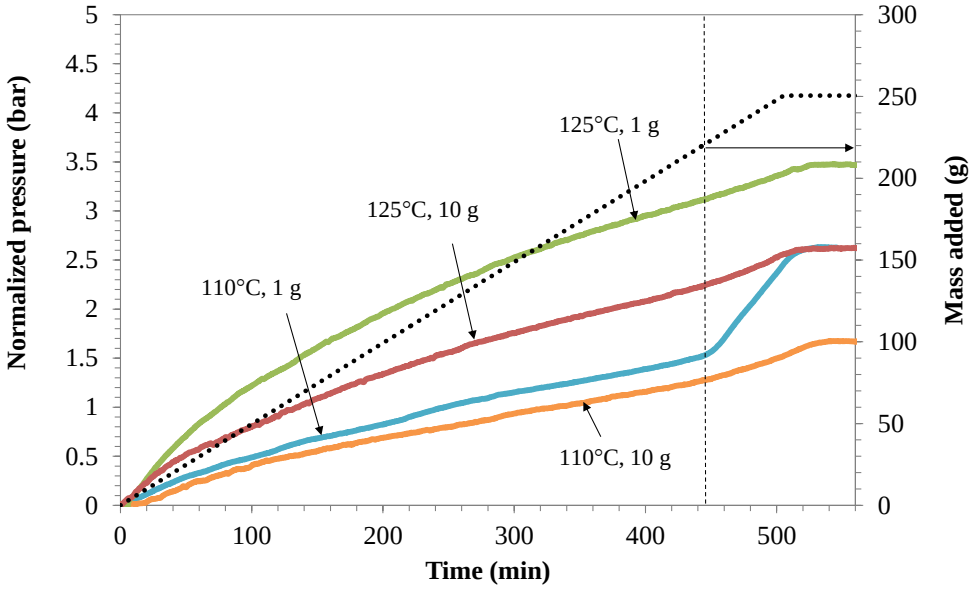

Figure 46. Normalized pressure increase during the *N*-oxidation of 3-picoline at different temperatures and masses of catalyst. All runs shown in this figure were performed at 250 rpm and 0.5 g/min (runs 1 to 4 from Table 14)

Figure 47 shows different runs performed at 0.5 g/min and 400 rpm. The same phenomenon as in Figure 46 was observed in the measurement at 110 °C and 1 g of catalyst; at a certain point, the slope of the pressure increase changes abruptly. However, in this case, the point where the slope changes occurs earlier, after 196 g of hydrogen peroxide solution have been added. At this point, the conversion of 3-picoline can be estimated at approximately 78%. Same as in Figure 46, the pressure increase in all

measurements shown in Figure 47 is linear up to a certain point, and then the pressure increase occurs much more rapidly.

From Figure 47, it can be seen that the measurements at 110 °C and 1 g of catalyst (run 9 in Table 14), 125 °C and 1 g of catalyst (run 10 in Table 14), and 125 ºC and 10 g of catalyst (run 18 in Table 14) follow almost the same pressure profile up to the point of the abrupt change. This abrupt change occurs at the point where the decomposition of hydrogen peroxide becomes more competitive. At this point, the concentration of 3-picoline is low enough to slow down the rate of the *N*-oxidation reaction. Because of this, hydrogen peroxide starts accumulating and the decomposition rate is accelerated.

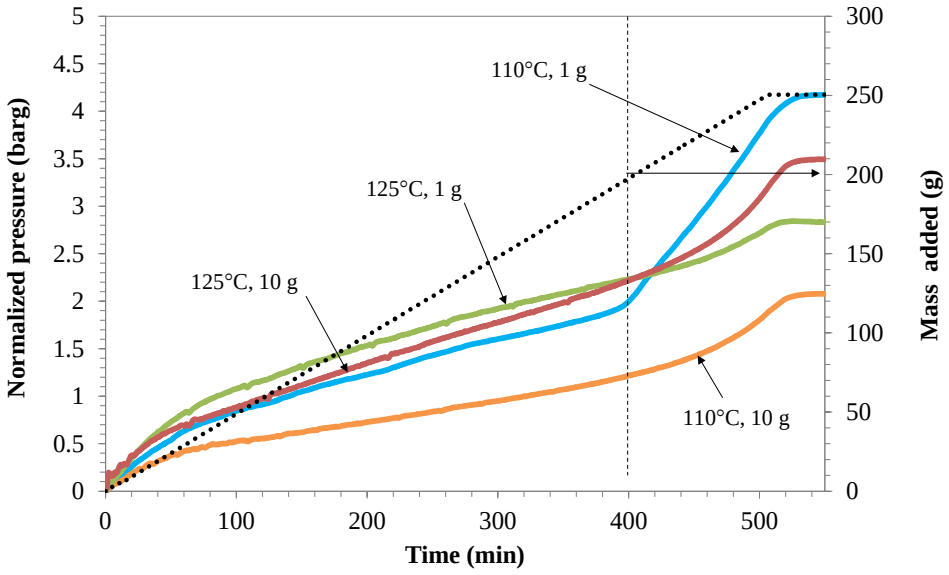

Figure 47. Normalized pressure increase during the *N*-oxidation of 3-picoline at different temperatures and catalyst mass (runs 9 to 12 in Table 14). All runs shown in this figure were performed at 0.5 g/min and 400 rpm

The plots in Figure 48 represent the interaction of catalyst and stirring rate, *i.e.*, it shows how the pressure changes when the experiments are run with the same mass of catalyst but different stirring rates, while the dosing rate and temperature are kept constant.

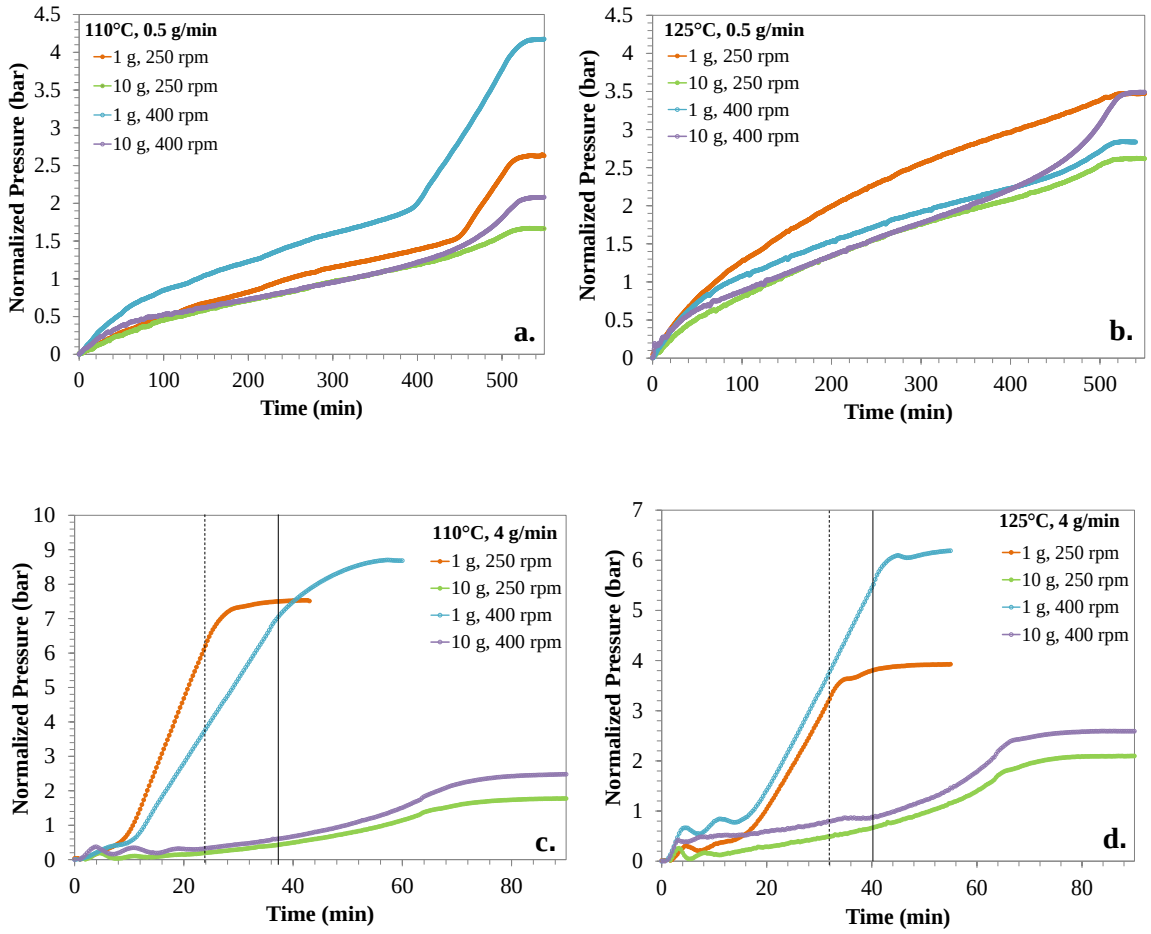

Figure 48. Normalized pressure during the *N*-oxidation of 3-picoline at different conditions. These plots represent the interaction of catalyst and stirring rate at constant temperature and dosing rate. a) 110 °C and 0.5 g/min (runs 1, 3, 9 and 12); b) 125 °C and 0.5 g/min (runs 2, 4, 10 and 16); c) 110 °C and 4 g/min (runs 5, 7, 13 and 15); d) 125 °C and 4 g//min (runs 6, 8, 11 and 14)

Although the catalyst-stirring rate interaction is not statistically significant according to the factorial design analysis, it can be seen in Figure 48 that there is a difference between experiments run at the same temperature, catalyst mass, and dosing rate but different stirring rate.

For the experiments performed at the high level of catalyst (10 g), it can be seen in Figure 48a-d that the experiments run at the high level of stirring rate (400 rpm) resulted

in higher pressure increases, and therefore, more decomposition and lower conversions. The normalized pressures are overlapped up to a certain point where the pressure of the experiment at higher stirring starts increasing slightly faster than that of the experiment at low stirring rate. This effect is more obvious in the experiments performed at a low dosing rate (Figure 48a-b). However, the difference in conversion for the experiments performed at the high levels of catalyst mass and stirring rate is equal or lower than 2%, which is close to the estimated experimental error of 1%. This finding indicates that the effect of the stirring rate when the mass of catalyst is high is practically insignificant, and that the differences observed in the normalized pressures may be purely visual. Nevertheless, these are preliminary observations. Mixing issues change with the size, geometry and configuration of a reactor, for which is necessary to perform appropriate mixing studies taking into account the specifics of the reactor to be used.

In contrast, most of the experiments performed at the low level of catalyst (1 g) seem to be benefited by the higher stirring rate, except the experiment performed at 110 °C, 1g and 0.5 g/min (run 9), which seemed to be affected negatively by the higher stirring rate.

The experiments performed at low catalyst (1 g) and high dosing rate (4 g/min) were favored by the high stirring rate (400 rpm), at both temperatures tested. In particular, the experiments performed at 110 °C, 1 g of catalyst and 4 g/min (runs 5 and 13) showed the biggest difference. The conversion obtained from the experiment with high stirring rate (run 13) was 11% higher than the corresponding experiment performed at low stirring rate (run 5). Figure 48c-d only show the first dosing step of runs 5, 6, 13, 14. The complete plots have already been shown in Figure 44a-b. In Figure 48d, which shows experiments conducted at 125 °C and 4 g/min, it seems like from the two experiments performed at low catalyst, the experiment performed at high stirring rate (run 14) presents a higher pressure increase than the respective experiment at low stirring rate (run 6). However, Figure **48**d only shows the first of two dosing steps of both

experiments; the final conversion obtained with the experiment at high stirring rate (run 14) was actually 2% higher than the experiment performed at low stirring rate (run 6).

5.2.2 Calorimetric analysis

A calorimetric analysis was conducted on the experiments performed as part of the factorial DOE in order to determine the heat of reaction, total energy released by the synthesis reaction, and power profiles during the experiments.

Calorimetric calculations were done based on an energy balance over the reactor previously shown in Equation 3. The dimensions of all terms in the equation are thermal power and the units used in calculations were Watt (W).

$$\dot{Q}_{rxn} = \dot{Q}_{flow} - \dot{Q}_{cal} + \dot{Q}_{dos} + \dot{Q}_{acc} + baseline \qquad \text{(Eq. 3)}$$

where

$\dot{Q}_{rxn}$ is the total power generated by both reactions, the *N*-oxidation of alkylpyridines and the decomposition of hydrogen peroxide

$\dot{Q}_{flow}$ is the power exchanged with the cooling medium (oil jacket)

$\dot{Q}_{cal}$ is the power from the electrical heater which is typically used during the calibrations, but can be also used during the experiment to assist fast heating; it is measured directly

$\dot{Q}_{dos}$ is the power needed to bring the dosed material to the temperature of the reaction mixture

$\dot{Q}_{acc}$ is the accumulated power. During isothermal operation this term is zero.

The term baseline includes the power due to stirring and the power losses

The power exchanged with the oil jacket, $\dot{Q}_{flow}$, can be calculated according to Equation 24:

$$\dot{Q}_{flow} = UA(T_r - T_j) \quad \text{(Eq. 24)}$$

where

U is the overall heat transfer coefficient, in W/($m^2 \cdot$°C);

A is the area of heat exchange (wet area), in m^2;

T_r is the temperature of the reactor, in °C; and

T_j is the temperature of the oil jacket, in °C.

The oil circulates in the jacket around the reactor at a very high speed, such that the difference between the temperature at the inlet and outlet of the jacket is practically zero. The power used to bring the dosed material to the reaction temperature, $\dot{Q}_{dos}$, is calculated using Equation 25:

$$\dot{Q}_{dosing} = \dot{m} C_p (T_r - T_{dos}) \quad \text{(Eq. 25)}$$

where

$\dot{m}$ is the flow mass of material dosed to the reactor

C_p is the heat capacity of the dosed material

T_{dos} is the temperature of the dosed material

As mentioned in Section 3.2.1, the lid of the reactor was heated with rapid circulating oil. It is expected that the dosing tube, which is inserted through the lid, would be heated up as well, along with the dosing material, particularly at low dosing rates. Since it was not possible to insert a thermometer inside the dosing tube, it has been assumed that the dosing temperature, T_{dos}, is equal to the ambient temperature in the laboratory. However, there is an unaccounted for power, which is provided to the dosed material as it crosses the lid.

The heat capacity, C_p, of the dosed material, *i.e.*, hydrogen peroxide 35 wt. % solution in water, was estimated as the weight-average heat capacity of the mixture, 3.635 J/(g·°C).

The *UA* and baseline values before and after the reaction are calculated by performing calibrations before dosing and following the reaction completion, according to the methodology of Papadaki and Nawada.[58] A calibration consists on applying a known constant power to the reaction mixture using an electrical heater for a determined period of time, typically 20 minutes. At steady state, *i.e.*, constant reactor and oil jacket temperatures, $\dot{Q}_{acc}$ is zero; in absence of reaction and dosing of material, the energy balance is rearranged and simplified as follows:

$$\dot{Q}_{cal} = UA\left(T_r - T_j\right) + baseline \qquad \text{(Eq. 26)}$$

Therefore, a plot of $\dot{Q}_{cal}$ versus $\left(T_r - T_j\right)$ gives a straight line where *UA* is the slope and the intercept with the y-axis corresponds to the $baseline$. Two points [$\left(T_r\text{-}T_j\right)$, $\dot{Q}_{cal}$] are the bare minimum to build the straight line. One point can be taken at steady-state before the electrical heater is turned on $\left(\dot{Q}_{cal} = 0\right)$, and the other point can be taken at steady-state while the electrical heater is supplying power to the reaction mixture ($\dot{Q}_{cal} = c$, where c is a constant). More calibrations result in a higher level of confidence in the value of UA and the $baseline$. In order to maintain the reactor contents at isothermal conditions before and during the calibration, the temperature of the jacket is automatically adjusted. Therefore, the quantity $\left(T_r - T_j\right)$ is different at different values of $\dot{Q}_{cal}$. Figure 49 illustrates the points used to estimate *UA* and the baseline.

The volume of the reaction mixture increases with dosing of material and so does the heat exchange area, *A*. Given the large amount of water in the reaction mixture, it is assumed that the transformation of the alkylpyridine into the corresponding *N*-oxide has an insignificant effect on the properties of the mixture, and consequently on the *U* value.

Since the dosing rate is constant, it is considered in this study that the *UA* and baseline vary linearly with the addition of hydrogen peroxide to the reactor.

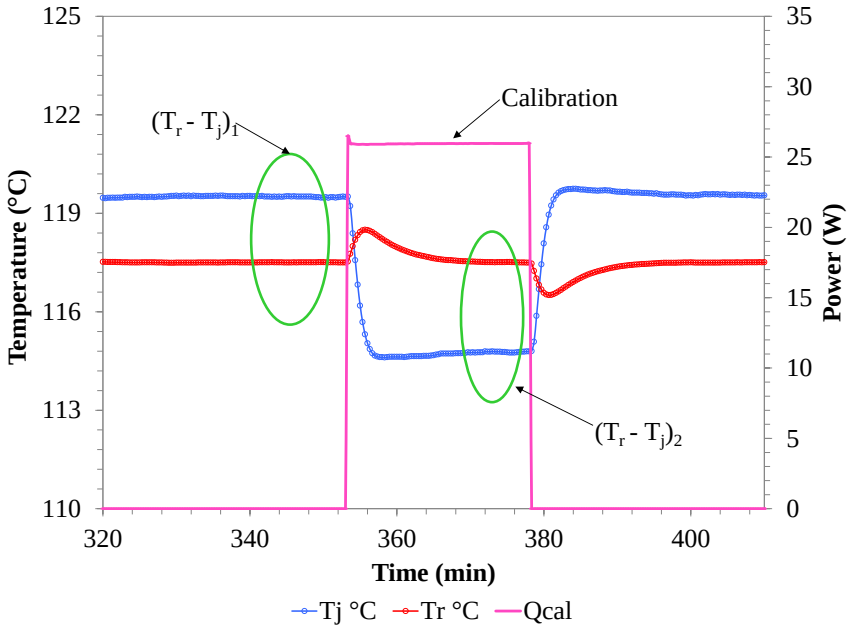

Figure 49. Typical reactor and jacket temperatures in the presence and absence of power supplied by the electrical calibration heater.

The total energy (in Joules) generated by the reaction, Q_{total}, can be calculated as the integral of $\dot{Q}_{rxn}$ over the total time of the reaction:

$$Q_{total} = \frac{\int_0^{t_f} \dot{Q}_{rxn}\, dt}{\int_0^{t_f} dt} \qquad \text{(Eq. 27)}$$

The energy generated by the decomposition of hydrogen peroxide, Q_{dec}, is calculated using the following equation:

$$Q_{dec} = -\Delta H_{dec} \cdot n_{H_2O_2\ dec} \quad [kJ] \qquad \text{(Eq. 28)}$$

where

ΔH_{dec} is the heat of decomposition of hydrogen peroxide, -98.3 kJ/mole[31, 32]

$n_{H_2O_2\,dec}$ are the moles of hydrogen peroxide decomposed, and are equal to twice the number of oxygen moles

The calculation of the oxygen moles at the end of the experiment to calculate the conversion of 3-picoline has been previously described in Section 5.1. However, it is also necessary to calculate the oxygen moles throughout the course of the reaction in order to calculate the power of the hydrogen peroxide decomposition. The calculation of the oxygen moles generated during the reaction is also based on pressure differences, as explained below.

Figure 50 shows a schematic description of the pressure changes that occur during the reaction. The reactor is initially sealed at atmospheric pressure and ambient temperature ($Pair_o$, T_o); the initial conditions are represented by the red dot in Figure 50. Then, the reactor is heated up to the desired reaction temperature (T_{rxn}), which causes an increase in the pressure. The pressure of the reactor right before dosing starts (point 1), is equal to:

$$P_1 = P_{vap1} + P_{air1} \quad \text{(Eq. 29)}$$

where P_{vap1} is the vapor pressure of the mixture at the temperature of the reaction and P_{air1} is the air pressure at the temperature of the reaction and at the initial reactor headspace volume. P_{air1} can be calculated using the ideal gas law as follows:

$$Pair_1 = Pair_o \times \frac{T_{rxn}}{T_o} \quad \text{(Eq. 30)}$$

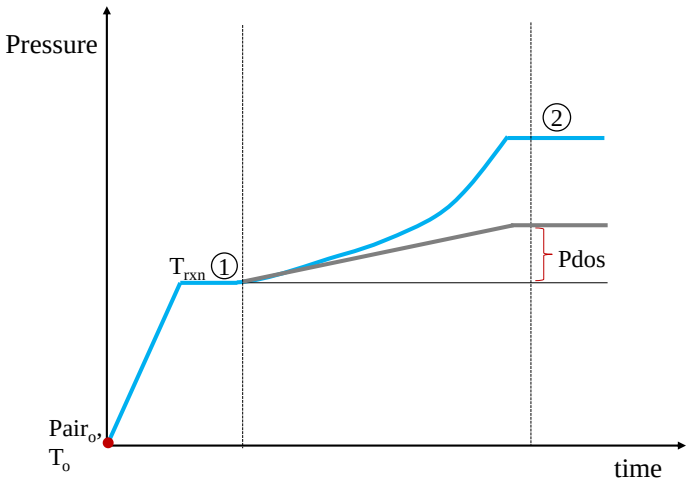

Figure 50. Schematic of the pressure changes during a typical 3-picoline *N*-oxidation experiment. The blue line represents the pressure of the reactor and the gray line represents the change in pressure due to dosing

Once dosing starts, the air pressure increases gradually due to the linear reduction of the headspace volume. The pressure at point 2 in Figure 50 corresponds to the pressure of the reactor after dosing has finished and the system has stabilized. The pressure at point 2 accounts for the air pressure at the final headspace volume, P_{air2}, the vapor pressure of the mixture, P_{vap2}, and the oxygen generated throughout the course of the reaction, P_{O_2}, as shown in the following equation:

$$P_2 = P_{vap2} + P_{air2} + P_{O_2} \quad \text{(Eq. 31)}$$

$Pair_2$ can be calculated from the ideal gas law as shown in Equation 32:

$$P_{air2} = P_{air1} \times \frac{V_i}{V_f} \quad \text{(Eq. 32)}$$

Where V_i and V_f are the initial and final headspace volumes, respectively. The difference between the air pressure at the final headspace volume and the air pressure at the initial

headspace volume is equal to the pressure increase due to the reduction of the headspace, due to dosing, ΔP_{dos}:

$$\Delta P_{dos} = P_{air2} - P_{air1} \quad \text{(Eq. 33)}$$

Therefore, the total pressure increase throughout the experiment is equal to:

$$\Delta P = P_2 - P_1 = \left(P_{vap2} + P_{air2} + P_{O_2}\right) - \left(P_{vap1} + P_{air1}\right) \quad \text{(Eq. 34)}$$

Due to lack of information in the literature, it was assumed that the vapor pressure of the initial and final mixtures is equal to the vapor pressure of water. Since the reaction is carried out isothermally, the vapor pressure terms, P_{vap1} and P_{vap2}, are cancelled out. Equation 34 can then be written as:

$$\Delta P = P_{O_2} + P_{dos} \quad \text{(Eq. 35)}$$

The pressure corresponding to the oxygen generated throughout the reaction can be calculated from Equation 36:

$$P_{O_2} = \Delta P - P_{dos} \quad \text{(Eq. 36)}$$

The oxygen moles generated during the reaction are then calculated with the ideal gas law and the moles of hydrogen peroxide decomposed are calculated by multiplying the oxygen moles by two.

Once the moles of hydrogen peroxide decomposed and the power of the decomposition are calculated, the heat of the *N*-oxidation reaction, Q_{Nox}, is calculated from the difference between the total heat and the heat produced from the decomposition:

$$Q_{Nox} = Q_{total} - Q_{dec} \quad \text{(Eq. 37)}$$

The enthalpy of the *N*-oxidation, ΔH_{Nox}, can be calculated dividing the heat of the *N*-oxidation by the number of moles of alkylpyridine reacted:

$$\Delta H_{Nox} = \frac{Q_{Nox}}{alkylpyridine\ moles\ reacted} \quad \left[\frac{J}{mol}\right] \quad \text{(Eq. 38)}$$

Table 16 summarizes the UA, baseline, energy released, and heats of reaction calculated for the experiments performed in this study. The heats of reaction found for the *N*-oxidation of 3-picoline at different conditions were between 120 and 190 kJ/mol. Both, the upper and lower values are consistent with previously reported values for the *N*-oxidation of 2-picoline.[59, 62] However, it must be pointed out that for measurements performed at the high level of stirring rate, power and heat of reaction calculations have a larger error associated to them. This is due to the fact that the heat transfer area affects a different quantity of reactant and therefore the coefficient calculated (UA) is not the same throughout the reaction vessel. Due to the high stirring rate, a deep vortex is formed. Consequently, the heat transfer to the liquid in the upper part of the reactor is different to the heat transfer in the lower part of the reactor.

It can also be seen in Table 16 that the heat generated by the decomposition in most cases was about 2-3% of the total heat generated, which is low compared with the error of the measurement. The exception were those experiments performed with low level of catalyst and high level of dosing rate (runs 5, 6, 13 and 14), for which the heat generated by the decomposition was up to 28% of the total energy released. Saenz-Noval[62] previously reported heats of decomposition accounting for 1% of the total energy release during the *N*-oxidation of 2-picoline. The experiments by Saenz-Noval[62] were done in slightly different conditions (more water added to initial mixture). However, the difference indicates that 3-picoline is slightly more difficult to oxidize.

Table 16. UA, baseline, energy released and heats of reaction calculated for the experiments discussed in this section

Run	Temp. (°C)	Catalyst (g)	Dosing rate (g/min)	Stirring rate (rpm)	UA1 (W/C)	UA2 (W/C)	Baseline1	Baseline2	Qtotal (kJ)	Qdec (kJ)	QNox (kJ)	ΔHnox kJ/mole
1	110	1	0.5	250	3.61	4.60	6.89	5.66	420.45	9.02	411.43	165
2	125	1	0.5	250	3.74	4.71	10.77	11.33	412.25	12.29	399.96	163
3	110	10	0.5	250	3.63	4.93	8.00	8.24	425.37	5.15	420.23	166
4	125	10	0.5	250	3.85	4.83	11.32	11.96	408.84	8.85	399.99	161
5	110	1	4	250	3.92	5.48	6.76	10.26	339.45	95.76	243.69	150
6	125	1	4	250	3.75	4.80	8.13	8.62	384.76	47.80	336.96	160
7	110	10	4	250	3.85	4.78	6.71	6.09	352.50	5.90	346.60	138
8	125	10	4	250	3.79	4.79	9.84	9.74	357.79	6.94	350.85	140
9	110	1	0.5	400	2.57	5.27	17.64	8.97	459.62	15.84	443.78	183
10	125	1	0.5	400	4.92	5.54	17.02	15.86	473.15	9.69	463.46	187
11	125	10	4	400	3.03	5.65	17.02	16.24	325.62	8.66	316.96	127
12	110	10	0.5	400	2.44	5.41	11.19	9.53	451.20	7.26	443.94	177
13	110	1	4	400	4.73	5.24	17.64	9.41	362.13	66.28	295.85	154
14	125	1	4	400	4.92	5.48	25.39	16.00	388.32	43.12	345.20	160
15	110	10	4	400	2.14	5.25	9.30	7.77	304.88	9.44	295.44	119
16	125	10	0.5	400	2.79	5.62	17.32	15.36	431.37	12.67	418.70	171
17	117.5	5.5	2.25	325	4.41	5.04	14.68	10.86	391.44	8.30	383.14	154
18	117.5	5.5	2.25	400	4.41	5.42	14.68	10.92	361.99	9.26	352.74	142

Figure 51a-b show the total power generated in the eight experiments conducted at the low level of dosing rate (0.5 g/min). It can be seen in Figure 51a-b that the amount of power generated was approximately the same and practically constant, even at different temperatures and catalyst concentrations, indicating a similar rate of reaction. However, the power calculated at 400 rpm is slightly larger than the power generated at 250 rpm most likely owing to the impact of the error in the assessment of heat effects and the size of the increased heat transfer area formed because of the vortex. The power profiles obtained confirm once again that the reaction is controlled by dosing. It can also be observed in Figure 51 that the there is a slight power increase around 260 min, time at which 130 g of hydrogen peroxide solution have been added (52% of total mass). This phenomenon is more noticeable in Figure 51a (250 rpm). The reason of this increase has not been confirmed. However, it is possible that this phenomenon is related to the evaporation in the mixture, *i.e.*, once dosing starts, the vapor pressure of the mixture increases drastically as the system tries to find a new equilibrium, but as the concentration of water increases in the mixture, the vapor pressure increase is slower. Therefore, it is likely that the energy-consuming evaporation process becomes much less significant at the point where the increase in the power profiles is observed.

It can also be observed in Figure 51a-b that once dosing is finished, the power decreases very rapidly to zero. This indicates that there is very little accumulation in the system and that the reaction finishes shortly after dosing.

Figure 52 shows the power profiles generated during the *N*-oxidation of 3-picoline at 110 °C, 1 g catalyst, 0.5 g/min and 250 rpm. The total power presents some oscillation during the first 150 minutes. This is due to the temperature fluctuations during this time, which is likely due to the strong heat of solution. Because the initial mixture is almost pure 3-picoline, the heat of solution is strong.

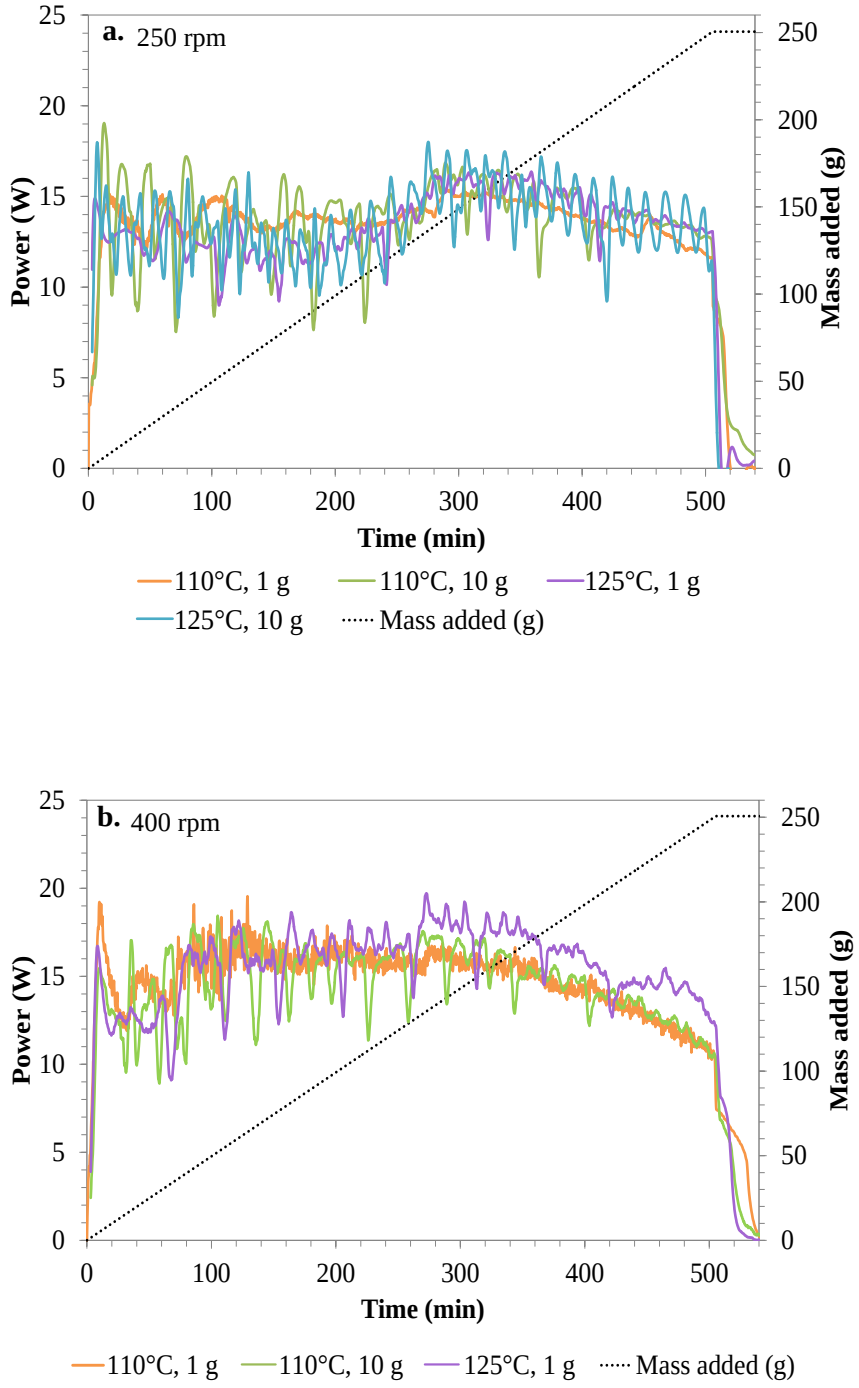

Figure 51. Total power generated during the *N*-oxidation of 3-picoline at different temperatures and catalyst mass using a dosing rate of 0.5 g/min and a stirring rate of a) 250 rpm (runs 1-4 in Table 16) and b) 400 rpm (runs 9,10, 12, 16 in Table 16)

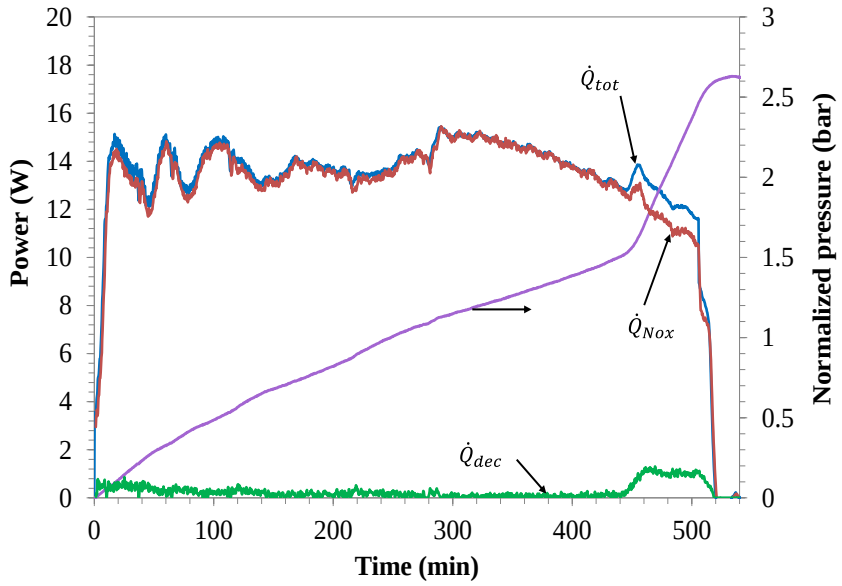

Figure 52. Total, *N*-oxidation and decomposition power generated during the *N*-oxidation of 3-picoline at 110°C, 1 g catalyst, 0.5 g/min and 250 rpm (run 1 in Table 16), along with the normalized pressure profile of the measurement, which is read on the right axis

The total power generated is practically equal to the power of the *N*-oxidation reaction until approximately 445 minutes, which corresponds to 222 g (2.28 moles) or 89% of hydrogen peroxide added. At this point, it is clear that the power of the decomposition increases from zero to approximately 1.5 W. This power increase is also observed as a small peak of the total power profile. At the same time, the pressure starts increasing dramatically (see Figure 46). This is the point where the decomposition of hydrogen peroxide becomes more competitive. It is not necessarily the point where the kinetic regime starts, as it can be seen that the *N*-oxidation power, and consequently, the total power, start decreasing at around 300 min, before the decomposition power and the rate of pressure rise start increasing more dramatically. Additionally, in this particular experiment, it is observed that the power generated by the decomposition is constant, indicating that the decomposition is also controlled by the availability of hydrogen peroxide; the same can be seen in the pressure profile, which although it increases at a faster rate, it continues to be linear.

Figure 53a-b show the averaged power of decomposition for different experiments. From Figure 53a, it is observed that during the first 150 minutes, it seems like there is more decomposition than at the end of the experiment. However, the power estimation during this time is not accurate. The power of decomposition is calculated from pressure differences, and due to temperature fluctuation at the beginning of dosing, the pressure also fluctuates. In addition, there is a dramatic change in the vapor pressure of the system. The fact that a stronger fluctuation is observed in the curves from experiments at 125 °C indicates that the effect of the vapor pressure was not completely eliminated from the calculations.

After the unstable period in Figures 54a, the power of decomposition drops to a value below 1 W. Then, in the last 100 min, the decomposition power increases due to the decrease in the concentration of 3-picoline, which leads to accumulation of hydrogen peroxide, and consequently, to an increase in the rate of the decomposition. It can also be seen that the decomposition becomes significant at around the same time (445 min) for all experiments shown in Figure 53a, although it is more intense for the experiment conducted at 110 °C and 1 g of catalyst (run 1 in Table 16).

Similar results were obtained from the experiments performed at 400 rpm, shown in Figure 53b. However, the fluctuation at the beginning of the experiments only lasts about 100 min. After that, the power of decomposition drops to a value below 0.5 W. The decomposition of hydrogen peroxide becomes more significant for most experiments shown in Figure 53b at 415 min, although its intensity varies according to the operating conditions. In the case of the experiment at 110 °C and 1 g of catalyst (run 9 in Table 16), the decomposition starts increasing at 380 min and remains constant until the end of the dosing period, indicating that the decomposition is controlled by the availability of hydrogen peroxide, as discussed earlier.

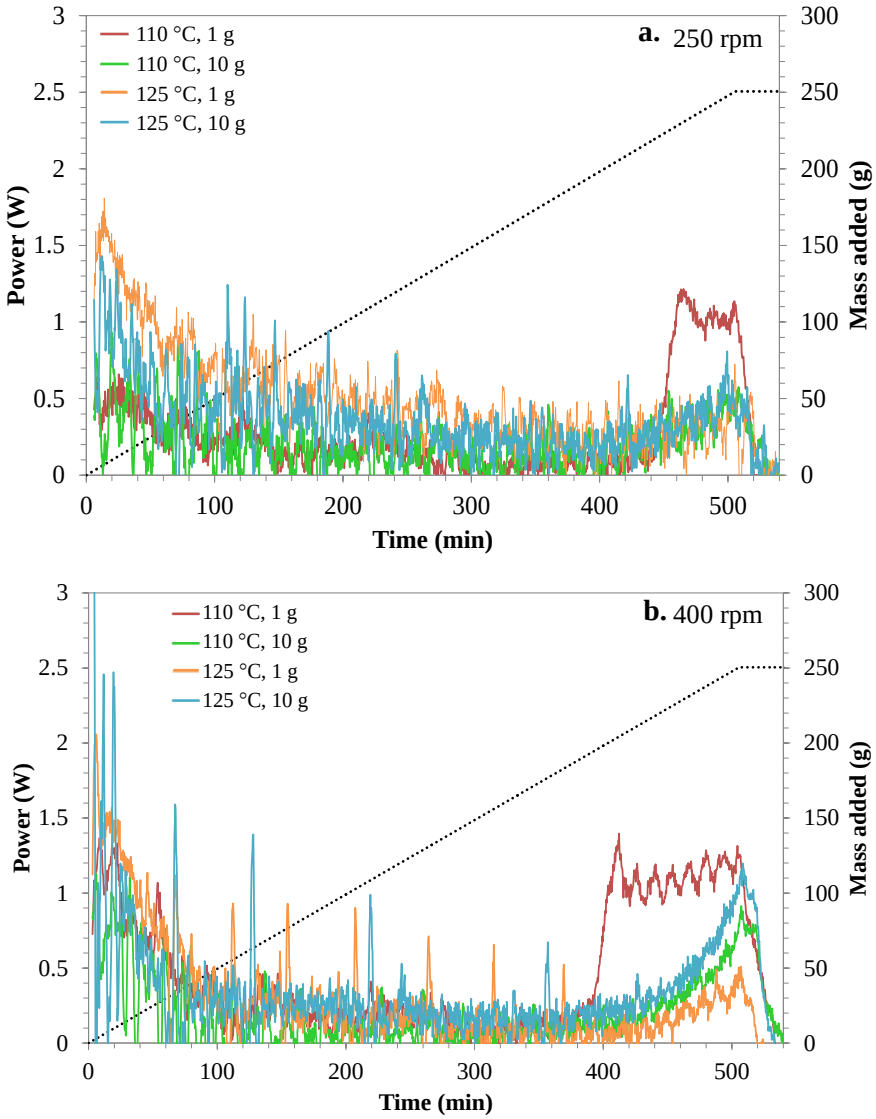

Figure 53. Power generated by the decomposition of hydrogen peroxide during the *N*-oxidation of 3-picoline at different temperatures and amounts of catalyst, using a dosing rate of 0.5 g/min and stirring rate of a) 250 rpm (runs 1-4 in Table 16) and b) 400 rpm (runs 9,10, 12, 16 in Table 16)

Figure 54 shows the power profiles generated during an experiment at the low levels of temperature, catalyst and stirring rate and high level of dosing rate (run 5 in Table 16). This was the experiment where the lowest conversion of 3-picoline was obtained. Due to severe hydrogen peroxide decomposition, it was necessary to perform this experiment in

three dosing steps. During the first dosing step, 93.54 g of hydrogen peroxide solution were added; 89.14 g were added in the second step, and 68.25 g were added in the third one.

In a single dosing step of the experiment shown in Figure 54, more decomposition power is generated than in any other complete experiment performed with a higher mass of catalyst or with a lower dosing rate. In the first two dosing steps, the decomposition power is as high as 30 W, while in the third step is as high as 20 W. The extent of the decomposition can be also observed from the amount of power generated once dosing has stopped. In the first step, dosing stops at 24.7 min, but the reaction does not finish until 32 min (7.3 min after). In the second step, dosing stops at 21.7 min and the reaction finishes at 32.7 min (10.3 min after). In the third step, dosing stops at 17.7 min and the reaction finishes at 29.7 min (12 min after). Even though the mass dosed in the second and third steps is lower than the dosed mass in the first step, the reaction takes longer to finish due to the high accumulation of hydrogen peroxide.

In the first dosing step of the experiment shown in Figure 55, it can be seen that there is an ‘overshoot’ in the power. This is due to the heat of solution and initial contact between the two reactants. In the second dosing step, the overshoot is smaller and in the third dosing step, it is barely noticeable. As hydrogen peroxide is added to the reactor, the concentration of water grows very rapidly. Therefore, after a certain mass of hydrogen peroxide has been added, the heat of mixing is negligible.

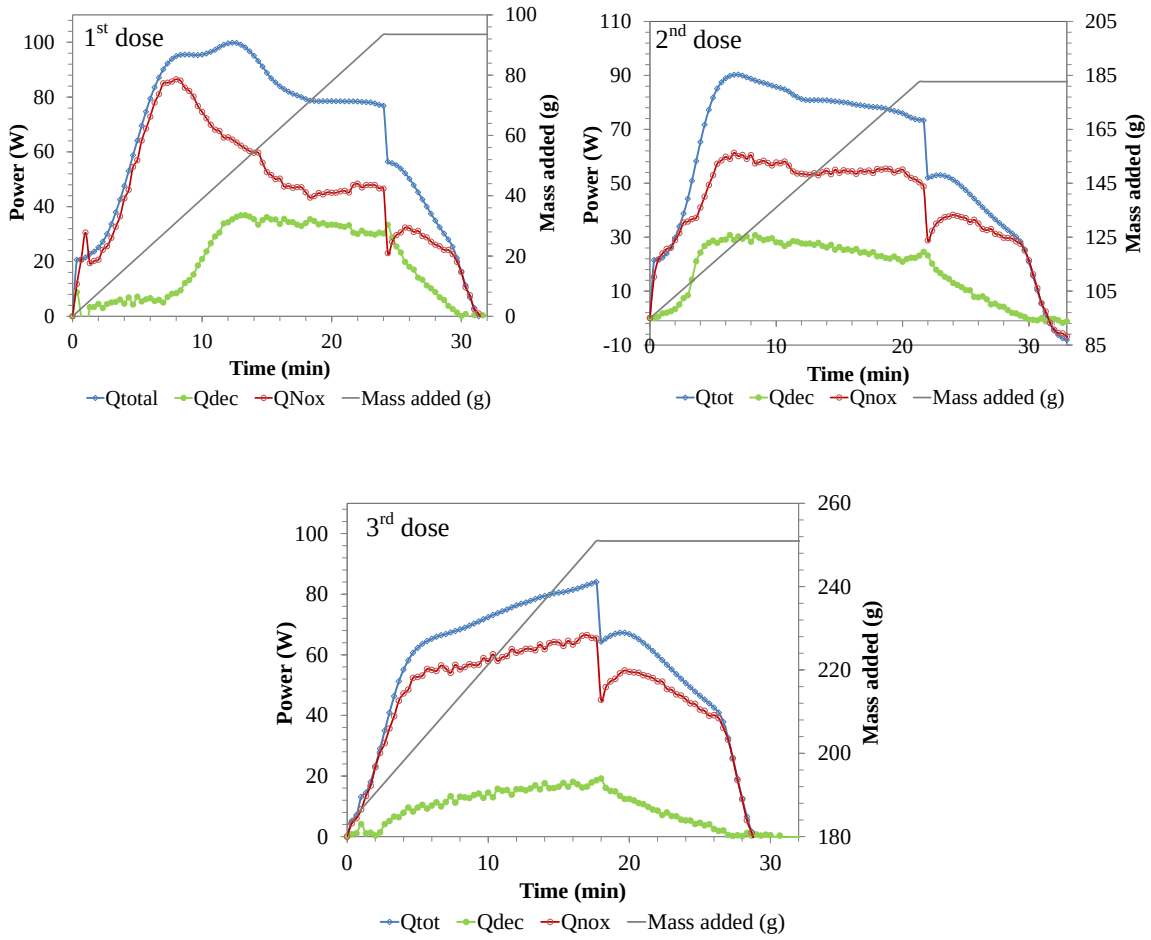

Figure 54. Total, *N*-oxidation and decomposition power profiles for the *N*-oxidation of 3-picoline at 110°C, 1 g of catalyst, 4 g/min and 250 rpm (run 5 in Table 16)

In the first and second dosing steps, it can be seen that after the 'overshoot', the power of the reaction is practically constant until dosing stops, despite the high dosing rate used in the experiment. Once dosing stops, the power of both, the *N*-oxidation and the decomposition decrease. It can also be observed that the total, and therefore, the *N*-oxidation power drop abruptly when dosing is stopped. Because of the high dosing rate used in this experiment, the ending of dosing causes an upset in the system. In addition, as mentioned earlier, it has been assumed in the calculations that the dosing temperature, T_{dos}, is equal to the ambient temperature in the laboratory. However, T_{dos} was likely higher than the ambient temperature, as the temperature of hydrogen peroxide could

have been increased while crossing the heated lid of the reactor. This error in the calculation of $\dot{Q}_{dos}$ is reflected in the calculation of the total and *N*-oxidation power.

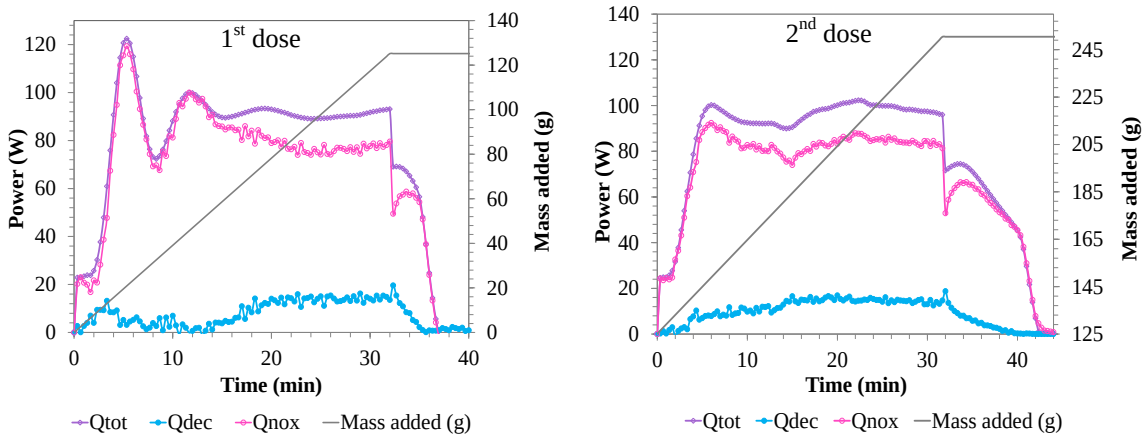

Figure 55. Total, *N*-oxidation and decomposition power profiles for the *N*-oxidation of 3-picoline at 125°C, 1 g of catalyst, 4 g/min and 250 rpm (run 6 in Table 16)

Figure 55 shows the power profiles generated during an experiment at the low levels of catalyst and stirring rate and high levels of temperature and dosing rate (run 6 in Table 16). It can be seen that the results are similar to those of Figure 54. However, the power generation is slightly higher due to the higher temperature. Also, due to the higher temperature, the accumulation of hydrogen peroxide is lower, and the maximum power generated by the decomposition is always below 20 W. Nonetheless, as shown in Figure 44 the pressure generated under the conditions of this experiment was high, which represents a hazardous situation.

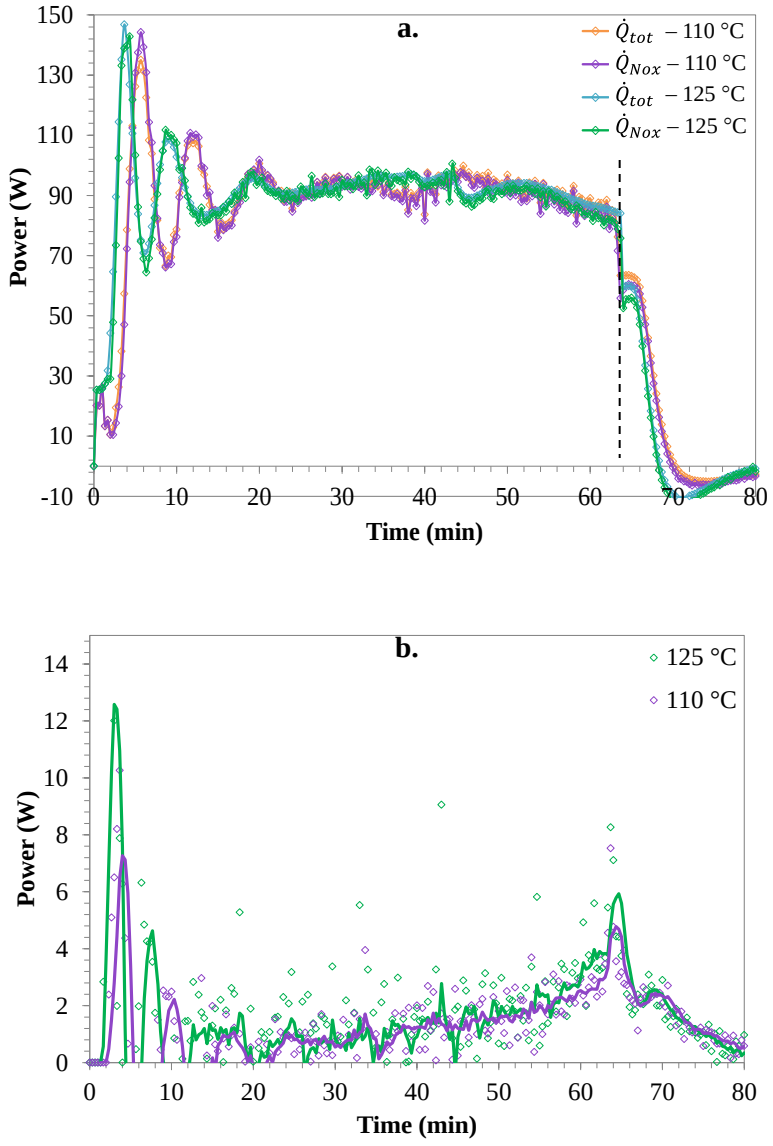

Figure 56. Power profiles for the *N*-oxidation of 3-picoline at two different temperatures using 10 g of catalyst, a dosing rate of 4 g/min and a stirring rate of 250 rpm. a) Total power; b) Averaged decomposition power

Figure 56a-b show the power profiles obtained from experiments conducted at high levels of catalyst mass and dosing rate, and different temperatures (runs 7 and 8 in Table 16). From Figure 56a, it can be seen that, similar to other experiments, there is some

fluctuation in the power profiles due to the temperature instability at the beginning of the reaction. After that, the power is practically constant until dosing is finished. By the time dosing stops (63.3 min), enough hydrogen peroxide has accumulated, such that both the *N*-oxidation and the decomposition continue, although the power generation decreases rapidly.

The averaged power of decomposition (Figure 56b) also presents some fluctuation in the first 15 min. As mentioned before, this is an inherent flaw in the calculation of decomposition power due to the variation of pressure with small temperature changes, and the drastic change in vapor pressure of the mixture. After the unstable period, the averaged power of the decomposition is below 2 W, and then increases toward the end of dosing due to the drop in concentration of 3-picoline. Once dosing finishes, the decomposition power decreases to zero. Overall, the decomposition power is very low compared to the average total power, which is approximately 90 W. The decomposition power accounts for only 1.7 and 1.9% of the total energy released for the experiments at 110 °C and 125 °C, respectively. Therefore, the power of the *N*-oxidation is practically equal to the total power throughout most of the experiment, which demonstrates the high efficiency achieved.

As can be seen in Figure 56a the power generated in both experiments is approximately the same, even though the temperature difference is 15 °C. This indicates that the reaction proceeds at approximately the same rate, which is equal to the dosing rate. Due to the high mass of catalyst used, the *N*-oxidation occurs very fast and its rate is limited by the availability of hydrogen peroxide. Similar power profiles were obtained for the experiments performed at the same conditions as the experiments shown in Figure 56, but using the high level of stirring rate, 400 rpm (runs 11 and 15 in Table 16).

It is worth pointing out that the heat generated during the experiments shown in Figures 55 to 57 was very high and fast. In some cases, the power output exceeded 100 W. This

fast and intense power generation would be difficult to handle by a typical batch or semi-batch reactor, since in general, these types of reactors have a heat removal capacity of approximately 30 W/L. Therefore, a typical semi-batch reactor would not be able to effectively remove the heat generated by the reaction under the conditions used for the experiments shown in Figure 54 to 55, and a runaway reaction would occur. In addition, not only a reaction under these conditions could overload the cooling system, but also the control system. Since the reaction occurs very fast, the heat of reaction goes from zero to 90-100 W almost immediately, *e.g.*, in Figure 54, the power went from zero to 90 W in approx. 7 min. However, a different type of reactor arrangement would probably be able to remove power more efficiently, as explained in Section 8.

5.3 Conclusions

The *N*-oxidation of 3-picoline has been studied in two different isothermal reaction calorimeters using a closed reactor at different conditions so as to test the effects that different parameters have on the hazards and the efficiency of the *N*-oxidation. The main findings are summarized below.

Preliminary experiments performed in the HEL-SIMULAR with the *N*-oxidation of 3-picoline demonstrated that higher temperatures can result in very high 3-picoline conversions and can dramatically decrease the amount of hydrogen peroxide which decomposes. In addition, a small quantity of catalyst may be sufficient for an efficient reaction performance when operation is at higher temperatures. Preliminary experiments also provided evidence that a careful selection of inert materials and a different reactor design may practically completely eliminate hydrogen peroxide decomposition.

Based on preliminary results, a full 2^4 factorial design of experiments was used to study the effect of temperature, catalyst mass, dosing rate and stirring rate on the conversion of 3-picoline. The factorial analysis revealed that the most influencing effects on the

conversion of 3-picoline are the mass of catalyst, the dosing rate, and the interaction between those two factors, with the effect of the catalyst mass being the largest. Combinations of low catalyst mass and high dosing rate are detrimental for the process, as they allow the accumulation of hydrogen peroxide in the reactor. The accumulation of hydrogen peroxide leads to a high rate of decomposition, since the rate is proportional to the square of the concentration of hydrogen peroxide. In contrast, the use of low dosing rates, combined with either a high or low mass of catalyst, does not allow hydrogen peroxide to accumulate; thus, the *N*-oxidation reaction becomes more competitive.

There is clear evidence that 3-picoline *N*-oxidation at 125 °C is not significantly better than operation at 110 °C. In fact, more decomposition was observed at 125 °C, particularly when a large mass of catalyst was used, likely because this temperature is higher than the onset temperature of the thermal decomposition of hydrogen peroxide, and because the presence of phosphotungstic acid accelerates the decomposition of hydrogen peroxide. Therefore, an increase in the temperature of the reaction and the mass catalyst of catalyst used is beneficial only up to certain extent.

There is no optimum operating condition for the *N*-oxidation of 3-picoline. Instead, there is a set of conditions that would minimize the decomposition of hydrogen peroxide and make the process inherently safer by practically eliminating the hydrogen peroxide decomposition, limiting the accumulation in the reactor, and eliminating the need to use an excess of hydrogen peroxide. The set of conditions consist of the appropriate combination of temperature, mass of catalyst and dosing rate.

Additional information about the *N*-oxidation of 3-picoline was obtained from the pressure history of the experiments, which revealed the point at which sufficient hydrogen peroxide has accumulated such that the decomposition becomes more competitive. However, the evaluation of the *N*-oxidation and decomposition rates via the

measurement of the pressure has inherent inaccuracies due to the lack of sufficient thermodynamic data regarding the vapor pressure of the mixture.

The heat of reaction for the *N*-oxidation of 3-picoline was found to be between 120 and 190 kJ/mole, which is in agreement with previous works. The evaluation of power generation showed that at high dosing rates, the power generated by the reaction may overload the cooling and control systems of a typical batch or semi-batch reactor as the power generation is high and fast. However, a different reactor configuration may allow a more efficient heat removal.

6. STUDY OF THE *N*-OXIDATION OF HIGHER ORDER ALKYLPYRIDINES USING ISOTHERMAL CALORIMETRY

This section presents the results of isothermal experiments to study the *N*-oxidation of 3,5-lutidine, 2,6-lutidine, and 2,4,6-collidine. Preliminary experiments with 3,5-lutidine were conducted in the HEL-SIMULAR isothermal calorimeter to study the effect of an increase of temperature on the *N*-oxidation reaction. Additional experiments with 3,5-lutidine *N*-oxidation were conducted in the RC1*e* to determine the influence of catalyst mass and dosing rate on the reaction, as well as the effect of the phase separation. The results of isothermal experiments conducted with 3,5-lutidine are discussed in Section 6.1 and 6.2. Experiments performed to study the *N*-oxidation of 2,6-lutidine and 2,4,6-collidine were performed in the RC1*e* and the results are discussed in Section 6.3. A calorimetric analysis to determine the power output and the heat of reaction of the *N*-oxidation of the different alkylpyridines studied here is also included in this section.

6.1 Study of the *N*-oxidation of 3,5-lutidine Using the HEL-SIMULAR Isothermal Calorimeter

Preliminary experiments with 3,5-lutidine were conducted in the HEL-SIMULAR isothermal calorimeter to study the effect of temperature on the *N*-oxidation reaction. The experiments consisted on loading 190 g of 3,5-lutidine in the reactor (1.77 moles), along with 6.33 g of catalyst dissolved in 15 g of water. Then, the reactor was sealed at atmospheric pressure and the mixture was heated up to 80 °C, when it was vented and sealed again at atmospheric pressure. The reaction mixture was then brought to the desired temperature of reaction. After a period of temperature stabilization, a calibration was performed. After that, a stoichiometric amount of aqueous solution of hydrogen peroxide 35 wt. % (172.3 g) was added at a slow rate of 0.24 g/min in order to prevent accumulation in the reactor. Once the dosing step finished, the reaction was allowed to

reach completion, and then another calibration was performed. The reactor was then cooled down to ambient temperature.

Table 17 shows the details of the preliminary measurements performed in the HEL-SIMULAR. The first two measurements in Table 17 were conducted to test the reproducibility of the experiments. However, toward the end of run 1, the connection between the computer and the balance was lost, which caused the pump to add an excess of hydrogen peroxide at a faster rate. Figure 57 shows the pressure increase during runs 1-4. It can be seen that the two experiments at 110 °C (runs 1 and 2) follow exactly the same path up to the point of the problem with the balance. The conversion obtained in runs 1 and 2 differ by 2.2% because of the excess added in run 1. Despite this issue, the two experiments confirmed the reproducibility of the experiments.

Besides confirming the reproducibility of the experiments, run 1 has been shown here to illustrate the potential hazard of a pump malfunction. Although the problem in run 1 was related to the balance, the consequences were the same as if it had been a pump malfunction. The problem with the balance lasted for 10 minutes before it was detected, and the fast addition during this period was enough to cause a pressure increase of 0.25 bar. At a large scale, a pump malfunction like the one shown here could lead to catastrophic consequences.

From Figure 57, it can be seen that the experiment performed at 120 °C (run 3) follows the same pressure profile as runs 1-2, despite the 10 °C temperature difference. This indicates that the reactions occurred at the same rate, which was controlled by the dosing of hydrogen peroxide to the reactor. Also, the moles decomposed in runs 2 and 3 and the conversion of 3,5-lutidine obtained are the same.

Table 17. Details of experiments with 3,5-lutidine in the HEL-SIMULAR calorimeter. Initial mass of 3,5-lutidine: 190 g (1.77 moles); catalyst mass: 6.33 g; stirring rate: 250 rpm; dosing rate: 0.24 g/min; P_o (pressure at 80 °C, when the reactor was sealed): 0.99 bar

Run		Temp. (°C)	Mass dosed (g)	P_i (bar)	P_f (bar)	$\triangle P^*$ (bar)	O_2 moles (nO_2)	H_2O_2 moles decomp.	H_2O_2 moles reacted in *N*-oxidation	3,5-lutidine conversion %
1		110	178.3	1.22	2.86	1.64	0.083	0.165	1.670	94
2		110	172.9	1.25	2.72	1.47	0.074	0.148	1.632	92
3		120	172.4	1.48	2.94	1.46	0.071	0.142	1.632	92
4	Dose 1	125	116.9	1.71	3.85	2.14	0.111	0.222	0.981	55
	Dose 2	125	57.1	2.04	2.68	0.64	0.031	0.062	0.525	85

Notes:

P_i is the pressure of the mixture at the temperature of reaction, before dosing

P_f is the pressure of the mixture at the temperature of reaction, after dosing, once the reaction has reached completion

$*\triangle P = P_f - P_i$

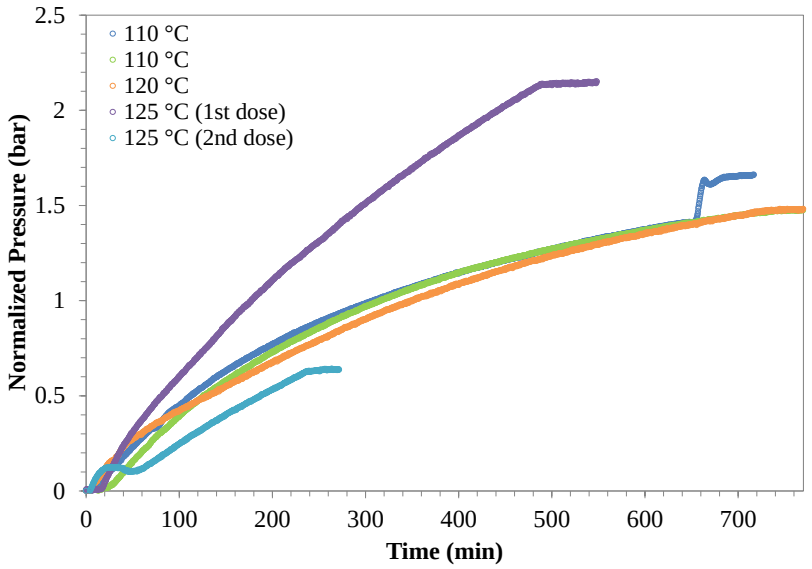

Figure 57. Normalized pressures during the *N*-oxidation of 3,5-lutidine at different temperatures using 6.33 g of catalyst (runs 1-4 from Table 17)

During the experiment conducted at 125 °C (run 4), the pressure generated reached the maximum operating limit of the reactor. For this reason, it was necessary to interrupt dosing, cool down the reactor to 80 °C and vent it. After that, the reactor was heated up again to the reaction temperature and dosing was resumed.

The *N*-oxidation of 3,5-lutidine is initially mass-diffusion controlled because 3,5-lutidine is not soluble in water. Thus the reacting mixture forms two phases, an aqueous phase where the catalyst is dissolved, and an organic phase. This is due to the limited solubility of 3,5-lutidine in water in a wide range of temperatures and concentrations.[90, 91] Consequently, the reaction occurs mostly at the interface of the two phases.

Typically, increased mixing, *i.e.*, higher stirring rates, helps when there are mass transfer issues. However, Saenz-Noval[62] has reported the use of different stirring rates for the *N*-oxidation of 2,6-lutidine without success. For this reason, and also considering the results of the DOE discussed in Section 5.2, a constant stirring rate of 250 rpm was used in all the experiments performed with 3,5-lutidine.

Hydrogen peroxide is miscible in water; therefore, when it is added to the reactor, it dissolves in the aqueous phase, accelerating the decomposition reaction. In addition the decomposition is exacerbated by the fact that the reaction temperature (125 °C) is higher than the temperature of decomposition of the hydrogen peroxide. Hydrogen peroxide was added through a tube that was approximately 8 cm higher than the liquid level. Therefore, it is expected that part of the hydrogen peroxide added evaporated before reaching the liquid and decomposed in the vapor phase.

In Figure 57 is observed that the pressure increase in the first dosing step of the experiment performed at 125 °C (run 4) is much higher than the other runs. It is believed that the higher pressure increase is due to the abovementioned reasons, in addition to the to the change in vapor pressure. After the first dosing step it is likely that the reaction mixture was homogeneous, and therefore, the *N*-oxidation reaction became more competitive, reducing the decomposition of hydrogen peroxide. This is why the pressure increase in the second step, in which only 57 g of hydrogen peroxide were added, is less steep than in the first step.

During the first dosing step of run4, the percentage of hydrogen peroxide that decomposed was 18.5%, while in the second step was 10.6%. The 57 g added in the second step increased the conversion of 3,5-lutidine by nearly a 30%. It is believed that the lower decomposition in the second step is due to a decrease in the mass transfer resistance caused by the formation of the two phases. However, there is no literature available on the thermodynamics and phase equilibrium of the 3,5-lutidine/3,5-lutidine-*N*-oxide/catalyst/water system to verify this hypothesis. In addition, after mixing 3,5-lutidine with the catalyst, a yellow milky mixture – possibly a suspension – was formed, which made very difficult the identification of different phases visually (see Figure 58)

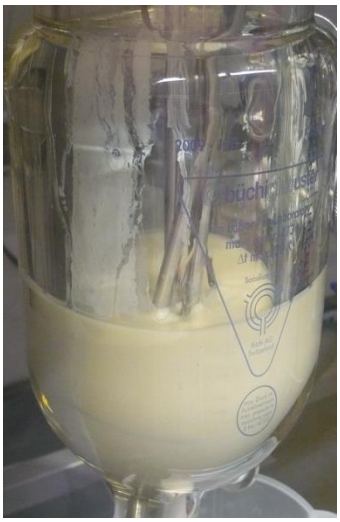

Figure 58. Resulting color of a mixture containing 190 g of 3,5-lutidine, 6.33 g of catalyst, and 15 g of water

From Table 17, it can be seen that the conversion of 3,5-lutidine obtained in runs 1-3 was high, even though only the stoichiometric amount of hydrogen peroxide was used. The lowest conversion was obtained in run 4, which was the experiment performed at the highest temperature. Also, it can be seen that the conversions obtained in runs 2 and 3 are identical. This contradicts previous findings that suggest that a higher temperature would favor the *N*-oxidation of alkylpyridines. Similar to the observations stated in Section 5.2, it was determined in this study that the increase of temperature positively affects the *N*-oxidation of 3,5-lutidine up to a certain temperature around 125 °C, after which a further increase in temperature promotes the thermal decomposition of hydrogen peroxide.

6.2 Study of 3,5-lutidine *N*-oxidation Using the RC1*e* Isothermal Calorimeter

Additional experiments to study the *N*-oxidation of 3,5-lutidine were conducted using the RC1*e* calorimeter to determine the influence of catalyst mass and dosing rate on the reaction. Table 18 show the details of the measurements performed with 3,5-lutidine in

the RC1*e* calorimeter, along with a summary of the results obtained from each experiment.

Experiments in the RC1*e* were performed as described in Section 3.2.1, and similar to the experiments performed in the HEL-SIMULAR, except that the reactor was not vented at 80 °C before the reaction started. Because the RC1*e* can withstand much higher pressure (10 bar) than the HEL-SIMULAR, the venting step was considered unnecessary.

In run 1 (Table 18), the stoichiometric amount of hydrogen peroxide was added in the first dosing step. Subsequently, the reactor was cooled down, vented and heated up again to the reaction temperature. A 20% excess of hydrogen peroxide (46 g) was added in order to see how the system responded. In run 2, due to the low catalyst used, vigorous decomposition occurred, which forced the interruption of dosing. After cooling down and venting, the system was brought to the reaction temperature and dosing was resumed; a 20% excess of hydrogen peroxide was also added in this case. In runs 3 and 4, only the stoichiometric amount of hydrogen peroxide was added.

Figure 59 shows the solubility diagram for the 3,5-lutidine/water.[90] The blue line indicates the phase separation, *i.e.,* inside the loop, a 3,5-lutidine/water mixture will have two phases, while a mixture outside the loop will be homogeneous. It can be seen that there is a wide range of conditions at which a 3,5-lutidine/water mixture forms a two-phase system. High temperatures and high concentrations of 3,5-lutidine would be required to achieve a homogeneous mixture. Therefore, in order to avoid early shifting of the phase equilibrium towards the two-phase region, no water was added to dissolve the catalyst in any of the experiments conducted in the RC1*e*. However, no benefit was observed as compared to the experiments performed in the HEL-SIMULAR, in which a small amount of water was used to dissolve the catalyst.

Table 18. Details of experiments with 3,5-lutidine in the RC1*e* calorimeter. Initial mass of 3,5-lutidine: 254 g (2.37 moles); stirring rate: 250 rpm; P_o (pressure at ambient temperature): 0 barg. Initial (T_i) and final temperature (T_f) for all measurements was 23 °C

Run		Temp. (°C)	Catalyst (g)	Dosing rate (g/min)	Mass dosed (g)	P_2 (barg)	△P (bar)	O_2 moles (nO_2)	H_2O_2 moles decomp.	H_2O_2 moles reacted in *N*-oxidation	3,5-lutidine conversion %
1	Dose 1	110	10	2	230.2	3.25	3.25	0.083	0.166	2.204	93
	Dose 2	110	10	2	46.0	3.78	3.71	0.161	0.321	2.356	100
2	Dose 1	110	1	0.5	141.4	4.27	4.24	0.212	0.423	1.032	44
	Dose 2	110	1	0.5	134.6	2.49	2.42	0.200	0.400	0.985	100
3		110	10	0.5	230.1	2.38	2.37	0.058	0.115	2.253	95
4		120	1	0.5	230.4	3.04	3.02	0.076	0.153	2.220	94

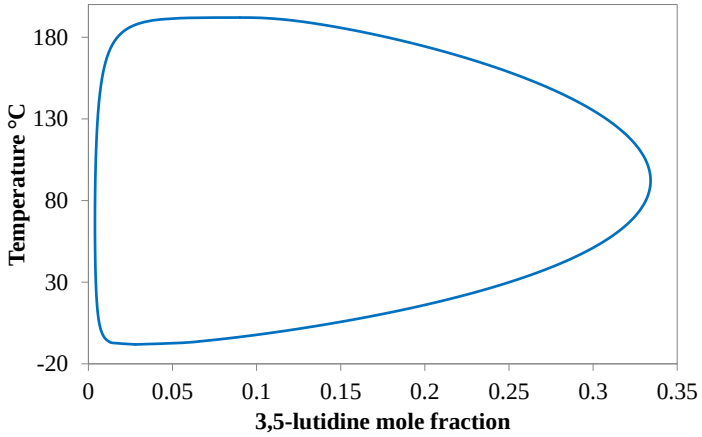

Figure 59. Solubility diagram for the 3,5-lutidine/water system[90]

Based on the diagram shown in Figure 60, it was expected that by starting the reaction with pure 3,5-lutidine, homogeneous conditions were attained, at least at the beginning of the reaction. Once dosing starts, the mole fraction of water increases rapidly due to the water that comes with the hydrogen peroxide solution and the production of water from both the *N*-oxidation and the decomposition reactions. Due to the higher polarity of the *N*-oxide, it is expected that it would positively affect the mixing of the system and reduce the mass transfer resistance. However, this is only a hypothesis as once the reaction starts and *N*-oxide is being produced, the solubility diagram shown in Figure 59 does not apply anymore and there is no literature data available to support this statement. Experiments and/or theoretical calculations to determine the phase-equilibrium during the *N*-oxidation of 3,5-lutidine would be required to verify the abovementioned hypothesis.

A milky yellow color was also observed during the experiments performed with the RC1*e* upon mixing the catalyst and 3,5-lutidine. Since there was no water to dissolve the catalyst, it is likely that the catalyst and 3,5-lutidine formed a suspension at the beginning of the reaction. In the experiments where 1 g of catalyst was used, the catalyst

was completely suspended in 3,5-lutidine, such that no catalyst could be seen at the bottom of the reactor, and the color of the mixture was opaque yellow (see Figure 60).

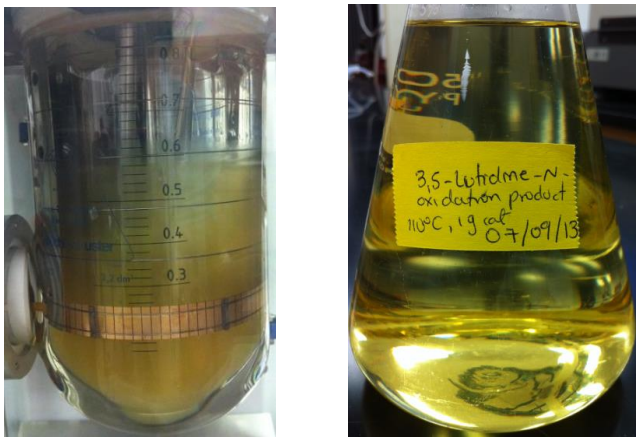

Figure 60. 3,5-lutidine *N*-oxidation mixture containing 254 g of 3,5-lutidine and 1 g of catalyst. Left: mixture as observed at the beginning of the reaction; right: final mixture

After adding approximately 200 g of hydrogen peroxide, the reaction mixture cleared up to give a bright yellow color (See Figure 60-right). The catalyst was completely soluble in the final mixture. Instead, when 10 g of catalyst were used, the color of the mixture was milky yellow and some undissolved catalyst could be seen at the bottom of the reactor. After adding approx. 200 g of hydrogen peroxide in the reactor, the catalyst could no longer be seen at the bottom of the reactor; however, even after adding the stoichiometric amount of hydrogen peroxide, the mixture was still milky yellow. Only in the experiments where a 20% excess was used the final mixture cleared up, but some of the catalyst precipitated after settling for several hours.

In order to compare experiments with different dosing rates and masses added, a dimensionless time was defined as follows:[62]

$$t^* = \frac{t - t_i}{t_f - t_i} \qquad \text{(Eq. 39)}$$

where

t is any time during the dosing and stabilization period

t_i is the time dosing starts

t_f is the final time, including dosing and stabilization period

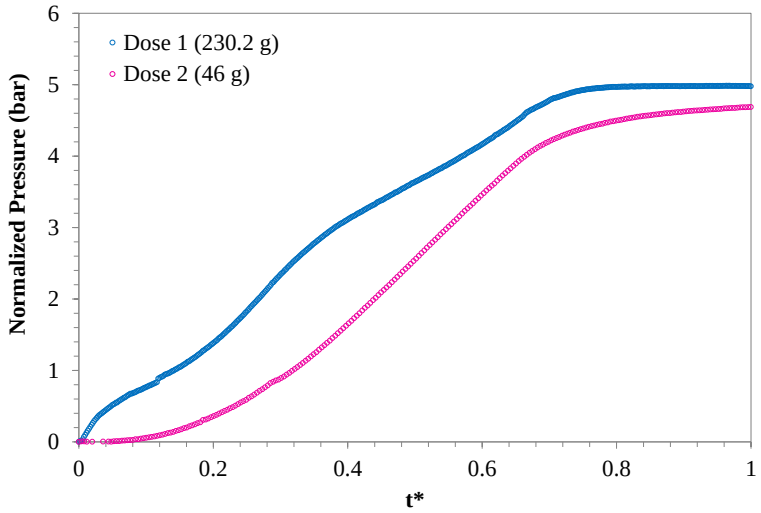

Figure 61. Normalized pressure of the two dosing steps during the *N*-oxidation of 3,5-lutidine at 110°C, 10 g of catalyst and a dosing rate of 2 g/min (run 1 in Table 18)

Figure 61 shows the normalized pressure for the two dosing steps in run 1 (Table 18). During the first dosing step, the stoichiometric amount was dosed (approx. 230 g), while in the second dosing step, a 20% excess of hydrogen peroxide was added (46 g). It can be seen in Figure 61 and Table 18 that a similar pressure was generated during the two dosing steps, even though only 46 g were added in the second step.

Some fluctuation in the pressure is observed during the first dosing step, which is consistent with changes in the temperature of the jacket (Figure 62). As mentioned

earlier, the *N*-oxidation of lutidines (and collidines) is limited by mass transfer issues due to the formation of two phases. Therefore, every experiment is different. In the first dosing step of run 1, the jacket temperature starts dropping as soon as dosing starts to remove the heat generated by the reaction and stabilizes at around 20 minutes. After 30 minutes, the jacket temperature starts decreasing further. At this point, it is very likely that the composition of the mixture has changed such that either the mixture is homogeneous or a higher mass transfer coefficient facilitates the *N*-oxidation reaction, which increases the power generated, as seen later in Figure 67. After 70 minutes the jacket temperature starts increasing. At this point, approximately 60% of the stoichiometric amount of hydrogen peroxide has been added (140 g), so the concentration of 3,5-lutidine has dropped and the power generation starts decreasing.

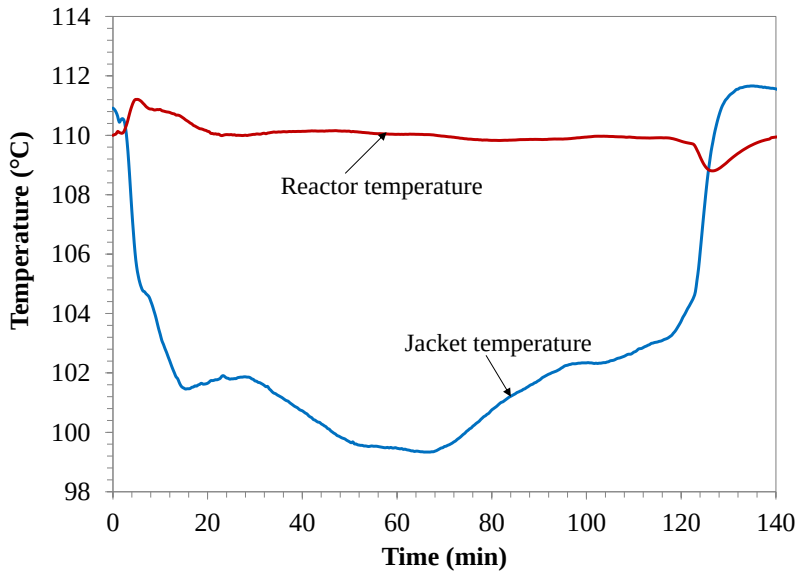

Figure 62. Reactor and oil jacket temperatures during the first dosing step of the *N*-oxidation of 3,5-lutidine at 110 °C employing 10 g of catalyst and a dosing rate of 2 g/min (run 1 in Table 18)

The conversion obtained after the first dosing step in run 1 is 93%. During the second dosing step, the concentration of 3,5-lutidine is very low; consequently, hydrogen

peroxide is accumulated and the rate of the decomposition is accelerated. For this reason, a significant amount of the hydrogen peroxide added in the second step is decomposed. From 0.473 moles (46 g) of hydrogen peroxide added in the second step, 41% decomposed (0.193 moles), versus 7% decomposed in the first step. In other words, in order to increase the conversion of 3,5-lutidine from 93% (using the stoichiometric amount of hydrogen peroxide) to 100%, a 20% excess is necessary, from which 41% decomposes. In addition, the increase in conversion is accompanied by a pressure increase equivalent to the pressure increase throughout the entire first dosing step.

Figure 63 shows the pressure increase during each of the dosing steps in run 2. It can be seen that although the mass of hydrogen peroxide added in each step is similar, the pressure increase widely differs. From Table 18, the total pressure increase ($\triangle$P) during the first dosing step is 4.24 bar, while in the second step is only 2.42 bar, even though a 20% excess is added in the second step. During the first dosing step, mass transfer dominates the reaction, as it has been mentioned earlier, which exacerbates the decomposition of hydrogen peroxide. In addition, the vapor pressure of the mixture changes dramatically as the mole fraction of water increases. In the second dosing step, although the concentration of 3,5-lutidine has dropped considerably, the mixture is likely homogeneous (or significantly less affected by mass transfer limitations), so the aqueous solution of hydrogen peroxide is better dispersed in the reaction mixture, which favors the *N*-oxidation.

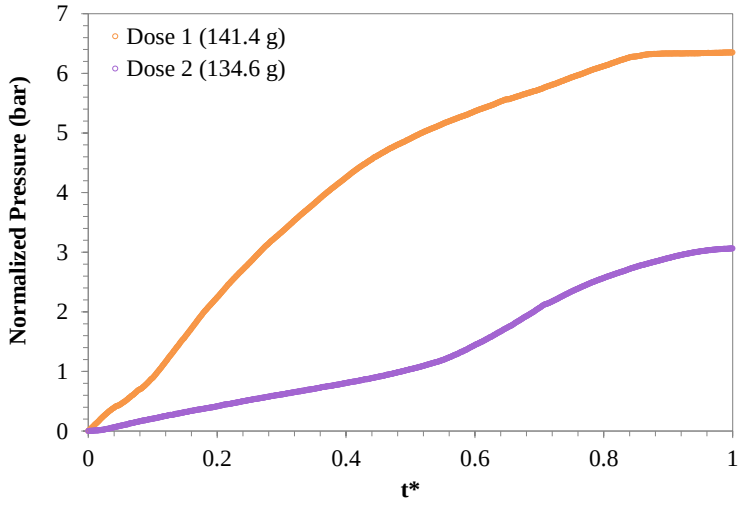

Figure 63. Normalized pressure increase during the *N*-oxidation of 3,5-lutidine at 110°C employing 1 g of catalyst and a dosing rate of 0.5 g/min (run 2 in Table 18)

As mentioned earlier, a 20% excess was added in runs 1 and 2. In both experiments the conversion obtained was 100%. However, the pressure profiles are very different. In run 1, the entire stoichiometric amount of hydrogen peroxide was added in a single step, obtaining a conversion of 93% with a net pressure increase of 3.25 bar. In contrast, in run 2, a pressure increase of 4.24 bar was generated in the first step, after only about 60% of the stoichiometric amount was added, giving a conversion of 50.5%. This clearly demonstrates the strong influence of the catalyst on the selectivity towards the *N*-oxidation.

On the other hand, the use of higher dosing rates affected negatively the *N*-oxidation of 3,5-lutidine. The reason why the pressure increase in the second step of run 1 is higher than in run 2 is because the dosing rate in run 1 was 4 times higher than in run 2. It was determined previously in Subsection 5.2 that the catalyst-dosing rate interaction was the most significant effect on the conversion of 3-picoline. It was also determined that when high catalyst was used the decomposition was minimal even when dosing rates as high as 4 g/minutes were used. However, in the case of the 3,5-lutidine, the dosing rate had a stronger effect than on 3-picoline. Even though 10 g of catalyst were used for the *N*-

oxidation of 3,5-lutidine in run 1, a dosing rate of 2 g/min appears to be too high for this system. It can be seen in Figure 63 that in run 2, where a low dosing rate of 0.5 g/min was used, the pressure increase for the second step was only 2.42 bar, and a final conversion of 3,5-lutidine of 100% was obtained, despite using only 1 g of catalyst and an excess of hydrogen peroxide.

A particular observation from Figure 63 is that in the second dosing step, the normalized pressure increase is similar to the profiles obtained during the *N*-oxidation of 3-picoline at the same conditions (110 °C, 1 g of catalyst and a dosing rate of 0.5 g/min). The pressure increases at a constant rate up to a point where the slope of the pressure increase becomes steeper. This point occurs when approximately 228 g of hydrogen peroxide have been added (99% of stoichiometric amount), as shown in Figure 64. However the transition is less sharp than it was observed in the *N*-oxidation of 3-picoline.

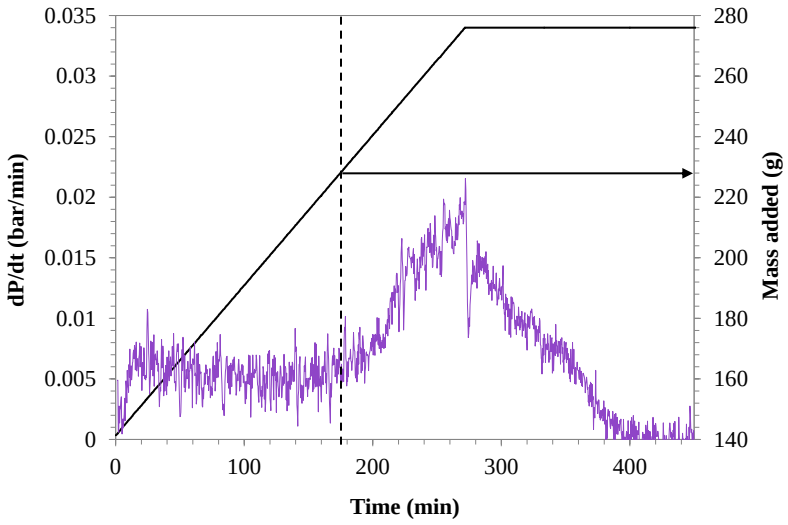

Figure 64. Averaged pressure rate during the second dosing step of the *N*-oxidation of 3,5-lutidine at 110°C employing 1 g of catalyst and a dosing rate of 0.5 g/min (run 2 in Table 18)

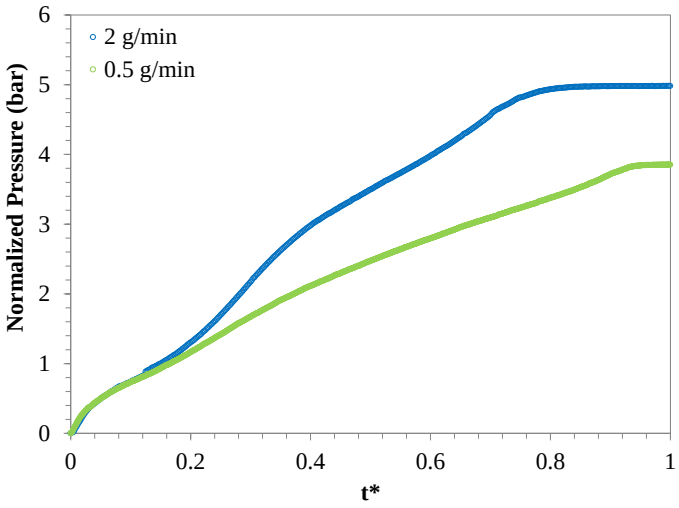

Figure 65. Normalized pressure increase during the *N*-oxidation of 3,5-lutidine at 110°C employing 10 g of catalyst and two different dosing rates (dose 1 of run 1, and run 3 in Table 18)

Figure 65 shows a comparison of the pressure increase of the first dosing step of run 1 and run 2. In both experiments compared, the stoichiometric amount (230 g) of hydrogen peroxide was added. This figure shows the influence of dosing rate on the reaction system. Even though a high mass of catalyst was used in both experiments, the experiment conducted at the higher dosing rate (run 1) resulted in a higher net pressure increase (3.25 bar at ambient temperature) and a lower conversion of 93%, as compared to the experiment at lower dosing rate (run 2), in which a net pressure increase of 2.37 bar (at ambient temperature) and a conversion of 95% were obtained.

However, it should be taken into account that the dosing time with a dosing rate of 0.5 g/min is 460 min, 4 times longer than the dosing time with a rate of 2 g/min (115 min), and the difference in conversion obtained is minimal. This demonstrates the importance of studying the effect of different dosing rates in order to find the fastest rate that minimizes the decomposition, so as to not comprise the safety of the operation and ensure an efficient process.

Figure 66 shows a comparison of the pressure increase of the first dosing step of run 2 and run 4. In both experiments compared, 1 g of catalyst was used. This figure shows the temperature effect on the reaction system. It can be seen that after t* = 0.27, the pressure increase for the experiment at 120 °C (run 4) is lower than in the experiment at 110 °C (dosing 1 of run 2), even though the quantity added in run 4 was the entire stoichiometric amount, while in the first dosing step of run 2, it was only 141.4 g. In this case, although the mass of catalyst used was only 1 g, the combination of a slow dosing rate (0.5 g/min) and high temperature favored the *N*-oxidation reaction. However, as shown in Section 6.1, further increase of temperature can cause more decomposition of hydrogen peroxide. At t*<0.27, it can be seen that the pressure increase of the experiment at 120 °C (run 4) is higher than that of the experiment at 110 °C. Nevertheless, this is likely due to the higher vapor pressure at 120 °C, which effect is not completely eliminated after normalizing the pressure.

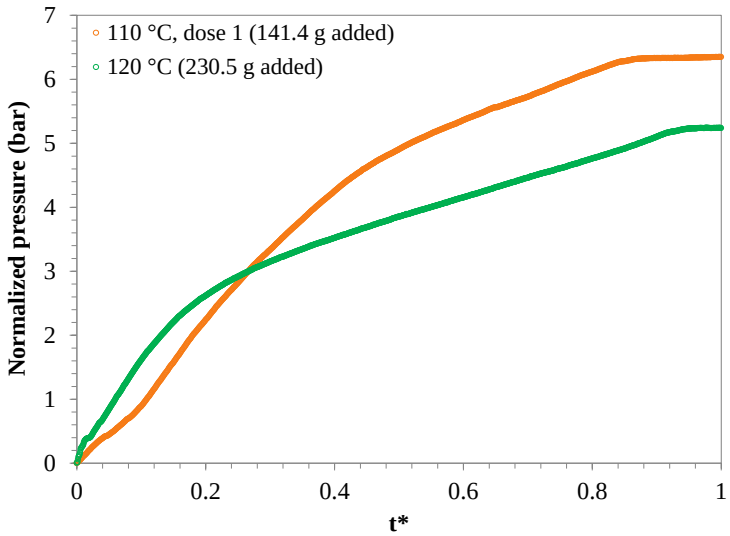

Figure 66. Normalized pressure increase during the *N*-oxidation of 3,5-lutidine at different temperatures using 1 g of catalyst and a dosing rate of 0.5 g/min (dose 1 of run 2, and run 4 in Table 18)

6.2.1 Calorimetric analysis

The power generated by the *N*-oxidation and decomposition reactions, as well as the heat of reaction of the *N*-oxidation of 3,5-lutidine were calculated following the procedure outlined in Subsection 5.2.2. The results are summarized in Table 19. The heat of reaction of the *N*-oxidation of 3,5-lutidine was found to be between 150 and 170 kJ/mole.

Figure 67a shows the total, *N*-oxidation, and decomposition power generated during the first step of run 1. As mentioned earlier, there was a fluctuation of the temperature of the jacket during the first dosing step of run 1, likely owed to the mass transfer limitation and to the moderately high dosing rate for this system (refer to Figure 62). The temperature fluctuations resulted in an irregular power profile, as shown in Figure 67a.

It can be seen in Figure 67a that there is a small accumulation of hydrogen peroxide in the reactor once dosing finishes because the power generation does not immediately fall to zero. By the end of the first dosing step and stabilization period the conversion is approximately 93%, having added the stoichiometric amount of hydrogen peroxide only. The concentration of 3,5-lutidine in the reactor is very low at this point. Due to the low concentration of 3,5-lutidine, hydrogen peroxide accumulates in the reactor. Thus, the decomposition reaction becomes more competitive than the *N*-oxidation. A reduction of the dosing rate at these later stages of the measurement would probably increase 3,5-lutidine conversion and reduce hydrogen peroxide decomposition.

Table 19. UA, baseline, energy released and heat of reaction calculated for 3,5-lutidine *N*-oxidation experiments performed in the RC1*e*

Run		Temp. (°C)	Catalyst (g)	Dosing rate (g/min)	UA1 (W/°C)	UA2 (W/°C)	Baseline1 (W)	Baseline2 (W)	Qtotal (kJ)	Qdec (kJ)	QNox (kJ)	ΔHnox kJ/mole
1	Dose 1	110	10	2	3.37	4.46	3.54	6.40	355.0	16.6	338.5	154
	Dose 2	110	10	2	4.46	4.68	6.40	7.95	65.6	19.3	46.3	165
2	Dose 1	110	1	0.5	3.37	4.12	3.21	5.81	227.4	26.0	201.5	168
	Dose 2	110	1	0.5	4.12	4.70	5.81	7.78	220.8	11.4	209.3	165
3		110	10	0.5	3.32	4.45	3.55	6.70	371.1	11.5	359.6	160
4		120	1	0.5	3.43	4.55	3.99	9.88	363.1	15.3	347.9	157

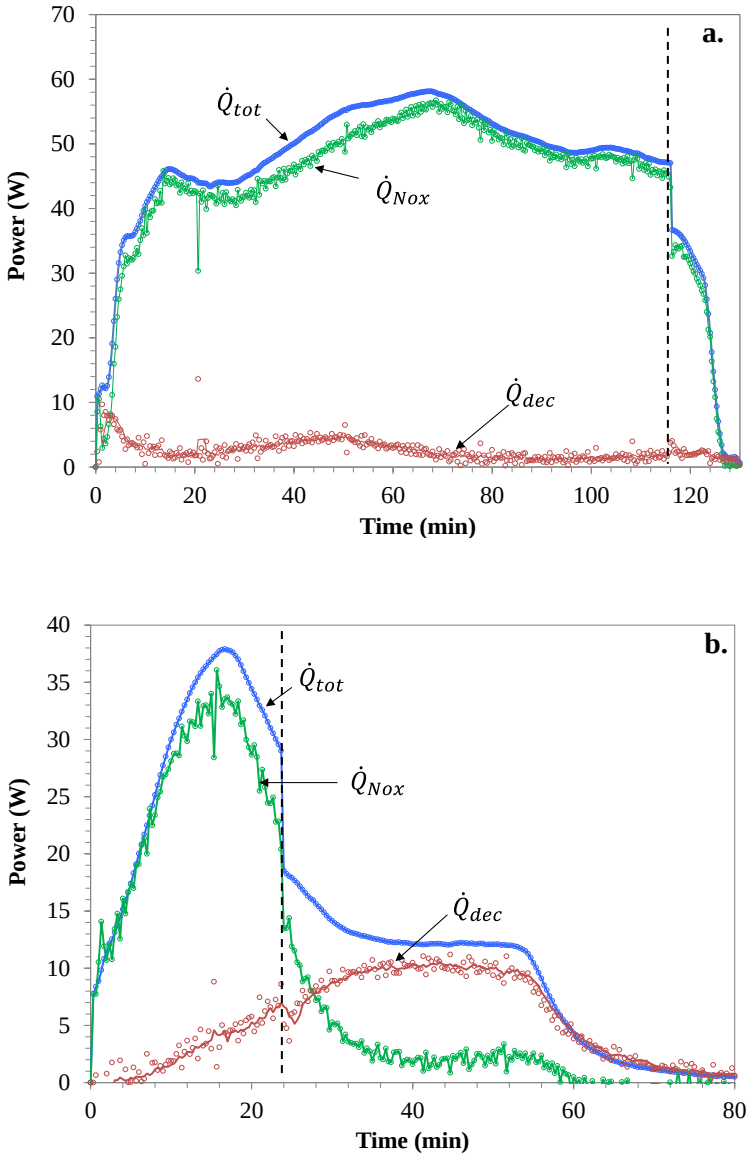

Figure 67. Total, *N*-oxidation and decomposition power during the *N*-oxidation of 3,5-lutidine at 110°C using 10 g of catalyst and a dosing rate of 2 g/min (run 1 in Table 19). a) First dosing step – stoichiometric amount of hydrogen peroxide added (230.2 g); b) Second dosing step – 20% hydrogen peroxide added (46 g). The dashed line represents the end of dosing

Figure 67b shows the total, *N*-oxidation and decomposition power for the second dosing step of run 1, in which a 20% excess of hydrogen peroxide was added. As seen in Figure 67b, the decomposition power surpasses the *N*-oxidation at ~28 min. It can also be seen

that after dosing is finished, the power profile decreases in a particular way. The change in the slope of the power profile indicates a change in the reaction order, after *N*-oxidation has practically finished. Sempere *et al.* have proposed a Langmuir-Hinshelwood type of kinetic model, which can reproduce the change of order:[51]

$$r_{dec} = \frac{k \cdot Z_0 \cdot [B]}{\left(\frac{1}{K_b \cdot [B]} + 1\right) \cdot V} \qquad \text{(Eq. 40)}$$

Such that reaction rate is first order at high hydrogen peroxide concentration:

$$r_{dec} = \frac{k \cdot Z_0 \cdot [B]}{V}, \qquad if \quad \frac{1}{K_b \cdot [B]} \ll 1 \qquad \text{(Eq. 41)}$$

but the reaction rate shifts to second order when hydrogen peroxide concentration drops

$$r_{dec} = \frac{K_b \cdot k \cdot Z_0 \cdot [B]^2}{V}, \qquad if \quad \frac{1}{K_b \cdot [B]} \gg 1 \qquad \text{(Eq. 42)}$$

where

r_{dec} is the rate of the decomposition reaction, mole/ (L*s)

k is the rate constant of the reaction, L/(mole*s)

Z_0 are the initial moles of catalyst

$[B]$ is the concentration of hydrogen peroxide, mole/L

K_b is the equilibrium constant for the formation of an intermediate between hydrogen peroxide and the catalyst

Consequently, at large hydrogen peroxide concentrations, the decomposition reaction is of first order with respect to hydrogen peroxide, while at low hydrogen peroxide concentrations, the reaction is second order. However, this change of order is observed only at specific conditions that require high concentrations of hydrogen peroxide

present, *i.e.*, when there is a high accumulation of hydrogen peroxide in the reactor.[56, 59] For this reason, this phenomenon was not observed in most experiments performed in this study.

The model proposed by Sempere *et al.*[51] was later improved by Papadaki and Gao,[57] so as to complete inadequacies of the former and to incorporate additional evidence collected at a later stage. However both models were based on experimental data collected at a relatively narrow range of temperature, *i.e.*, between 85 and 100°C. The profile obtained in Figure 67b indicates that the kinetic mechanism is the same at higher temperature and therefore, a kinetic model written as Equation 40 can be used for this reaction.

Figure 68a-b shows the power generated during both dosing steps of run 2. During the first dosing step, the power of decomposition reaches a maximum at around 50 min, and then it starts decreasing until it becomes insignificant at 190 min. At this point, the power of the *N*-oxidation is practically equal to the total power. The maximum in the decomposition is caused by the mass transfer resistance for the transport of hydrogen peroxide from the aqueous to the organic phase, and by the low mass of catalyst used. However, as mentioned earlier, there are inherent flaws in the calculation of the power of decomposition, particularly at the beginning of the reaction, as it is based on pressure differences. At the beginning of the reaction the pressure changes largely due to the increase of vapor pressure and to any decomposition occurring at the same time. Although the increased decomposition at the beginning of the reaction is logical, because of the mass transfer resistance, it is difficult to distinguish between the increase of pressure due to vapor pressure and the increase due to any oxygen produced. Thermodynamic data would be needed in order to achieve a better estimation.

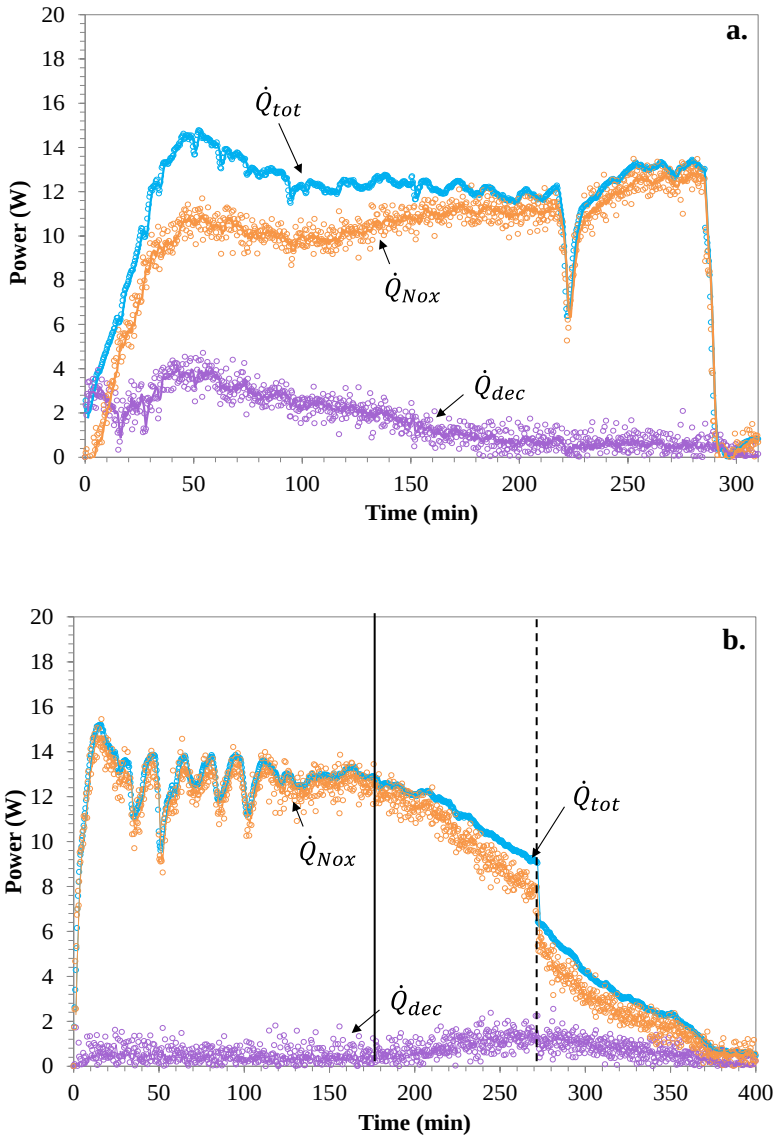

Figure 68. Total, *N*-oxidation and decomposition power during the *N*-oxidation of 3,5-lutidine at 110°C employing 1 g of catalyst and a dosing rate of 0.5 g/min (run 2 in Table 19). a) First dosing step – 141.4 g of hydrogen peroxide added; b) Second dosing step – 134.6 g of hydrogen peroxide added; this amount included a 20% excess. The solid vertical line indicates the time at which the stoichiometric amount of hydrogen peroxide has been added. The dashed line indicates the end of dosing.

After 190 min, 95 g of hydrogen peroxide have been added, and the mass transfer resistance is less significant. However, the power is constant because the reaction is still limited by the dosing of material to the reactor. It can also be seen in Figure 69a that the

power falls to zero immediately after dosing is stopped, which confirms that there was no accumulation in the system at this point. In Figure 68a, the power fall observed at 222 min is due to a temporary interruption of dosing.

Figure 68b shows that the power resumed basically at the same point where it left off in the previous step. The total power generated is basically the power of the *N*-oxidation; the decomposition power is negligible up to the point where the stoichiometric amount of hydrogen peroxide is added. At this point, the power of the *N*-oxidation starts decreasing and the power of the decomposition increases. Once dosing finishes, both the *N*-oxidation and decomposition power slowly decrease to zero, indicating an accumulation of hydrogen peroxide in the reactor due to the low catalyst and excess hydrogen peroxide added.

Figure 69 and Figure 70 show the power generated during runs 3 and 4, respectively. In general, runs 3 and 4 show similar power profiles, indicating similar reaction rates. In Figure 69, it can be seen that there is some fluctuation in the power in the first 100 minutes. This is due to temperature fluctuation as a result of the heat of solution. After that, the power is practically constant throughout the reaction. Once dosing ends, the power drops to zero immediately. This is thanks to the combination of high mass of catalyst and low dosing rate, which limits the accumulation of hydrogen peroxide.

Similar to Figure 68a, the power of decomposition shown in Figure 71 is larger at the beginning of the reaction because of the low mass of catalyst used and the mass transfer limitations. However, after 100 minutes the decomposition power drops to practically zero, and the power profiles are comparable to those shown in Figure 69. It is believed this is the point at which the mixture becomes homogeneous. Because of the milky/opaque color of the mixture, it was not possible to verify this visually.

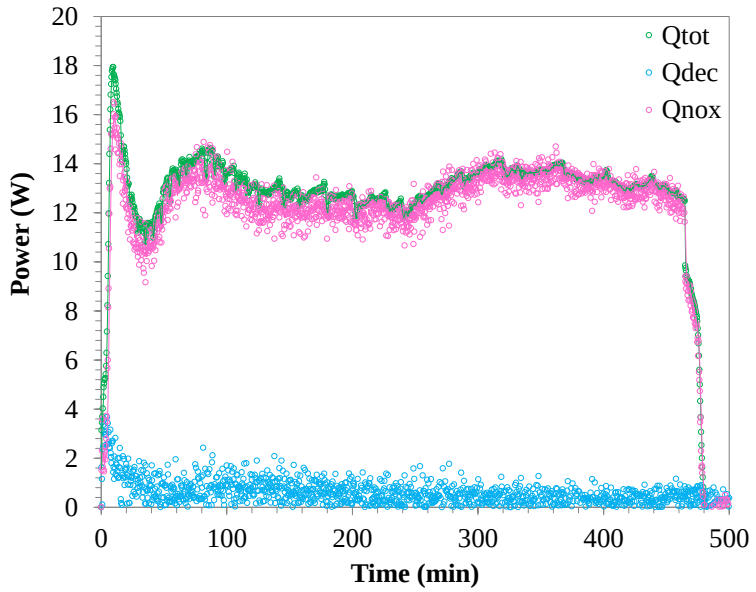

Figure 69. Total, *N*-oxidation and decomposition power generated during the *N*-oxidation of 3,5-lutidine at 110°C using 10 g of catalyst and a dosing rate of 0.5 g/min (run 3 in Table 19)

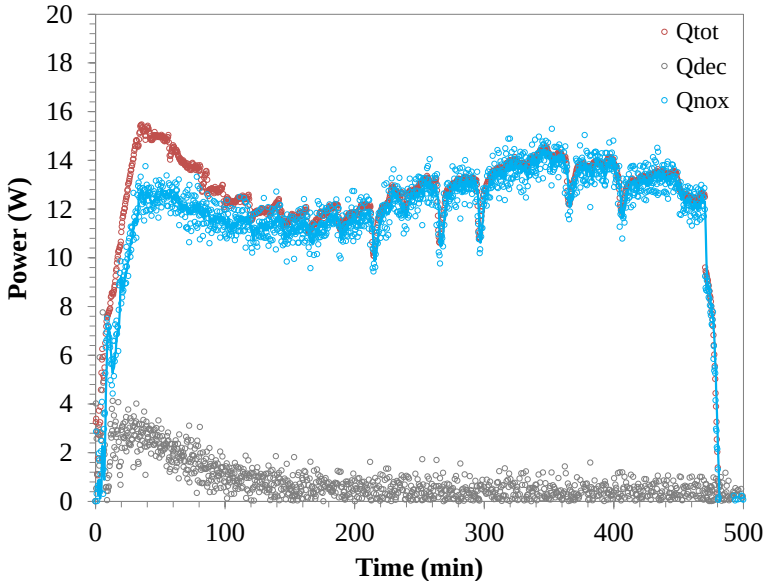

Figure 70. Total, *N*-oxidation and decomposition power generated during the *N*-oxidation of 3,5-lutidine at 120°C, 1 g of catalyst and dosing rate of 0.5 g/min (run 4 in Table 19)

It can be seen in Figure 69 and Figure 70 that approximately the same amount of power is generated in both experiments, even though they were performed at different temperature and catalyst concentrations. Also, the total and *N*-oxidation power profiles in Figure 69 and Figure 70 show a slight increase around 240 min. At this point 120 g (1.23 moles) of hydrogen peroxide have been added, which is the 52% of the total addition. This is exactly the same phenomenon observed in the *N*-oxidation of 3-picoline. The reason of this increase has not been confirmed. As mentioned in Section 5.2.2, it is possible that this phenomenon is related to the evaporation in the mixture, *i.e.*, as dosing advances, the vapor pressure of the mixture finds a new equilibrium. It is likely that the energy-consuming evaporation process becomes much less significant at the point where the increase in the power profiles is observed.

6.3 *N*-oxidation of 2,6-lutidine and 2,4,6-collidine

The *N*-oxidation of 2,6-lutidine and 2,4,6-collidine was briefly studied using the RC1*e* calorimeter and following the experimental procedure described in Subsection 6.2. The purpose of this study was to compare the behavior of the *N*-oxidation of these compounds to that of 3-picoline and 3,5-lutidine. For this study, previous observations were tested versus a single experiment with 2,6-lutidine and 2,4,6-collidine, respectively. Both experiments were performed at a temperature of 110 °C, using a slow dosing rate of 0.5 g/min and high catalyst mass equal to 10 g, since this combination seemed to be beneficial in experiments performed with the other alkylpyridines studied in this work. Also, even though the *N*-oxidation of 3,5-lutidine did not benefit from the lack of water in the initial mixture, no water was used in the experiments performed with 2,6-lutidine and 2,4,6-collidine in order to reduce as much as possible the formation of two phases in the initial stage of the reaction.

6.3.1 N-oxidation of 2,6-lutidine

Table 20 shows the details of the measurement performed with 2,6-lutidine and summarizes the results in terms of conversion and moles of hydrogen peroxide decomposed. Severe decomposition during the experiment forced the interruption of dosing. Two steps were required to complete the addition of the stoichiometric amount of hydrogen peroxide. Then, the reactor was cooled down and vented and the reaction mixture was heated up to the reaction temperature again. A 20% excess of hydrogen peroxide was then added in a third dosing step. The purpose of adding the excess was to observe the behavior of the system at a wide range of concentrations of 2,6-lutidine, and compare it with other alkylpyridines.

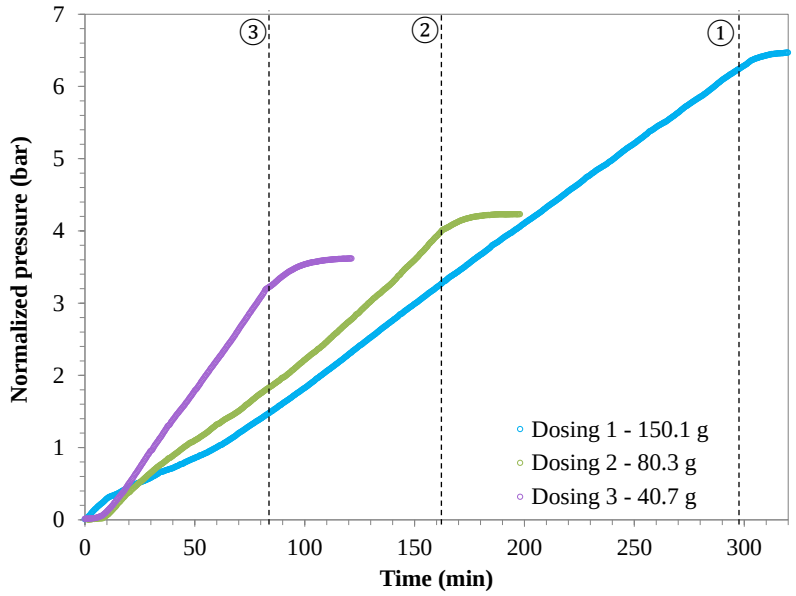

Figure 71. Normalized pressure increase during the different dosing steps in the *N*-oxidation of 2,6-lutidine at 110 °C, using 10 g of catalyst and a dosing rate of 0.5 g/min. The dashed lines indicates the point at which dosing was stopped for each dosing step.

Table 20. Details of experiment performed with 2,6-lutidine. Initial mass of 2,6-lutidine: 254 g (2.37 moles); stirring rate: 250 rpm; Initial pressure (pressure at ambient temperature): 0 barg; Initial (Ti) and final temperature (Tf): 23°C

	Temp. (°C)	Catalyst (g)	Mass dosed (g)	P_2 (barg)	△P (bar)	O_2 moles (nO2)	H_2O_2 moles decomp.	H_2O_2 moles reacted in *N*-oxidation	2,6-lut conv. %
Dosing 1	110	10	150.1	5.66	4.64	0.140	0.280	1.266	53
Dosing 2	110	10	80.3	4.34	3.28	0.089	0.178	0.649	81
Dosing 3	110	10	40.7	3.94	2.93	0.076	0.153	0.266	92

Table 21. UA, baseline, energy released and heats of reaction calculated for the experiment performed with 2,6-lutidine in the RC1*e*

	Temp. (°C)	Catalyst (g)	Dosing rate (g/min)	UA1 (W/°C)	UA2 (W/°C)	Baseline1 (W)	Baseline2 (W)	Qtotal (kJ)	Qdec (kJ)	QNox (kJ)	ΔHnox kJ/mole
Dose 1	110	10	0.5	3.523	4.207	4.289	7.062	222.51	27.97	194.54	154
Dose 2	110	10	0.5	4.207	4.431	7.062	7.358	126.19	17.80	108.40	167

Figure 71 shows the pressure increase during the experiment performed with 2,6-lutidine. As mentioned earlier in Section 6.2, there are several factors that influence the pressure increase, particularly at the beginning of dosing, including mass transfer resistance and vapor pressure changes. It can be seen in Figure 72 that during the first dosing step, the pressure increases linearly. This indicates that the decomposition reaction is controlled by dosing and proceeds at a constant rate. In the second dosing step, the pressure increases at a slightly higher rate than in the first dosing step. The conversion of 2,6-lutidine obtained after the second dosing step, in which the addition of the stoichiometric amount of hydrogen peroxide was completed, was 81%. The third dosing step, in which a 20% excess hydrogen peroxide was added, presented the steepest pressure increase, even though only 40.7 g of the material were added. This is because by the end of the second dosing step, the concentration of 2,6-lutidine had already dropped to a value that allowed the accumulation of hydrogen peroxide and therefore, increased the decomposition.

A final conversion of 2,6-lutidine equal to 92% was obtained. Overall from the hydrogen peroxide added to the reactor, only 77% was used in the *N*-oxidation. These findings indicate that the conditions found to work well for the *N*-oxidation of 3-picoline and 3,5-lutidine are not sufficient to reduce the decomposition of hydrogen peroxide in the N-oxidation of 2,6-lutidine.

It can also be seen in Figure 72 that the pressure stops increasing almost immediately after dosing has ceased in the first and second dosing steps. This further verifies the lack of accumulation of hydrogen peroxide. Instead, in the third step, the pressure continues to increase by about 0.5 bar after dosing stops, indicating some accumulation during this step.

From Table 20, it can be seen that the mass added in the third step was half of that added in the second step. In turn, the mass added during the second step was almost half of that

added in the first step. However, the net pressure increase (at ambient temperature) obtained during the third step (2.93 bar) was only 0.35 bar higher than the net pressure increase generated during the second dosing step (3.28); while the net pressure increase generated during the first dosing step was 1.28 bar higher than in the second step. These calculations show an increase in the amount of hydrogen peroxide decomposed in each step.

It was observed that the lack of water in the initial reaction mixture does not appear to have had any effect on the phase-equilibrium of the mixture. There was significant decomposition during the experiment, and the results obtained are similar to those of Saenz-Noval[62] who performed experiments with an initial mixture containing of 50 mole % 2,6-lutidine in water. Consequently, it is necessary to continue the search for alternatives that minimize the phase separation during the *N*-oxidation of 2,6-lutidine in order to ensure an inherently and more efficient process.

Calorimetric analysis

The power of the *N*-oxidation of 2,6-lutidine, and the power of the hydrogen peroxide decomposition reactions were estimated using the procedure outlined in Section 5.2.2. The quantities obtained are summarized in Table 21. The heat of reaction of the *N*-oxidation of 2,6-lutidine was between 150 and 170 kJ/mole.

Figure 72a-b shows the power profiles generated during the first two dosing steps in the *N*-oxidation of 2,6-lutidine. It can be seen that the power generated during the *N*-oxidation of 2,6-lutidine slowly increases all throughout the first dosing step. This is because of the mass transfer resistance; hydrogen peroxide slowly dissolves in 2,6-lutidine and starts reacting with the alkylpyridine until the power of the reaction reaches a fairly constant value around 14 W, as seen in Figure 72b. The power generated by the decomposition during the *N*-oxidation of 2,6-lutidine was significant throughout the

entire course of the reaction and stayed practically constant at a value around 2 W, which is consistent with the linear pressure profiles obtained. The power generated by the decomposition was approximately 13% of the total energy released.

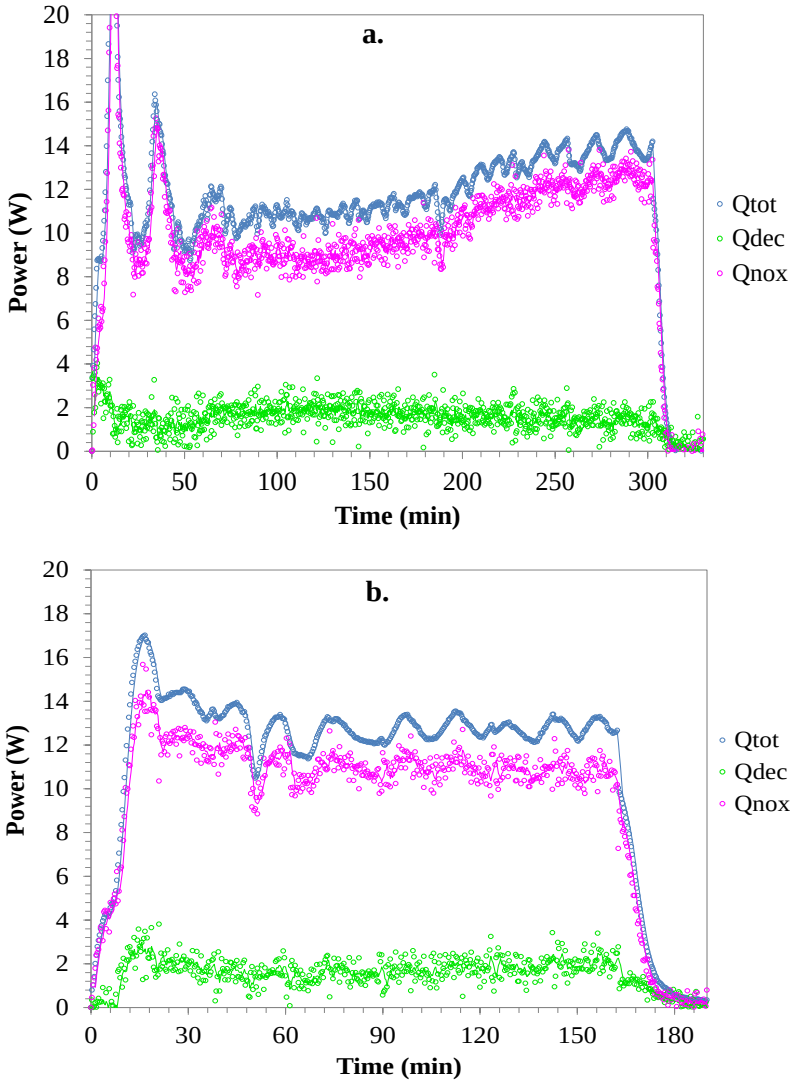

Figure 72. Total, *N*-oxidation and decomposition power generated during the *N*-oxidation of 2,6-lutidine at 110 °C, using 10 g of catalyst and a dosing rate of 0.5 g/min. a) Dosing 1 – 150.1 g of H_2O_2 added, b) Dosing 2 – 80.3 g of H_2O_2 added

6.3.2 N-oxidation of 2,4,6-collidine

Table 22 show the details of the measurement performed with 2,4,6-collidine and summarizes the results in terms of conversion of 2,4,6-collidine and moles of hydrogen peroxide decomposed. Similar to the experiment with 2,6-lutidine, severe decomposition during the experiment forced the interruption of dosing, requiring two steps to complete the addition of the stoichiometric amount of hydrogen peroxide. A 20% excess of hydrogen peroxide was then added in a third dosing step.

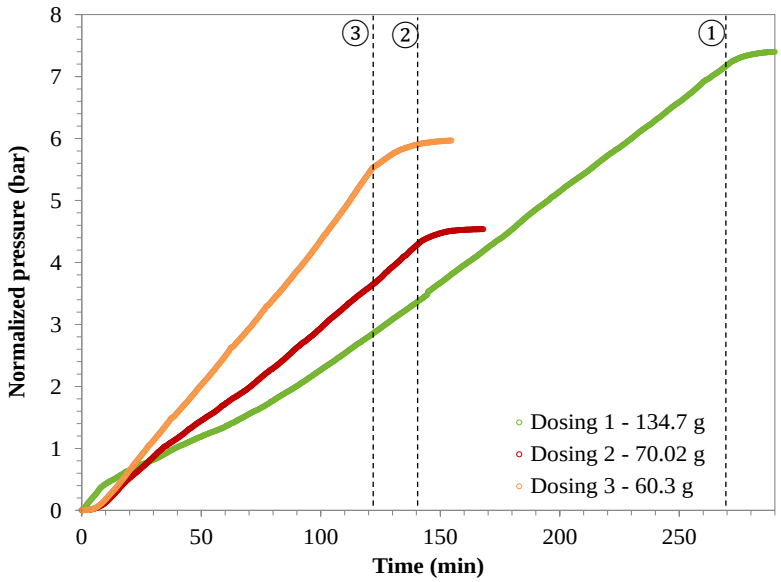

Figure 73. Normalized pressure increase during the different dosing steps in the *N*-oxidation of 2,4,6-collidine at 110 °C, using 10 g of catalyst and a dosing rate of 0.5 g/min. The dashed lines indicates the point at which dosing was stopped for each dosing step.

Figure 73 shows the pressure increase during the experiment performed with 2,4,6-collidine. In each dosing step, a linear pressure increase was observed, which indicates a decomposition controlled by dosing. However, the slope of the pressure increase was steeper in each dosing step.

Table 22. Details of experiment performed with 2,4,6-collidine. Initial mass of 2,4,6-collidine: 254 g (2.10 moles); stirring rate: 250 rpm; Initial pressure (pressure at ambient temperature): 0 barg; Initial (Ti) and final temperature (Tf): 23 °C

	Temp. (°C)	**Catalyst (g)**	**Mass dosed (g)**	**P_2 (barg)**	**△P (bar)**	**O_2 moles (nO2)**	**H_2O_2 moles decomp.**	**H_2O_2 moles reacted in *N*-oxidation**	**2,4,6-collidine conv. %**
Dosing 1	110	10	134.7	6.14	5.13	0.159	0.317	1.069	51
Dosing 2	110	10	70.0	4.58	3.56	0.101	0.202	0.519	76
Dosing 3	110	10	60.3	7.45	7.42	0.122	0.243	0.377	94

Table 23. UA, baseline, energy released and heats of reaction calculated for the experiment performed with 2,4,6-collidine in the RC1*e*

	Temp. (°C)	**Catalyst (g)**	**Dosing rate (g/min)**	**UA1 (W/°C)**	**UA2 (W/°C)**	**Baseline1 (W)**	**Baseline2 (W)**	**Qtotal (kJ)**	**Qdec (kJ)**	**QNox (kJ)**	**ΔHnox kJ/mole**
Dosing 1	110	10	0.5	3.383	4.117	2.973	6.810	180.74	31.75	148.99	139
Dosing 2	110	10	0.5	4.117	4.375	6.810	8.806	113.36	20.21	93.15	180
Dosing 3	110	10	0.5	4.375	4.608	8.806	7.470	89.79	24.33	65.46	174

The behavior of 2,4,6-collidine is similar to that of the sister compound 2,6-lutidine. It can be seen in Figure 73 that the highest pressure increase was obtained during the first dosing step. This is due to the mass transfer resistance, which promotes the decomposition, and to vapor pressure changes. Besides, the mass dosed in the first dosing step is almost double the mass dosed in the second step. Figure 73 also shows that once dosing stops, the pressure stops increasing almost immediately, indicating no or little accumulation.

After the second dosing step, in which the addition of the stoichiometric amount of hydrogen peroxide was completed, the conversion of 2,4,6-collidine obtained was equal to 76%. Same as in the experiment with 2,6-lutidine, the third dosing step, in which a 20% excess hydrogen peroxide was added, presented the steepest pressure increase, even though only 60.3 g of the material were added. This is because by the end of the second dosing step, the concentration of 2,4,6-collidine had already dropped to a value that allowed the accumulation of hydrogen peroxide and therefore, increased the decomposition. The final conversion of 2,4,6-collidine after the third dosing step, in which a 20% hydrogen peroxide was added, was of 94%.

Although a high conversion of 2,4,6-collidine was obtained, it must be taken into account that a 20% excess of hydrogen peroxide was required to achieve this result. However, the main issue is that the decomposition of hydrogen peroxide was significant throughout the entire course of the reaction, which made the process hazardous and inefficient. Compared to 2,6-lutidine, 2,4,6-collidine seemed more difficult to oxidize. For each dosing step in the *N*-oxidation of 2,4,6-collidine, the net pressure increase (at ambient temperature) was always higher than the net pressure increase obtained for each step in the *N*-oxidation of 2,6-lutidine.

From Table 22, it can be seen that although the mass added in the second step (70 g) was 10 g lower that the mass added in the third step (60.3 g), the net pressure increase (at ambient temperature) obtained during the third step (7.42 bar) was more than double the net pressure increase obtained in the second step (3.52 bar). These calculations show an increase in the amount of hydrogen peroxide decomposed in each step and the effect of accumulation on the decomposition reaction.

Same as 2,6-lutidine, no benefit was obtained from the lack of water in the initial reaction mixture for the *N*-oxidation of 2,4,6-collidine. As mentioned earlier, this compound was the most difficult to N-oxidize and there was significant decomposition throughout the experiment. Alternatives to achieve a homogeneous mixture are much needed in order to improve the safety and efficiency of the N-oxidation of 2,4,6-collidine.

Calorimetric analysis

The power of the *N*-oxidation 2,4,6-collidine, and the power of the hydrogen peroxide decomposition were estimated and the quantities obtained are summarized in Table 23. The heat of reaction of the *N*-oxidation of 2,4,6-collidine was between 140 and 180 kJ/mole. The power of decomposition was higher in the *N*-oxidation of 2,4,6-collidine, than in the *N*-oxidation of 2,4,6-lutidine, indicating that this molecule is more difficult to oxidize.

Figures 74a-c show the power profiles generated during the three dosing steps in the *N*-oxidation of 2,4,6-collidine. It can be seen that the power profiles for 2,4,6-collidine are very similar to those of 2,6-lutidine, meaning that both compounds behave similarly.

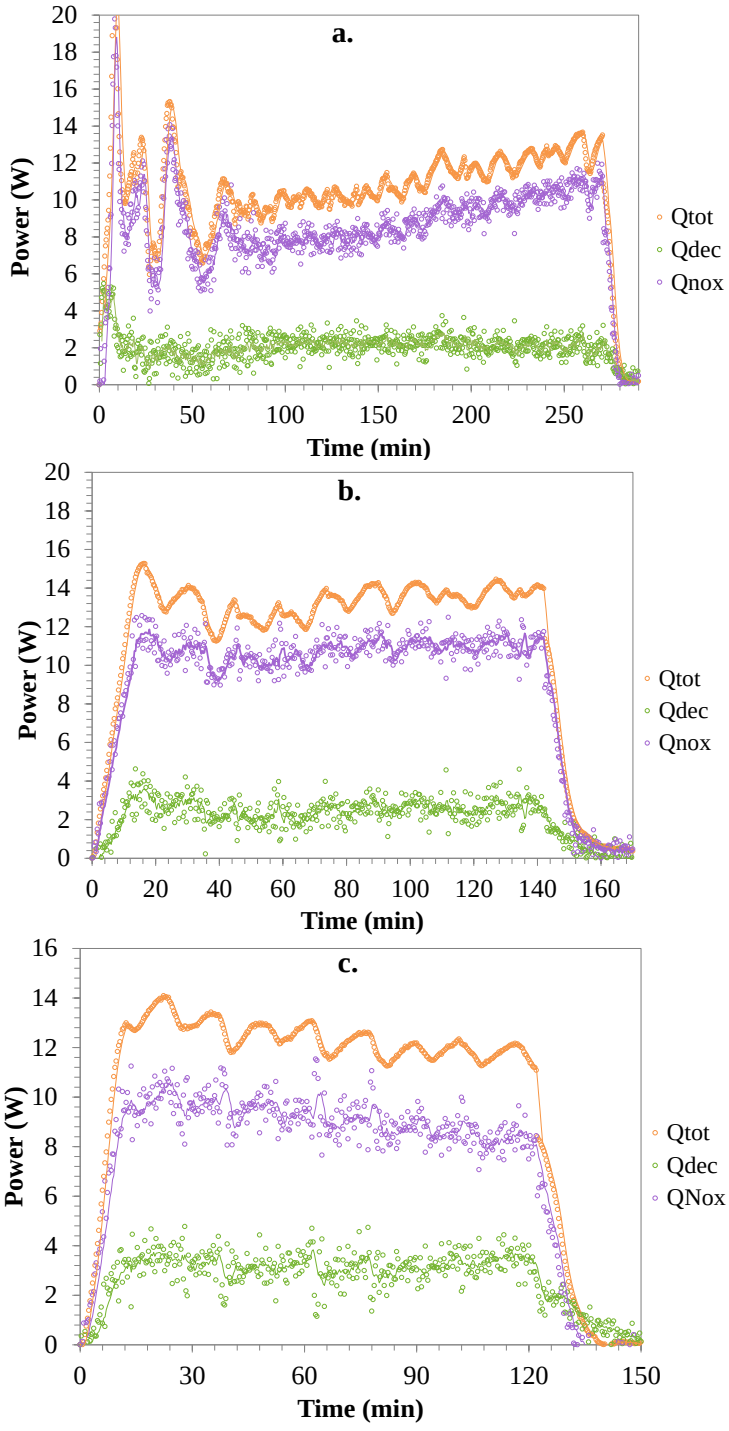

Figure 74. Total, *N*-oxidation and decomposition power generated during the *N*-oxidation of 2,4,6-lutidine at 110°C using 10 g of catalyst and a dosing rate of 0.5 g/min. a) Dosing 1 – 134.7 g of H_2O_2 added, b) Dosing 2 – 70.02 g of H_2O_2 added , c) Dosing 3 – 60.26 g of H_2O_2 added
Similar results were obtained for the *N*-oxidation of 2,4,6-collidine, as shown in

Figure 74 shows that during the first dosing step, the power of decomposition was at a constant value of 2 W. This value increased to 3 W in the second step and reached the 4 W in the third dosing step. In total, the power generated by the decomposition amounted 20% of the total energy released. This is a large percentage compared to the total decomposed in the *N*-oxidation of other alkylpyridines included in this study.

It can also be seen in the power profiles shown in
Figure **74** that the power profiles drop to zero almost immediately after dosing is stopped, which indicates that there was no accumulation of hydrogen peroxide in the mixture, even though a 20% excess of hydrogen peroxide was used in the experiment. This is because of the minimal accumulation of hydrogen peroxide in the mixture. Therefore, the severe decomposition in the *N*-oxidation of 2,4,6-collidine is not owed to hydrogen peroxide accumulation, but to the mass transfer resistance.

Discussion

The experiments conducted with 2,6-lutidine and 2,4,6-collidine show a different behavior than the sister compounds 3-picoline and 3,5-lutidine. Although the power of the *N*-oxidation reaction is similar, *i.e.*, practically constant throughout the reaction, the power generated by the decomposition is much stronger. It was previously shown in Figure 69 and Figure 70 that the decomposition of hydrogen peroxide during the *N*-oxidation of 3,5-lutidine becomes insignificant after a certain point in the reaction. Instead, the decomposition power in the *N*-oxidation of 2,6-lutidine remains constant, and in the case of 2,4,6-collidine, it increases. This may indicate that 2,6-lutidine and 2,4,6-collidine are molecules more difficult to oxidize due to their chemical structure, or that the two phases, *i.e.*, aqueous and organic, do not dissolve throughout the course of the reaction. However, as mentioned earlier, there is no information available in the literature on the phase-equilibrium on these reacting systems. Further research on the phase-equilibrium the compounds involved in the *N*-oxidation of higher order alkylpyridines is necessary to improve the safety and efficiency of the process.

6.4 Conclusions

The *N*-oxidation of 3,5-lutidine was studied using two different isothermal reaction calorimeters, with the reactor operating under pressure, and different conditions to examine their effect on the hazards and efficiency of the *N*-oxidation.

The experiments conducted showed that it is possible to obtain high conversions of 3,5-lutidine without using an excess of hydrogen peroxide. It was also shown that the behavior of 3,5-lutidine is similar to that of 3-picoline. However, 3,5-lutidine appears to be more negatively affected by high dosing rates than 3-picoline. Therefore, it is recommended to use slow dosing rates for the *N*-oxidation of this compound.

The evaluation of the power profiles showed the point at which the mixture becomes homogeneous, which is the point where the decomposition power drops to a value close to zero. However, as mentioned earlier, thermodynamic data would be needed in order to achieve a better estimation of the decomposition power.

The *N*-oxidation of 2,6-lutidine and 2,4,6-collidine was studied using the RC1*e* isothermal calorimeter to compare their behavior with that of sister compounds included in this study. It was found that these compounds are less amenable to the N-oxidation than 3-picoline and 3,5-lutidine. Vigorous decomposition of hydrogen peroxide occurred throughout the entire course of the reaction, which required several dosing steps to add the required mass of hydrogen peroxide. Conditions that affect positively the *N*-oxidation of 3-picoline and 3,5-lutidine, *i.e.*, higher temperature, low dosing rate, high mass of catalyst, do not seem to significantly increase the safety and efficiency of the *N*-oxidation of 2,6-lutidine and 2,4,6-collidine. Therefore, it is imperative to find alternatives that can minimize the formation of two-phases in the reaction mixture.

The heat of reaction for all higher alkylpyridines studied here was found to be between 150 and 170 kJ/mole of alkylpyridine reacted, which is consistent with previous works.

7. STUDY OF THE N-OXIDATION OF ALKYLPYRIDINES BY MEANS OF *IN-SITU* FTIR

Reaction calorimetry is a sensitive technique, which can be affected by minimum disturbances during an experiment. During a calorimetric experiment, typically samples are taken at regular intervals to determine the extent of the reaction, as well as concentrations of the different species involved in the reaction under study. This information can later be used for kinetic analysis. However, the extraction of samples during a calorimetric measurement not only disturbs the system, but it also reduces the volume of reaction, contributing to the error in the measurement. Furthermore, short living intermediates may disappear from the sample before it is analyzed using an off-line technique such as gas chromatography (GC), high performance liquid chromatography (HPLC), or nuclear magnetic resonance (NMR). Therefore, it is desirable to use a non-intrusive method, which can provide reliable concentration data.

Previous works have reported the use of *in-situ* FTIR spectroscopy as an analytical tool to obtain quantitative data on concentration for different purposes. For example, da Silva and Cajaiba da Silva[92] have used attenuated total reflectance (ATR) FTIR spectroscopy and heat flow calorimetry to determine the solubility curve of adipic acid in acetone to illustrate a methodology that can be used for the development of crystallization processes; de Souza and Cajaiba da Silva[93] used real-time ATR-FTIR spectroscopy to obtain quantitative data on the yield during the synthesis of biodiesel. Hamminga *et al.*[94] have used the same technique to study the kinetics and reaction mechanism of liquid phase hydrogenation of γ-butyrolactone to 1,4-butanediol over a copper zinc oxide catalyst at high temperature and pressure. Many other examples and applications of *in-situ* FTIR are available in the literature.[95-99]

In this work, the *N*-oxidation of alkylpyridines is studied by means of *in-situ* FTIR, simultaneously with calorimetric measurements described in Section 5.2. The key and target objective is to identify reaction kinetics and reaction pathways via the measurement of concentrations of reactants products and intermediates. This is a formidable task by itself, which requires the accomplishment of several targets, as outlined below.

The first objective is to obtain reliable concentration data to compare with concentrations obtained from calorimetric data. Concentration data is not only useful for kinetic analysis but also to evaluate reactant accumulation in the reactor and subsequent evaluation of runaway scenarios.

The procedure to obtain concentrations from calorimetric data (power output) in an open system has been outlined by Sempere *et al.*[51] and Papadaki.[59] As mentioned in Section 5.2.2., the power of the *N*-oxidation is calculated by subtracting the power of the decomposition from the total power. In an open system, an oxygen mass flow meter can be used to estimate the mass of hydrogen peroxide decomposed, and thus the power generated by the decomposition. However, in a semi-closed system operating under pressure, the calculation of the power of the decomposition of hydrogen peroxide is based on pressure differences. Therefore, the accurate estimation of concentration from calorimetric data, for a closed system, depends on the measurement of the pressure, which accounts for the generation of gas and vapors. In order to determine the increase of pressure due to oxygen generation only, it is necessary to know how the vapor pressure of the mixture changes throughout the reaction; however, this information is not available in literature, for which it is necessary to make some assumptions, as noted in Section 5. These assumptions have an inherent error associated to them, which is reflected in the estimation of concentration data. In addition, the measurement of pressure is very noisy, particularly at high temperatures, and it is affected by temperature

fluctuations in the reactor, which are more pronounced at the beginning of dosing and at higher dosing rates.

The second objective is to estimate the end point of the reaction. Even though it has been shown that high conversions can be achieved, it is necessary to estimate the point at which the reaction advances so slowly that it is not worth continuing it. In the context of the *N*-oxidation of alkylpyridines, the end point of the reaction is also useful for the design of an inherently safer process, *i.e.,* the reaction should be stopped when the *N*-oxidation proceeds so slowly that the decomposition of hydrogen peroxide predominates.

The third objective is to identify the formation of intermediates and other events throughout the course of the reaction. *In-situ* FTIR allows further insight of the reaction by providing a 'movie' of the reaction. Lastly, the purpose of this study is also to evaluate the performance of *in-situ* FTIR and determine its advantages and disadvantages as an analytical tool for the study of complex reactions. In order to illustrate the methodology, the infrared study was conducted for the *N*-oxidation of 3-picoline.

7.1 Infrared Probe Calibration

According to the Beer-Lambert law,[100] the absorbance of a compound is directly proportional to the path length of the beam in the absorbance medium and to the concentration:

$$A=\varepsilon bC$$

where A is the absorbance of the compound, b is the path length of the beam, C is the concentration of the compound, and ε is the constant of proportionality, which is called the molar absorptivity.[101] Therefore, at a constant path length, the absorbance is directly

proportional to the concentration, *i.e.*, a plot of absorbance versus concentration will give a straight line.

The infrared probe was calibrated by performing a series of experiments in the RC1*e* calorimeter. The goal of the calibration experiments was to find the relationship between peak absorbance and concentration of the chemicals of interest, in this case, 3-picoline and 3-picoline-*N*-oxide (3Nox).

The FTIR probe was calibrated at 60, 80, and 110 ^{o}C according to the methodology outlined here: 350 ml of water were added in the reactor and heated to the desired temperature, which was maintained constant for the whole measurement. A total of 400 ml of 3-picoline were added in a step-wise process using 20 ml in each step. The temperature was allowed to stabilize after each addition step. After the temperature was stabilized in its set value, infrared (IR) spectra were collected every 1 minute.

Characteristic peaks of the 3-picoline IR spectra were selected and their peak heights were tracked throughout the experiment. A similar process was employed for the correlation of the infrared light absorption of the 3Nox/water solution. Pure water was employed and small quantities of 3Nox were added in a step-wise mode. Then, the influence of the absorbance of the product on the reactant, and vice versa, was examined by adding 3Nox in a step-wise mode to an aqueous solution containing 3-picoline, and the peak heights were measured at the selected frequencies. The calibration was done at different temperatures in order to observe the effect of the temperature on the absorbance.

In the next sections, the spectra of the compounds involved in the *N*-oxidation of alkylpyridines are shown and the most distinct IR bands of each one of them are determined. Then, the method used to perform the calibrations is described and the results are discussed. In addition, the synergistic effects between different compounds

are also assessed, *e.g.*, effect of water and/or catalyst on the spectra, influence of 3Nox on the absorption of 3-picoline and vice versa.

7.1.1 Selection of peaks

Figure 75 and Figure 76 show the spectra of 3-picoline and 3Nox, respectively, as obtained during the collection of reference spectra using the ReactIR 15^{TM}. No data treatment, *e.g.*, subtraction of water, has been applied to the spectra shown in Figure 75 and Figure 76.

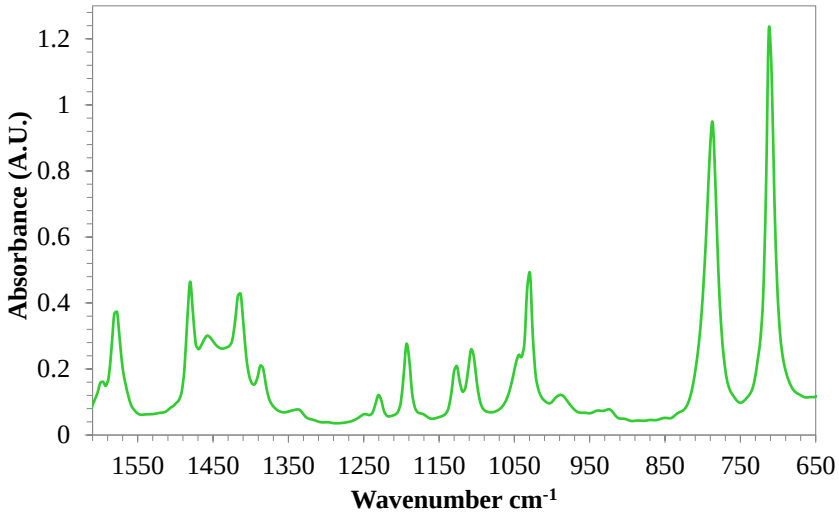

Figure 75. Infrared spectrum of 3-picoline used as reference for the calibration of the infrared probe

Both 3-picoline and 3Nox present most of their characteristic peaks in the 1800-650 cm^{-1} region. Other peaks can also be observed at wavenumbers higher than 1800 cm^{-1}. However, the probe tip has a diamond-composite sensor, which absorbs infrared light in the 1950-2250 cm^{-1} region; consequently, this region is considered a 'blind spot' and no

useful information can be obtained from there. Therefore, the region of the infrared spectra selected for the study of the *N*-oxidation of 3-picoline was 1800-650 cm^{-1}.

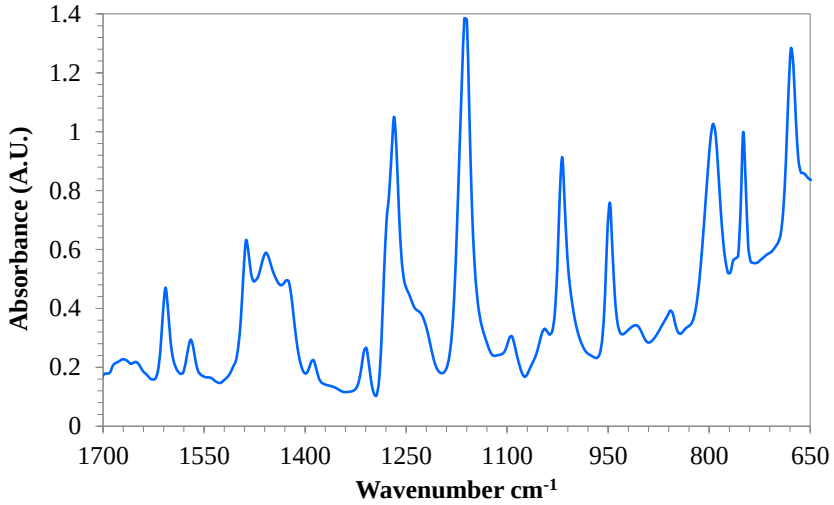

Figure 76. Infrared spectrum of 3-picoline-*N*-oxide used as reference for the calibration of the infrared probe

Table 24 shows the vibrational frequencies observed in the spectra of 3-picoline and 3Nox in the selected range of study. The assignment of the vibrational frequencies for the spectrum of 3-picoline was done according to the work of Lopez-Tocon *et al.*[102] and for 3Nox, the work of Katritzky *et al.* was followed.[103] Table 25 shows the assignment of the bands observed for the catalyst, according to the work of Mane *et al.*[104]

3Nox is highly hygroscopic; for this reason, the sample used to obtain the reference spectra contained a small amount of water. The effect of the water in the 3Nox spectrum can be seen in the band around 1640 cm^{-1} and also at wavenumbers below 1000 cm^{-1}, where the spectrum show an upwards trend similar to the spectrum of water.

Table 24. Assignment of vibrational frequencies for the IR spectra of 3-picoline and 3Nox

3-picoline		3Nox	
Character	**Frequency (cm^{-1})**	**Character**	**Frequency (cm^{-1})**
$\boldsymbol{\nu}_{ring}$	1599	ν(CC, CN)	1607
$\boldsymbol{\nu}_{ring}$	1579	ν(CC, CN)	1569
δ(CH)	1480	ν(CC, CN)	1487
$\delta_{as}(CH_3)$	1457	ν(CC, CN)	1428
δ(CH)	1416	$\nu^{+}N–O^{-}$	1268
$\delta_{s}(CH_3)$	1386	?	1165
$\boldsymbol{\nu}$(CX)	1230	Ring	1018
δ(CH)	1192	γ(CH)	947
$\boldsymbol{\nu}_{ring}$	1126		
$\boldsymbol{\nu}_{ring}$	1045		
δ_{ring}	1029		
γ(CH)	990		
$\boldsymbol{\nu}_{ring}$	786		
τ_{ring}	712		

Table 25. Assignment of vibrational frequencies for the IR spectrum of phosphotungstic acid.[104]

Assignment	Frequency (cm^{-1})
W-O-W $\boldsymbol{\upsilon}_1$	770
W-O-W $\boldsymbol{\upsilon}_2$	884
W=O	973
P-O	1087

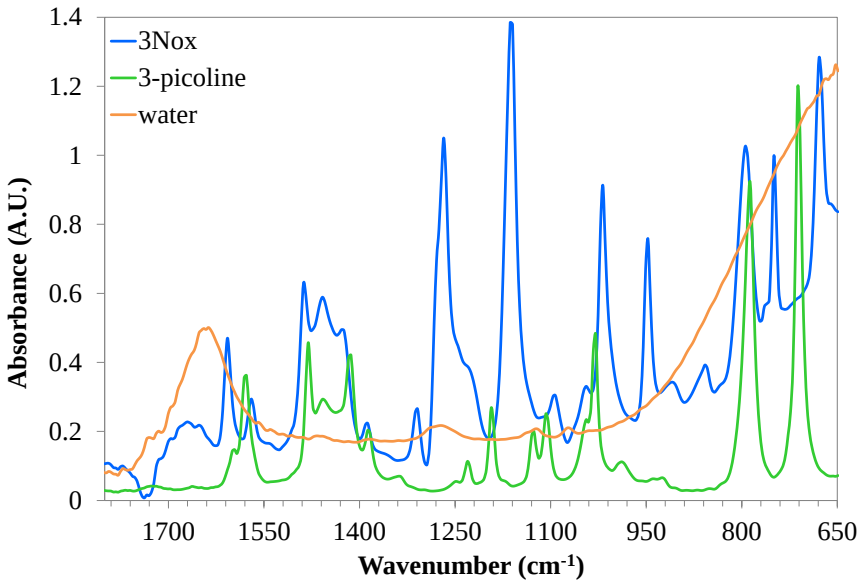

Figure 77. Infrared spectra of 3-picoline, 3Nox, and water

Figure 77 shows the spectra of 3-picoline, 3Nox, and water in the region selected for this study. It can be seen that the infrared spectrum of 3Nox contains strong bands that overlap many of the characteristic bands of 3-picoline. Also, water absorbance is very strong at wavenumbers below 1000 cm^{-1} and in the range 1550-1750 cm^{-1}. Therefore, water may interfere with the measurements in these ranges.

Figure 78 shows the spectra of 3-picoline with different amounts of phosphotungstic acid dissolved in a small quantity of water (20-30 g). The ReactIR 15 instrument usually does not "see" the solids in solution. However, as shown in Figure 78, when the concentration of catalyst is high enough, the instrument can detect the presence of phosphotungstic acid. The increased height of the bands at 712 and 786 cm^{-1} is due to additional water in the mixture, from the phosphotungstic acid, which is a hydrate.

For the selection of the peaks to be used for each compound, two criteria should be fulfilled: a distinct absorption of the compound at the selected wavenumber and a negligible or minimal absorption of the rest of the compounds in that specific

wavenumber if possible. Clearly, 3-picoline and 3Nox have very similar structures and therefore share several characteristic peaks. However, because molecular, chemical, and physical environment have a strong effect on the infrared spectrum, bands corresponding to the same vibrations can be shown in slightly different locations.[105] This difference offers an advantage for the calibration, because there are more peaks available to track. In addition, the band corresponding to the N–O (1268 cm^{-1}) bond in the infrared spectrum of 3Nox is strong and unique, and could therefore be used for the calibration.

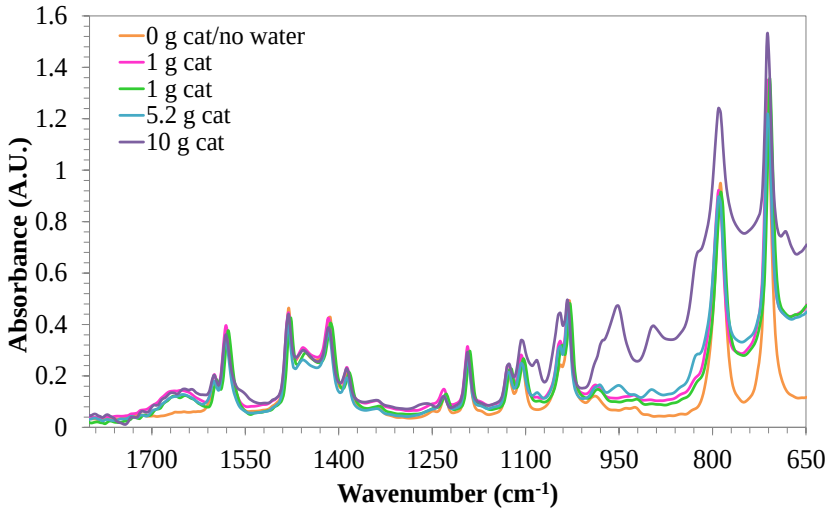

Figure 78. IR spectra of pure 3-picoline, and 3-picoline with a small quantity of water and different amounts of phosphotungstic acid.

In order to obtain more clear and defined peaks and eliminate some of the peak overlap, the second derivative was applied to the spectra. The second derivative also reduces the effect of water in the spectra. Figure 79a-c show the spectra of 3-picoline, 3Nox, and water after the second derivative was applied.

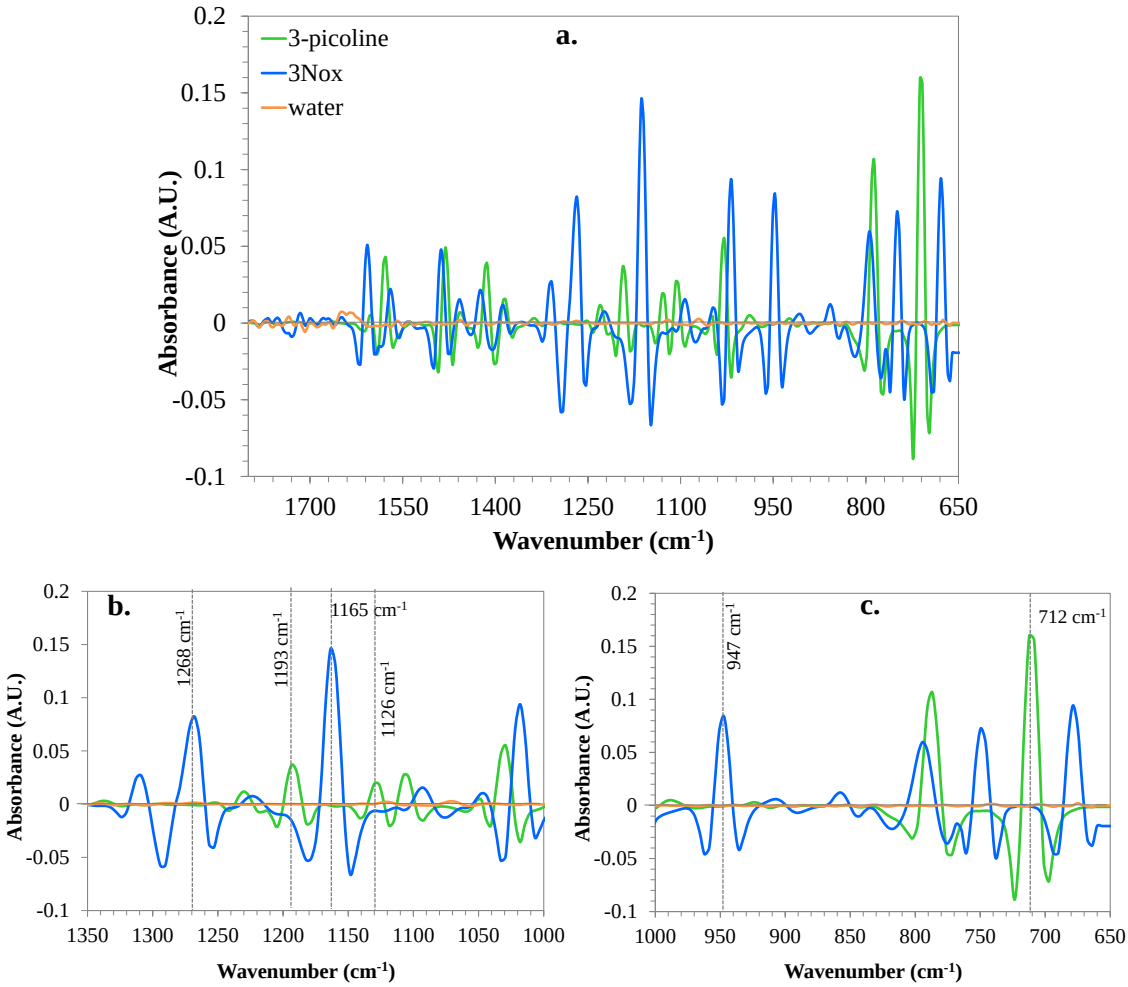

Figure 79. Infrared spectra of 3-picoline, 3Nox, and water with second derivative applied. a) Full region of study shown; b) Zoom-in region 1350-1000 cm^{-1}; c) Zoom-in region 1000-650 cm^{-1}

By using the second derivative, it was possible to trend some peaks characteristic of 3-picoline, *e.g.,* 1192 and 1126 cm^{-1}, which were not clear or were overlapped before. It can also be seen in Figure 79 that the spectrum of water was reduced to an almost flat line, which does not overlap with other compounds. The bands selected for trending are listed in Table 26.

Table 26. Selected frequencies for the calibration of the infrared probe

	3-picoline	3Nox
Frequency (cm^{-1})	712	749
	1126	947
	1192	1165
		1268

Once the characteristic peaks of the spectra were selected, their peak heights to zero were followed throughout the experiment. Figure 80 shows the change of peak height with concentration at different frequencies throughout the calibration experiment performed at 110 °C with 3-picoline. Low peak heights correspond to lower concentrations of 3-picoline. Figure 81 shows the peak trends for 3-picoline with respect to time (only part of the experiment time is shown) during one of the calibration experiments with 3-picoline performed at 110 °C. The addition steps are clearly shown in Figure 81, which demonstrates the sensitivity of the probe. For each concentration (each addition step), the peak heights were averaged; then, the average was used as the reference value for the corresponding solution concentration to develop a univariate model.

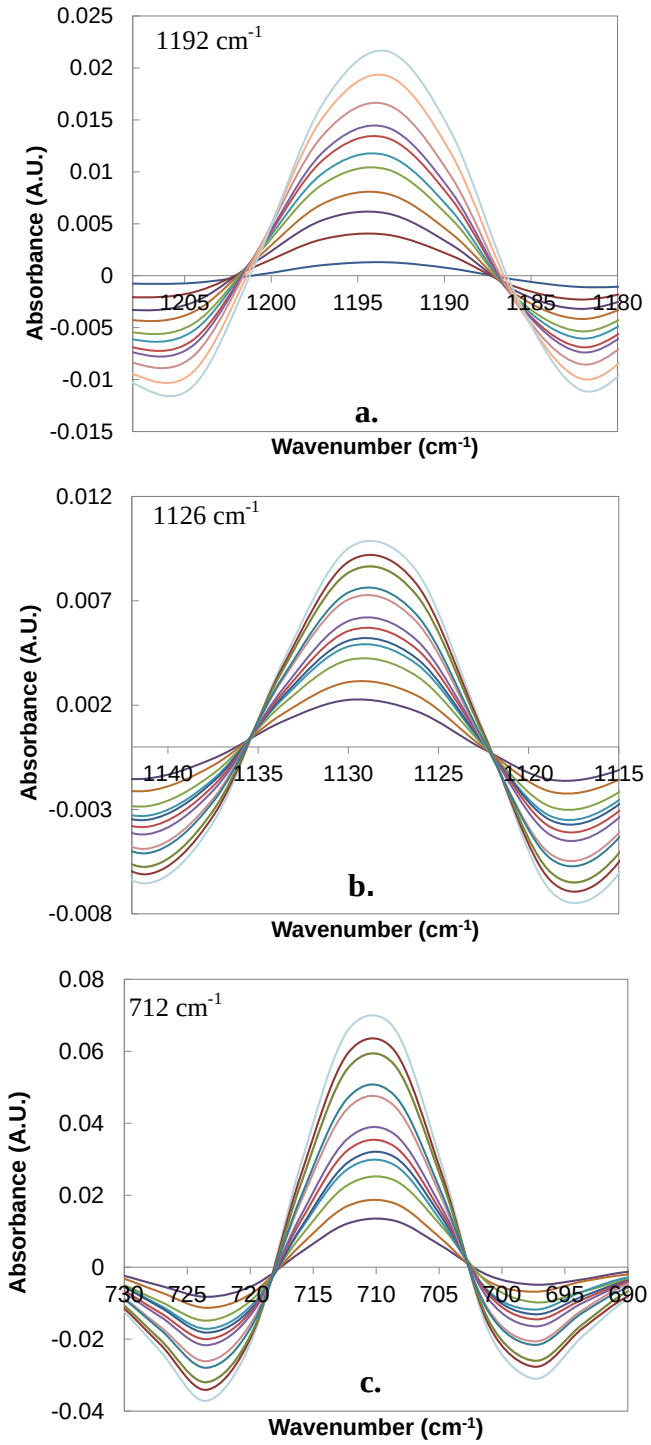

Figure 80. Peak height variation with concentration of 3-picoline at the selected frequencies during a calibration experiment performed at 110 °C. a) Peak height at 1192 cm^{-1}; b) Peak height at 1126 cm^{-1}; and c) Peak height at 712 cm^{-1}

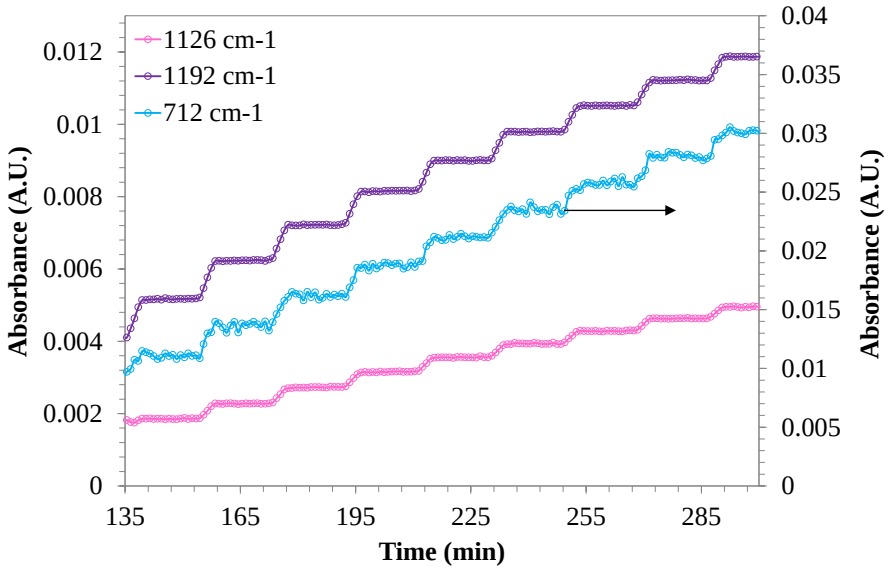

Figure 81. Peak trends for 3-picoline at the selected frequencies showing the addition steps

Figure 82a-c show the peak height of different absorption bands as a function of 3-picoline concentration at 110 °C in an aqueous solution containing only 3-picoline. As can be seen in Figure 82 the absorption at 1192 cm^{-1} changed linearly with concentrations up to 5.5 mole/L, while absorption at 712 cm^{-1} was not linear throughout the entire concentration range. Instead, the peak at 712 cm^{-1} shows a quadratic trend.

The absorption at 1126 cm^{-1} was also linear up to 5.5 mole/L; however, the absorption at this frequency loses its linearity at concentrations below 2 mole/L. The concentration of 3-picoline during a reaction lies in the range of 9.5 mole/L to zero, while the concentration of its *N*-oxide is between zero and 4.9 mole/L.

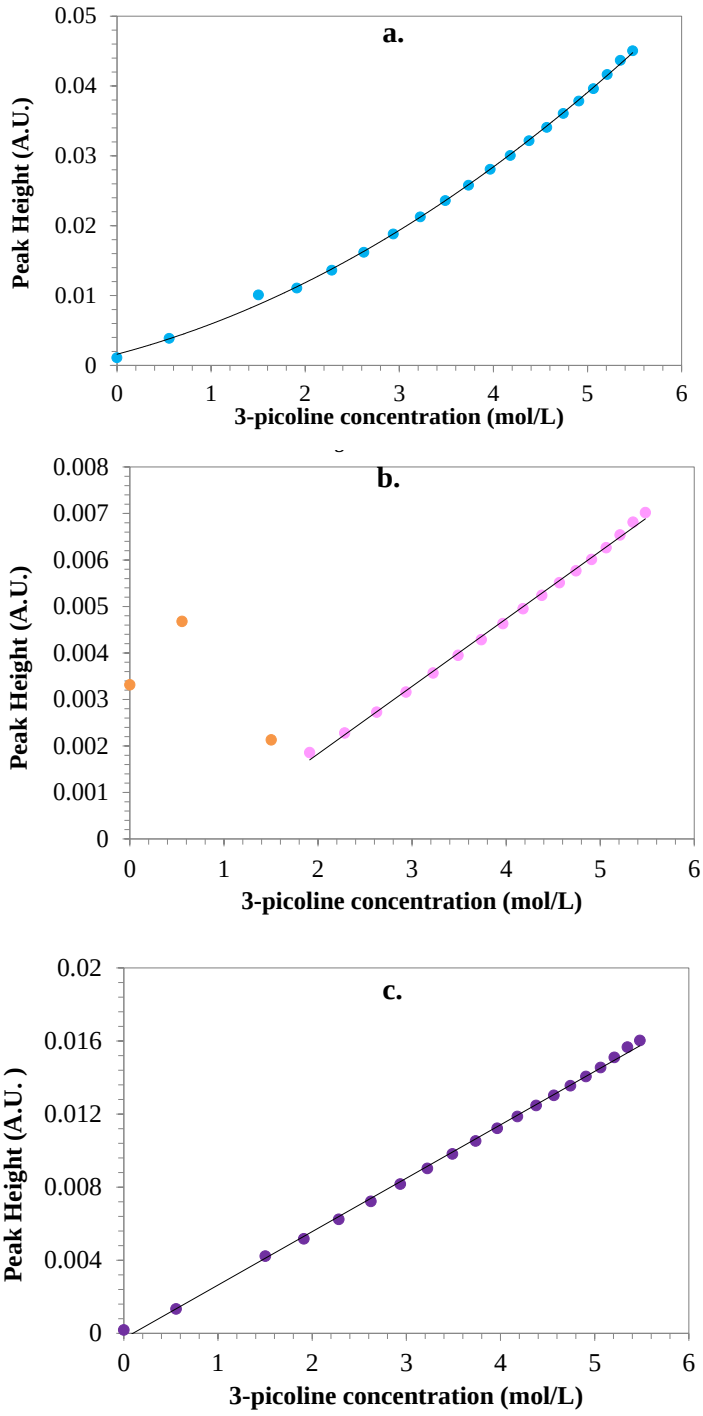

Figure 82. Linear relationship between peak height and concentration of 3-picoline at the selected frequencies: a) 712 cm^{-1}; b) 1126 cm^{-1}; and c) 1192 cm^{-1}

A blank *N*-oxidation experiment performed at 110 °C was used to evaluate the infrared absorption at higher concentrations than those shown in Figure 82. In the blank experiment, pure 3-picoline was loaded to the reactor and brought to the experiment temperature. Then, instead of adding hydrogen peroxide, an amount of water equal to that of hydrogen peroxide was added at a rate of 4 g/min. Thus, the *N*-oxidation reaction did not occur and the concentration of 3-picoline decreased only due to the dilution effect. During the experiment, infrared spectra were taken every minute and the aforementioned infrared bands were followed. Due to the constant dosing of water, the concentration of 3-picoline changed continuously, as opposed to steps, from 9.5 mole/L to 4.9 mole/L.

Figure 83 shows the peak height vs. 3-picoline concentration for both the calibration experiment and the blank experiment. Although two separate experiments are shown in the plots, the overlap is almost perfect, except in the case of the band at 1126 cm^{-1}. As in Figure 82, the peak height at 712 cm^{-1} shows a quadratic relationship with 3-picoline concentration. In the case of the absorptions at 1192 and 1126 cm^{-1}, the trends seem to lose linearity at concentrations above 8.8 mole/L.

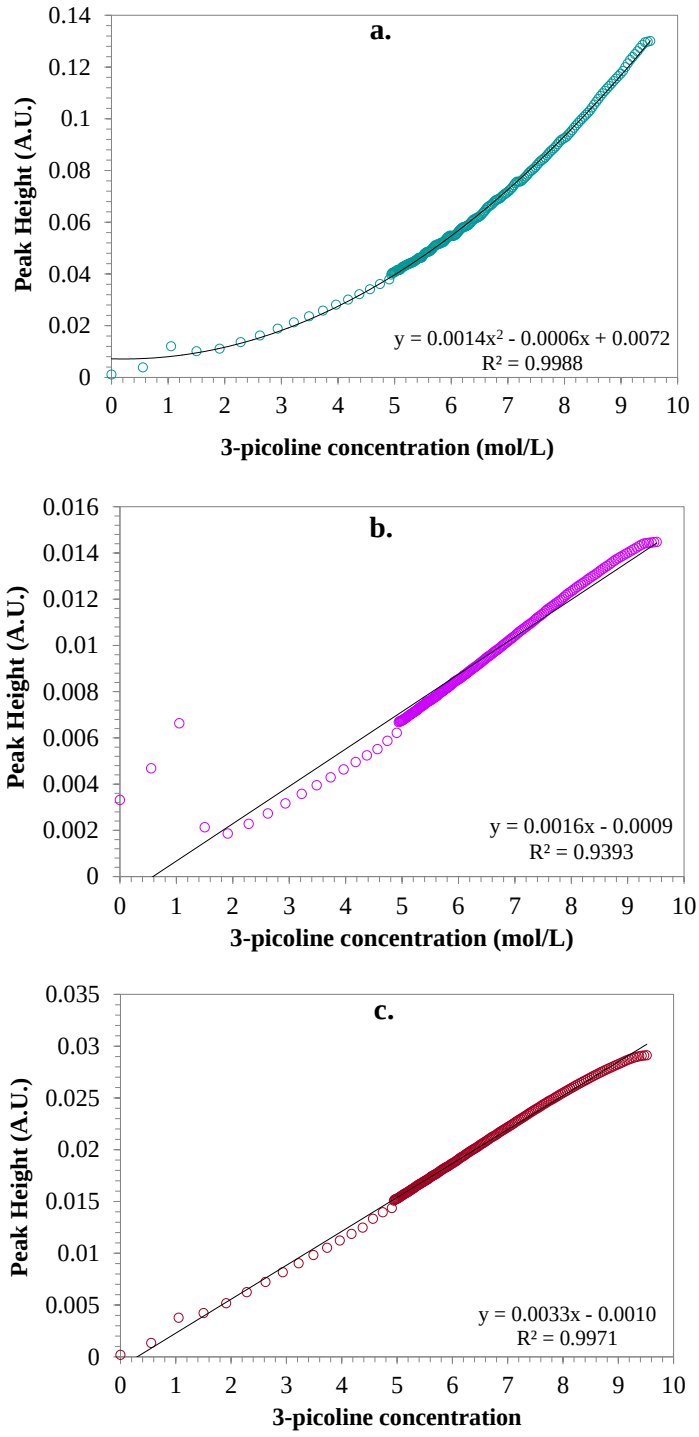

Figure 83. Peak heights as a function of 3-picoline concentration in water at 110 °C, at the selected frequencies: a) 712 cm^{-1}; b) 1126 cm^{-1}; and c) 1192 cm^{-1}

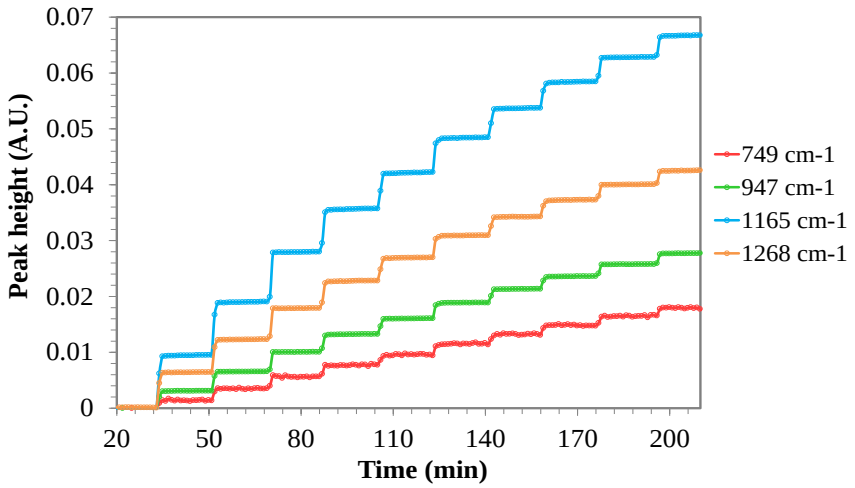

Figure 84. Peak trends for 3Nox at different frequencies showing the addition steps

A similar process was employed for the correlation of the absorption 3Nox solutions. Figure 84 shows the peak trends for 3Nox with respect to time (only part of the experiment time is shown) during one of the calibration experiments with 3Nox performed at 60 °C. The addition steps are clearly shown in Figure 84.

Figure 85a-d show the peak height of different absorption bands as a function of 3Nox concentration in an aqueous solution at 60°C. As can be seen in
Figure 85, all the 3Nox selected absorption peaks change linearly with 3Nox concentrations up to 2.5 mole/L.

7.1.2 Temperature effect

In order to see the effect of temperature on the infrared spectra, calibration experiments with 3-picoline/water solutions were performed at 60, 80, and 110°C, following the procedure outlined in Section 7.1. Figure 86a-c show the peak height as a function of 3-picoline concentration at different temperatures.

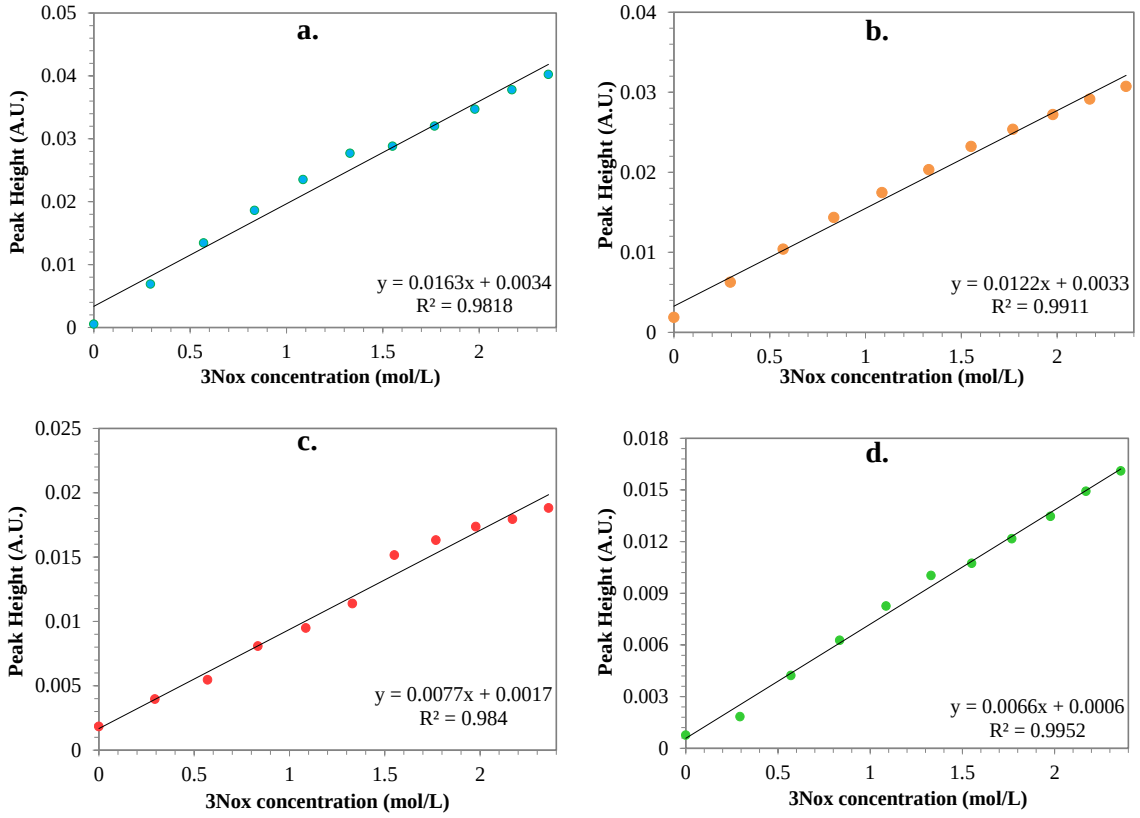

Figure 85. Peak heights as a function of 3Nox concentration in water at 60 ^{o}C at the selected frequencies: a) 1165 cm^{-1}; b) 1268 cm^{-1}; and c) 749 cm^{-1}; and d) 947 cm^{-1}

It can be seen from Figure 86 that the temperature has a slight effect on the infrared absorption at the selected frequencies. The peak height at 712 cm^{-1} is the least affected by temperature changes. Higher temperatures lead to lower absorption, and the effect of the temperature is more pronounced at high concentrations. The comparison shown in Figure 86 emphasizes the importance of performing the calibration at the temperature of the reaction; extrapolations from other temperatures can lead to serious mistakes in the prediction of concentration.

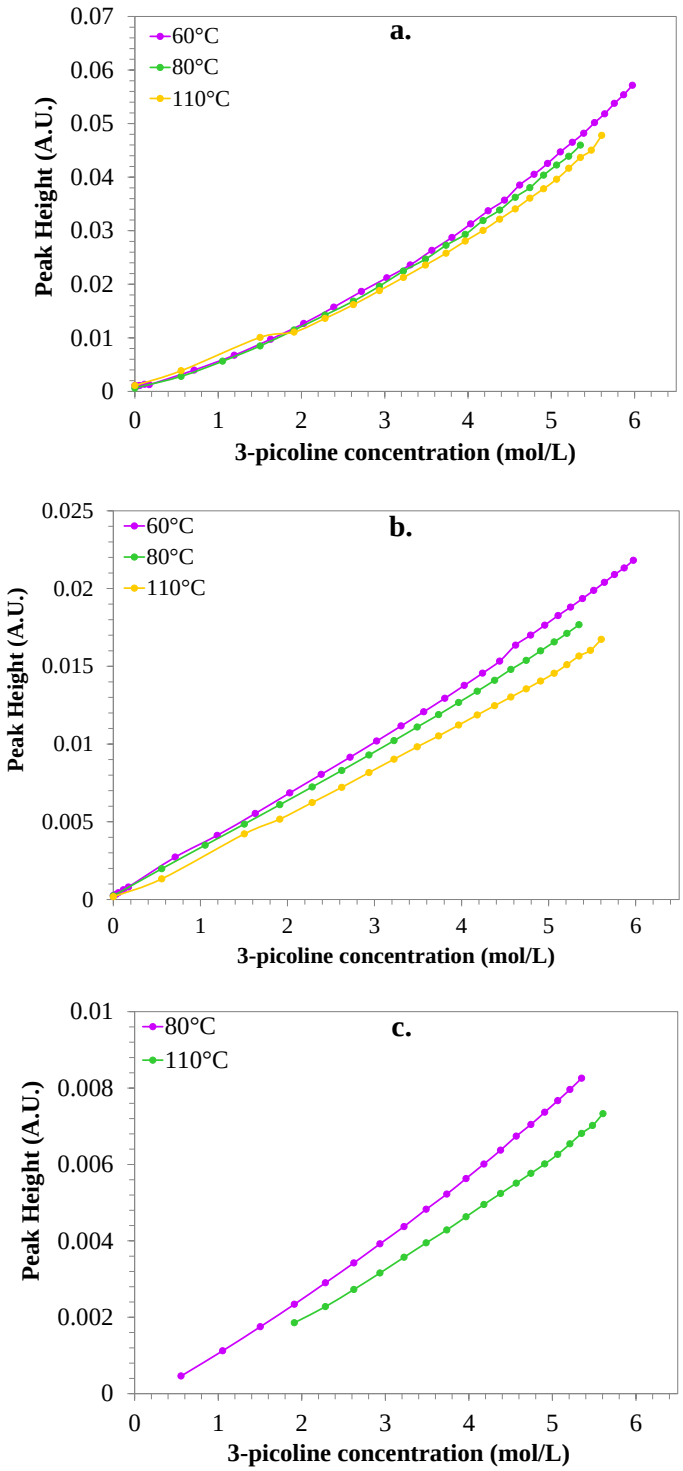

Figure 86. Peak height as a function of 3-picoline concentration at different temperatures, at the selected frequencies: a) 712 cm^{-1}; b) 1192 cm^{-1}; and c) 1126 cm^{-1}

7.1.3 Synergistic effects in the infrared spectra

In order to examine the influence that the absorbance of the product has on the reactant and vice versa, 3Nox was added in a step-wise mode on an aqueous solution containing 3-picoline, and the peak heights were measured at the aforementioned frequencies.

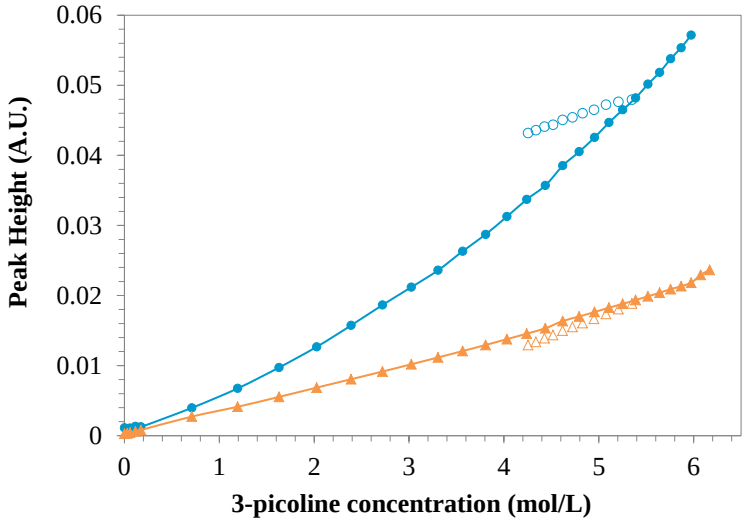

Figure 87. Peak height as a function of 3-picoline concentration at 60°C, at the selected frequencies of 712 cm^{-1} (blue) and 1192 cm^{-1} (orange), in presence of 3Nox (open markers) and without 3Nox (closed markers)

Figure 87 shows that the peak height is affected by the presence of the 3Nox, in particular, the peak at 712 cm^{-1}. The change in the peak at 1192 cm^{-1} is less noticeable; however, due to the few data points, it is not possible to determine with certainty the magnitude of the difference over the entire concentration range.

Figure **88** shows the effect of 3-picoline on the peak heights of 3Nox. Evidently, the peak heights change dramatically in presence of 3Nox. As mentioned earlier, the molecular, chemical, and physical environment have a strong effect on the infrared spectrum.[105] Therefore, in order to have more accurate calibration, it is necessary to have a calibration environment as similar as possible to the reaction mixture. An alternative way to

calibrate the infrared probe would be to perform a reaction and take samples at regular intervals to be analyzed offline using a GC or HPLC. Then, concentration data may be used for the calibration.

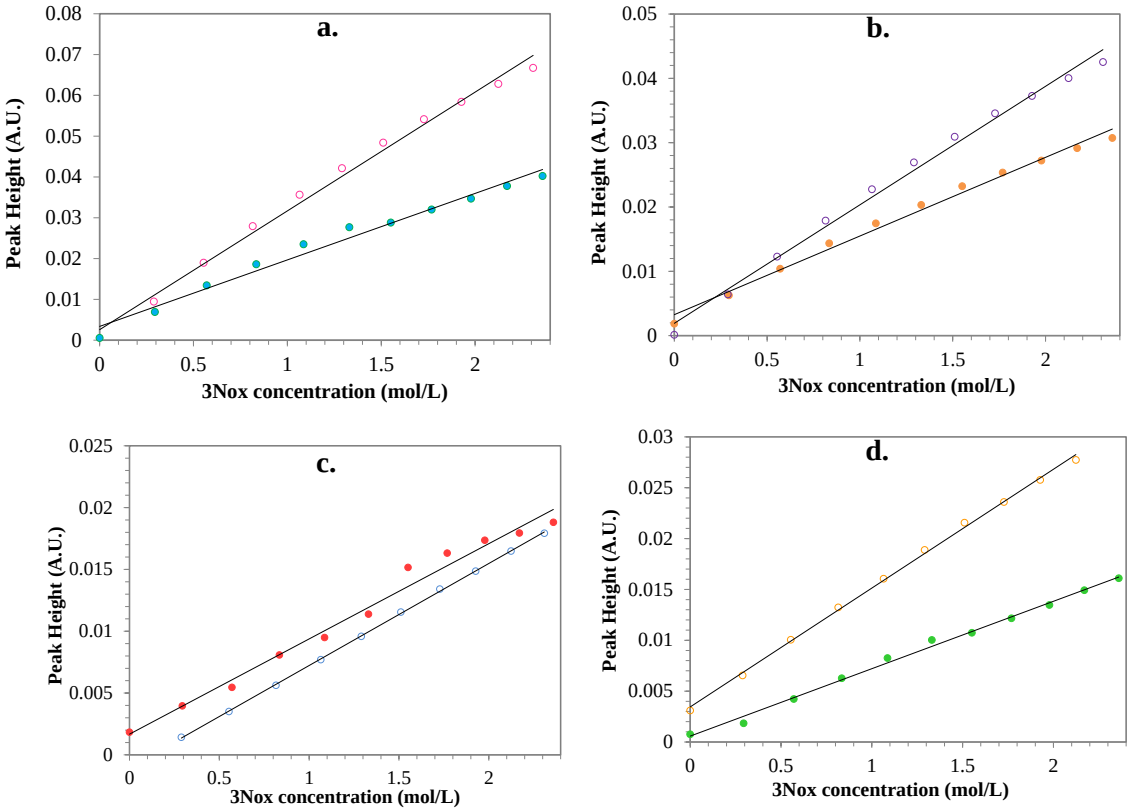

Figure 88. Peak height as a function of 3Nox concentration at 60°C at the selected frequencies in the presence of 3-picoline (open markers) and without 3-picoline (closed markers); a) 1165 cm^{-1}; b) 1268 cm^{-1}; c) 749 cm^{-1}; d) 948 cm^{-1}

7.2 Estimation of Concentration from IR Data

Once the linear relationships between peak height and concentration were found, concentrations calculated calorimetrically were compared with those calculated using the linear relationships obtained from the IR calibration.

Figure 89 shows a comparison of concentrations calculated calorimetrically and using the IR calibration for an experiment performed at 110 °C, with 10 g catalyst, a dosing rate of 4 g/min and a stirring rate of 250 rpm (part of factorial design, see Section 5.2).

As shown in Figure 87, the peak at 712 cm^{-1} is not ideal for the measurement of 3-picoline concentration because it is strongly affected by the presence of 3Nox. Further evidence is provided by Figure 89. It is clear that the peak at 712 cm^{-1} does not accurately represent the concentration of 3-picoline throughout the experiment.

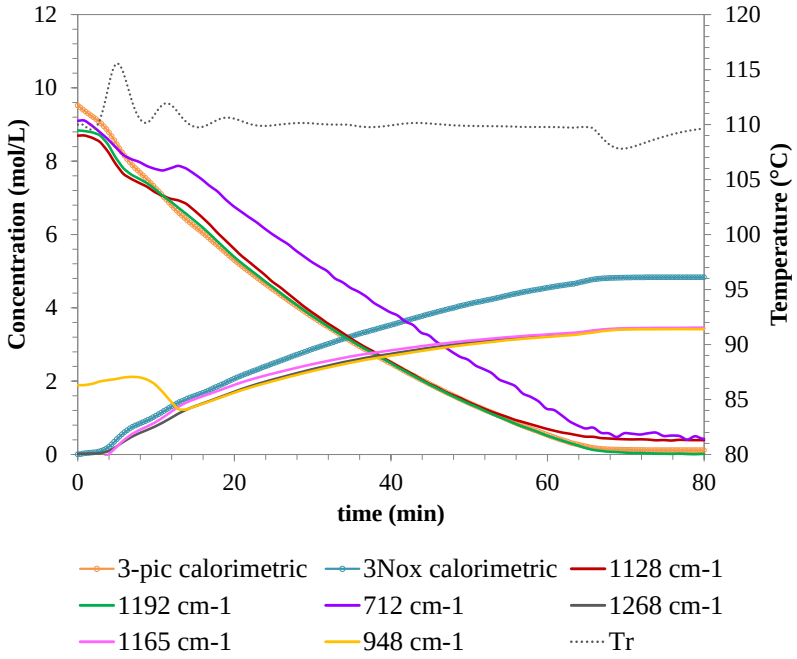

Figure 89. Comparison of concentrations calculated calorimetrically and using *in-situ* FTIR for an *N*-oxidation of 3-picoline performed at 110 °C using 10 g of catalyst

For the prediction of the concentration of 3-picoline, peaks at 1126 cm^{-1} and 1192 cm^{-1} show a much better agreement with calorimetric concentration. However, there are some differences at the beginning and at the end of the measurement.

Differences at the beginning can be explained in part due to the temperature variation in the reactor. In the first five minutes of the measurement, there is a temperature overshoot of approximately 5 °C caused by the initiation of dosing to the reactor and the heat of mixing. Subsequently, the temperature slowly stabilizes. Additionally, the disagreement between concentrations at the beginning of the reaction may be because the infrared probe is not sensitive to high concentrations. As mentioned earlier, for the frequencies tracked, the peak height loses linearity with concentration at around 8.8 mole/L, so the prediction at higher concentrations is not accurate (See Figure 83). There is also some disagreement at the end of the experiment between the concentrations calculated calorimetrically and using the IR. This is because the probe was not sensitive to low concentrations. As shown in Figure 82, peak heights at 712 cm^{-1} and 1126 cm^{-1} were not linear at concentrations below 2 mole/L. In addition to the inaccurate spectrometric measurement of concentration, the absolute error in the power of the reaction is comparable to the measured power itself, thus rendering the reliable calorimetrically calculated concentration also problematic.

With regards to 3Nox, it can be seen in Figure 89 that concentrations calculated using the IR calibration are widely underpredicted, except the first 13 minutes for the concentration calculated from peak height at 947 cm^{-1}, which show erroneous behavior; it is impossible that the concentration of 3Nox starts at a value other than zero. This disagreement is likely due to the fact that the catalyst has some interference at this frequency (947 cm^{-1}), as shown in Figure 78. After 13 minutes, the correlation for 947 cm^{-1} shows agreement with the 3Nox concentrations calculated from peak heights at other frequencies.

During experiments performed in the RC1*e*, it was observed that when 10 g of catalyst were used, some of the catalyst precipitated. The catalyst typically dissolved after adding approximately 50 g of the hydrogen peroxide 35 wt. % aqueous solution. The experiment shown in Figure 89 was performed using a dosing rate of 4 g/min; at this

rate, 52 g would be added after 13 min, which supports the hypothesis that undissolved catalyst may have interfered with the peak height measurement at this frequency.

7.2.1 Estimation of concentration from conversion data

Figure 90 shows a 3D plot of the infrared absorption evolution during the *N*-oxidation of 3-picoline. The plot consists of all the IR spectra taken throughout the dosing and stir-out period, and it allows for seeing the change in absorption intensity at different frequencies over time.

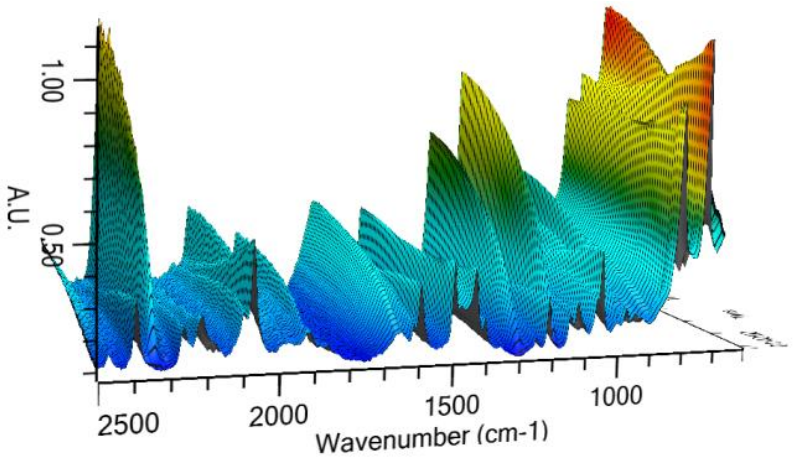

Figure 90. 3D plot of the infrared absorption evolution during an *N*-oxidation of 3-picoline at 110°C using 1 g of catalyst

Figure **91** shows a set of selected spectra taken from the plot shown in Figure 90 at specific times, *i.e.*, each spectrum shown in

Figure **91** is a 'slice' of the 3D plot at a certain time.

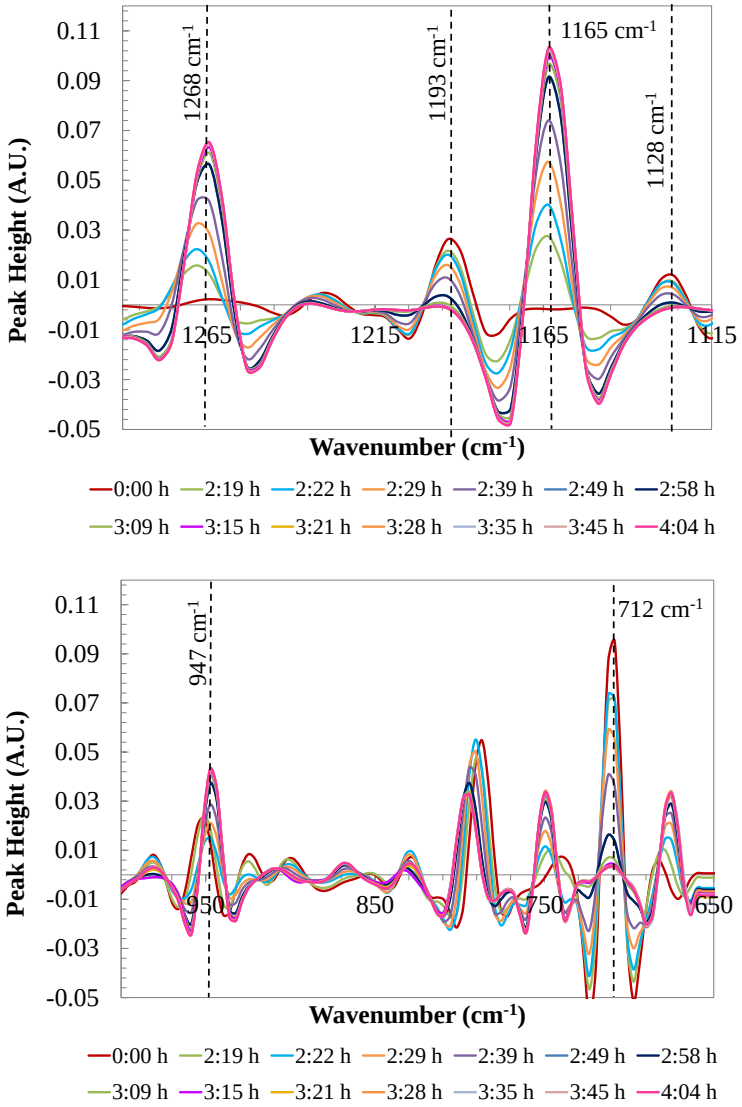

Figure 91. Variation of absorption intensity at different frequencies during the *N*-oxidation of 3-picoline at 110 °C and 10 g of catalyst using a dosing rate of 4 g/min and a stirring rate of 250 rpm

The conversion of 3-picoline at any time *t* can be calculated as:[80]

$$\%\ conversion\ (t) = 1 - \frac{peak\ height\ (t)}{\max. peak\ height} \times 100 \qquad \text{(Eq. 43)}$$

Peak height (t) is the height of the peak at the selected frequency at any given time. For 3-picoline, the maximum peak height is the peak height at the selected frequency right before dosing starts. Figure 92 shows the conversions for three different experiments, calculated using Equation 43 and the peak height at 1192 cm^{-1}. This frequency was selected because of its linearity with 3-picoline concentration throughout most of the range of concentrations of the experiment. From Figure 92, it can be seen that all three measurements follow approximately the same path. This indicates that the reaction is controlled by dosing. Temperature does not provide any benefit. Although the reaction certainly occurs at a faster rate at 125 °C, it is controlled by dosing, so no difference is observed with the experiments performed at lower temperatures.

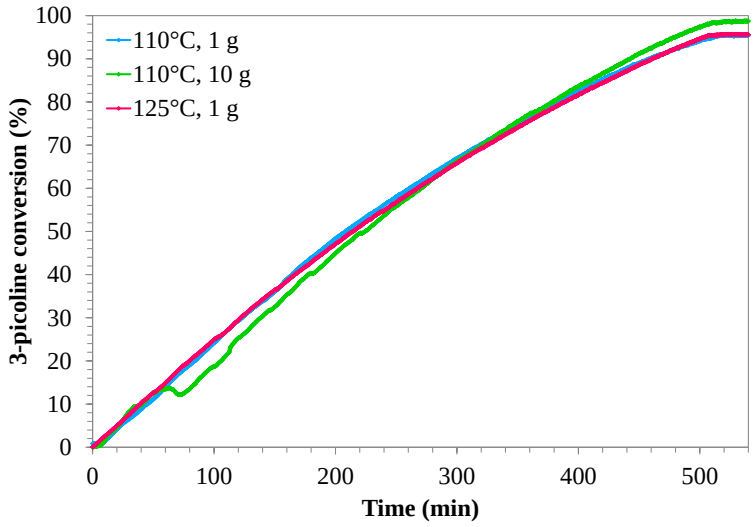

Figure 92. 3-picoline conversions for three *N*-oxidation experiments performed at different temperature and catalyst concentrations. In all experiments, a dosing rate of 0.5 g/min and a stirring rate of 250 rpm were used

Table 27 shows a comparison of the conversions of 3-picoline calculated using Equation 43 and the conversions calculated using the method described in Section 5.1, for the three experiments shown in Figure 92. It can be seen in Table 27 that the conversions calculated using the two different methods agree well, with the greatest difference being 1.1%. Experiment 2 leads to a higher conversion due to the positive effect of the

catalyst. However, the achieved increase in conversion of experiment 2 is only 3.3%, using 10 times as much catalyst as in experiment 1.

Table 27. Comparison of final conversions obtained from IR data and conversions calculated from pressure differences for the experiments shown in Figure 92

Exp.	Conditions	% Conversion (from IR)	%Conversion (from pressure calculations)
1	110°C, 1 g catalyst	95.4	96.5
2	110°C, 10 g catalyst	98.7	98.0
3	125°C, 1 g catalyst	95.6	95.2

Conversions obtained using Equation 43 were also used to calculate concentrations, using the following equation:

$$[3pic] = \frac{n_{3-pic,0} \cdot (1 - X)}{V} \qquad \text{(Eq. 44)}$$

where,

$[3pic]$ is the concentration of 3-picoline,

$n_{3-pic,0}$ are the initial moles of 3-picoline in the reactor,

X is the conversion, calculated with Equation 36, and

V is the volume of the reaction mixture

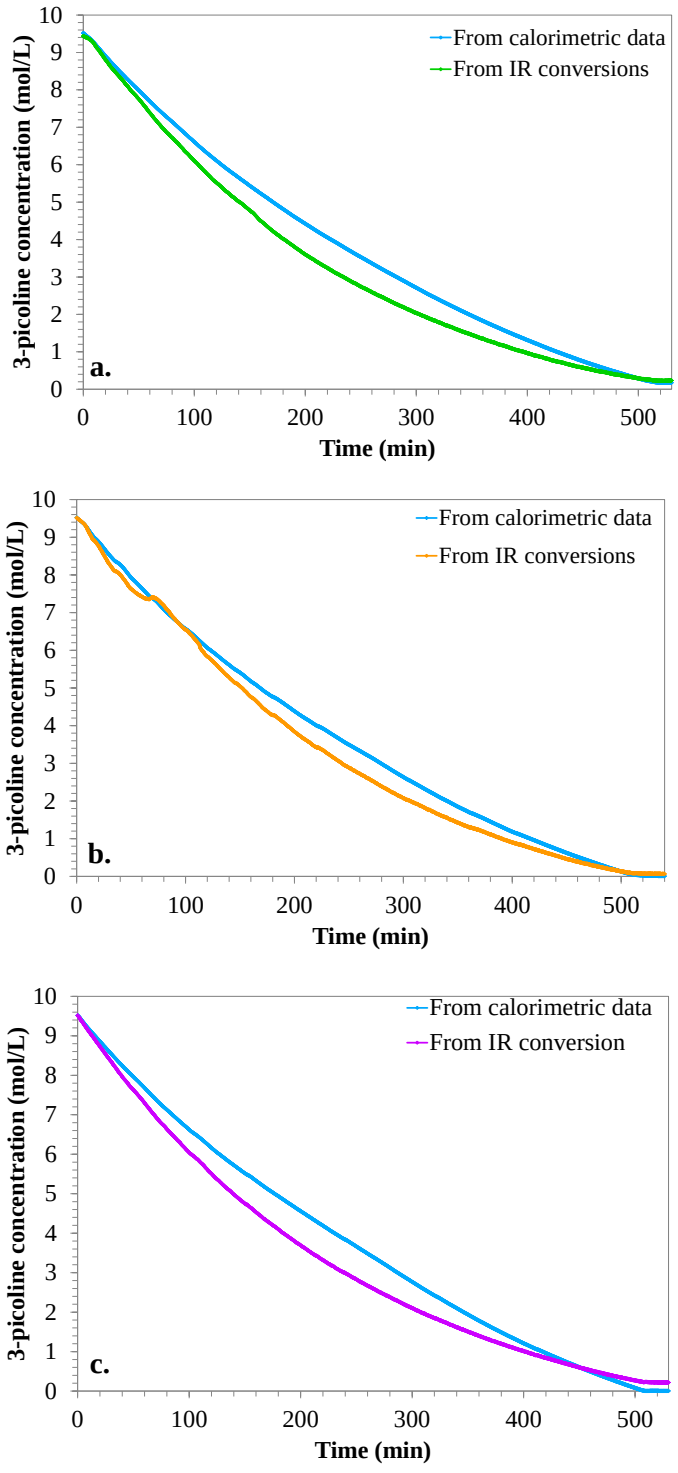

Figure 93. Comparison of concentrations calculated from calorimetric data and from Equation 38 for the *N*-oxidation of 3-picoline at different temperatures and mass of catalyst. a) 110 °C and 1 g of catalyst; b) 110 °C and 10 g of catalyst; a) 125 °C and 1 g of catalyst;

Figure 93 shows a comparison of 3-picoline concentration calculated from calorimetric data and concentrations calculated using Equation 44. In all cases, the concentrations estimated from IR conversions and from calorimetric data have similar start and finish values, but they do not follow exactly the same path. As will be shown in Section 7.3, it appears that an intermediate forms in the reaction. The intermediate has peaks that correspond to both 3-picoline and 3Nox, including the peak at 1192 cm^{-1}. Thus, the concentration obtained from IR conversions may represent more than one compound (3-picoline and an intermediate) and it cannot be directly compared to concentrations obtained from calorimetric data, where it is assumed that the concentration of 3-picoline decreases according to a single reaction.

7.3 Study of the *N*-oxidation of Alkylpyridines Using ConcIRT™

ConcIRT™ is a curve-resolution algorithm that searches the collected infrared spectra to identify groups of wavenumbers that change in the same manner, *i.e.*, at the same rate. The algorithm assumes that the wavenumbers that change in the same way belong to the same component, and thus, it provides an individual spectrum for each identified component. At the same time, ConcIRT™ also calculates the relative concentration profiles of each component.[80] ConcIRT™ can be used in real time, while the spectra are being collected, but it can also be used during an offline analysis.

ConcIRT™ offers several advantages over other analytical techniques. It is fast, it can be used in real-time and it is possible to detect unstable, fast-disappearing intermediates.[94] Because of those advantages, ConcIRT™ has been previously used in different studies, including kinetic and mechanistic studies, polymer synthesis, and homogeneous- and bio-catalysis.[94]

A time frame as well as a frequency interval must be specified for the ConcIRT™ analyses. In this study, the time frame has been limited to the dosing of material and

stabilization period once dosing has finished. By default, ConcIRT™ analyzes the "fingerprint" region of the infrared spectrum, which is located between 1900 cm^{-1} and 900 cm^{-1}. As mentioned earlier, most changes in *N*-oxidation of 3-picoline occur between 1800 cm^{-1} and 650 cm^{-1}; therefore, the ConcIRT™ analysis was limited to this region. No second derivative or any other data treatment was applied to the data before running the ConcIRT™ software, as data treatment could lead to overprediction and wrong estimations of the software. It must be emphasized that ConcIRT™ is based on mathematical models, and has no "chemical sense". Therefore, it is necessary to carefully interpret the results with chemical knowledge.[106]

Figure 94 shows the relative concentrations profiles obtained from ConcIRT™ for the *N*-oxidation of 3-picoline performed at 110 °C, using 1 g of catalyst, a dosing rate of 0.5 g/min, and a stirring rate of 250 rpm. It can be seen from Figure 94 that ConcIRT™ identified three components. ConcIRT™ compares the reference spectra with the spectra of the identified components and automatically labels any known components. For the analysis shown in Figure 94, ConcIRT™ labeled Component #1 as 3-picoline and Component #3 as 3Nox. It is clear from the profiles of components #1 and #3 that one of them is the reactant (#1) and the other one is the product (#3). Component #2 is an unidentified reaction intermediate.

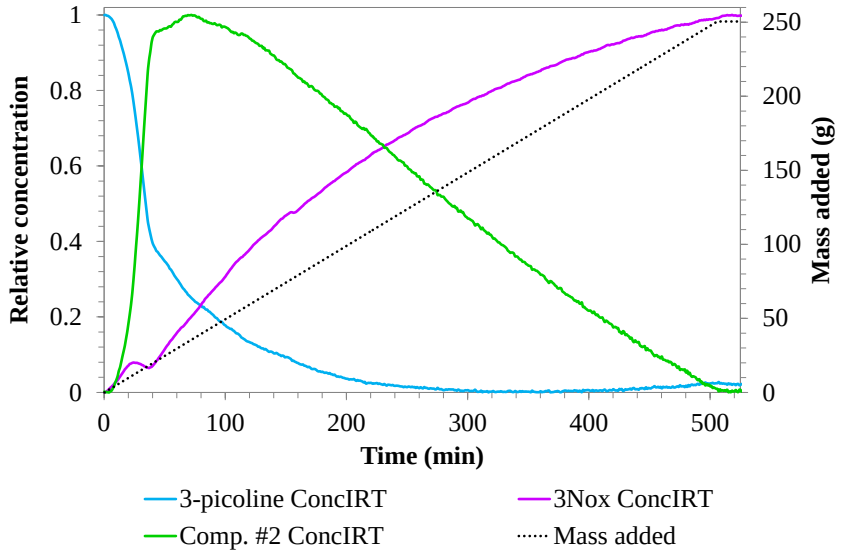

Figure 94. Relative concentration profiles identified by ConcIRT™ for the *N*-oxidation of 3-picoline at 110 °C using 1 g of catalyst, a dosing rate of 0.5 g/min, and a stirring rate of 250 rpm

Figure 95 and Figure 96 show a comparison of the reference spectra of 3-picoline and 3Nox and the spectra calculated by ConcIRT™. It can be seen that the reference and calculated spectra match almost perfectly.

Figure 97 shows the spectrum of the intermediate and it is compared to the spectrum of 3-picoline. It can be seen that the spectrum of the intermediate follows the spectrum of 3-picoline very closely. However, it also presents characteristic peaks of 3Nox at 1271 cm^{-1} and 1167 cm^{-1}, although the frequencies are slightly shifted by 2-3 cm^{-1}. Given the spectrum of the intermediate, it can be hypothesized that the intermediate is formed by some type of complex between the 3-picoline molecule and oxygen from the hydrogen peroxide/catalyst, such that the complex intermediate presents vibrations at the same frequencies as the *N*-oxide.

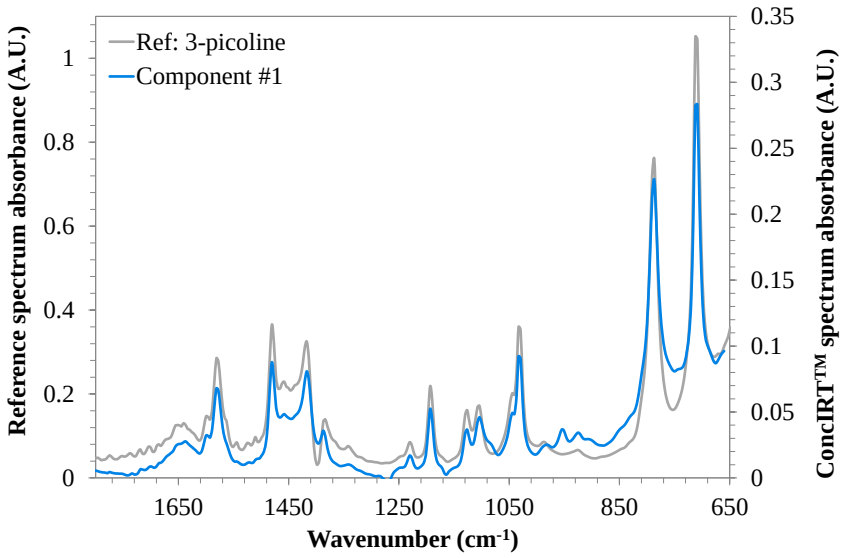

Figure 95. Comparison of the reference spectrum of 3-picoline and the calculated spectrum for Component #1 by ConcIRT™

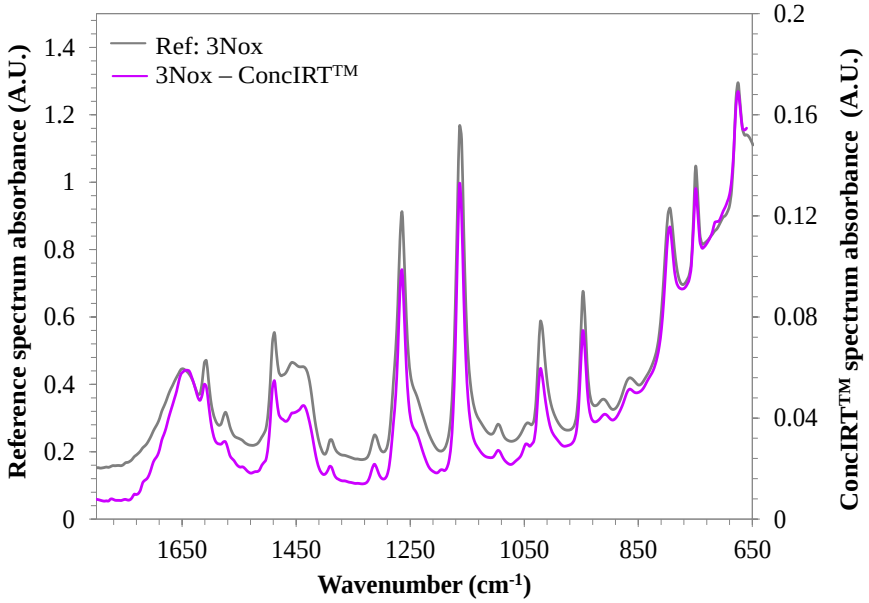

Figure 96. Comparison of the reference spectrum of 3Nox and the calculated spectrum for 3Nox (component #3) by ConcIRT™

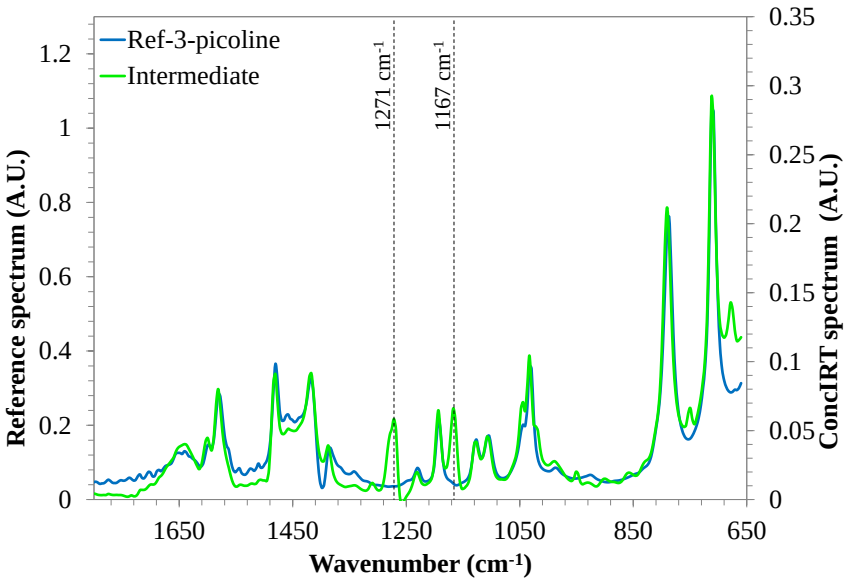

Figure 97. Comparison of the reference spectrum of 3-picoline and the spectrum of the intermediate component identified by ConcIRT™

In order to identify the intermediate, the infrared spectrum of a mixture of 3-picoline and hydrogen peroxide (35 wt. %) was taken, as well as the spectrum of hydrogen peroxide 35 wt. % by itself. The spectrum of a mixture of hydrogen peroxide and phosphotungstic acid was also taken, but it showed to be the same as the spectra of hydrogen peroxide. The spectra taken are shown in Figure 98. Also, the spectrum of the initial reaction mixture composed of 3-picoline, phosphotungstic acid and water was taken, and it was shown earlier in Figure 78.

From the spectra shown in Figure 98 and Figure 78, it can be seen that none of the spectra present peaks at the same frequency as the characteristic peaks of 3Nox. Therefore, the intermediate formed should be a combination of hydrogen peroxide, phosphotungstic acid and 3-picoline.

It has been reported in the literature that heteropolyacids, such as phosphotungstic acid, form peroxotungsten species with hydrogen peroxide, amongst other species,

$[PO_4\{WO(O_2)_2\}_4]^{3-}$ and $[W_2O_3(O_2)_4]^{2-}$.[107] Since neither hydrogen peroxide, nor phosphotungstic acid have strong absorbance in the infrared probe used, it was not possible to observe the peroxotungsten species in this study. It has also been suggested that the peroxotungsten species provide an oxygen to 3-picoline, which is then oxidized to 3Nox.[108]

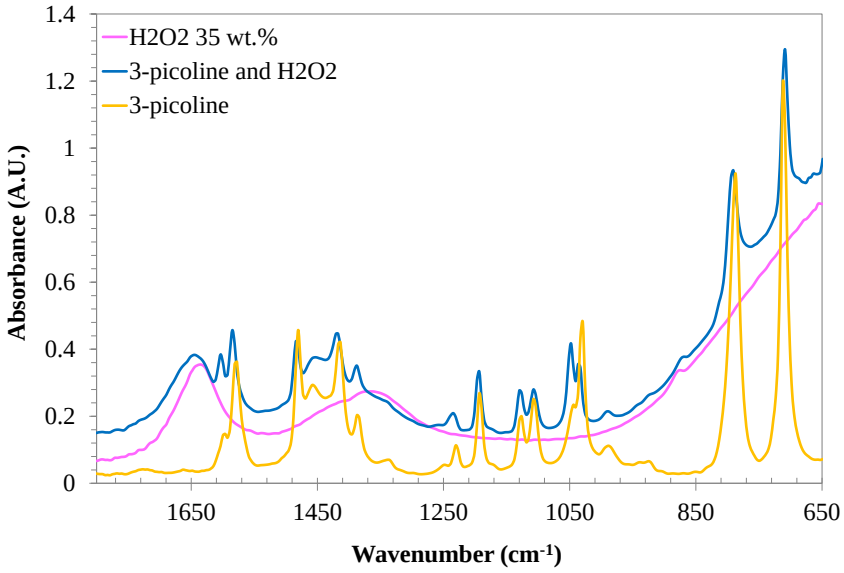

Figure 98. IR spectra of aqueous hydrogen peroxide 35 wt.%, a mixture of hydrogen peroxide and 3-picoline, and pure 3-picoline.

Papadaki and Gao[57] have proposed two possible reaction pathways for the *N*-oxidation of alkylpyridines, an interaction between a peroxotungsten species and the alkylpyridine, and the interaction between the stabilized alkylpyridine with hydrogen peroxide by hydrogen bonding with the peroxotungsten species. It is possible that the intermediate structures formed in those pathways coincide with the intermediate detected in this study; however, since the details of the molecular interactions are unknown, this hypothesis cannot be supported with certainty.

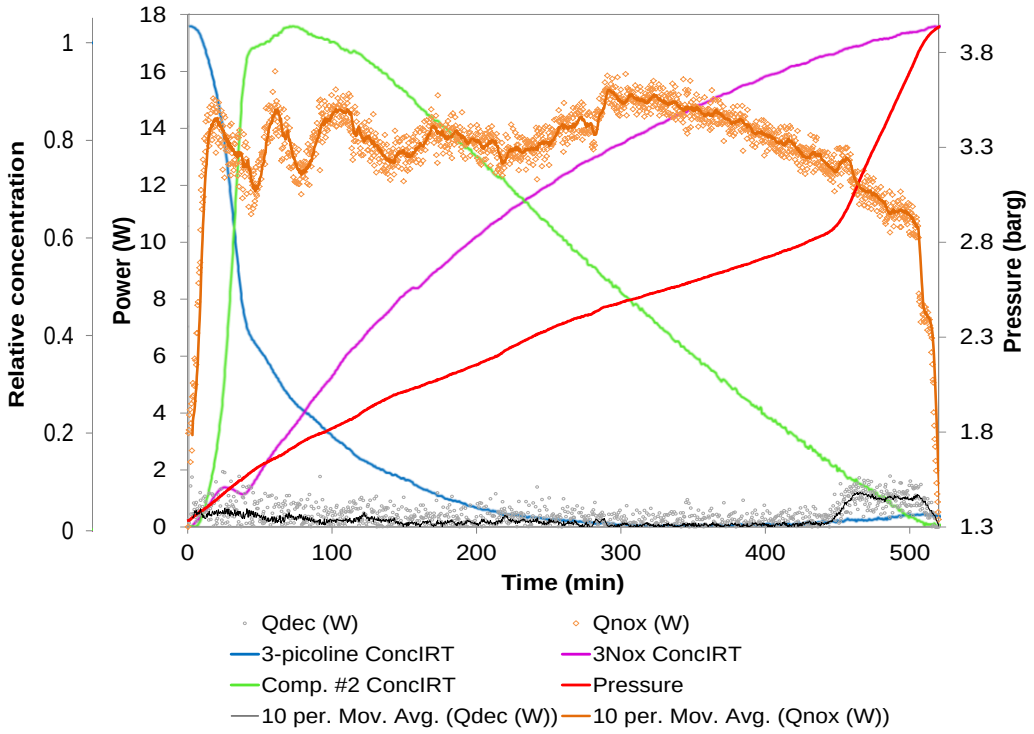

Figure 99. Curves generated during the *N*-oxidation of 3-picoline at 110 °C using 1 g of catalyst, a dosing rate of 0.5 g/min, and a stirring rate of 250 rpm

It can be observed in Figure 99 that the intermediate is formed quickly after dosing starts and as the concentration of the intermediate decreases, the concentration of 3Nox increases. In Figure 100, it can be seen that the production of 3Nox stops at the same time the intermediate is finished, indicating that the intermediate is essential for the formation of 3Nox. Also, due to the low accumulation of hydrogen peroxide, the *N*-oxidation finishes almost right after dosing.

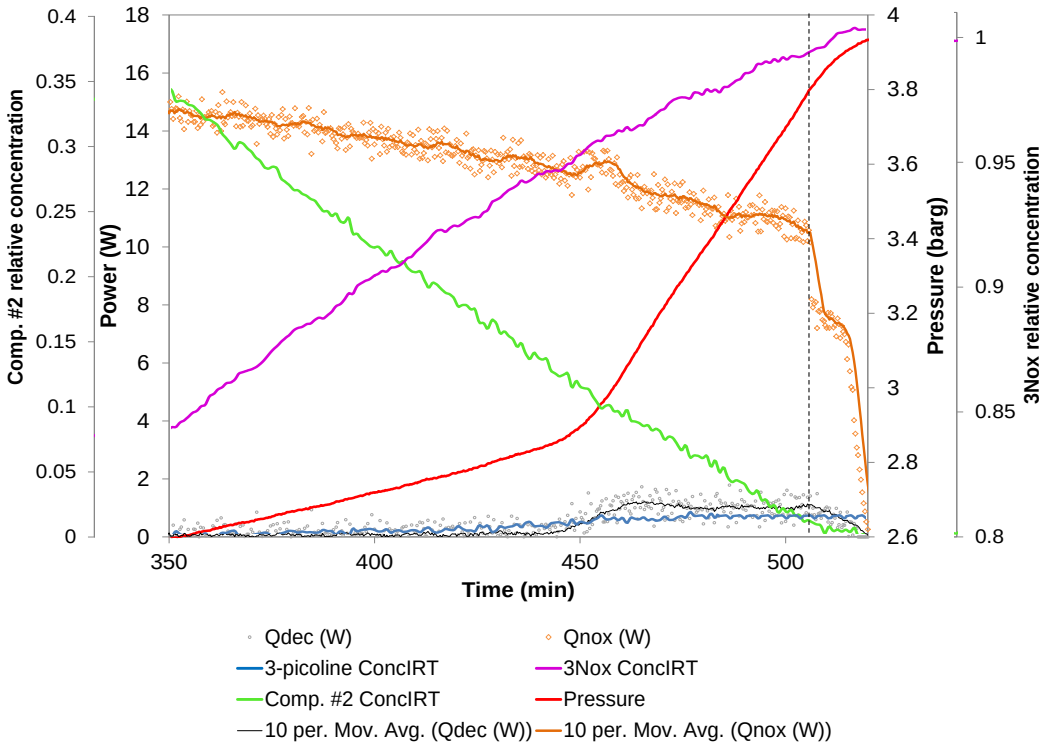

Figure 100. Magnification of Figure 99. Curves generated during the *N*-oxidation of 3-picoline at 110 °C using 1 g of catalyst, a dosing rate of 0.5 g/min, and a stirring rate of 250 rpm

Figure 101 shows the results of an experiment performed at 110 °C, with 10 g of catalyst and a dosing rate of 4 g/min. It can be seen in Figure 101 that the intermediate relative concentration goes to zero soon after dosing stops and so does the production of 3Nox. Due to the much faster rate, hydrogen peroxide accumulates in the reaction. Once dosing stops, the pressure continues to increase due to the generation of oxygen from the hydrogen peroxide decomposition, which indicates that the intermediate is not involved in the decomposition of hydrogen peroxide.

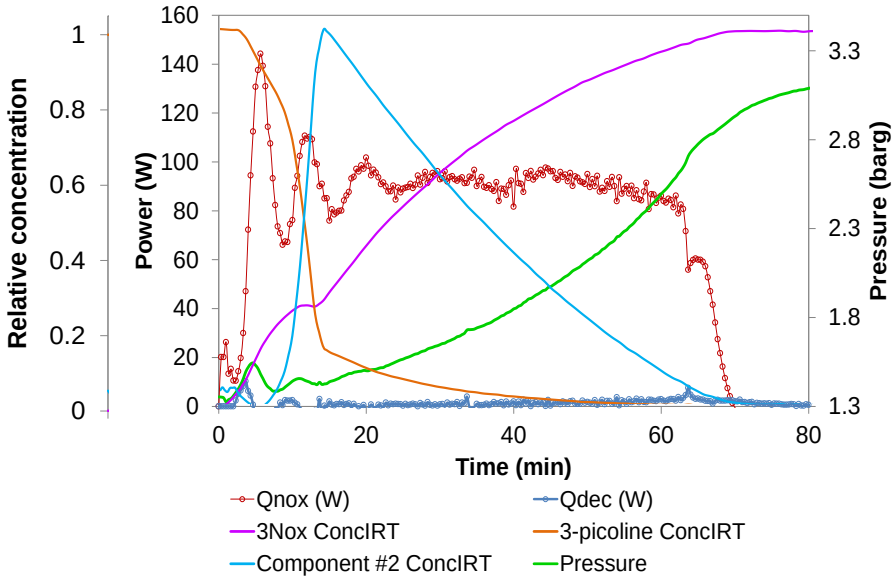

Figure 101. Curves generated during the *N*-oxidation of 3-picoline at 110 °C using 10 g of catalyst, a dosing rate of 4 g/min, and a stirring rate of 250 rpm

7.4 Conclusions

The infrared probe ReactIR 15^{TM} was calibrated using an univariate model based on the Beer-Lambert law, in which the concentration is proportional to the absorption of a compound. The frequencies chosen for the calibration were based on the distinct absorption of the compound at the selected frequency and a negligible absorption of the rest of the compounds at that specific frequency. The second derivative was applied to the spectra to further differentiate the peaks. The selected wavenumbers included 712, 1126 and 1192 cm^{-1} for 3-picoline and 749, 947, 1165, and 1268 cm^{-1} for 3Nox.

For 3-picoline, it was found that the peak at 712 cm^{-1} followed a quadratic relationship with concentration, rather than a linear one. The peak at 1126 cm^{-1} was not sensitive at concentrations below 2 mole/L. The peak at 1193 cm^{-1} provided the best results, although it was linear only up to 8.8 mole/L. In the case of 3Nox, all peaks presented

linearity at concentrations up to 2.5 mole/L. However, the peaks at 1165 and 1268 cm^{-1} are not sensitive at concentrations below 0.3 mole/L

The effect of the temperature on the calibration of 3-picoline indicates that the absorption decreases at higher temperatures, and that the effect is greater at higher concentrations. Therefore, it is necessary to perform the calibrations at the conditions at which the reaction is performed. However, it is unlikely that a change in temperature lower than 5 °C will have a large effect on the predicted concentrations.

The synergistic effects in the infrared spectra were also evaluated to determine the influence of one compound on the absorption of the other one. It was found that the absorption of 3-picoline at 712 cm^{-1} dramatically changes in presence of the *N*-oxide. The absorption at 1192 cm^{-1}, although not identical with and without *N*-oxide, does not present a major difference. On the other hand, the absorption of the *N*-oxide at all selected wavenumbers significantly changes in presence of 3-picoline.

It was found that although the calibrations for both 3-picoline and 3Nox showed linearity, the prediction of concentrations during the real experiment was poor. The comparison of concentrations calculated from calorimetric data and from the infrared probe calibration show significant differences, particularly at the beginning (too high concentrations) and at the end of the experiment (too low concentrations). This is likely due to the synergistic effects abovementioned. Also, poor prediction could be due to lack of sensitivity of the probe at too high (>8.8 mole/L) concentrations.

The conversion of several experiments was calculated using the peak height at a selected frequency and dividing it by the maximum peak height (Equation 36). Conversions obtained through this method were in good agreement with conversions calculated using the method of the pressure difference described in Section 5.1. Concentrations were also calculated from conversions values. The concentrations showed good agreement at the

beginning and at the end with concentrations calculated from calorimetric data. However, the concentration of 3-picoline is underpredicted throughout the experiment. It is possible that the underprediction is due to an intermediate formed which has the same peaks as 3-picoline, so the peak height represents more than one compound, *i.e., the* concentrations calculated from conversions do not represent the concentration of 3-picoline only.

The analyses of the surface generated using the curve-resolution algorithm ConcIRT™ revealed an unidentified intermediate in the reaction. Said intermediate presents peaks characteristic of both 3-picoline and 3Nox. This might be a compound where an oxygen atom is attached to the nitrogen so the molecule presents absorption at the characteristic frequency of an N-O bond. The production of the intermediate finishes almost as soon as dosing is finished. As soon as the intermediate is finished, so is the production of 3-picoline *N*-oxide.

The use of *in-situ* FTIR spectroscopy is a useful method for analyzing complex reactions such as the *N*-oxidation of alkylpyridines. Useful qualitative information can be obtained, such as peak profiling and identification of new substances. This can be useful for developing kinetic mechanisms. However, in order to extract quantitative information, a thoroughly planned and detailed calibration is necessary. The calibration must be done at the reaction conditions and taking into account the synergistic effects between different compounds at different concentrations in a reaction mixture.

An alternative approach to perform a calibration would be to perform a reaction and take samples at regular intervals to be analyzed offline, using a GC or HPLC. Then, concentration data could be used for the calibration. However, at the reaction conditions used in this study, the extraction of samples for off-line analysis was a complex and hazardous task.

8. INHERENTLY SAFER REACTORS: APPLICATION ON THE *N*-OXIDATION OF ALKYLPYRIDINES*

The purpose of this section is to demonstrate how an inherently safer process can be built by designing a reactor operating in a way which addresses the key issues that make the process hazardous after an assessment of the conditions that reduce or eliminate the key hazards. Furthermore, it is shown that such improvements, which primarily target the inherent safety of the process, also result in an increased efficiency and economic viability of the process.

This research work, as well as previous works on the *N*-oxidation of alkylpyridines[50, 57, 62] demonstrate that the operating conditions in the process currently used facilitate the decomposition of hydrogen peroxide and do not inhibit the possibility for a runaway reaction to develop. Moreover, the reactor design itself does not adequately suit this type of reaction. As such, this process presents an opportunity to implement inherently safer alternatives proposed by Kletz[109] and be used as a model for the design of inherently safer reactors. Kletz emphasized that the meticulous study of the reaction can suggest the reaction conditions and the appropriate reactor design for an intensified and inherently safer process where the process hazards can be inherently minimalized.[109]

So far, the knowledge acquired on the *N*-oxidation of alkylpyridines indicates that reaction efficiency, selectivity and safety can be greatly improved (a) by increasing the operating temperature, (b) by using an alternative reactor design, and (c) in the case of the higher order alkylpyridines, by avoiding operating conditions where a heterogeneous

* Part of this section is reprinted with permission from "Toward an inherently safer design and operation of batch and semi-batch processes: The *N*-oxidation of alkylpyridines" by A. Pineda-Solano, L.R. Saenz, V. Carreto, M. Papadaki and M. S. Mannan, 2012. *Journal of Loss Prevention in the Process Industries*, 25, 797-802, Copyright [2012] by Elsevier.

mixture is formed. Each one of these issues will be discussed in the following subsections.

8.1 Operating at Higher Temperatures

As mentioned earlier, an increase in the operating temperature could lead to increased selectivity and safety. More specifically, the benefits obtained from operating the process at higher temperatures include: a dramatic increase in *N*-oxidation selectivity resulting in a respective reduction of hydrogen peroxide decomposition, decreased reaction and overall process times, and elimination of the need for hydrogen peroxide excess.

Experiments performed in this and previous studies using an isothermal closed system at temperatures over 100 °C confirmed that for the case of the picolines (methylpyridines), which form homogeneous mixtures with water, a relatively small temperature increase has a dramatic impact on *N*-oxidation selectivity. Thus, hydrogen peroxide decomposition is practically eliminated if its addition is conducted at an appropriately slow rate. Additionally, the conversions achieved are as high as 98% using only the stoichiometric amount of hydrogen peroxide. This subsequently obviates the need for excess hydrogen peroxide. It can be observed in Figure 102 that the power generated by the hydrogen peroxide decomposition is negligible and barely measurable throughout the reaction. It can also be seen that the power generated by the *N*-oxidation is practically constant throughout the reaction, indicating that the reaction is controlled by dosing. This means that the *N*-oxidation reaction occurs very fast, so the rate of reaction is limited by the rate of addition of hydrogen peroxide, rather than by the reaction kinetics.

Because of the dependency of the reaction rate upon temperature, the operation at higher temperatures implies a much faster rate of the desired reaction. In turn, a faster rate of reaction results in shorter reaction times. Consequently, a smaller reactor could be used,

where the effects of a runaway reaction would be limited by the amount of reactants in the reactor.

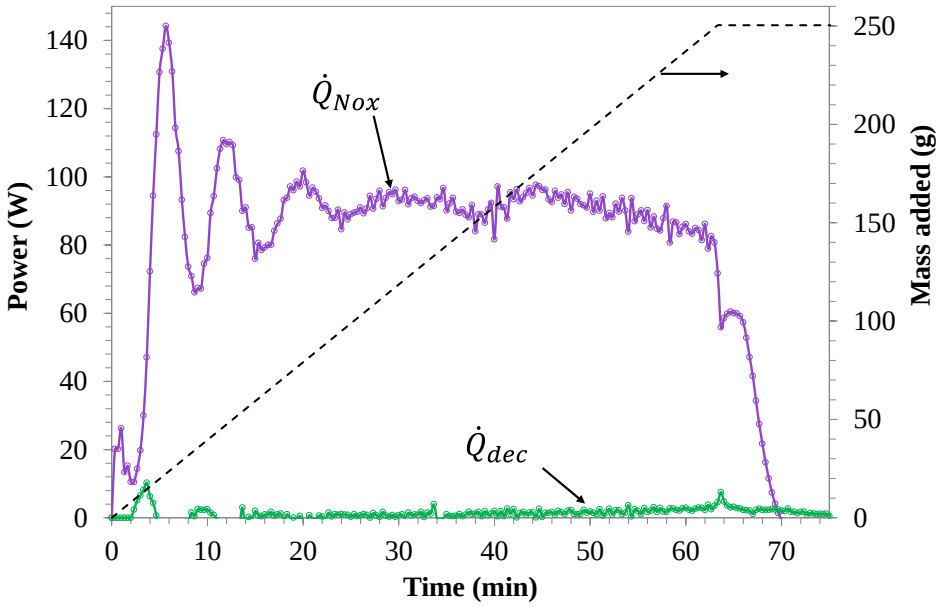

Figure 102. *N*-oxidation and decomposition power for the *N*-oxidation of 3-picoline at 110°C using 10 g of catalyst, performed in the RC1*e* isothermal calorimeter. A stoichiometric amount (with 3-picoline) of H_2O_2 was added to the reactor at a rate of 4 g/min. The dashed line shows the mass of H_2O_2 added as a function of time and is read on the right-hand ordinate

In the traditional process, the reaction takes longer to complete because the lower temperature and the dilution due to hydrogen peroxide excess lowers the rate of reaction. Moreover, the excess of hydrogen peroxide added imposes an additional process step which is its subsequent neutralization. Longer times increase the opportunities for something to go wrong; the longer the process, the higher the likelihood for equipment to fail, people to make mistakes, and consequently, for an accident to occur. Prolonged reaction/process times slowly wear the equipment and controls, resulting in decreased equipment reliability. Additionally, the hydrogen peroxide accumulation in the reactor could lead to a runaway scenario with serious consequences, as previously explained.

By operating the process at higher temperatures, hydrogen peroxide would be effectively consumed in the *N*-oxidation, such that the excess would not be necessary. The excess of hydrogen peroxide used in the currently employed process is the main cause of decreased safety and efficiency.

Regarding safety, while part of the excess decomposes, a good amount of hydrogen peroxide is accumulated; increasing the severity of the consequences should a runaway develop. At higher reaction temperatures, hydrogen peroxide accumulation in the reactor would be constantly low, so it would not impose any threat in terms of safety, while the rate of its decomposition would also be minimized.

Another implication of using an excess of hydrogen peroxide in the current process is the need for increased inventory and transportation. As mentioned before, hydrogen peroxide is a reactive chemical very sensitive to contamination. Although commercial hydrogen peroxide is stable at room temperature, it can easily decompose in the presence of impurities, even if they exist at very low concentrations.[110] By eliminating the excess of hydrogen peroxide used in the reaction, the inventory need would be reduced. As Kletz stated, "*what you don't have, can't leak*",[111] and in this case, it cannot runaway.

Regarding efficiency, the use of higher temperatures eliminates a step required in the traditional process. Because the excess of hydrogen peroxide is not necessary, the extra step required to neutralize the remaining hydrogen peroxide can be eliminated. The elimination of the neutralization step has an influence on the environmental impact and the economics of the process. Due to the large amount of excess hydrogen peroxide used and the chemicals needed to neutralize it, there is a large quantity of waste generated. This results in higher expenses for waste disposal. Additionally, the extra time needed for adding the excess of hydrogen peroxide and neutralizing it increases the overall batch time, reducing the efficiency of the process. Furthermore, larger process equipment (reactor and separation equipment) and more time and energy are required to process

larger amounts of materials, which also affect the efficiency and profitability of the process.

As Kletz indicated,[112-114] the development of intensified and inherently safer processes also leads to reductions in costs. In the proposed process, hydrogen peroxide is effectively consumed in the *N*-oxidation and since the temperatures used are higher, the rate of the desired reaction is much faster. Thus, higher conversions of alkylpyridine can be obtained, which increases the efficiency of the process. In addition, the accumulation of hydrogen peroxide is kept to a minimum, enhancing the safety of the process.

8.2 The Importance of a Process-Specific Reactor Design

Kletz has previously emphasized that changing the mixing pattern in the reactor can improve the efficiency of the reaction, leading to an intensified process.[109] In the case of the *N*-oxidation of alkylpyridines, increased selectivity, and hence efficiency, towards the *N*-oxidation can be achieved if the reactor operates as ideal mixed flow for hydrogen peroxide and ideal plug flow for the alkylpyridine. The latter cannot be achieved in the reactor currently employed for the *N*-oxidation. By modifying the mixing pattern in the *N*-oxidation of alkylpyridines, an intensified and inherently safer process of improved efficiency and economics can be achieved.

In the currently used open system, the safety of the process relies merely on the controlled addition of hydrogen peroxide and the ability of the generated gas to leave the system. Should an upset in the process occur, the reaction could lose thermal control and runaway. For example, consider a pump failure. If the pump fails to deliver the correct flow rate of hydrogen peroxide, and instead sends a higher flow rate to the reactor, the concentration of hydrogen peroxide will quickly increase. If the vent line of the reactor is not capable of removing all the produced gas and vapor, as the rate of decomposition is proportional to the square of the concentration of hydrogen peroxide, the oxygen

generation and temperature will rapidly increase, possibly causing the reactor or the vent line to burst.

While it could be argued that an open reactor is suitable for the operation because oxygen is allowed to escape, a closed reactor would be inherently safer. Besides, even if oxygen can escape from the system and prevent the reactor from over-pressurizing (assuming it is adequately vented), the vapors above the liquid are still rich in oxygen. Consequently, the hazard of fire is still present. As calorimetric measurements have shown, in a closed system working at higher temperatures, oxygen would not be produced in the first place or would be produced in negligible amounts. The present work sets the foundation for the development of an intensified process, which under normal conditions the hydrogen peroxide decomposition will be negligible (oxygen generation almost eliminated), while in abnormal conditions the low reactant accumulation and the small reactor size will not allow for a hazardous runaway to develop.

Because the reaction is controlled by dosing, the heat of reaction is released practically at a constant rate, which simplifies the heat exchanger design. Furthermore, since the *N*-oxidation is highly exothermic (ΔH_r =130-190 kJ/mole), the energy integration of the process may be evaluated by utilizing the heat of reaction to preheat the feed or for product separation.[115]

Due to the inherent benefits provided by a tubular reactor, Kletz and Amyotte[113] have suggested that this should always be considered as an alternative to the traditional batch or semi-batch reactor. Thus, it has been thought that a small diameter tubular reactor with radial distribution of hydrogen peroxide would be a good fit for the *N*-oxidation of alkylpyridines, because it is economical and safer to operate at high pressures. Furthermore, because the capacity of pharmaceutical reactions are relatively small, appropriately small size reactors dedicated to a specific process are likely to be a better

alternative to the use of larger multi-purpose units. Although further studies are needed before such a reactor is designed, all the aforementioned evidence suggests that there is a much safer and efficient alternative to the existing process.

8.3 Avoiding Non-Homogeneous Mixtures

As mentioned in previous sections, the catalyst and hydrogen peroxide are water soluble. At conditions where the alkylpyridine does not fully mix with water, the reaction mixture forms two liquid phases like in the case of the *N*-oxidation of high order alkylpyridines (*e.g.*, lutidines and collidines) at 100 °C. In those cases, the *N*-oxidation is controlled by the slow mass transfer of hydrogen peroxide to the organic phase while the homogeneously catalyzed decomposition of hydrogen peroxide is dramatically favored. In order to obtain an inherently safer and more efficient *N*-oxidation, the operation at homogeneous conditions is of interest. Therefore, it is important to study the thermodynamics of the process to determine the conditions at which the reaction can be performed in a single phase. Temperature, pH, and the presence of third compounds are the key factors which affect phase solubility. When temperature is to be considered as a factor, product decomposition "onset" has to be considered and it can be used so as to set an upper limit for reactor operation.

For a 2,6-lutidine/water system, the liquid-liquid phase region is present over a wide range of conditions (*i.e.,* temperatures between 30 and 230 °C and concentrations between 5 and 80 2,6-lutidine wt. %).[116] However, Andon and Cox[117] demonstrated a reduction in the two-liquid region when adding 3-picoline in different proportions. Based on these findings, the addition of a third component in the system 2,6-lutidine/water could increase the homogeneous region of the mixture, and as a consequence, the efficiency of the *N*-oxidation for alkylpyridines with limited miscibility in water can be addressed. Saenz-Noval[62] showed that a similar reduction in the two-liquid phase region is obtained when adding acetic acid to the 2,6-lutidine/water mixture.

Acetic acid has been employed as a catalyst in alternative, less efficient methods for the *N*-oxidation of different alkylpyridines.[25, 118]

In general, the addition of a third component in the mixture is an alternative to develop an inherently safer *N*-oxidation by reducing the presence of two phases. This alternative is an example of the "hybridization" or "transformation" inherent safety concept as proposed by Edwards[119], in which the chemistry of the process remains unchanged but the process is made inherently safer by adding another component to the mixture; however, the third component should not form byproducts with the reactants. Moreover, the effect of such a component on the runaway behavior and the cost of separation posterior to the reaction should be taken into account. The role of pH has to be investigated in the future, as well as the effect of the catalyst or the addition of product, which could positively affect homogeneity.

8.4 Discussion

In general, inherently safer alternatives are associated with using lower operating temperatures and pressures.[120] However, these process conditions are not always the best option. It has been shown that for the *N*-oxidation of alkylpyridines, a closed reactor operating at higher temperatures – and consequently, higher pressures – looks very promising in terms of an inherently safer process. Kletz has previously explained that an intensified process working at high temperatures and pressures may be inherently safer than one working at milder conditions.[111] That is the case for the *N*-oxidation of alkylpyridines. By increasing the temperature of the reaction, the major hazards of the process, namely the decomposition and accumulation of hydrogen peroxide, are greatly reduced. The hazard represented by the accumulation of hydrogen peroxide is much more significant than that of the temperature and pressure, as the accumulation can worsen the consequences of a runaway reaction. Moreover, because of the fast rate of reaction, a small reactor can be used, limiting the effects of the hazards posed by the

operation at higher temperature and pressure. In addition, the reduction of hazards in the process is accompanied by many other benefits, as explained earlier.

8.5 Conclusions

This work proposed alternatives that would result in an inherently safer process for the *N*-oxidation of alkylpyridines. It was also demonstrated that understanding the reaction system and its hazards is of paramount importance for the development of inherently safer technologies. As an example, the study of the *N*-oxidation of alkylpyridines system has revealed operating conditions that increase the selectivity of the synthesis reaction, leading to an intensified and inherently safer process. In addition, it was shown that such a process would be accompanied by increased efficiency and cost reduction.

In the development of intensified processes, special attention should be given to the reactor design, as mixing is crucial. The reactor design must be based on the thorough study of the kinetics and thermochemistry of the reaction system. Finally, as illustrated here, thermodynamics can have a dramatic effect on the safety as well as on the design of the process. Important consideration should be given to the properties of the system, especially those related to phase equilibrium because the elimination of two phases is the key to the design of a good performance and a safe reactor.

9. CONCLUSIONS AND FUTURE WORK

This section summarizes the main findings of the work presented in this dissertation (Section 9.1) and it outlines the opportunities to continue this research (Section 9.2).

9.1 Conclusions

This dissertation involved novel calorimetric, analytical, and computational work for the investigation of complex aspects of the *N*-oxidation of alkylpyridines, a reaction used in the pharmaceutical industry, which paved the way toward inherently safer hazardous reactive processes and the application of inherent safety principles. From a safety perspective, the *N*-oxidation of alkylpyridines itself is of interest because of the hazards resulting from the undesired, gas-generating decomposition of hydrogen peroxide, the oxidizing agent. The generation of oxygen, combined with the flammability of the alkylpyridines, represents a serious fire and explosion hazard for the process. However, the focus of this work was not limited to this reaction. This complex reaction system was also used as a case study for the development of tools and methodologies which illustrate how an inherently safer process can be achieved by assessing conditions that reduce or eliminate the hazards. Furthermore, this work showed that the study of the reactivity of the participating compounds, and of the thermodynamics of the process, should form an essential part of chemical production before full scale application. These studies can result in a process-specific reactor design, which not only brings improvements in the safety and the efficiency of the process, but also results in a reduction of time and resources

.

As many of the hazards associated with the *N*-oxidation of alkylpyridines are typical of other batch reaction systems, especially of those involving hydrogen peroxide, the

methodologies and the design approaches used in this dissertation can be incorporated to other systems involving batch or semi-batch reactions.

The topics covered in this research involved:

a. The assessment of the decomposition of the participating compounds in isolation and in combination, in order to evaluate the hazards originated by each of the individual compounds and by their synergies. Those measurements were combined with liquid end-product analysis.

b. Isothermal calorimetric measurements in different calorimeters at a wide variety of conditions in order to assess the role of different factors in the reactive behavior, the thermodynamics and the overall efficiency of the process.

c. Factorial design of experiments in order to reveal the key factors affecting the process and their synergies

d. Application of real-time FTIR spectroscopy for the analysis and monitoring of complex reactions, and implementation of specific techniques for its combined use with reaction calorimetry to obtain further understating on the chemical reaction.

Thermal stability analyses were conducted in the Automatic Pressure Tracking Adiabatic Calorimeter (APTAC) to ensure that the operating conditions studied would not lead to secondary decompositions. The analyses indicated that all alkylpyridines involved in this study (3-picoline; 3,5-lutidine; 2,6-lutidine; and 2,4,6-collidine) are thermally stable up to 400 °C. Conversely, all corresponding alkylpyridine *N*-oxides decompose at temperatures above 230 °C. Isothermal tests conducted on 3-picoline-*N*-oxide showed that increasing temperature accelerates the rate of the decomposition.

With regards to the effect of the catalyst, 3-picoline-*N*-oxide appears to have low sensitivity to small changes in the catalyst concentration. In fact, in all experiments performed isothermally at different temperatures, the rate of the decomposition reaction

using 0.1 g of catalyst was faster than when using 0.3 g of catalyst. This possibly suggests a change in the mechanism of the decomposition with the amount of catalyst used. Only when large amounts of catalyst were used, the decomposition of 3-picoline-*N*-oxide was accelerated.

The decomposition of alkylpyridine *N*-oxides involves a complex reaction mechanism in which non-condensable gases are generated, and in which the main pathway appears to be the detachment of the oxygen atom from the parent alkylpyridine molecule. However, multiple other compounds were found during GC/MS and LC/MS analysis, which show evidence that some polymerization occurred during the decomposition reaction. Further research is needed to determine the reaction mechanism of the decomposition of alkylpyridine *N*-oxides.

An evaluation of operating conditions was conducted for the *N*-oxidation of 3-picoline; 3,5-lutidine; 2,6-lutidine; and 2,4,6-collidine. A 2^4 full factorial design of experiments (DOE) was used to study the factors (operating conditions) that affect the conversion of 3-picoline into 3-picoline-*N*-oxide. The factors studied included temperature (110 and 125°C), catalyst amount (1 and 10 g), dosing rate (0.5 and 4 g/min), and stirring rate (250 and 400 rpm). The factorial DOE revealed that in the range of conditions used in the study the conversion of 3-picoline is most influenced by the interaction of catalyst mass and dosing rate, *i.e.*, a high dosing rate may be used if the quantity of catalyst is high, while a slow dosing rate is required if the amount of catalyst is small. In both cases, the conversions of 3-picoline obtained were above 94% and as high as 98% using only a stoichiometric amount of hydrogen peroxide, and the decomposition reaction was kept to a minimum. This finding shows that in addition to the improvement in the safety of the process, an increase in efficiency is achieved as the excess hydrogen peroxide is no longer needed. In contrast, a combination of low catalyst amount and high dosing rate led to conversions as low as 63%.

The catalyst mass–dosing rate factor interaction is of importance due to its effect on the accumulation of hydrogen peroxide. High amounts of catalyst (10 g) accelerate the *N*-oxidation reaction rate, such that the accumulation of hydrogen peroxide in the reactor is constantly low, even at high dosing rates. A low accumulation of hydrogen peroxide is of paramount importance for the safety of the process, as the decomposition of accumulated hydrogen peroxide during a cooling failure could increase the temperature of the mixture and trigger the decomposition of the product (3nox), as shown in adiabatic tests. However, a large increase in the catalyst amount can promote the decomposition of hydrogen peroxide, particularly when combined with a temperature increase.

The utilization of high dosing rates imposes other safety issues. Fast reactions are usually difficult to control initially, due to the abrupt increase in the power output; the reaction generates heat at a very fast rate, and therefore, the safe operation of a reactor operating at a high dosing rate depends on the heat removal capability of the reactor. A typical batch reactor can remove approximately 30 W/L. In comparison, some of the experiments conducted in this work generated a power overshoot as high as 150 W/L. This issue highlights the importance and the advantages that a smaller, intensified reactor can offer towards the safety and efficiency of the process.

The effect of the temperature in the range 110-125 °C is not statistically significant. Although preliminary experiments in this work and previous works showed the indisputable positive effect of a temperature increase, particularly when compared to experiments performed at temperatures below 100 °C, the factorial DOE showed that, at the range of temperatures studied, the effect is small compared to the effect of other factors such as catalyst mass and dosing rate. That is, while a temperature increase of 10 °C over the typical temperature of 100 °C dramatically favors the selectivity of the synthesis reaction, a further increase does not show a significant benefit. High

conversions (>97%) can be obtained using a temperature of 110 °C, when combined with a sufficient amount of catalyst and appropriate dosing rate.

In general, it was shown that temperature should be increased only to a certain extent. Safety considerations are involved when increasing the temperature further. While a higher temperature reduces the accumulation of hydrogen peroxide, it also promotes its decomposition, particularly when high amounts of catalyst are used.

The effect of the temperature-catalyst factor interaction is important, but it is not statistically significant. In previous studies, it has been argued that an increase in temperature and catalyst concentration could reduce the decomposition of hydrogen peroxide. While this statement is true, it holds only if an appropriate dosing rate is used. This finding emphasizes the importance of taking into account all factors that can affect a chemical reaction when evaluating the most suitable operating conditions.

The effect of the stirring rate is not statistically significant under the conditions of the study. This is due to the small volume of the reactor and the type of stirrer used in this study. However, the study of mixing effects during the development of the intensified reactor suggested in this work is of paramount importance.

There is no “optimum” operating condition for the *N*-oxidation of alkylpyridines. Instead, there exists a set of operating conditions at which the process can operate safely and efficiently. This set consists of an appropriate combination of catalyst mass, dosing rate, and temperature. The selection of the operating conditions is strongly influenced by the reactor design and cooling system capability.

In general, the findings from the factorial DOE on 3-picoline-*N*-oxidation can be applied to other members of the alkylpyridine family. However, for higher order alkylpyridines, it is necessary to evaluate the phase-equilibrium during the reaction in order to determine

conditions or alternatives where a homogeneous liquid phase can be achieved, and thus an inherently safer and more efficient process.

The behavior of 3,5-lutidine is similar to that of 3-picoline during the *N*-oxidation. Conversions as high as 95% were obtained using only the stoichiometric amount of hydrogen peroxide; and the power generated by the reaction was practically constant. However, the effect of the accumulation of hydrogen peroxide is stronger in the case of 3,5-lutidine, which is worsened with the use of high dosing rates and low amounts of catalyst. When a low amount of catalyst is used, the pressure increase can be high, even if a slow dosing rate is used. This effect is mitigated with an increase in temperature. Nevertheless, the increase in temperature favors the *N*-oxidation only up to certain extent. Temperatures between 110 and 120 °C were beneficial, while a further increase promoted the decomposition of hydrogen peroxide.

The *N*-oxidation of 3,5-lutidine is easier than the *N*-oxidation of 2,6-lutidine and 2,4,6-collidine, with the latter being the most difficult to *N*-oxidize. The behavior of 2,6-lutidine and 2,4,6-collidine during the *N*-oxidation is similar. Both compounds showed constant power profiles and generated approximately the same amount of energy per mole, indicating similar reaction rates, controlled by the availability of the oxidant. There is significant decomposition of hydrogen peroxide throughout the entire reaction, which dramatically reduces the efficiency.

The conversion of 2,6-lutidine obtained using only the stoichiometric amount of hydrogen peroxide was 81%, with the energy released by the hydrogen peroxide decomposition being 13% of the total energy released. A conversion of 76% was obtained in the case of 2,4,6-collidine, and the power of the decomposition reaction amounted to 20% of the total energy released. Adding an excess of 20% of hydrogen peroxide increased the conversions to 92% and 94%, respectively, although approximately 40% of the excess added decomposed. Therefore, a small excess of

hydrogen peroxide in the *N*-oxidation of 2,6-lutidine and 2,4,6-collidine can be carefully used if high conversions are to be achieved in a single stage. In such case, a very slow addition of the excess under careful supervision of the process is recommended. In order to further increase the efficiency of the *N*-oxidation of higher order alkylpyridines, it is imperative to study the thermodynamics of the system and find alternatives to achieve a homogeneous mixture.

In general, as the rate of reaction of the *N*-oxidation is controlled by the availability of hydrogen peroxide, the power generated by the *N*-oxidation is practically constant, which would simplify a heat exchanger reactor design. Based on this fact, the use of an intensified, small tubular reactor with radial distribution of hydrogen peroxide has been suggested as an alternative reactor design. Such design is economical, safer to operate at higher pressures, and would ensure adequate mixing between the alkylpyridine and hydrogen peroxide to maximize efficiency. In addition, energy integration could be achieved by using the heat released by the *N*-oxidation to preheat the feed or for product separation. The suggested process would also alleviate the environmental impact due to the *N*-oxidation. Since the excess hydrogen peroxide is no longer needed, there is no need to use additional chemicals for neutralization of the remaining hydrogen peroxide. Therefore, the waste generation is reduced. It would also decrease the risk associated with the storage and transportation of large amounts of hydrogen peroxide.

The use of *in-situ* FTIR spectroscopy is a suitable method for analyzing complex reactions such as the *N*-oxidation of alkylpyridines. Useful qualitative information can be obtained, such as trending of compounds, identification of new substances, and determination of the end point of the reaction. This information can be helpful for decision-making and cost-benefit analyses. The trends of compounds show the moment when the concentration of the product is no longer increasing or is increasing very slowly. Therefore, a decision can be made to stop or continue the process depending on the value of the product and the cost associated with extending the time of the process.

Qualitative data, combined with quantitative concentration data can also be useful for developing kinetic mechanisms. However, in order to extract quantitative information, a careful calibration is necessary. The calibration must be done at the reaction conditions and taking into account the synergistic effects between different compounds in a reaction mixture.

Two different methods were used to calculate the concentration of 3-picoline in the mixture; the first one consisted of calibrating the probe using mixtures of known concentrations of 3-picoline and developing a linear model relating peak height to concentration. The second one consisted of using the peak profiling technique in which conversion is calculated by dividing the peak height at a selected frequency by the maximum peak height; concentrations were then calculated from conversion data. The conversions calculated were in good agreement with conversions calculated using pressure differences. However, the prediction of concentrations throughout the experiments show significant differences with concentrations calculated from calorimetric data. The difference is likely owed to the lack of sensitivity of the probe at concentrations of alkylpyridine higher than 8.8 M and possibly due to an intermediate formed which has the same peaks as 3-picoline, so the peak height at the selected frequencies represents more than one compound. Further research would be required before accurate concentration data can be obtained from infrared data for kinetic analyses.

The analysis of the reaction using an *in-situ* FTIR probe and the curve-resolution algorithm ConcIRT^{TM} indicated the presence of an unidentified intermediate in the reaction. The intermediate shows characteristic peaks of both 3-picoline and 3-picoline-*N*-oxide. It is clear that said intermediate plays an important role in the *N*-oxidation, as the production of *N*-oxide ends when the intermediate is finished. Further research is needed on the mechanism of this system of reactions to identify the structure of the intermediate.

Overall, this dissertation provides sufficient information to select operating conditions that maximize the safety and efficiency of the *N*-oxidation of alkylpyridines, and it also represents a step forward toward an inherently safer process. The data, tools, and techniques utilized in this dissertation illustrate a methodology through which the design of inherently safer processes is based on the thorough study of the reaction of interest. In addition, it was demonstrated that it is possible to develop safer processes without negatively impacting its efficiency.

9.2 Future Work

This section summarizes the opportunities to continue the development of an inherently safer process for the *N*-oxidation of alkylpyridines. It also provides recommendations for future work, based on the challenges faced during this study.

9.2.1 Kinetics of the N-oxidation of alkylpyridines

In order to ensure the reliable prediction of runaway reactions, it is necessary to develop theoretically sound and accurate kinetic models that represent a system of reactions. For this reason, it would be worth investigating the kinetics of the *N*-oxidation of alkylpyridines over an extended temperature range.

During this study, conditions were identified, in which the *N*-oxidation of 3-picoline occurred in the kinetic regime. The conditions used were a low amount of catalyst and high dosing rate, which cause a high accumulation of hydrogen peroxide, *e.g.*, 1 g of catalyst and a dosing rate of 4 g/min. Temperatures between 110 and 125 °C were used in this study (see Section 5.2). At 125 °C, there is less accumulation of hydrogen peroxide in the reactor, however, a kinetic regime is observed as the concentration of 3-picoline decreases. It was found that the model proposed by Papadaki and Gao,[50] although it was developed based on calorimetric measurements performed in a narrow

temperature range (85-95 °C), has the potential to represent the reaction system at higher temperatures. However, there are several limitations that need to be overcome in order to accurately estimate the rate and equilibrium constants involved in the model.

Figure 103 shows the experimental and simulation power profiles generated using the model by Papadaki and Gao.[50] The differences between the model and the experimental data are caused by deviation from isothermal conditions, inaccurate prediction of hydrogen peroxide decomposition, heat of mixing and because the coefficients used for the simulation were found by trial and error and may not provide the best fit. However, the simulation shows the potential of the model to fit the data.

For the estimation of the parameters of the kinetic model, it is essential to develop a better method to measure the decomposition of hydrogen peroxide. This could be done by evaluating the thermodynamics of the reacting system and determine how the vapor pressure changes throughout the reaction.

In addition, the reaction should be performed in a vessel that can withstand high pressures. In order to obtain data for kinetic analysis, hydrogen peroxide must be allowed to decompose. Therefore, the pressure in a closed system will increase very rapidly, and due to the high temperature used, even a small amount of oxygen generated can cause a large increase in the pressure. The reactor used in this study could withstand pressures up to 10 barg, so sometimes, it was necessary to interrupt dosing and vent the reactor.

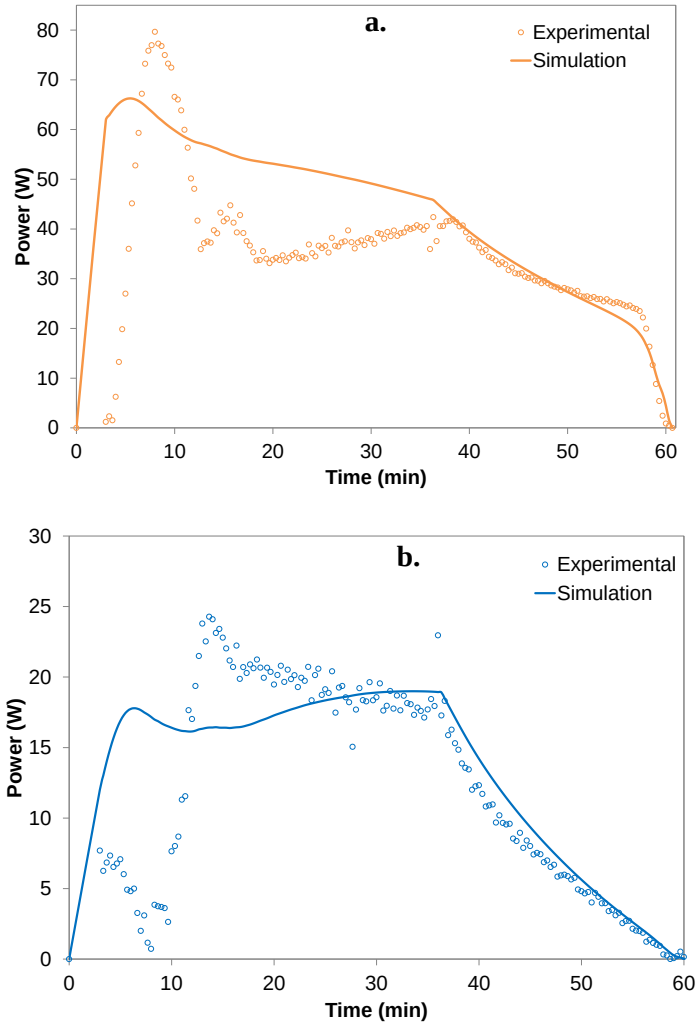

Figure 103. Experimental and simulated power profiles during the *N*-oxidation of 3-picoline at 110 °C using 1 g of catalyst and a dosing rate of 4 g/min. a) *N*-oxidation power; b) decomposition power

Further research is also needed to identify chemical intermediates in the *N*-oxidation of alkylpyridines. As mentioned in Section 7.3, an unknown chemical intermediate was detected using *in-situ* FTIR and the ConcIRT™ software from Mettler-Toledo. The identification of this intermediate would help define the mechanism involved in the *N*-oxidation of alkylpyridines and confirm the findings from Papadaki and Gao.[50] Deep understanding of infrared spectroscopy and organic chemistry is needed for this purpose.

9.2.2 Study of the phase-equilibrium during the N-oxidation of higher order alkylpyridines

The *N*-oxidation of 2,6-lutidine and 2,4,6-collidine showed that an increase in temperature and a high concentration of catalyst does not actually eliminate the decomposition of hydrogen peroxide. As mentioned in Section 6, due to the limited miscibility of these alkylpyridines in the aqueous phase, the decomposition of hydrogen peroxide is promoted, particularly at the beginning of the reaction when the concentration of alkylpyridine is high. As the reaction advances and *N*-oxide is produced, the two phases slowly disappear until a homogeneous mixture is obtained near the end of the reaction. Therefore, it is imperative to study the phase equilibrium of this system throughout the reaction, experimentally and computationally. Experimentally, the first alternative to study should be the addition of *N*-oxide to the initial reacting mixture As the *N*-oxides are more soluble in water, it is expected that its addition to the mixture can reduce the formation of two phases. Computationally, the use of the Gibbs minimization method, which combines phase equilibrium and chemical equilibrium may be used, as suggested by Saenz-Noval.[62] However, the scarce information of alkylpyridine *N*-oxide properties may be a limitation for using the Gibbs minimization method, as also pointed out by Saenz-Noval.

9.2.3 Reactor design for the N-oxidation of alkylpyridines

It was mentioned in Section 8 the benefits that could be achieved if an intensified, plug-flow-heat-exchanger type of reactor is used for the *N*-oxidation of alkylpyridines. Therefore, it is worth to further research this possibility by constructing a reactor prototype that incorporates the findings of this and previous research works. However, several limitations must be first overcome. For example, it is necessary to determine how the catalyst could be introduced in the reactor, the delivery method of hydrogen peroxide

and all the physical parameters of a reactor, such as size, geometry and materials of construction.

9.2.4 Study of the mechanism of decomposition of alkylpyridine N-oxides

The formation of multiple compounds during the decomposition of alkylpyridine *N*-oxides indicates that a complex reaction mechanism is involved. Additional studies are necessary to identify the different steps and intermediates involved in the mechanism. Computational chemistry may be used for such purpose.

REFERENCES

1. Westerterp, K. R.; Molga, E. J., No More Runaways in Fine Chemical Reactors. *Industrial & Engineering Chemistry Research* **2004,** 43, (16), 4585-4594.

2. Zaldivar-Comenges, J. M., Fundamentals on Runaway Reactions: Prevention and Protection Measures. In *Safety of Chemical Batch Reactors and Storage Tanks*, Kluwer Academic Publishers: Netherlands, 1991; pp 19-47.

3. Coker, A. K., *Modeling of Chemical Kinetics and Reactor Design*. Gulf Professional Publishing: Houston, TX, 2001.

4. Gielens, B.; Bizzarri, D.; Dobet, C.; Germain, A., *Manual for Identifying and Evaluating Thermal Runaway Reaction Hazards*. Federal Ministry of Employment and Labour: Brussels, 2001.

5. Sheldon, R. A., Catalysis and Pollution Prevention. *Chemical Industry* **1997,** 1, 12-15.

6. Barton, J. A.; Nolan, P. F., Incidents in the Chemical Industry Due to Thermal-Runaway Chemical Reactions. *IChemE Symposium Series* **1989,** 115, 3-13.

7. U.S. Chemical Safety and Hazard Investigation Board *Hazard Investigation: Improving Reactive Hazard Management*; CSB: Washington, D.C., 2002.

8. U.S. Chemical Safety and Investigation Board *Fire and Explosion: Hazards of Benzoyl Peroxide*; CSB: Washington, D.C., 2003.

9. U.S. Chemical Safety and Investigation Board *Toxic Chemical Vapor Cloud Release*; CSB: Washington, D.C., 2006.

10. U.S. Chemical Safety and Investigation Board *Runaway Chemical Reaction and Vapor Cloud Explosion*; CSB: Washington, D.C., 2007.

11. U.S. Chemical Safety and Investigation Board *T2 Laboratories, Inc. Runaway Reaction*; CSB: Washington, D.C., 2009.

12. Barbas, R.; Botija, M.; Camps, H.; Portell, A.; Prohens, R.; Puigjaner, C., Safety Evaluation of an Unexpected Incident with a Nitro Compound. *Organic Process Research & Development* **2007,** 11, (6), 1131-1134.

13. Sachdev, A.; Todd, J., Incident Investigation of Mono-Nitro Toluene Still Explosion. *Journal of Loss Prevention in the Process Industries* **2005,** 18, (4–6), 531-536.

14. Joseph, G.; Kaszniak, M.; Long, L., Lessons after Bhopal: CSB a Catalyst for Change. *Journal of Loss Prevention in the Process Industries* **2005,** 18, (4–6), 537-548.

15. Center for Chemical Process Safety, *Inherently Safer Chemical Processes: A Life Cycle Approach.* AIChE/CCPS: New York, 2009.

16. Johnson, R. W.; Rudy, S. W.; Unwin, S. D., Essential Practices for Managing Chemical Reactivity Hazards. Center for Chemical Process Safety/AIChE: 2003.

17. Lutz, W. K., Take Chemistry and Physics into Consideration in All Phases of Chemical Plant Design. *Process Safety Progress* **1995,** 14, (3), 153-160.

18. Mosley, D. W.; Ness, A.; Hendershot, D. C., Screen Reactive Chemical Hazards Early in Process Development. *Chemical Engineering Progress* **2000,** 96, (11), 51-63.

19. Aldeeb, A. A. Systematic Approach for Chemical Reactivity Evaluation. Texas A&M University, College Station, 2003.

20. Leggett, D. J., Safe Process Development from Reaction Hazards Testing. *Thermochimica Acta* **2001,** 367-368, 351-365.

21. Mannan, S., Reactive Chemicals. In *Lees' Loss Prevention in the Process Industries* 3rd ed.; Mannan, S., Ed. Butterworth-Heinemann: Burlington, 2005; Vol. 33, pp 1-47.

22. Kletz, T., *Process Plants: A Handbook for Inherently Safer Design*. Taylor & Francis: Ann Arbor, MI, 1998.

23. Scriven, E.; Murugan, R., Pyridine and Pyridine Derivatives. In *Kirk-Othmer Encyclopedia of Chemical Technology*, John Wiley & Sons, Inc.: 2005; Vol. 20, pp 1-53.

24. Dressler, H., Pyridine and Derivatives. In *Van Nostrand's Encyclopedia of Chemistry*, John Wiley & Sons, Inc.: 2005.

25. Shimizu, S.; Watanabe, N.; Kataoka, T.; Shoji, T.; Abe, N.; Morishita, S.; Ichimura, H., Pyridine and Pyridine Derivatives. In *Ullmann's Encyclopedia of Industrial Chemistry*, Wiley-VCH Verlag GmbH & Co. KGaA: 2000.

26. Joule, J. A.; Mills, K., Pyridines: Reactions and Synthesis. In *Heterocyclic Chemistry* 5th ed.; John Wiley and Sons: 2010.

27. Sigma-Aldrich. 3-picoline [Material Safety Data Sheet]. http://www.sigmaaldrich.com/catalog/product/aldrich/p42053?lang=en&region=US (January 15, 2014).

28. Sigma-Aldrich. 3,5-lutidine [Material Safety Data Sheet]. http://www.sigmaaldrich.com/catalog/product/aldrich/l4206?lang=en&region=US (January 15, 2014).

29. Sigma-Aldrich. 2,4,6-collidine [Material Safety Data Sheet]. http://www.sigmaaldrich.com/catalog/product/fluka/27692?lang=en&region=US (January 15, 2014).

30. Sigma-Aldrich. 2,6-lutidine [Material Safety Data Sheet]. http://www.sigmaaldrich.com/catalog/product/sial/l3900?lang=en&region=US (January 15, 2014).

31. Jones, C. W., *Applications of Hydrogen Peroxide and Derivatives*. Royal Society of Chemistry: 1999.

32. Goor, G.; Glenneberg, J.; Jacobi, S., Hydrogen Peroxide. In *Ullmann's Encyclopedia of Industrial Chemistry*, Wiley-VCH Verlag GmbH & Co. KGaA: 2000.

33. Yaws, C. L., *Yaws' Critical Property Data for Chemical Engineers and Chemists*. Knovel: 2012.

34. Arkema. Hydrogen Peroxide. http://emea.brightenyourfuture.com/export/sites/byf-emea/.content/medias/downloads/literature/hydrogen-peroxide-brochure.pdf (February 17, 2014).

35. Eul, W.; Moeller, A.; Steiner, N., Hydrogen Peroxide. In *Kirk-Othmer Encyclopedia of Chemical Technology*, John Wiley & Sons, Inc.: 2000.

36. Mackenzie, J., Considerations for the Safe Design of Processes Using Hydrogen Peroxide and Organics. *Plant/Operations Progress* **1991,** 10, (3), 164-170.

37. Greene, B.; Baker, D. L.; Frazier, W. *Hydrogen Peroxide Accidents and Incidents: What We Can Learn from History*; NASA: 2005.

38. Klais, O., Hydrogen Peroxide Decomposition in the Presence of Organic Material: A Case Study. *Thermochimica Acta* **1993,** 225, (2), 213-222.

39. Kumasaki, M., An Explosion of a Tank Car Carrying Waste Hydrogen Peroxide. *Journal of Loss Prevention in the Process Industries* **2006,** 19, (4), 307-311.

40. Lacoursiere, J. P., An Explosion Caused by Mixing Incompatible Liquids. *Process Safety Progress* **2005,** 24, (2), 115-119.

41. Wehrum, W. L., Case Study of a Hydrogen Peroxide Related Deflagration in a Wastewater Treatment Tank. *Process Safety Progress* **1993,** 12, (4), 199-202.

42. Keggin, J. F., The Structure and Formula of 12-Phosphotungstic Acid. *Proceedings of the Royal Society of London. Series A* **1934,** 144, (851), 75-100.

43. Kozhevnikov, I. V., Sustainable Heterogeneous Acid Catalysis by Heteropoly Acids. *Journal of Molecular Catalysis A: Chemical* **2007,** 262, (1-2), 86-92.

44. Romanelli, G. P.; Autino, J. C., Recent Applications of Heteropolyacids and Related Compounds in Heterocycles Synthesis. *Mini-Reviews in Organic Chemistry* **2009,** 6, (4), 359-366.

45. Bamoharram, F. F., Role of Polyoxometalates as Green Compounds in Recent Developments of Nanoscience. *Synthesis and Reactivity in Inorganic, Metal-Organic, and Nano-Metal Chemistry* **2011,** 41, (8), 893-922.

46. Kozhevnikov, I. V., Advances in Catalysis by Heteropolyacids. *Russian Chemical Reviews* **1987,** 56, (9), 811-825.

47. Misono, M., Recent Progress in the Practical Applications of Heteropolyacid and Perovskite Catalysts: Catalytic Technology for the Sustainable Society. *Catalysis Today* **2009,** 144, (3–4), 285-291.

48. Misono, M.; Ono, I.; Koyano, G.; Aoshima, A., Heteropolyacids. Versatile Green Catalysts Usable in a Variety of Reaction Media. *Pure Applied Chemistry* **2000,** 72, (7), 1305-1311.

49. Palomo-Coll, A. A Process for the Preparation of Omeprazol. ES 2026761 (A6), January 5th, 1992.

50. Gao, J.; Papadaki, M., Global Kinetic Model: A Case Study on the *N*-oxidation of Alkylpyridines. *Journal of Hazardous Materials* **2006,** 130, 141-147.

51. Sempere, J.; Nomen, R.; Rodriguez, J. L.; Papadaki, M., Modelling of the Reaction of *N*-oxidation of 2-Methylpyridine Using Hydrogen Peroxide and a Complex Metal Catalyst. *Chemical Engineering and Processing* **1998,** 37, 33-46.

52. Saenz, L.; Carreto, V. H.; Liu, L.; Rogers, W. J.; Mannan, M. S.; Papadaki, M., 2-Methylpyridine-*N*-oxidation Runaway Studies. *Journal of Loss Prevention in the Process Industries* **2009,** 22, 839-843.

53. Saenz, L. R.; Carreto-Vazquez, V. H.; Rogers, W. J.; Papadaki, M.; Mannan, M. S., Thermal Decomposition of 2-Methylpyridine-*N*-oxide: Effect of Temperature and Influence of Phosphotungstic Acid as the Catalyst. *Catalysis Communications* **2011,** 12, (14), 1370-1373.

54. Papadaki, M.; Marques-Domingo, E.; Gao, J.; Mahmud, T., Catalytic Decomposition of Hydrogen Peroxide in the Presence of Alkylpyridines: Runaway Scenarios Studies. *Journal of Loss Prevention in the Process Industries* **2005,** 18, 384-391.

55. Pineda-Solano, A.; Saenz, L. R.; Carreto, V.; Papadaki, M.; Mannan, M. S., Toward an Inherently Safer Design and Operation of Batch and Semi-Batch Processes: The *N*-oxidation of Alkylpyridines. *Journal of loss prevention in the process industries* **2012,** 25, (5), 797-802.

56. Papadaki, M.; Emery, R. J.; Serra, E.; Nomen, R.; Sempere, J., Sensitivity Analysis of the 2-Methylpyridine *N*-oxidation Kinetic Model. *Green Chemistry* **2002,** 4, 199-205.

57. Papadaki, M.; Gao, J., Kinetic Models of Complex Reaction Systems. *Computers and Chemical Engineering* **2005,** 29, 2449-2460.

58. Papadaki, M.; Nawada, H. P., Towards Improved Reaction Runaway Assessment Methods I. Simple Calorimetric Method of Evaluation of Heat Transfer Coefficient and Reactor Thermal Mass. *International Journal of Chemical Reactor Engineering* **2003,** 1, (Article A40).

59. Papadaki, M.; Stoikou, V.; Mantzavinos, D.; Miranda, J. L. R., Towards Improved Reaction Runaway Studies; Kinetics of the *N*-oxidation of 2-Methylpyridine Using Heat-Flow Calorimetry. *Trans IChemE* **2002,** 80, (Part B), 186-196.

60. Baxendale, J., Decomposition of Hydrogen Peroxide by Catalysts in Homogeneous Aqueous Solution. In *Advances in Catalysis*, 1952; Vol. 4, p 31.

61. Schumb, W.; Satterfield, C.; Wentworth, R., American Chemical Society Monograph Series, Hydrogen Peroxide. *Reinhold, New York* **1955**.

62. Saenz-Noval, L. R. Evaluation of Alternatives for Safer and More Efficient Reactions: A Study of the *N*-oxidation of Alkylpyridines. Texas A&M University, 2011.

63. Hendershot, D. C., Inherently Safer Chemical Process Design. *Journal of Loss Prevention in the Process Industries* **1997,** 10, (3), 151-157.

64. Stoessel, F., *Thermal Safety of Chemical Processes: Risk Assessment and Process Design*. Wiley-VCH: 2008.

65. Khan, F. I.; Amyotte, P. R., How to Make Inherent Safety Practice a Reality. *The Canadian Journal of Chemical Engineering* **2003,** 81, (1), 2-16.

66. Hendershot, D. C., Conflicts and Decisions in the Search for Inherently Safer Process Options. *Process Safety Progress* **1995,** 14, (1), 52-56.

67. Hurme, M.; Rahman, M., Implementing Inherent Safety Throughout Process Lifecycle. *Journal of Loss Prevention in the Process Industries* **2005,** 18, (4–6), 238-244.

68. Wei, C.; Rogers, W. J.; Mannan, M. S., Application of Screening Tools in the Prevention of Reactive Chemical Incidents. *Journal of Loss Prevention in the Process Industries* **2004,** 17, (4), 261-269.

69. Saraf, S. R.; Rogers, W. J.; Mannan, M. S., Using Screening Test Data to Recognize Reactive Chemical Hazards. *Journal of Hazardous Materials* **2003,** 104, (1–3), 255-267.

70. Aldeeb, A. A.; Rogers, W. J.; Mannan, M. S., Theoretical and Experimental Methods for the Evaluation of Reactive Chemical Hazards. *Process Safety and Environmental Protection* **2002,** 80, (3), 141-149.

71. Stoessel, F., Applications of Reaction Calorimetry in Chemical Engineering. *Journal of Thermal Analysis and Calorimetry* **1997,** 49, (3), 1677-1688.

72. Papadaki, M., Use of Reaction Calorimetry in Thermal Risk Assessment Studies and Safe Design of Batch Reactions That Can Lead to a Runaway: Application on Hydrogen Peroxide. *Topics in Catalysis* **2004,** 29, (3-4), 207-213.

73. Landau, R. N., Expanding the Role of Reaction Calorimetry. *Thermochimica Acta* **1996,** 289, (2), 101-126.

74. Fisher, H. G., An Overview of Emergency Relief System Design Practice. *Plant/Operations Progress* **1991,** 10, (1), 1-12.

75. Chippet, S.; Ralbovsky, P.; Granville, R. In *The APTAC: A High Pressure, Low Thermal Inertia, Adiabatic Calorimeter*, International Symposium on Runaway Reactions, Pressure Relief Design, and Effluent Handling, New Orleans, LA, March 11-13, New Orleans, LA, 1998; pp 81-108.

76. Gygax, R., Chemical Reaction Engineering for Safety. *Chemical Engineering Science* **1988,** 43, (8), 1759-1771.

77. Stoessel, F., Assessment of Thermal Risks. In *Thermal Safety of Chemical Processes: Risk Assessment and Process Design*, Wiley-VCH Verlag GmbH & Co. KGaA: 2008; pp 59-80.

78. Townsend, D. I.; Tou, J. C., Thermal Hazard Evaluation by an Accelerating Rate Calorimeter. *Thermochimica Acta* **1980,** 37, (1), 1-30.

79. Mettler-Toledo, RC1*e* High Performance Thermostat. Operating Instructions. 2012.

80. Mettler-Toledo, Hardware Manual: ReactIR 15^{TM} - Improve Chemistry Understanding. 2012.

81. Wei, C.; Rogers, W. J.; Mannan, M., Detection of Autocatalytic Decomposition Behavior of Energetic Materials using APTAC. *Journal of Thermal Analysis and Calorimetry* **2006,** 83, (1), 125-130.

82. Antony, J., *Design of Experiments for Engineers and Scientists*. Butterworth-Heinemann: 2003.

83. Krishna Prasad, R.; Srivastava, S. N., Sorption of Distillery Spent Wash onto Fly Ash: Kinetics, Mechanism, Process Design and Factorial Design. *Journal of Hazardous Materials* **2009,** 161, (2–3), 1313-1322.

84. Montgomery, D. C., *Design and Analysis of Experiments*. 7th ed.; John Wiley & Sons: 2008.

85. NIST/SEMATECH, e-Handbook of Statistical Methods. National Institute of Standards and Technology: 2012.

86. Design Institute for Physical Properties, DIPPR Project 801 - Full Version. Design Institute for Physical Property Research/AIChE: 2010.

87. Andon, R. J. L.; Cox, J. D.; Herington, E. F. G., Phase Relationships in the Pyridine Series. Part 6. The Thermodynamic Properties of Mixtures of Pyridine, and of Three of its Homologues, with Water. *Transactions of the Faraday Society* **1956,** 53, 410-426.

88. Katsoni, A.; Frontistis, Z.; Xekoukoulotakis, N. P.; Diamadopoulos, E.; Mantzavinos, D., Wet air oxidation of table olive processing wastewater: Determination of key operating parameters by factorial design. *Water Research* **2008,** 42, (14), 3591-3600.

89. Chowdhury, P.; Gomaa, H.; Ray, A. K., Factorial design analysis for dye-sensitized hydrogen generation from water. *International Journal of Hydrogen Energy* **2011,** 36, (21), 13442-13451.

90. Góral, M.; Shaw, D. G.; Mączyński, A.; Wiśniewska-Gocłowska, B.; Oracz, P., IUPAC-NIST Solubility Data Series. 96. Amines with Water Part 3. Non-Aliphatic Amines. *Journal of Physical and Chemical Reference Data* **2012,** 41, (4), 043108-52.

91. Stephenson, R. M., Mutual Solubility of Water and Pyridine Derivatives. *Journal of Chemical & Engineering Data* **1993,** 38, (3), 428-431.

92. da Silva, A. d. P. M.; Cajaiba da Silva, J. o. F., Determination of the Adipic Acid Solubility Curve in Acetone by Using ATR-FTIR and Heat Flow Calorimetry. *Organic Process Research & Development* **2011,** 15, (4), 893-897.

93. de Souza, A. V. A.; Cajaiba da Silva, J. F., Biodiesel Synthesis Evaluated by Using Real-Time ATR-FTIR. *Organic Process Research & Development* **2012,** 17, (1), 127-132.

94. Hamminga, G. M.; Mul, G.; Moulijn, J. A., Real-Time In Situ ATR-FTIR analysis of the liquid phase hydrogenation of γ-butyrolactone over Cu-ZnO catalysts: A mechanistic study by varying lactone ring size. *Chemical Engineering Science* **2004,** 59, (22–23), 5479-5485.

95. Lewiner, F.; Klein, J. P.; Puel, F.; Févotte, G., On-line ATR FTIR Measurement of Supersaturation During Solution Crystallization Processes. Calibration and Applications on Three Solute/Solvent Systems. *Chemical Engineering Science* **2001,** 56, (6), 2069-2084.

96. Merayo, N.; Hermosilla, D.; Negro, C.; Blanco, Á., On-line FTIR as a Novel Tool to Monitor Fenton Process Behavior. *Chemical Engineering Journal* **2013,** 232, (0), 519-526.

97. Poljanšek, I.; Šebenik, U.; Krajnc, M., Characterization of Phenol–Urea–Formaldehyde Resin by Inline FTIR Spectroscopy. *Journal of Applied Polymer Science* **2006,** 99, (5), 2016-2028.

98. Zilian, A., *In situ* Analytics for Hydrogenation Reactions. *CHIMIA International Journal for Chemistry* **2001,** 55, (9), 704-707.

99. Zogg, A.; Fischer, U.; Hungerbühler, K., A New Approach for a Combined Evaluation of Calorimetric and Online Infrared Data to Identify Kinetic and Thermodynamic Parameters of a Chemical Reaction. *Chemometrics and Intelligent Laboratory Systems* **2004,** 71, (2), 165-176.

100. Swinehart, D. F., The Beer-Lambert Law. *Journal of Chemical Education* **1962,** 39, (7), 333.

101. Stuart, B., *Infrared Spectroscopy : Fundamentals and Applications*. J. Wiley: Chichester, England, 2004.

102. López Tocón, I.; Woolley, M. S.; Otero, J. C.; Marcos, J. I., Vibrational Spectrum of 3-Methyl and 4-Methylpyridine. *Journal of Molecular Structure* **1998,** 470, (3), 241-246.

103. Katritzky, A. R.; Beard, J. A. T.; Coats, N. A., 748. *N*-oxides and Related Compounds. Part XVI. Infrared Spectra of 3-Substituted Pyridine 1-oxides. *Journal of the Chemical Society (Resumed)* **1959**, 3680-3683.

104. Mane, S. R.; Kharade, R. R.; Mane, R. M.; Gawale, S. N.; Patil, S. M.; Bhosale, P. N., Influence of Ti+ Doping on Opto-Structural and Electrical Properties of Chemically Grown Tungsten Heteropolyoxometalate Thin Films. *Digest Journal of Nanomaterials & Biostructures* **2011,** 6, (2), 451-466.

105. Coates, J., Interpretation of Infrared Spectra, A Practical Approach. In *Encyclopedia of Analytical Chemistry*, John Wiley & Sons, Ltd: 2006.

106. Bacchi, S.; Yahyah, M.; Carangio, A.; Ribecai, A.; Cerrato Oliveros, M. C., Fit for Purpose Experimental Designs and Analyses in Chemical Development. *Organic Process Research & Development* **2010,** 14, (2), 332-338.

107. Bailey, A. J.; Griffith, W. P.; Parkin, B. C., Heteropolyperoxo- and Isopolyperoxo-Tungstates and -Molybdates as Catalysts for the Oxidation of Tertiary Amines, Alkenes and Alcohols. *Journal of the Chemical Society, Dalton Transactions* **1995**, (11), 1833-1837.

108. Ding, Y.; Zhao, W.; Song, W.; Zhang, Z.; Ma, B., Mild and Recyclable Catalytic Oxidation of Pyridines to *N*-oxides with H_2O_2 in Water Mediated by a Vanadium-Substituted Polyoxometalate. *Green Chemistry* **2011,** 13, (6), 1486-1489.

109. Kletz, T. A., Inherently Safer Plants: An Update. *Plant/Operations Progress* **1991,** 10, (2), 81-84.

110. Eto, I.; Akiyoshi, M.; Matsunaga, T.; Miyake, A.; Ogawa, T., Influence of Heavy Metal Ion on the Thermal Explosion of Hydrogen Peroxide. *Journal of Thermal Analysis and Calorimetry* **2006,** 85, (3), 623-627.

111. Kletz, T., What You Don't Have, Can't Leak. *Chemistry and Industry* **1978,** May 6, 287-292.

112. Kletz, T., Inherently Safer Design—Its Scope and Future. *Process Safety and Environmental Protection* **2003,** 81, (6), 401-405.

113. Kletz, T.; Amyotte, P., *Process Plants: A Handbook for Inherently Safer Design*. 2nd ed.; CRC Press: 2010.

114. Kletz, T. A., Inherently Safer Plants. *Plant/Operations Progress* **1985,** 4, (3), 164-167.

115. Pineda-Solano, A.; Saenz-Noval, L.; Papadaki, M.; Carreto-Vazquez, V. H.; Waldram, S.; Nayak, S.; Gao, J.; Rogers, W. J.; Mannan, M. S. In *Inherently Safer Reactor Design for Complex Reactions Based on Calorimetry Studies*, 7th Global Congress on Process Safety, Chicago, Illinois, March 13-16, AIChE, Ed. Chicago, Illinois, 2011.

116. Andon, R. J. L.; Cox, J. D., 896. Phase relationships in the pyridine series. Part I. The miscibility of some pyridine homologues with water. *Journal of the Chemical Society (Resumed)* **1952**, 4601-4606.

117. Andon, R. J. L.; Cox, J. D., 896. Phase Relationships in the Pyridine Series. Part I. The Miscibility of Some Pyridine Homologues with Water. *Journal of the Chemical Society (Resumed)* **1952**, (0), 4601-4606.

118. Shaw, E. N., Pyridine *N*-oxides. In *Chemistry of Heterocyclic Compounds*, John Wiley & Sons, Inc.: 2008; pp 97-153.

119. Edwards, V. H., Designing SAFER Process Plants. *Chemical Engineering* **2011,** 118, (4), 44-48.

120. Center for Chemical Process Safety, *Inherently Safer Chemical Processes - A Life Cycle Approach* 2nd ed.; CCPS/AIChE: 2009.